

Gene re-activation mechanisms
in the context of acquired drug resistance

de-silence of the lmn_s

Anna González Manjón

Gene re-activation mechanisms in the context of acquired drug resistance

De-silence of the LMNs

Anna González Manjón

Author: Anna González Manjón

Cover lay-out: Alex Gómez (@alex_soma6). The cover is a reference to the movie The silence of the lambs, and represents the importance of the Nuclear Lamina and its components in gene regulation. Original idea from Miguel López Venegas.

Printing: Ridderprint, www.ridderprint.nl

Layout and design: Nino Bolink, persoonlijkproefschrift.nl

Copyright 2021 © Anna González Manjón

The Netherlands. All rights reserved. No parts of this thesis may be reproduced, stored in a retrieval system or transmitted in any form or by any means without permission of the author.

Gene re-activation mechanisms in the context of acquired drug resistance

De-silence of the LMNs

**Reactiveringsmechanismen van genen in de context van
verworven resistentie tegen geneesmiddelen**

(met een samenvatting in het Nederlands)

Proefschrift

ter verkrijging van de graad van doctor aan de
Universiteit Utrecht
op gezag van de
rector magnificus, prof.dr. H.R.B.M. Kummeling,
ingevolge het besluit van het college voor promoties
in het openbaar te verdedigen op

donderdag 13 januari 2022 des ochtends te 10.15 uur

door

Anna González Manjón

geboren op 10 juli 1993
te Barcelona, Spanje

PROMOTOREN

Prof. dr. R.H. Medema

Prof. dr. B. van Steensel

"Who knows? Have patience. Go where you must go, and hope!"
Gandalf

J.R.R Tolkien



TABLE OF CONTENTS

Chapter 1	General Introduction and thesis outline	9
Chapter 2	TUBB3 overexpression has a negligible effect on the sensitivity to Taxol in cultured cell lines	25
Chapter 3	Perturbations in 3D genome organization can promote acquired drug resistance	47
Chapter 4	DNA damage-dependent chromatin dynamics as a potential cause of therapy resistance	83
Chapter 5	Unexpected gene activation following CRISPR-Cas9-mediated genome editing	111
Chapter 6	Uncovering the role of DDR factors on regulating repair pathway choice in the context of chromatin	131
Chapter 7	General discussion	145
Apendix	Nederlandse samenvatting	164
	Resumen en español	165
	Curriculum Vitae	166
	Publication list	167
	Acknowledgements	168



1

General Introduction

Anna G. Manjón, René H. Medema

DNA from the beginning

The human genome is made up of approximately three billion base pairs of deoxyribonucleic acid, better known as DNA. As first described in 1953 by Watson, Crick and Franklin, DNA is a macromolecule consisting of two strands twisting around a common axis in a shape called the double helix¹. At the most basic level, the DNA is wrapped around proteins known as histones, which together with DNA form a structure called the nucleosome (**Fig. 1**).

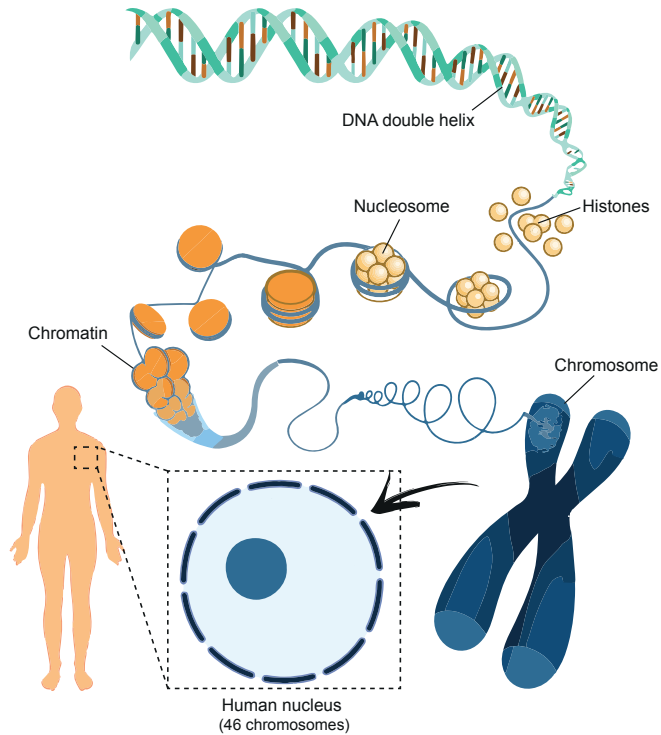


Figure 1. Organization of genetic information in the nucleus of human cells.

(Adapted from Genome Research Limited). The DNA is formed by two linear strands containing different pairing bases. The double helix is further wrapped with histone proteins forming the nucleosome that will be organized in chromatin. When cells want to divide the chromatin is packed into chromosomes. Human cells contain 46 chromosomes that will form the human body.

A nucleosome is comprised of the histones H2A, H2B, H3 and H4 in an octamer form (2 of each) which binds and wraps approximately 146 base pairs of DNA^{2,3}. The N-terminal of histones can be modified – by acetylation, methylation, ubiquitination or phosphorylation – to manipulate DNA accessibility⁴. In the eukaryotic cells, the highly organized complex of DNA, RNA and proteins found within the nucleus is called chromatin. Nucleosomes fold up to form 30 nanometer chromatin fibers,

which are further wrapped into bigger structures to form chromosomes. Humans have 46 chromosomes in each cell, divided into 22 pairs of autosomes and 2 sex chromosomes. Each chromosome is thus a long chain of compacted chromatin, that allows for storing two meters of genetic information in a cell that is only a few micrometers (**Fig. 1**). Even though the DNA carries all the genetic information, this needs to be transcribed into messenger RNA in order for a cell to conduct its functions. The messenger RNA will be used as a template to determine the amino acid sequence to form proteins. Remarkably, only a little portion of the genome encodes for proteins, what we call genes^{5,6}. Genes are often surrounded by huge noncoding deserts that may contain repetitive DNA sequences such as telomeres and centromeres, regulatory sequences such as promoters and enhancers, and non-coding RNA molecules that are all essential to preserve the nuclear and cellular integrity.

Euchromatin and heterochromatin

Chromatin has traditionally been categorized into two main classes based on structural and functional criteria. Euchromatin contains the majority of genes, and it is often under active transcription allowing the recruitment of transcription factors and enzymes to interact with the DNA. Heterochromatin is a highly conserved and compacted domain of eukaryotic genomes typically transcriptionally repressed and responsible for several genome functions⁷⁻⁹ (**Fig. 2**). Heterochromatin can be classified into two major types, constitutive and facultative. Constitutive heterochromatin (CH) is typically situated at pericentromeric and telomeric domains which contains relatively low transcriptional levels, repetitive DNA sequences such as DNA satellites and transposons elements. This type of heterochromatin is also enriched for di- and trimethylated histone H3 lysine 9 (H3K9me2 and me3) which is recognized by the heterochromatin protein 1 (HP1). HP1 can later promote the spreading of heterochromatin along the chromosome^{7,10}. Facultative heterochromatin (FH) is associated with transcriptional regulation of developmental genes and depends on Polycomb group protein complexes 1 and 2 (PRC1 and PRC2), which initiate silencing by deposition of H3K27me3¹¹ (**Fig. 2**). Moreover, heterochromatin can also be found interspersing non-repetitive euchromatic regions (IH). As some examples mention above, in order to maintain the desired chromatin environment and gene expression programs, a wide variety of proteins are able to modify, remove and sense specific amino acids at the histone tails. These are the so-called writers, erasers and readers, respectively¹².

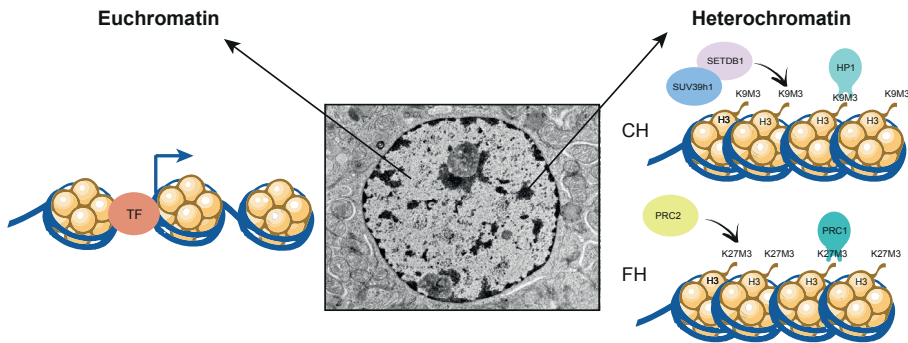


Figure 2. The states of chromatin in the nucleus.

Middle - Electron microscopy image of a nucleus with clear active chromatin (euchromatin) and dark repressive chromatin (heterochromatin). Left - Euchromatin contains less nucleosomes which allows transcription factors to bind and activate transcription. Right - Heterochromatin is divided in Constitutive (CH) or Facultative (FH) and is densely packed with nucleosomes and specific repressive histone marks.

Large-scale structural compartmentation of the nucleus

Within the eukaryotic nucleus, DNA – regardless of its chromatin status – is intricately folded. Chromosome organization is important to facilitate very long DNA molecules to fit into the nucleus as well as to ensure that the DNA is properly regulated^{13,14}. Powerful insights into the organization of the DNA in the nucleus have followed from the development of genome-wide methods including Hi-C or Dam-ID among others (**Fig. 3**).

Topological associated domains: TADs

Hi-C analysis – a type of chromosome conformation capture technique – revealed two levels of chromatin organization: topological associated domains (TADs) and compartments. A TAD is a chromosome region whose DNA sequences are preferentially found interacting together by CTCF and cohesin-dependent loop formation¹⁵. Hi-C maps also reveal longer range interactions known as compartments, which involve interactions between many TADs. Compartments are divided into active (A) and inactive (B) regions which correspond to euchromatin and heterochromatin, respectively¹⁶ and is proposed to occur via a microphase separation mechanism¹⁷ (**Fig. 3**).

Lamina associated domains: LADs

Another genome-wide approach to study genome architecture is the mapping of DNA interactions with the Nuclear Lamina (NL), mostly by means of the DamID technology^{18,19}. The DamID method tethers a bacterial DNA adenine methyltransferase (Dam) to a NL protein (such as Lamin B1) that leads to methylation

of DNA in contact with that protein²⁰. Lamina associated domains (LADs) are defined as genomic regions that make molecular contact with the NL and poses several features from heterochromatin, mostly comprising H3K9me3 and H3K27me3 histone marks²¹. It has been shown that genes located in LADs are expressed at very low levels, suggesting that nuclear periphery is more restrictive for transcriptional activity²² (**Fig. 3**).

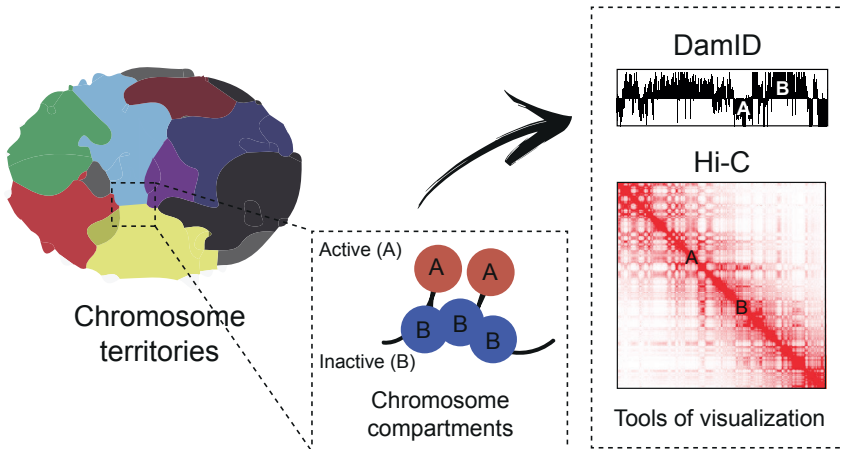


Figure 3. Chromosome territories in the nucleus forming different compartments and methods for their visualization.

Adapted from (Hildebrand EM & Dekker J 2020). Left - cell nucleus showing different chromosomes in different colors that illustrate chromosome territories. Middle - Each chromosome has regions of active (A) and inactive (B) chromatin, which separates within compartments. Right - A and B compartments are visible in DamID plots and Hi-C matrices.

Transcription regulation

Transcription regulation in the context of chromatin

Genes do not work as isolated and single units. Their expression is modulated by chromatin and influenced by the three-dimensional organization of the genome²³. Gene activation often involves the displacement of nucleosomes located at the gene regulatory regions. ATP-dependent nucleosome remodeling protein complexes are able to alter the position of nucleosomes thus creating nucleosome-free regions more accessible to transcription factors²⁴. Another mechanism of gene regulation is via DNA methylation, usually associated with gene silencing. DNA methyltransferase enzyme catalyzes the addition of a methyl group to cytosine of CG dinucleotides. This covalent modification can interfere with transcription factor binding and spread other repressive chromatin marks²⁵ (**Fig. 4**, top). Histone modifications are associated with both inactive and active transcriptional program. One of the most widely studied histone modification is acetylation, which adds a negative charge

that repel the negatively charged DNA therefore resulting in chromatin relaxation and gene expression. On the contrary, histone methylation can be associated both with transcriptional repression or activation. For example, while H3K9me3 and H3K27me3 are associated with heterochromatin and gene repression, both mono- and tri-methylation on K4 of histone H3 (H3K4me1 and H3K4me3) are activation markers found on gene regulatory regions²⁶⁻²⁸.

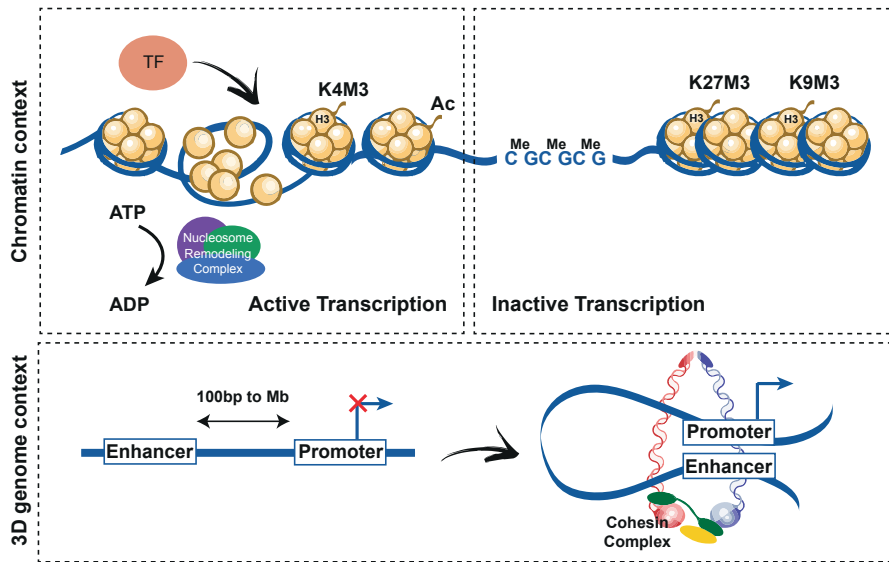


Figure 4. Transcription regulation in the chromatin and three-dimensional genome context. Top - From the nucleosome resolution perspective, Nucleosome remodeling together with changes in histone modifications can make the DNA accessible to TFs leading to transcription activation. DNA methylation and other repressive chromatin marks (H3K9me3 or H3K27me3) correlate with low levels of transcription. Bottom - From the 3D genome perspective, enhancers and promoters need to be in close proximity forming loops with the help of cohesin complex to fully activate gene transcription.

Transcription regulation in the context of the three-dimensional genome

The process of transcriptional regulation is not carried out on a linear DNA molecule; rather, transcription regulation also depends on long range physical interactions between DNA regulatory sequences described as promoters and enhancers. Promoters are proximal elements located within a few hundred base pairs upstream of the transcription start site. Enhancer sequences can be located hundreds of kilobases away from the start of transcription²⁹. For most of the genes, interaction between enhancer and promoter is required for full gene activation, therefore, the three-dimensional context of the genome plays a crucial role in transcriptional regulation. As first described in the β -globin locus, promoter-enhancer interactions

are achieved by a process called DNA loop formation, which involves the CTCF protein and the cohesin complex. It is known that these loops form within the context of TADs which delimit regulatory hubs. The promoter-enhanced functionality is achieved by the binding of transcription factors, other co-regulators and the chromatin structure^{5,30,31} (**Fig. 4**, bottom). Therefore, in order to accomplish proper control of gene transcription, a cross-talk between chromatin modifications, gene-regulatory elements and the three-dimensional genome is crucial to achieve.

Preserving genome integrity

Considering that DNA is the source code for human life, each cell in the human body receives thousands of DNA lesions per day³². These lesions, if not repaired properly, can perturb the integrity of the DNA and lead to larger genomic aberrations that will compromise the organism viability. DNA damage can arise from normal biological processes - such as DNA replication - or due to environmental exposure of cells to DNA damaging agents - for instance the solar ultraviolet radiation³³. DNA bases can be damaged by oxidative processes, alkylation or hydrolysis, bulky adduct formation or DNA crosslinking. However, the most deleterious form of DNA lesions are double strand breaks (DSBs), which induce a breakage in both sides of the double helix^{33,34}. Remarkably, organisms possess an elaborate network of mechanisms to repair those DNA lesions. This complex network is known as the DNA damage response (DDR). Here we will describe the damage response induced by DSBs.

The DNA damage response

The DNA damage response includes several signal transduction pathways which detect DNA lesions and recruit DNA repair proteins in order to fix the damage. The first proteins to be recruited to DSBs are the ataxia teleangiectasia-mutated protein (ATM) and DNA-dependent protein kinase (DNA-PK)³⁵. These kinases consequently phosphorylate residue 139 of the histone variant H2AX (gH2AX) at proximal sites of the DSB³⁶. gH2AX rapidly spreads and amplifies the response to damage binding a sensor protein called MDC1 which will recruit more ATM and repair factors³⁷. Among other repair factors recruited we find the MRN complex - formed by Mre11, Rad50 and Nbs1 - and the RING finger E3 ubiquitin ligases RNF8 and RNF168 proteins³⁸. Together, these factors are essential for the recruitment of downstream DDR factors such as p53-binding protein 1 (53BP1) and the BRCA1 complex, which will have a major influence on the choice of the repair mechanism employed (**Fig. 5**, top)^{39,40}.

Canonical non-homologous end joining (NHEJ)

NHEJ repairs a DSB by ligating the broken DNA ends together and can take place throughout the cell cycle. This pathway initiates by the high affinity binding of the Ku70/80 heterodimer to the double-stranded DNA ends^{41,42}. Subsequently, DNA-PKcs binds Ku70/80 tethering the two broken ends together and auto phosphorylates in

order to recruit other DNA damage factors⁴³. The ends are then minimally processed in a reaction involving the MRN complex. Finally, a complex consisting on Ligase IV, XRCC4, XLF and PAXX is recruited and ligates the broken DNA ends⁴⁴. Due to the end-processing and the lack of DNA template for repair, small insertions and deletions can be formed at the break site. (**Fig. 5**, left). Therefore, NHEJ is considered an error-prone pathway.

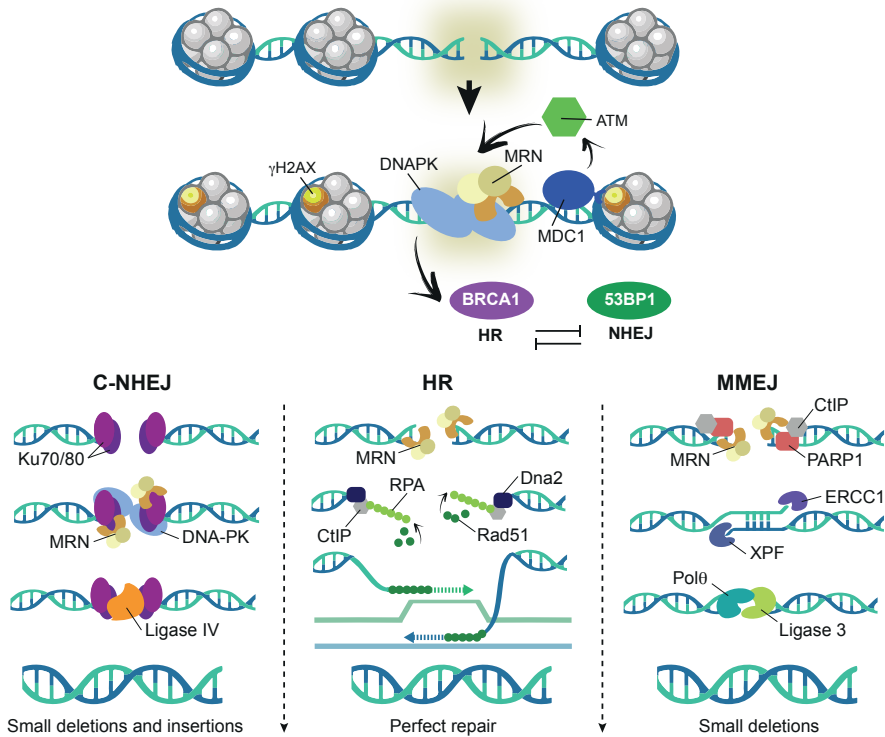


Figure 5. The DNA damage response and repair pathway choice. Top - Schematic representation of the general DNA damage response. Bottom left - Canonical non-homologous end joining repair pathway. Bottom middle - Homologous recombination repair. Bottom right - Micro-homology end joining repair.

Homologous recombination (HR)

On the other hand, HR is considered an error-free repair pathway as it uses the undamaged sister chromatid as a template for accurate repair. HR is mostly active in S and G2 cell cycle phases^{45,46}. The initial steps involve the recruitment of the MRN complex, which - in conjunction with Exo1, Dna2 and other factors - resects the DNA at the break sites⁴⁷. This creates a single-stranded DNA (ssDNA) in both sites of the break that is stabilized by the RPA complex. This complex is then displaced

by the Rad51 recombinase which forms a nucleoprotein filament. Once Rad51 is load, this initiates DNA homology search and strand invasion by pairing with the complementary strand of the DNA template⁴⁸. This results in a D-loops structure formation, where DNA polymerase will use the DNA template to fill the resected DNA (**Fig. 5**, middle). The DNA synthesis allows for the formation of a join molecule with a double Holliday junction, which can be resolved by multiple endonucleases⁴⁹.

Microhomology-mediated end joining (MMEJ)

In addition to these two main repair pathways, an alternative repair mechanism can be used to repair DSBs. This pathway relies on both DNA resection and end joining, yet, it uses small homologies found close to the break site (microhomologies) to anneal the broken ends^{50,51}. The MRN complex together with PARP1 and CtIP perform DNA end processing, allowing for base pairing of the ssDNA molecules with the microhomologies. After microhomology annealing, the non-homologous DNA tails are removed by XPF and ERCC1 endonucleases to allow for DNA polymerase η to fill the gaps and stabilize the annealed intermediate. The final step involves Ligase III to mediate the end ligation (**Fig. 5**, right)^{51,52}. As a result of the DNA flap processing, MMEJ repair creates small deletions and therefore is an error-prone DSB repair pathway.

DNA repair in the context of chromatin

As described in earlier sections, chromatin is organized into high-order structures that form the three-dimensional genome. It is well known that the chromatin structure and its dynamics changes in response to DNA damage and repair. It has been proposed that upon DSBs, chromatin needs to decondense in order to allow for repair proteins to have access to the DNA lesion. In 2002, Green and Almouzni presented the Access-Repair-Restore model where they integrate nucleosome dynamics in the repair response. It is now known that the chromatin dynamics after DNA damage are more complex than the mere recruitment of chromatin remodelers. More recent versions of this model include histone modifications during the access and repair process as well as new histone incorporation during the restoration⁵³. On the other hand, it has also been suggested that damaged DNA loci are able to relocate to different nuclear compartments in order for DNA repair to take place. Therefore, we need to understand DNA repair as a cross-talk between repair pathways, chromatin modifications and structural changes within the three dimensions of the nucleus.

Histone mobility and modifications

It has been widely described that during early steps in the UV damage response histone proteins are mobilized from the break site⁵³. The destabilization of damaged nucleosomes is carried out by ATP-dependent chromatin remodeler complexes,

such as INO80, SWR1 and TIP60-p400, and it is known to be involved in efficient repair of DSBs^{54,55}. Importantly, histone mobilization has also been described in other model organisms and sources of DNA damage^{56,57}. As exemplified before with H2AX, besides histone remodeling, these proteins can undergo posttranslational modifications during the DNA damage response. Paradoxically, both active and repressive chromatin marks can be deposited in histones surrounding the DSB^{53,58}. For instance, histone acetylation will lead to chromatin relaxation and recruitment of DNA damage factors for correct repair⁵⁹. However, repressive factors such as HP1 and Polycomb group proteins can also be recruited to DSBs, where they are involved in transcription inhibition during repair of DNA lesions (**Fig. 6A**)^{60,61}. Thus, chromatin compaction cannot simply be considered as a barrier for DSB repair, yet, it can also play a role in regulating a correct damage response.

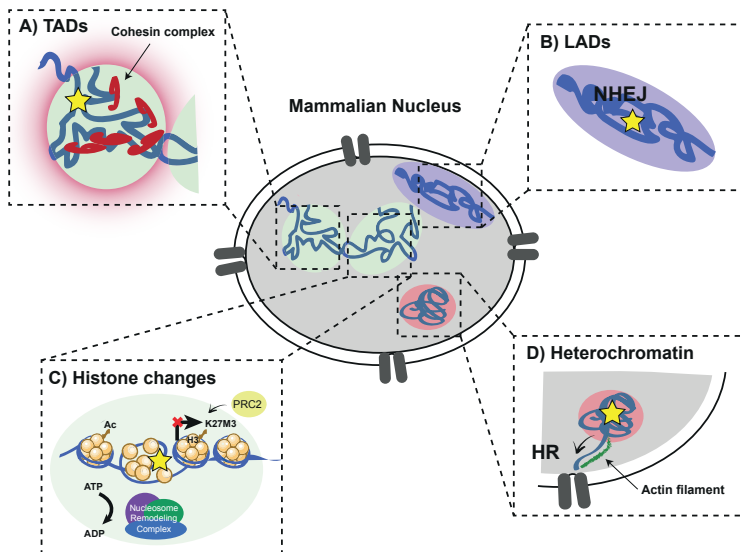


Figure 6. Impact of nuclear organization on DNA damage response and repair. Adapted from (Dabin J et al 2016). A) DSBs and γ H2AX are thought to cluster within TAD structures via cohesin loading. B) Repair in LADs occur by NHEJ mainly inside the domain. C) Several histone modifications take place during DSB repair at the nucleosome level. D) Pericentromeric heterochromatin relocalize to the nuclear periphery in order to be repaired by HR. This mechanism is thought to be driven by nuclear actin polymerization.

DNA mobility upon DNA damage and repair

Advances in live-cell imaging analysis have made possible the visualization of DNA mobility in real time. It is now clear that DNA mobility is dramatically increased in the presence of DSBs. In *Drosophila* and mammalian cells, DSBs induced in pericentromeric heterochromatin are relocalized outside of this domain to

be repaired by HR^{62,63}. This relocalization depends on nuclear pores and inner nuclear membrane which allow for DNA anchoring^{64,65}. It has been hypothesized that the DNA spatial dynamics help preventing aberrant recombination between repetitive regions of heterochromatin. Most recently, nuclear actin and myosins have been proposed to drive relocalization of these heterochromatin breaks (**Fig. 6B**)^{66,67}. The mechanism of DNA mobility is not limited for DSBs in pericentromeric heterochromatin, as telomeres and replication stress loci also move to the nuclear periphery upon damage induction and repair^{68,69}.

Organizing DNA repair within the three-dimensional genome

The DNA repair also occurs in the higher-order chromatin structure within the influence of chromosome compartments, TADs and LADs. A study in 2014 in human cells showed that the nuclear position of a locus determined the DNA repair pathway choice⁷⁰. In contrast to earlier findings in yeast⁷¹⁻⁷⁴, this research proposes that Scel-induced DSBs within LADs do not migrate to more permissive chromatin environments and are repaired by NHEJ or MMEJ (**Fig. 6C**). Several other studies have suggested the role of chromosome architecture in controlling the clustering and spreading of gH2AX in specific domains⁷⁵. Indeed, gH2AX was found to spread within TAD structures, where the cohesin complex helped to confine this gH2AX signaling⁷⁶. Moreover, a model where cohesin-dependent DNA loop extrusion provides a way to signal the DSB repair response has been recently proposed (**Fig. 6D**)⁷⁷.

Restoration of the initial chromatin organization

As described in the previous sections, we now have an increase understanding on how chromatin is modified upon DNA damage. However, the restoration of chromatin and genome architecture after repair is completed is still not well understood⁷⁸. Returning to the previous chromatin state would ensure the maintenance of the genome integrity. Yet, the stable inheritance of the DNA damage-dependent chromatin modifications could induce genome plasticity, contributing to alterations of the transcriptional program and/or changes in cell identity. So far, few studies have suggested the contribution of DNA damage and repair in producing stable chromatin alterations leading to changes in gene expression. In one study, the induction of a DSB in an exogenous promoter was shown to, in a very low incidence, silence the associated gene due to DNA methylation spreading⁷⁹. In another, replication stress was found to induce loss of H3K4me3 which lead to low gene transcription in a reporter locus⁸⁰. However, it is still a matter of debate whether the observed epigenetic changes are transient or long term and whether they could contribute to transcription and cell reprogramming in endogenous locus.

DNA damage response and transcription

Even though in response to DSBs global DNA transcription is inhibited^{81,82}, increasing evidences have shown that DNA damage can as well have a positive role in transcription activation. It is well known that transcription can induce genomic instability, for example by obstructions to replication-fork progression or formation of DNA:RNA hybrids⁸³. Paradoxically, the generation of small non-coding RNAs (sncRNAs) upon damage have been well documented in the last years. These are known as DNA damage response RNAs (DDRNs)^{84,85}. The observations of this process were first reported by the recruitment of TFs and RNA binding proteins (RBPs) to DNA damage sites. It was latter suggested that DNA-dependent PARP1-mediated PARylation could facilitate chromatin remodeling leading to the recruitments of several TFs and other DDR proteins⁸⁶. Whether open chromatin and recruitment of TFs are needed for DDRNs formation is still not described.

In mammalian cells, DDRNs are generated from proximal sequences to the broken ends and need to be processed by two components of the RNA interference pathway (RNAi): DROSHA and DICER. Impairment of DDRNs processing - by DROSHA and DICER depletion - caused a reduction on DDR protein recruitment to damage sites, suggesting a direct role for DDRNs in the control of the DNA damage response⁸⁷. Specifically, reduced HR repair has been observed upon DICER and AGO2 downregulation^{88,89}. But most recently, DROSHA was reported to induce NHEJ in DNA damage sites via the MRN complex⁹⁰. Therefore, the mechanisms of action of the DDRNs in the repair response are not fully characterized. Notably, DDRNs biogenesis in mammals does not require preexisting transcription, as exogenous locus lacking transcription regulatory elements can as well generate DDRNs⁸⁷. It is interesting to hypothesize that *de novo* formation of small RNA transcripts - for example by RNA Polymerase II recruitment - could lead to transcription activation of repressed genes upon DNA damage. Yet, the study of transcription regulation at damage sites is relatively recent, and much more insights are needed to fully understand the paradox of both inhibiting canonical transcription and generating *de novo* DDRNs.

CRISPR as a tool for genome editing

As previously introduced, eukaryotic genomes are composed of billions of DNA bases. In recent year, several genome editing technologies have been developed making possible to introduce sequence-specific modifications in the DNA. Since the discovery of bacterial nucleases able to cleave DNA molecules in the early 70s^{91,92}, many useful applications of genome editing have been developed in different research fields. A particularly area of interest is that of introducing DSBs in a specific DNA sequence by using special nucleases. Nuclease-induced DSBs are able to activate the endogenous repair machinery of the target organism to repair

the DNA damage^{93,94}. Thus, genome editing technologies opened the possibility to easily study the DNA damage response in specific DNA locations.

The most common genome editing tools to introduce endogenous DSBs are zinc-finger nucleases (ZFNs), transcription activator-like effector nucleases (TALENs) and clustered regularly interspaced short palindromic repeat associated 9 nuclease (CRISPR-Cas9) (**Fig. 7**)^{95,96}. Certainly, the bacterial CRISPR-Cas9 nuclease has revolutionized the genome editing field, largely because of its easy manipulation and specificity of the cleavage. CRISPR was first discovered to have a role in the bacterial immune system⁹⁷⁻⁹⁹. It was demonstrated that after a viral infection, bacteria were able to integrate viral DNA repeats that were transcribed into two short RNAs: the mature crRNA (crRNA) and the trans-activating crRNA (tracrRNA). The crRNA contains a foreign sequence that serves as a guiding sequence, which binds the tracrRNA forming a crRNA-tracrRNA hybrid. This RNA hybrid is able to recruit Cas9 enzymes to bind and cleave pathogenic viral particles infecting the host cells (**Fig. 7**)(reviewed at⁹⁶).

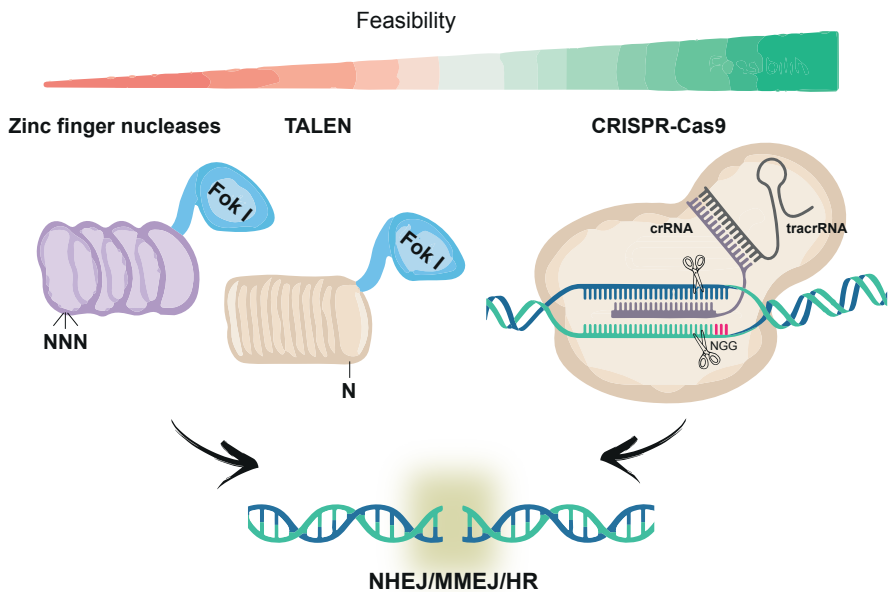


Figure 7. The major tools for genome-editing organized according to its feasibility. Adapted from (Adli M 2018). Zinc finger nuclease are engineered in order to recognize triple DNA nucleotides. TALE recognizes an individual base. The CRISPR technology uses RNA-DNA base pairing, where the crRNA gives the specificity of the cleavage sequence. The cleavage happens within in the context of the PAM sequence, consisting on 3 nucleotides NGG. All these tools induce DSBs that are either repair by NHEJ, MMEJ or HR.

These studies were shortly followed by revolutionary publications describing the use of CRISPR for *in vivo* genome editing of eukaryotic cells¹⁰⁰⁻¹⁰². Today, CRISPR-Cas9 is a worldwide used system that has been largely optimized and modified to serve many genome-editing purposes as well as many other genome and chromatin manipulation studies. In the field of DNA damage and repair, the CRISPR-Cas9 system allowed to induce DSBs at desired endogenous locations by generating a 20-nucleotides target recognition sequence in the crRNA. The resulting DSBs, as well as g-IR or chemically-induced, are able to be repaired with the endogenous repair machinery by NHEJ, HR or MMEJ repair^{103,104}.

Drug resistance in cancer

The understanding of cancer biology and therapy has dramatically increased over the last decades, which has significantly improved patient survival and quality of life. Yet, despite the arrival of immunotherapy and targeted therapies for cancer treatment, surgery, radiotherapy and chemotherapy still remain the three main pillars of cancer therapy. However, drug resistance is still one of the major obstacles to achieve cures in cancer patients^{105,106}. Drug resistance results in the tolerance of the cancer cells to pharmaceutical treatments, including chemotherapeutic compounds. In the early 70s, the P-glycoprotein was the first membrane transporter to be identified to confer multidrug resistance to several chemotherapeutic compounds in Chinese hamster ovarian cells^{107,108}. These first findings triggered the study of many other membrane transporters also known to be involved in multidrug resistance as well as diverse human physiological processes. All of these transporters belong to the ATP-binding cassette (ABC) family, which include proteins like the multidrug resistance-associate protein 1 (MRP1) or the breast cancer resistance protein (BCRP). For all proteins of the family, ATP binding and hydrolysis drives a cycle of conformational changes that allows a substrate to bind on one site of the membrane and to be released on the other side. Therefore, ABC transporters are capable of pumping out of toxic compounds out of cells.

ABCB1 is the gene that encodes for the P-glycoprotein, also known as multidrug resistance 1 (MDR1) protein. It is well-described that *ABCB1* expression acts as a mechanism of resistance to taxane related drugs such as doxorubicine or paclitaxel (Taxol) in cellular systems and mouse models. In cellular models, mechanisms such as increased *ABCB1* copy number, single nucleotide polymorphisms (SNPs) or epigenetic modifications have been described to explain the overexpression of *ABCB1* and consequent multi drug resistance¹⁰⁹⁻¹¹³. Additionally, the use of mouse models has confirmed the role of P-glycoprotein and other ABC transporters in impairing anticancer drugs absorption and brain exposure^{114,115}. Although the importance of P-glycoprotein in pharmacokinetics is largely understood, its role in drug resistance in human tumors is still debatable. Due to the clear observations in cellular systems and mouse, many clinical trials were performed with P-glycoprotein inhibitors to

improve the availability of chemotherapeutic drugs in tumors. Unfortunately, the majority of these clinical trials failed to enhance therapeutic efficiency and improve patient survival¹¹⁶⁻¹¹⁸. However, it is important to point out that these clinical trials were performed decades ago, without the appropriate tools for the genetic characterization of tumors with high levels of P-glycoprotein. Indeed, patients were not selected based on P-glycoprotein expression¹¹⁹⁻¹²¹. Interestingly, more recent investigations in ovarian cancer and leukemia have found that a low proportion of taxane-resistant patients harbor recurrent promoter fusions associated with overexpression of *ABCB1*¹²²⁻¹²⁴. Therefore, some scientists propose to re-evaluate whether P-glycoprotein and other transporters may play a clinical role in multi drug resistance in specific cancer types and patients.

Thesis outline

In this thesis we aim to better understand the molecular mechanisms that cells employ to upregulate genes undergoing chemotherapeutic drug treatments. We use the *ABCB1* gene as our model gene to study this process as its role in Taxol resistance is well characterized. In **Chapter 2** we demonstrate that *ABCB1* upregulation is the major mechanism of acquired taxane-related drug resistance in the untransformed retinal pigmented epithelial (RPE-1) cells. In **Chapter 3**, we characterize the molecular mechanisms underlying *ABCB1* upregulation in this cell line. We show that Nuclear Lamina (NL) interactions are required to maintain *ABCB1* repressed. Perturbations in NL lead to heterogeneous population with increase number of cells acquiring Taxol resistance. In **Chapter 4**, we aim to understand whether chromatin and three-dimensional genome changes, previously reported in literature upon DSB induction, could lead to upregulation of *ABCB1*. We also investigate whether the observed genome alterations could be stable inherited and consequently contribute to Taxol drug resistance. **Chapter 5** describes an unexpected event leading to *ABCB1* gene activation following CRISPR-Cas9 genome editing. When inducing a DSB with a lentiviral-based sgRNA vector, this can integrate into the endogenous genomic target location, leading to undesired activation of the target gene. Finally, in **Chapter 6**, we aim to further understand the DNA damage response in the context of chromatin. We demonstrate that CRISPR-Cas9 screens can be successfully implemented in the recently reported multiplexed reporter assay from Schep et. al to uncover the role of DDR factors on regulating repair pathway choice in the context of chromatin. Lastly, in **Chapter 7** we summarize and review the results described in this thesis. While the role of *ABCB1* in acquired multi drug resistance in patients is still debatable, we propose a set of novel molecular mechanisms that lead to upregulation of this gene.



2

TUBB3 overexpression has a negligible effect on the sensitivity to Taxol in cultured cell lines

Mihoko A. Tame*, Anna G. Manjón*, Daria Belokhvostova, Jonne A. Raaijmakers, René H. Medema

* Contributed equally

Published in Oncotarget

ABSTRACT

Microtubules are cellular targets for a variety of anticancer therapies because of their critical function in mitosis. Taxol belongs to a class of microtubule targeting agents that suppresses microtubule dynamics and interferes with the functioning of the mitotic spindle, thereby effectively blocking cell cycle progression of rapidly proliferating tumor cells. Despite its antitumor activity, drug resistance remains a common obstacle in improving its overall clinical efficacy. Previous studies have shown that the expression of a specific β -tubulin isotype, β III-tubulin/TUBB3, is dysregulated in drug-refractory tumors. However, whether enhanced TUBB3 expression is directly involved in promoting Taxol resistance remains a subject of debate. Here, we have used several approaches to assess the functional relation of TUBB3 overexpression and Taxol resistance. First, we generated a number of Taxol-resistant cell lines, to find that TUBB3 expression was elevated in a resistant cell line (RPE-20) derived from untransformed retinal pigment epithelial (RPE) cells, but the abundance of TUBB3 remained unchanged in four other cell lines after Taxol treatment. However, although RPE-20 cells displayed enhanced TUBB3 levels, we find that simultaneous up-regulation of the P-glycoprotein (P-gP) drug-efflux pump is responsible for the resistance to Taxol. Indeed, we could show that TUBB3 levels were dynamically regulated upon Taxol exposure and withdrawal, unrelated to the resistance phenotype. Next, we generated cell lines in which we could induce robust overexpression of TUBB3 from its endogenous locus employing the CRISPRa system. We demonstrate that solely enhancing TUBB3 expression results in a very minor decrease in the sensitivity to Taxol. This was further substantiated by selective depletion of TUBB3 in a series of breast cancer cell lines expressing high levels of TUBB3. We find that TUBB3 depletion had a minimal effect on the sensitivity to Taxol in one of these cell lines, but had no effect in all of the others. Based on these findings we propose that TUBB3 overexpression can only marginally affect the sensitivity to Taxol in cultured cell lines.

INTRODUCTION

Microtubules, polymers of α/β heterodimers, are dynamic cytoskeletal structures that are essential for many cellular functions, including cell movement, intracellular transport and cell division. Particularly during cell division, cells depend on the formation of a highly dynamic microtubule network, the mitotic spindle, which facilitates faithful segregation of chromosomes to the two new daughter cells [1]. Since uncontrolled cycles of cell divisions and chronic cell proliferation is a hallmark of many cancers [2], microtubules (MTs) have been exploited as therapeutic targets to curb proliferation of transformed cells using a variety of microtubule-targeting agents (MTAs), also known as anti-mitotics [3].

Paclitaxel (hereafter referred to as Taxol) is an MTA that suppresses microtubule dynamics and thereby disrupts mitotic progression. This mode of action is thought to be responsible for the potent ability of Taxol to prevent cell proliferation in tumors [4,5]. Taxol is used for the treatment of a variety of solid tumors, such as ovarian, breast and lung cancers [6]. However, in spite of its initial antitumor activity, the overall clinical efficacy of this drug is often limited due to intrinsic or acquired drug resistance [3,7]. Determining molecular mechanisms of Taxol resistance is therefore of great clinical value for the design of treatment plans.

Taxol specifically targets the β -subunit of tubulin [6], of which eight isotypes exist in humans [8]. The β -tubulin isotypes are highly conserved in their core globular domain; however they display subtle differences in their unstructured C-terminal tails, a region of the protein that is positioned at the exterior surface of the polymerized MT lattice and provides sites for a variety of post-translational modifications as well as binding sites for microtubule-associated proteins [9,10]. Expression of most of the β -tubulin isotypes is confined to specific cell types or tissues, and certain compositions of tubulin isotypes may assemble into discrete MT species with unique properties and functions [11,12].

Interestingly, tumors that have become refractory to Taxol treatment frequently express different sets of β -tubulin isotypes that are not expressed in their tissue of origin. In particular, the selective over-expression of class III β -tubulin (TUBB3) has been reported to be associated with Taxol resistance in an overwhelming number of translational studies (reviewed in [13,14]). Functional studies subsequently corroborated a direct role of TUBB3 in enhancing Taxol resistance. TUBB3 knockdown in cancer cell lines that have aberrantly high expression of this gene product were shown to result in increased sensitivity to Taxol [15-17], whereas ectopic over-expression of this gene in cell lines with low basal expression level of TUBB3 is accompanied by increased resistance to Taxol [18,19]. Furthermore, *in vitro* studies demonstrated that TUBB3 enhances the rate of tubulin depolymerization in the presence of Taxol [18,20,21], indicating that TUBB3 overexpression might directly render microtubules less sensitive to the MT-stabilizing activity of Taxol.

Based on these studies, the overexpression of TUBB3 has been initially considered as a promising predictive marker for Taxol resistance in tumors.

However, several other studies have since then implicated a broader function for TUBB3 in drug resistance or as a general cell survival factor. For instance, increased expression of TUBB3 confers cells with resistance to other chemotherapeutic drugs, including vinca alkaloids and DNA damaging agents [15,22]. Furthermore, TUBB3 overexpression has been observed upon exposure of cells to challenging growth conditions, such as nutrient deprivation [23] and hypoxia [24]. Moreover, increased expression of TUBB3 has been associated with aggressive tumor phenotypes in patients that have never been treated with Taxol-containing regimens (reviewed in [25]).

In this study, we addressed the regulation and functional significance of TUBB3 in Taxol resistance with multiple different experimental set-ups and a variety of cell lines. We have identified in multiple incidences a correlation between Taxol sensitivity and increased TUBB3 expression. However, although induced overexpression of TUBB3 is sufficient for a minor Taxol-resistance phenotype, TUBB3 depletion experiments show that it has no major role in driving drug resistance, therefore, other β -isotypes may contribute to this process. Our work highlights the multifactorial nature of Taxol resistance in cultured cell lines, and shows that TUBB3 overexpression in untransformed cells has a very minor effect on the Taxol sensitivity.

RESULTS

Taxol-resistance of RPE-20 is mediated through P-gP

We generated Taxol-resistant cell lines derived from hTERT-immortalized, untransformed RPE-1 (RPE) cells through prolonged exposure and clonogenic outgrowth in the presence of an increasing dose of Taxol. After polyclonal selection of Taxol-resistant cells for at least 4 weeks, we obtained a cell line that could proliferate under constant exposure to 20 nM of Taxol (RPE-20) (**Fig. 1A**). In terms of IC₅₀, the RPE-20 cell line displayed a 14-fold increased resistance to Taxol compared to the parental counterpart (RPE-0) (**Fig. 1B**; IC₅₀=3.0 for RPE-0, IC₅₀=43.5 for RPE-20). A predominant mechanism of Taxol resistance reported in studies utilizing cultured cell lines is the up-regulation of the drug efflux pump P-glycoprotein (P-gP)/ ABCB1 (reviewed in [26]). Thus, we decided to first test if Taxol resistance in the RPE-20 cells is mediated through P-gP. Relative survival plots revealed that RPE-20 cells became highly sensitive to Taxol when treated in combination with tariquidar, a specific inhibitor of P-gP [27]. While the RPE-20 cells have an IC₅₀ for Taxol of 41.1 nM in the absence of the inhibitor, their resistance dropped to an IC₅₀ of 3.8 nM after tariquidar addition, similar to the IC₅₀ for the parental RPE cells (**Fig. 1C**). This result suggests that an increased efflux of the drug mediated by P-gP predominantly

facilitates Taxol resistance in the RPE-20. Furthermore, these cells display cross-resistance to vincristine (**Fig. 1D**), an MTA that is also a well-described substrate of P-gP [26]. In line with this idea, we confirmed that RPE-20 cells express increased amount of P-gP both in protein (**Fig. 1E**) and mRNA level (**Fig. 1F**). In an attempt to establish a P-gP-independent Taxol-resistant RPE cell line, we cultured RPE cells in the presence of 5 nM Taxol and 40 nM of tariquidar. However, this approach did not yield any surviving clones (data not shown). Furthermore, we repeated the same approach with a p53-deficient RPE cell line. Although RPE p53^{-/-} cells grew out resistant colonies and were viable after increasing the dose of Taxol to 10 nM, their proliferation was severely reduced in the presence of tariquidar (**Fig. 1G**). Thus, this suggests that P-gP is an important driver of Taxol resistance in RPE cells and their proliferative capacity is severely compromised when forced to adapt to Taxol through alternative mechanisms. Nonetheless, we observed that the RPE-20 cells remain slightly more resistant to Taxol even in the presence of tariquidar (IC₅₀=3.8 nM) compared to the RPE-0 cells (IC₅₀=2.9 nM) (**Fig. 1C**). Moreover, RPE-20 cells were hypersensitive to the MT-destabilizing drug vincristine, when treated in combination with tariquidar (**Fig. 1D**). These results suggest that while the induction of P-gP activity provides the major mechanism of Taxol-resistance in RPE cells, they may have also adapted their MT dynamics to the stabilizing effect of Taxol, albeit that the contribution of the altered MT dynamics to the overall sensitivity to Taxol appears to be very minor.

TUBB3 protein levels are dynamically regulated upon Taxol exposure and withdrawal and does not correlate with the timing of resistance acquisition

Next, we set out to examine whether TUBB3 levels are altered in the RPE-20 cells compared to the Taxol-naïve RPE cells to account for the minor decrease in Taxol-sensitivity that we observed in the presence of tariquidar (**Fig. 1C**). Surprisingly, we observed an increase in TUBB3 protein levels in Taxol-resistant RPE cells compared to control DMSO-treated cells (**Fig. 2A**), similar to what was observed previously in the A549-T24 non-small-cell lung cancer [16] and DU-145 prostate carcinoma cells [28]. We confirmed the specificity of the TUBB3 antibody by western blotting of cell lysates collected after siRNA-mediated knockdown of this protein (**Fig. 2A**). Continuous exposure of RPE cells to a dose of Taxol at which cell proliferation is not affected (up to 2 nM, **Fig. 1A** and **B**) did not affect the expression level of TUBB3 (**Fig. 2A**). Next, we conducted siRNA-mediated knockdown of β III-tubulin to assess its role in the resistance of the RPE-20 cell line. Two of our siRNAs targeting TUBB3 displayed strong anti-proliferative effects (**Sup. Fig. 1A**), but a third (siTUBB3 #9) achieved an equally efficient knock-down of TUBB3, without affecting cell proliferation, indicating that siRNAs #6 and #8 induce off-target effects, whereas #7 induces a relatively mild depletion. Using siTUBB3 #9, we achieved almost complete TUBB3 knockdown (Fig.

S1A), but the sensitivity of RPE-20 to Taxol was unchanged as assessed by viability assays (**Sup. Fig. 1B**). Hence, we conclude that β III-tubulin has no role in the Taxol-resistance of the RPE-20 cells.

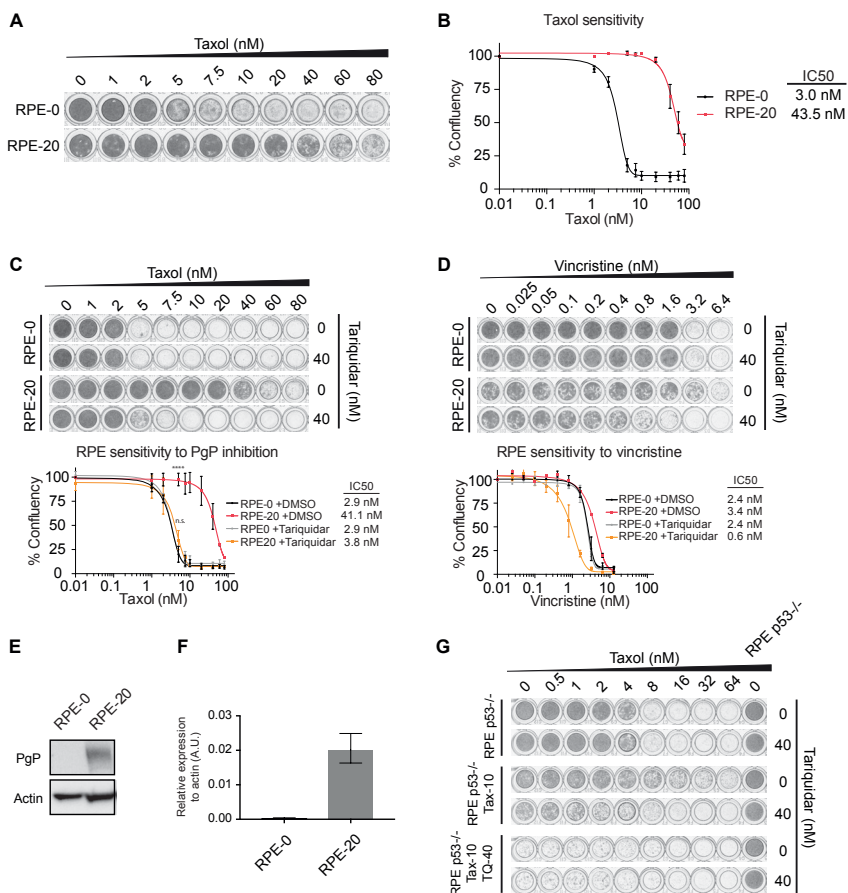


Figure 1. Taxol-resistance in RPE-20 is predominantly mediated through the up-regulation of the P-gp drug pump.

A) Crystal violet staining of viability assay with Taxol-naïve RPE-0 and resistant RPE-20 cell lines. **B)** Relative survival plots of the RPE-0 and RPE-20 cell lines. Shown are the average \pm s.d. of three independent experiments and the calculated IC₅₀. **C)** Relative survival plots of the same cell lines as in **A)** and **B)** in an increasing dose of Taxol and 0 and 40 nM of Tariquidar. ANOVA Turkey's multiple comparisons test. Graph shows mean \pm SEM. (****P<0.0001). **D)** Relative survival plots of RPE-0 and RPE-20 cells in an increasing dose of vincristine and 0 and 40 nM of Tariquidar. For all conditions, viability assays were carried out by growing ~1000 cells for 7 days. **E)** Western blot showing increased levels of P-gp in the Taxol-resistant RPE-20 cell line compared to RPE-0. **F)** P-gp mRNA levels were determined by qRT-PCR. Values were normalized to actin expression levels. Error bars are obtained from experimental triplicates. **G)** Relative survival plots with a drug-naïve RPE p53^{-/-}, a Taxol-resistant RPE p53^{-/-} (Tax-10), and a Taxol-resistant RPE p53^{-/-} cell line that was generated by a combined treatment with 40 nM of the P-gp inhibitor (Tax-10, TQ-40).

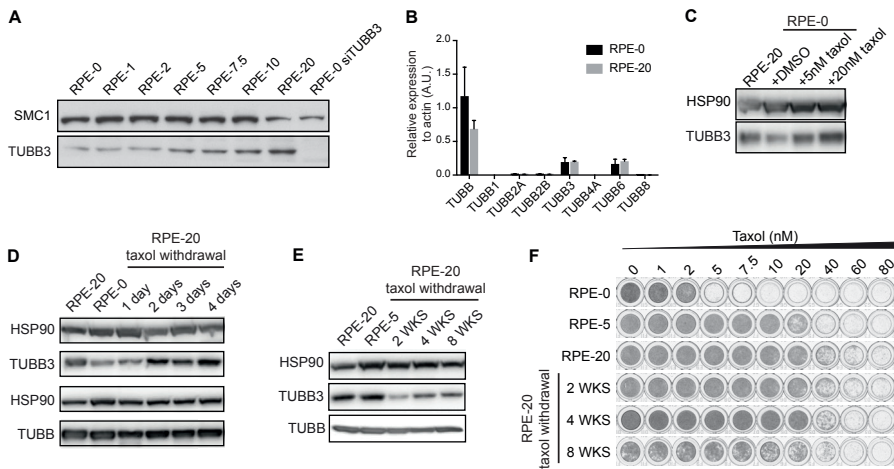


Figure 2. TUBB3 levels are dynamically regulated in RPE cells upon Taxol exposure and withdrawal.

A) Western blot showing TUBB3 levels in cell lysates prepared from Taxol-resistant RPE cells. Taxol-naïve RPE cells (RPE-0) exhibit low basal levels of TUBB3. Note that RPE-1 and RPE-2 indicate cell lines that have been continuously cultured in the presence of 1 and 2 nM of Taxol, respectively, while cell proliferation and viability of RPE cells was not visibly affected at these drug concentrations (see Fig. 1A)). The RPE-5, -7.5, -10, and -20 are cell lines derived from polyclonal selection of resistant cells that have survived Taxol treatment over a drug selection period of 4-6 weeks. **B)** β -tubulin isotypes mRNA levels were determined by qRT-PCR. Values were normalized to actin expression levels. Error bars are obtained from two independent experiments. **C)** Western blot showing the rapid induction of TUBB3 levels after a short-term, 30-hour treatment of RPE-0 cells with 5 and 20 nM of Taxol. **D)** Fluctuating TUBB3 levels immediately after Taxol withdrawal from the resistant RPE-20 cells and a further reduction of TUBB3 levels observed after up to 8 weeks of Taxol-withdrawal in **E)**. **F)** Viability assays were performed with the RPE-20 cells after different periods of Taxol withdrawal, corresponding to the time-points examined in **E)**.

Nonetheless, Taxol affected TUBB3 levels in a dose-dependent manner (**Fig. 2A**). In order to determine whether other β -tubulin isotypes were up- or down-regulated in RPE-20, we performed qRT-PCRs to examine the mRNA levels of other isotypes (**Fig. 2B**). Interestingly, we observed a similar expression profile in RPE-20 compared to RPE-0, indicating that the elevated levels of TUBB3 protein are not due to transcriptional up-regulation. We next performed Mass-spectrometry-based quantitative proteomics in RPE-20 to investigate the protein levels of various beta-tubulin isotypes (**Sup. Fig. 2A**). We find that expression of TUBB3 is most prominently increased, but also observe more modest increases in expression of TUBB4A/ β IV-tubulin and TUBB6/ β V-tubulin, whereas expression of TUBB/ β I-tubulin is somewhat decreased. This indicates that several beta-tubulin isotypes are stabilized in the Taxol-resistant RPE-20. However, given the primary role for P-gP

in the observed resistance (**Fig.1**), we can conclude that these changes have very limited effects on the overall response to Taxol.

To test whether TUBB3 overexpression is induced in other cell lines selected for Taxol-resistance, we generated Taxol-resistant cell lines derived from a colorectal carcinoma (HCT116), an osteosarcoma (U2OS), and two triple-negative breast cancer cell lines (Cal-51 and HCC1806). After polyclonal selection of Taxol-resistant cells, we obtained cell lines that could tolerate at least twice the dose of Taxol when compared to their parental counterparts (**Sup. Fig. 3A**). Next, we examined the levels of TUBB3 expression in these resistant cell lines and found no altered TUBB3 levels in the four Taxol resistant cancer cell lines relative to their respective parental cell lines (**Sup. Fig. 3B**). Thus, although some cell lines exhibit elevated levels of TUBB3 upon selection with Taxol, as was observed with the RPE-20 cell line in this study and a number of other cancer cell lines in other studies [16,28,29], this is by no means a phenomenon that occurs ubiquitously.

We further examined TUBB3 regulation after exposure of Taxol-naïve RPE cells to this drug for a short period of time. Surprisingly, we observed an increase of TUBB3 levels relative to control cells after 30 hours of Taxol at concentrations of 5 and 20 nM, respectively (**Fig. 2C**). Inversely, we observed a rapid reduction in TUBB3 abundance, to a level comparable to Taxol-naïve cells, after one day of removing Taxol from the culture medium of RPE-20 cells (**Fig. 2D**). A low level of TUBB3 was maintained after prolonged Taxol withdrawal of up to eight weeks (**Fig. 2E**). Relative survival plots conducted in parallel showed that while TUBB3 levels are reduced after Taxol withdrawal, cells remained as resistant to Taxol as the RPE-20 cells (**Fig. 2F**). These rapid and reversible changes in TUBB3 levels occurring after Taxol treatment of RPE cells (**Fig. 2C**), and considering that the mRNA levels in RPE-20 remain similar to RPE-0 (**Fig. 2B**), indicate that TUBB3 protein stabilization is dynamically regulated. This same trend could also happen with particular isotypes like TUBB, TUBB4A or TUBB6, but more work is required to resolve this. Altogether, this may indicate part of a more general cellular response to stress, analogous to TUBB3 up-regulation observed after exposure of cells to toxic microenvironments, such as hypoxia or nutrient deprivation [23,24].

Overexpression of TUBB3 in RPE cells plays a minor role in Taxol resistance

To further corroborate the notion that TUBB3 expression levels have a negligible effect on the sensitivity to spindle poisons like Taxol and vincristine, we introduced the SunTag-Cas9 (CRISPRa) system in RPE cells, which allows specific and robust transcriptional activation of genes of interest through sgRNA-Cas9-mediated targeting of synthetic transcriptional activators to upstream regions of transcriptional start sites (TSS) (**Fig. 3A**, [30,31]). Examination of the TUBB3 gene locus in the USCS genome browser (<https://genome.ucsc.edu/>) revealed the presence of two prominent histone3 lysine27 acetylation (H3K27Ac)-rich regions, a type of histone modification known as a marker of active gene regulation [32].

ABCB1 upregulation leads to Taxol resistance in cultured cells

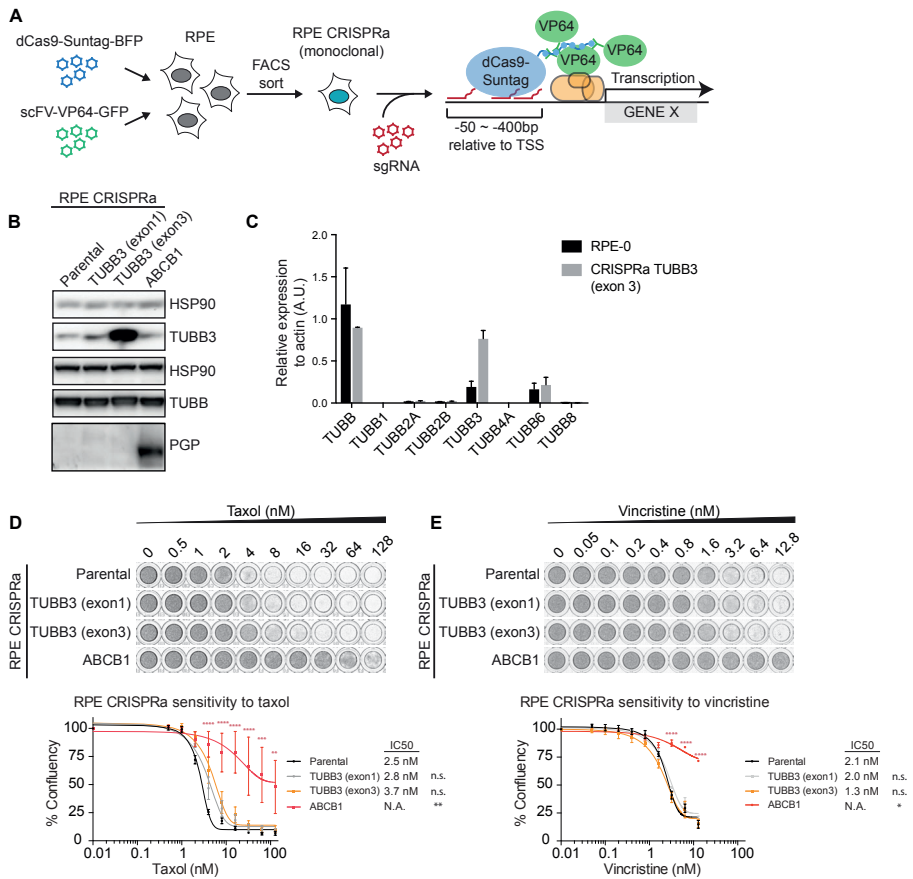


Figure 3. Overexpression of TUBB3 in RPE cells plays a minor role in Taxol resistance. **A)** Schematic depicting the procedure for generating CRISPRa cell lines. **B)** Western blots showing the expression levels of TUBB3 and P-gP after transduction of the CRISPRa cell lines with pools of sgRNAs targeted at putative enhancer regions of the respective genes. **C)** β -tubulin isotypes mRNA levels were determined by qRT-PCR. Values were normalized to actin expression levels. Error bars are obtained from two independent experiments. **D)** Relative survival plots of the TUBB3 and P-gP-overexpressing CRISPRa cell lines in increasing doses of Taxol and **E)** vincristine. ANOVA Turkey's multiple comparisons test. Graph shows mean \pm SEM. (**** $P < 0.0001$, *** $P < 0.001$, ** $P < 0.01$).

The first H3K27Ac-rich region is located upstream of exon 1 and a second region is flanked by exon 2 and 3 of the TUBB3 gene locus. This indicates the presence of an intragenic enhancer for the transcriptional regulation of TUBB3, aside of a conventional enhancer at the 5'-UTR. Thus, we decided to design two separate sets of sgRNA pools, each targeting one of the H3K27Ac-rich regions (Table 1). In addition to using this system for the transcriptional activation of TUBB3, we sought to generate a CRISPRa cell line for the activation of P-gP/ABCB1 as a positive control (Table 1). We packaged the three pools of sgRNAs (sgTUBB3 exon 1, sgTUBB3 exon

3, and sgABCB1) into separate lentiviral particles and transduced monoclonal RPE cells stably expressing CRISPRa (**Fig. 3A**).

By western blot analysis, we confirmed the specific induction of P-gP in the CRISPRa cell lines co-expressing sgRNAs targeted against ABCB1 (**Fig. 3B**). As expected, P-gP over-expression (RPE CRISPRa sgABCB1) promoted a significant level of drug resistance against Taxol (**Fig. 3D**) as well as vincristine (**Fig. 3E**). For TUBB3, we observed that the two distinct sgTUBB3 pools induced differential levels of TUBB3. While the expression of sgTUBB3 exon 1 induced a minor increase in TUBB3 protein levels, we achieved highly efficient over-expression of TUBB3 with the sgTUBB3 targeting upstream of exon 3 (**Fig. 3B**). This over-expression was also confirmed by qRT-PCR, where the CRISPRa showed a ~4-fold increase in TUBB3 mRNA levels (**Fig. 3C**). Although the overall β -tubulin levels were comparable between the parental and the TUBB3 over-expressing cells (**Fig. 3B**), none of the other β -tubulin isotypes were down-regulated or up-regulated at the mRNA levels (**Fig. 3C**). Furthermore, mass-spectrometry experiments performed with CRISPRa TUBB3 (exon 3) show that the TUBB3 protein is the only isotype that is upregulated in these cells (**Sup. Fig. 2B**). Interestingly, relative survival plots revealed that the sensitivity of the TUBB3 over-expressing cell lines to Taxol is very comparable to the parental cell line. The IC₅₀ of RPE CRISPRa cells expressing sgTUBB3 exon 1 was 2.8 nM, a 1.1-fold increase compared to parental cells (IC₅₀ of 2.5 nM), while those expressing sgTUBB3 exon 3 showed an IC₅₀ of 3.7 nM (1.5-fold) (**Fig. 3D**). Over-expression of TUBB3 also minimally altered the sensitivity of these cells to vincristine (**Fig. 3E**). We therefore conclude that induced overexpression of TUBB3 is unable to promote a clear Taxol resistance phenotype. Given the fact that we find that protein levels of none of the other detectable beta-tubulin isotypes change (**Sup. Fig. 2B**), it is also unlikely that different expression of other β -tubulin isotypes affects Taxol- resistance and sensitivity in CRISPRa TUBB3 cell lines.

Differential functional requirement for TUBB3 in breast cancer cell lines

Lastly, we set out to examine the functional relevance of TUBB3 overexpression in Taxol resistance in a panel of breast cancer cell lines. We determined Taxol sensitivity in 13 cell lines, most of which are triple negative breast cancer cells (**Fig. 4A**, [33]). The panel of cell lines comprised a maximum ~7-fold difference in Taxol sensitivity between the most and least sensitive cell lines, with an IC₅₀ of 0.7 nM up to 4.3 nM. Next, we examined TUBB3 levels and found relatively high expression of this protein in five of the cell lines (CAL120, BT549, HCC1395, HCC70, and HS578T), while TUBB3 was barely detectable in the remaining eight cell lines (**Fig. 4B**). Interestingly, despite the limited sample size, comparison of TUBB3 levels with IC₅₀ revealed a slight positive correlation ($R^2=0.06846$) between these two factors (**Sup. Fig. 54**). To test whether there is a functional role of TUBB3 in conferring these cells with decreased sensitivity to Taxol, we performed viability assays after TUBB3 depletion

ABC1 upregulation leads to Taxol resistance in cultured cells

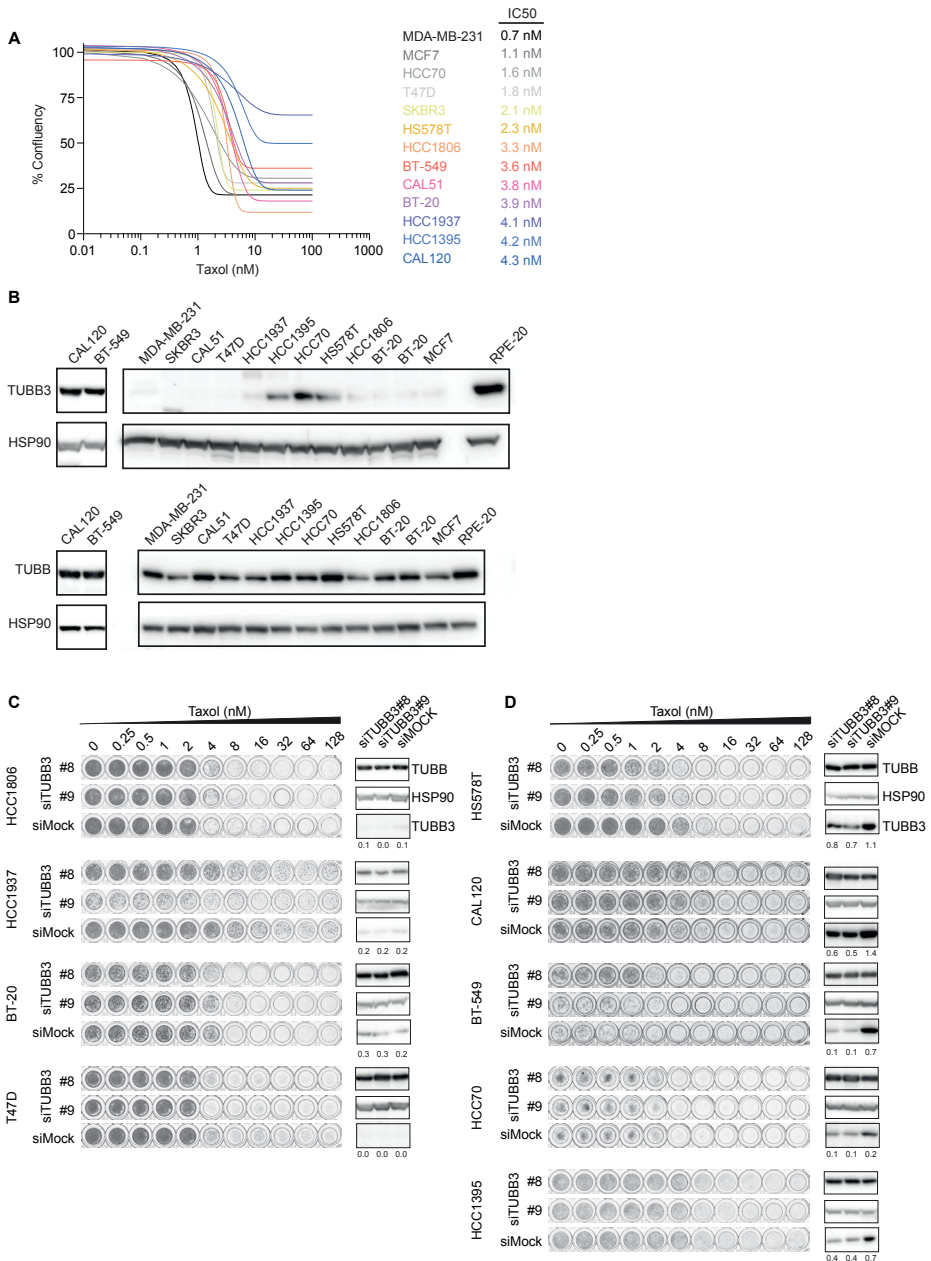


Figure 4. TUBB3 expression in breast cancer cell lines and Taxol sensitivity.

A) Sensitivity of breast cancer cell lines to Taxol determined by relative survival plots with increasing concentrations of Taxol for 7 days. Relative survival plots and IC50 were determined from at least three independent viability assays. For better visibility, the s.d. was excluded from this graph. **B)** Western blots showing the TUBB3 (top) and overall β -tubulin levels (bottom) in the breast cancer cell lines. **C)** Relative survival plots of four cell lines with low and **D)** five cell lines with high levels

of TUBB3 treated with different doses of Taxol for 7 days after knockdown of TUBB3. Cells were transfected with siRNA targeted against TUBB3 for 48 hours prior to re-plating them into new plates containing an increasing concentration of Taxol. Numbers below each TUBB3 blot indicate relative levels of TUBB3 normalized by loading controls.

using two independent siRNAs. As expected, in control cell lines with low or undetectable levels of TUBB3 (HCC1806, HCC1937, BT20, and T47D), Taxol sensitivity was unaffected after transfection of cells with siRNA targeted against TUBB3 as compared to Mock-depleted cells (**Fig. 4C**). Similarly, in four out of the five cell lines that had high levels of TUBB3 (CAL120, BT549, HCC70, and HCC1395), depletion of this protein did not sensitize the cells to Taxol (**Fig. 4D**). In one cell line (HS578T), we observed a minimal but consistent increase in Taxol sensitivity after depletion of TUBB3 with both siRNAs (**Fig. 4D**), but again the enhancement of Taxol sensitivity after TUBB3 depletion was minor. This suggests that TUBB3 overexpression has a very limited effect on sensitivity to Taxol in certain cell types. Nonetheless, this functional role of TUBB3 is not generally applicable, as Taxol treatment after TUBB3 depletion in the majority of cell lines tested has no significant effect on cell viability.

DISCUSSION

We have generated a number of Taxol-resistant cell lines in culture and examined changes in their β -tubulin isotypes expression levels compared to their parental counterparts, specially focusing on TUBB3. While we observed no induction in TUBB3 expression in multiple cancer cell lines, we did detect a prominent increase in TUBB3 protein levels in Taxol-resistant RPE cells. However, further analysis revealed that TUBB3 levels are dynamically regulated upon Taxol-treatment in Taxol-naïve RPE cells, and in response to Taxol-withdrawal from the resistant RPE-20 cells. This regulation occurred unrelated to the timing of acquisition of the Taxol-resistance phenotype. This observation makes it difficult to sustain the idea that deregulated TUBB3 overexpression is responsible for the acquisition of Taxol-resistance of RPE-20 cells. Rather, the induction of TUBB3 levels appears to occur as a cellular response, perhaps analogous to what has been observed after exposure of cells to other types of cellular stress [23,24]. Indeed, we find that the major mechanism of Taxol-resistance in the RPE-20 cells can be attributed to the activity of P-gP drug efflux pump, a factor that frequently contributes to multi-drug resistance in cell culture [26].

In order to determine whether other β -tubulin isotypes could play a role in Taxol resistance, we also assessed their expression levels in RPE-20. While we could not observe over-expression of any isotype at the transcriptional level, we found that TUBB3 protein was most prominently up-regulated, while expression of the TUBB4 and TUBB6 isotypes was slightly enhanced. On the other hand, TUBB levels appear

to be slightly down-regulated, perhaps to compensate the increase of the other isoforms. Although TUBB3 is the most described isoform to play a role in Taxol resistance, other β -tubulin classes, such as b-IV (TUBB4) and b-V (TUBB6) can also affect sensitivity to tubulin binding drugs [16,34,35]. While we focused our study in TUBB3 expression upon Taxol exposure and withdrawal, it would seem that the changes in TUBB4 and TUBB6 expression observed in the RPE-20 cells also have little effect on Taxol-sensitivity. Nonetheless, it would be interesting to test if mere expression of TUBB4 or TUBB6 at higher levels, like we did for TUBB3 using the CRISPRa-system, can affect the sensitivity to Taxol.

As an alternative approach for the direct functional assessment of TUBB3 in chemotherapy resistance, we have further established an RPE cell line that efficiently over-expresses TUBB3 from its endogenous locus by utilizing the CRISPRa technology. Interestingly, CRISPRa-mediated recruitment of the transcriptional machinery to both the 5'-UTR as well as to an intragenic region flanking exons 2 and 3 induces enhanced expression of TUBB3. Under hypoxic conditions, the recruitment of hypoxia-induced transcription factors HIF-1 α and HIF-2 α to an E-box motif located at the 3'-UTR of the TUBB3 locus induces TUBB3 expression [24]. Although additional experiments are needed to determine the function and regulation of these two new putative enhancer regions, our data indicate that additional mechanisms of TUBB3 transcriptional regulation, aside of regulation by HIFs at the 3'-UTR, are likely to exist. It remains an interesting question for the future to identify transcription factors that regulate these sites.

Importantly, we show that CRISPRa-mediated TUBB3 over-expression leads to a very limited change in Taxol sensitivity, which is in line with previous studies that failed to find a clear link between Taxol-sensitivity and TUBB3 expression levels [18,20,21]. Furthermore, the overexpression of TUBB3 confers cells with minimally, but consistently increased sensitivity to the MT-destabilizing drug vincristine. Overexpression of this particular β -tubulin isoform may alter MT dynamics to counteract the activity of MT-stabilizing agents, while synergizing with MT-destabilizers. This is in line with the observation that microtubules assembled from TUBB3 exhibit increased dynamicity compared to microtubules composed of other β -tubulin isoforms [36-38], and are more refractory to the suppressive effect of Taxol on MT dynamics in vitro [20]. However, in cells these changes have a very limited impact on the sensitivity to Taxol, insufficient to establish robust Taxol resistance. We also confirmed that other isoforms were not down-regulated as a result of the CRISPRa over-expression, thus, we can conclude that high expression of TUBB3 alone is not sufficient to affect the sensitivity to Taxol in RPE cell lines.

Finally, we have examined the functional significance of TUBB3 expression in several breast cancer cell lines that had inherently relatively high expression of this β -tubulin isoform. We find that RNAi-mediated depletion of TUBB3 induced a very minor shift in the sensitivity to Taxol in one out of five cell lines analyzed. This finding indicates that TUBB3 expression in breast cancer cell lines is certainly

not always linked to Taxol resistance. This is exemplified by our observation that TUBB3 levels are dynamically regulated in RPE cells upon short-term exposure of cells to Taxol. TUBB3 expression might be rapidly induced in certain cell types upon exposure to conditions of cellular stress. Whether TUBB3 has a functional role in such a stress response remains to be established. All in all, this study, together with previous ones, shows very limited effects of TUBB3 overexpression on the sensitivity to Taxol in cultured cell lines.

MATERIALS AND METHODS

Cell culture, transfection, and drug treatment

RPE-1, HCT-116, U2OS, CAL51, MDA-MB-231, MCF7, BT20, CAL-120, and SKBR-3 were grown in DMEM (Lonza, Basel, Switzerland), and HCC1937, HCC1187, HCC1806, HCC1395, T47D, BT-549, HCC70, and HS578T were grown in Gibco Advanced RPMI 1640 medium (Fisher Scientific) Supplemented with 6% fetal calf serum (Clontech, Mountain View, CA, USA), 50 µg/ml penicillin–streptomycin (Invitrogen, Waltham, MA, USA) and 2 mM L-glutamine (Lonza). RPE-11 was obtained from the American Type Culture Collection, and the breast cancer cell lines described in [42,43]. All cell lines were tested for mycoplasma contamination every three months. siRNA transfections were performed using RNAiMax (Invitrogen) in a reverse transfection protocol following the manufacturer's guidelines. TUBB3 siRNA OTP Human (siTUBB3#8: GCAACUACGUGGGCGACUC, siTUBB3#9: GAAGGAGUGUGAAAACUGC) was purchased from Thermo Scientific and used at a final concentration of 20 nM. Drugs were dissolved in DMSO and prepared at the following concentrations before usage at varying final concentrations as indicated in each Figure: Taxol at 100 µM, Vincristine at 1 mM, and Tariquidar at 100 µM.

Relative survival plots

Cells were plated on 96-well plates (BD Biosciences, Franklin Lakes, NJ, USA) at a starting density of ~1000 cells per well. Drugs were added the following day. On day 7, plates were fixed for 15 min with 96% methanol at -20 °C, stained with 0.1% crystal violet and washed with dH₂O. Dried plates were scanned and analyzed with ImageJ software (NIH, Bethesda, MD, USA). Cell survival graphs were prepared and IC50 calculations were performed using GraphPad Prism (La Jolla, CA, USA).

Immunoblot analysis

Cells were lysed in Laemmli buffer. Samples were separated by sodium dodecyl sulfate-polyacrylamide gel electrophoresis and transferred to nitrocellulose

membranes, blocked with 4% milk at room temperature, and incubated with primary antibodies at 4 °C overnight. The following antibodies were used: anti-TUBB (1:1000; TUB2.1, Sigma-Aldrich), anti-TUBB3 (1:500; TU-20, Millipore), anti-SMC1 (1:1000; A300-055A, Bethyl), anti-HSP90 (1:1000; H114, Santa Cruz), and anti-PGP (1:200; H-241, sc-8313). After incubation with secondary antibody (1:2000, DAKO) at room temperature for 1 hr, the membranes were developed with chemi-luminescence ECL reagent (Amersham, UK) and images were taken with the ChemiDoc XRS+ (Bio-Rad, Hercules, CA, USA). Images were processed and analyzed using ImageJ software (NHI, Bethesda, MD, USA).

Plasmids

sgRNA sequences for TUBB3 exon3 and ABCB1 were adapted from the genome-wide CRISPRa library [31]. sgRNA sequences for TUBB3 exon1 were selected from a -400 to -50 bp region upstream of the TUBB3 TSS using publically available CRISPR design tool (crispr.mit.edu). sgRNA oligos were cloned into a lentiviral vector (Lentiguide-Puro; Addgene#52963) using the BsmBI restriction site. sgRNA sequences are summarized in Supplementary table 1.

Generation of CRISPRa cell lines

RPE cells were co-transduced with viral particles containing SunTag-dCas9-BFP (Addgene# 60910) and scFV-VP69-GFP (Addgene# 60904). After two weeks of culturing, fluorescence activated cell sorting (FACS) was used to select for cells that were both BFP and GFP positive. Monoclonal CRISPRa cell lines were obtained, which were subsequently transduced with viral particles containing pools of sgRNAs targeted at enhancer regions of the ABCB1, TUBB3 exon1 or TUBB3 exon3 loci. Cells were selected for 2 weeks with puromycin to obtain stable polyclonal cell lines for the sgRNA expression.

RNA isolation and qRT-PCR analysis

Total RNA was extracted from RPE-0, RPE-20 and RPE-CRISPRa TUBB3 (exon3). RNA isolation was performed by using Qiagen RNeasy kit and quantified using NanoDrop (Thermo Fisher Scientific). cDNA was synthesized using superScript III reverse transcription, oligo dT (Promega), and 1000 ng of total RNA according to the manufacturer's protocol. Primers were designed with a melting temperature close to 60 degrees to generate 90–120-bp amplicons, mostly spanning introns. cDNA was amplified for 40 cycles on a cycler (model CFX96; Bio-Rad Laboratories) using SYBR Green PCR Master Mix (Applied Biosystems). Target cDNA levels were analyzed by the comparative cycle (Ct) method and values were normalized against

actin expression levels. qRT-PCR oligo sequences are summarized in supplementary table 2.

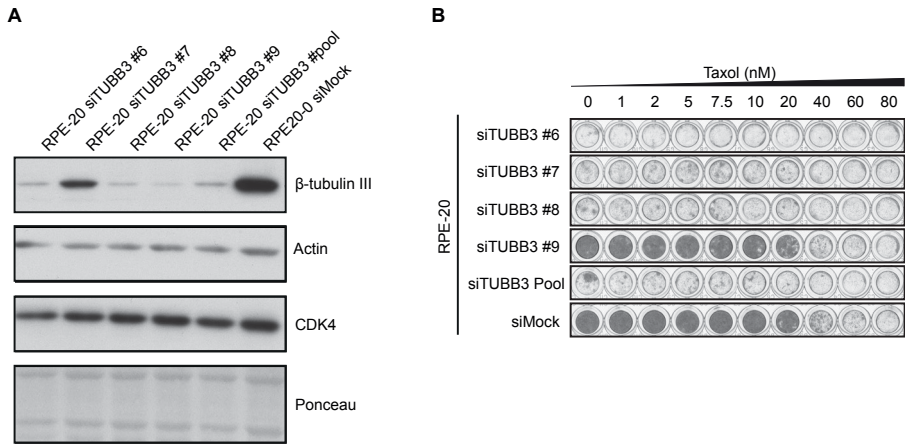
Mass spectrometry

Tubulin bands were excised from the coomassie stained gel, after which proteins were reduced with dithiothreitol and alkylated with iodoacetamide. Proteins were digested with trypsin (mass spec grade, Promega) overnight at 37°C and peptides were extracted with acetonitrile. Digests were dried in a vacuum centrifuge and reconstituted in 10% formic acid for MS analysis. Peptide mixtures (10% of total digest) were loaded directly on the analytical column and analyzed by nanoLC-MS/MS on an Orbitrap Fusion Tribrid mass spectrometer equipped with a Proxeon nLC1000 system (Thermo Scientific) as described previously [39]. Solvent A was 0.1% formic acid/water and solvent B was 0.1% formic acid/80% acetonitrile. Peptides were eluted from the analytical column at a constant flow of 250 nl/min in a 90-min gradient, containing a 74-min linear increase from 5% to 24% solvent B, followed by a 16-min wash at 80% solvent B.

Mass spectrometry data analysis

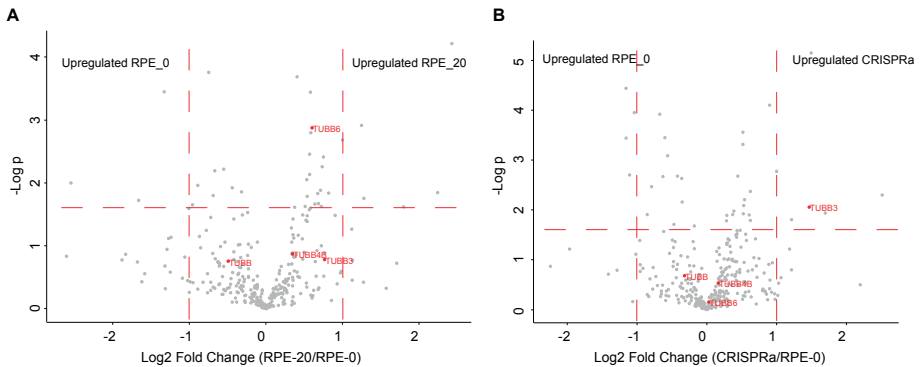
Raw data were analyzed by MaxQuant (version 1.5.8.3) [40] using standard settings for label-free quantitation (LFQ). MS/MS data were searched against the human Swissprot database (20,183 entries, release 2017_03) complemented with a list of common contaminants and concatenated with the reversed version of all sequences. Trypsin/P was chosen as cleavage specificity allowing two missed cleavages. Carbamidomethylation (C) was set as a fixed modification, while oxidation (M) was used as variable modification. LFQ intensities were Log₂-transformed in Perseus (version 1.5.5.3) [41], after which proteins were filtered for at least three valid values (out of 4 total). Missing values were replaced by imputation based a normal distribution using a width of 0.3 and a downshift of 1.8. Differentially expressed proteins were determined using a t-test (threshold: $P \leq 0.05$) and $[x/y] > 1$ | $[x/y] < -1$.

ABC11 upregulation leads to Taxol resistance in cultured cells



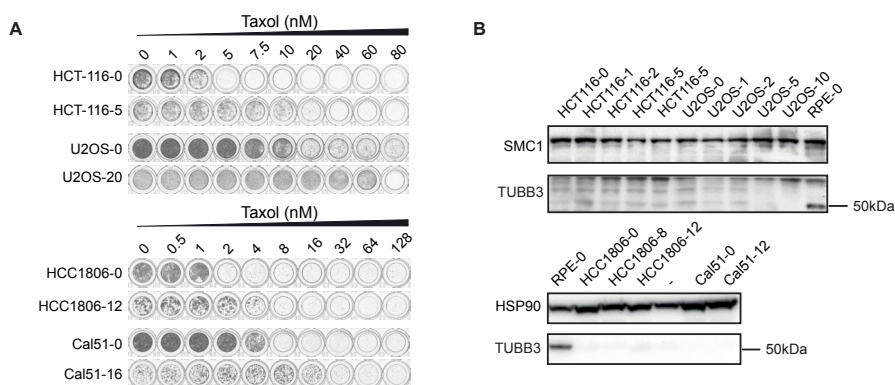
Supplementary Figure 1. β III-tubulin knockdown does not affect the sensitivity of RPE-20 to Taxol.

A) Western blot of RPE-20 cells transfected with single siRNAs targeted against TUBB3 for 48 hours. **B)** Relative survival plots of RPE-20 cells treated with different doses of Taxol for 7 days after knockdown of TUBB3 as described in **A**).



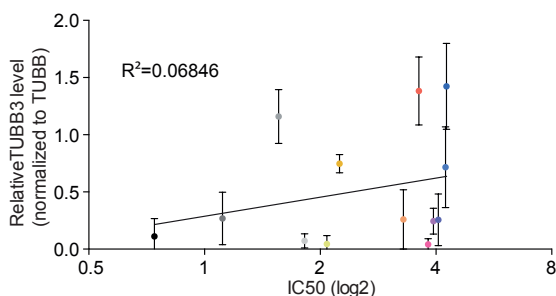
Supplementary Figure 2. Protein quantification of β -tubulin isotypes by mass spectrometry.

A volcano plot demonstrating magnitude of the protein comparisons between RPE-0 and RPE-20 in **A**) and RPE-0 and CRISPRa TUBB3 (exon 3) in **B**). The vertical axis indicates $-\log_{10}(p\text{-value})$. The horizontal axis indicates \log_2 fold change. The β -tubulin isotypes found are labeled in red. Data was obtained from two sample replicates.



Supplementary Figure 3. Induction of TUBB3 levels is not observed in multiple Taxol-resistant cancer cell lines.

A) Relative survival plots of Taxol-resistant cell lines derived from a colorectal carcinoma (HCT116), an osteosarcoma (U2OS), two triple-negative breast cancer cell lines (HCC1806 and Cal51), and their respective Taxol-sensitive parental cell lines. The values added behind the cell lines indicate the concentration of Taxol at which the resistant cell lines were grown in (e.g. HCT-116-5 indicates an HCT-116 cell line cultured continuously at 5 nM of Taxol). **B)** Whole cell lysates prepared from the parental and Taxol-resistant cancer cell lines showing their TUBB3 levels.



Supplementary Figure 4. Slight correlation between relative TUBB3 levels and IC50. The IC50 values were plotted against the relative TUBB3 levels determined for each breast cancer cell line. TUBB3 levels depicted here are averages from three independent experiments and normalized against whole β -tubulin levels.

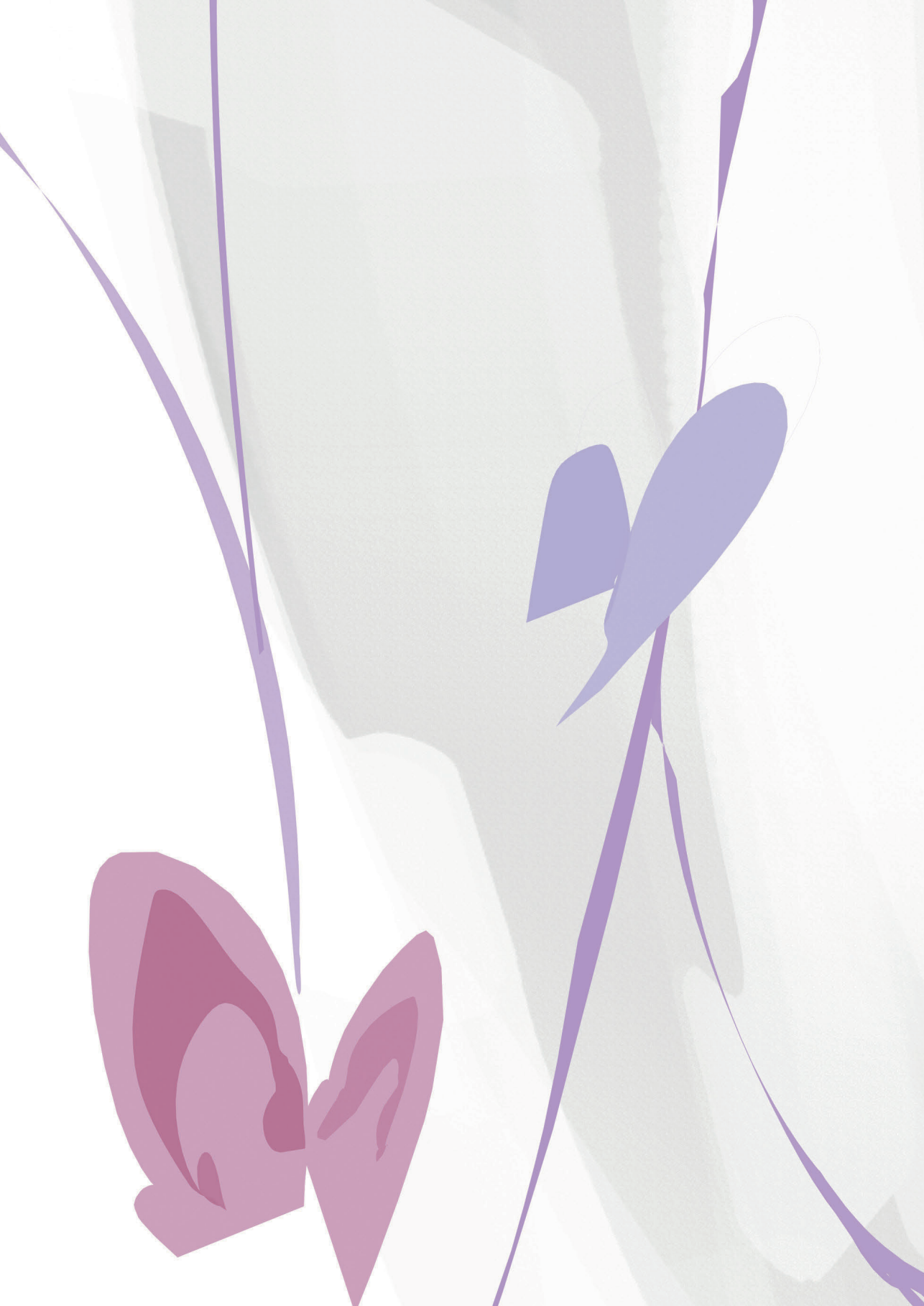
REFERENCES

- Walczak CE, Cai S, Khodjakov A. Mechanisms of chromosome behaviour during mitosis. *Nat Rev Mol Cell Biol.* 2010; 11: 91–102.
- Hanahan D, Weinberg RA. Hallmarks of Cancer: The Next Generation. *Cell.* 2011; 144: 646–674.
- Perez EA. Microtubule inhibitors: Differentiating tubulin-inhibiting agents based on mechanisms of action, clinical activity, and resistance. *Mol Cancer Ther.* 2009; 8: 2086–2095.
- Derry WB, Wilson L, Jordan MA. Substoichiometric Binding of Taxol suppresses Microtubule Dynamics. *Biochemistry.* 1995; 34: 2203–2211.
- Yvon AM, Wadsworth P, Jordan MA. Taxol suppresses dynamics of individual microtubules in living human tumor cells. *Mol Biol Cell.* 1999; 10: 947–959.
- Downing KH. Structural basis for the interaction of tubulin with proteins and drugs that affect microtubule dynamics. 2000; *Annu Rev Cell Dev Biol* 16: 89–111.
- Kavallaris M. Microtubules and resistance to tubulin-binding agents. *Nat Rev Cancer.* 2010; 10: 194–204.
- Luduena RF, Banerjee A (2008) The isotypes of tubulin: Distribution and functional significance. Humana Press.
- Janke C, Chloë Bulinski J. Post-translational regulation of the microtubule cytoskeleton: mechanisms and functions. *Nat Rev Mol Cell Biol.* 2011; 12: 773–786.
- Garnham CP, Roll-Mecak A. The chemical complexity of cellular microtubules: tubulin post-translational modification enzymes and their roles in tuning microtubule functions. *Cytoskeleton (Hoboken).* 2012; 69: 442–463.
- Verhey KJ, Gaertig J. The tubulin code. *Cell Cycle.* 2007; 6: 2152–2160.
- Sirajuddin M, Rice LM, Vale RD. Regulation of microtubule motors by tubulin isotypes and post-translational modifications. *Nature Cell Biology.* 2014; 16: 335–344
- Mariani M, Karki R, Spennato M, Pandya D, He S, Andreoli M, Fiedler P, Ferlini C. Class III β -tubulin in normal and cancer tissues. *Gene.* 2015; 563: 109–114.
- Sève P, Dumontet C. Is class III β -tubulin a predictive factor in patients receiving tubulin-binding agents? *The Lancet Oncology.* 2008; 9: 168–175.
- McCarroll JA, Sharbeen G, Liu J, Youkhana J, Goldstein D, McCarthy N, Limbri LF, Dischl D, Ceyhan GO, Erkan M, et al. β III-tubulin: a novel mediator of chemoresistance and metastases in pancreatic cancer. *Oncotarget.* 2015; 6: 2235–2249.
- Kavallaris M, Burkhart CA, Horwitz SB. Antisense oligonucleotides to class III β -tubulin sensitize drug-resistant cells to Taxol. *British Journal of Cancer.* 1999; 80: 1020–1025.
- Kavallaris M, Kuo DY, Burkhart CA, Regl DL, Norris MD, Haber M, Horwitz SB. Taxol-resistant epithelial ovarian tumors are associated with altered expression of specific beta-tubulin isotypes. *J Clin Invest.* 1997; 100: 1282–1293.
- Hari M, Yang H, Zeng C, Canizales M, Cabral F. Expression of class III beta-tubulin reduces microtubule assembly and confers resistance to paclitaxel. *Cell Motil Cytoskeleton.* 2003; 56: 45–56.
- Stengel C, Newman SP, Leese MP, Potter BVL, Reed MJ, Purohit A. Class III beta-tubulin expression and in vitro resistance to microtubule targeting agents. *British Journal of Cancer.* 2009; 102: 316–324.
- Derry WB, Wilson L, Khan IA, Luduena RF, Jordan MA. Taxol differentially modulates the dynamics of microtubules assembled from unfractionated and purified beta-tubulin isotypes. *Biochemistry.* 1997; 36: 3554–3562.
- Kamath K, Wilson L, Cabral F, Jordan MA. BetaIII-tubulin induces paclitaxel resistance in association with reduced effects on microtubule dynamic instability. *Journal of Biological Chemistry.* 2005; 280: 12902–12907.
- Gan PP, Pasquier E, Kavallaris M. Class III beta-tubulin mediates sensitivity to chemotherapeutic drugs in non small cell lung cancer. *Cancer Research.* 2007; 67: 9356–9363.
- Raspaglio G, De Maria I, Filippetti F, Martinelli E, Zannoni GF, Prislei S, Ferrandina G, Shahabi S, Scambia G, Ferlini C. HuR regulates beta-tubulin isotype expression in ovarian cancer. *Cancer Research.* 2010; 70: 5891–5900.
- Raspaglio G, Filippetti F, Prislei S, Penci R, De Maria I, Cicchillitti L, Mozzetti S, Scambia G, Ferlini C. Hypoxia induces class III beta-tubulin gene expression by HIF-1 α binding to its 3' flanking region. *Gene.* 2008; 409: 100–108.
- Karki R, Mariani M, Andreoli M, He S, Scambia G, Shahabi S, Ferlini C. β III-Tubulin: biomarker of taxane resistance or drug target? *Expert Opin Ther Targets.* 2013; 17: 461–472.
- Gottesman MM, Fojo T, Bates SE. Multidrug resistance in cancer: role of ATP-dependent transporters. *Nat Rev Cancer.* 2002; 2: 48–58.
- Mistry P, Stewart AJ, Dangerfield W, Okiji S, Liddle C, Bootle D, Plumb JA, Templeton D, Charlton P. In vitro and in vivo reversal of P-glycoprotein-mediated multidrug resistance by a novel potent modulator, XR9576. *Cancer Research.* 2001; 61: 749–758.
- Ranganathan S, Benetatos CA, Colarusso PJ, Dexter DW, Hudes GR. Altered beta-tubulin isotype expression in paclitaxel-resistant human prostate carcinoma cells. *British Journal of Cancer.* 1998; 77: 562–566.
- Liu B. Taxotere resistance in SUIT Taxotere resistance in pancreatic carcinoma cell line SUIT 2 and its sublines. *World Journal of Gastroenterology.* 2001; 7: 855.
- Tanenbaum ME, Gilbert LA, Qi LS, Weissman JS, Vale RD. A Protein-Tagging System for Signal Amplification in Gene Expression and Fluorescence Imaging. *Cell.* 2014; 159: 635–646.

31. Gilbert LA, Horlbeck MA, Adamson B, Villalta JE, Chen Y, Whitehead EH, Guimaraes C, Panning B, Ploegh HL, Bassik MC, et al. Genome-Scale CRISPR-Mediated Control of Gene Repression and Activation. *Cell*. 2014; 159: 647–661.
32. ENCODE Project Consortium. An integrated encyclopedia of DNA elements in the human genome. *Nature*. 2012; 489: 57–74.
33. Lehmann BD, Bauer JA, Chen X, Sanders ME, Chakravarthy AB, Shyr Y, Pietersen JA. Identification of human triple-negative breast cancer subtypes and preclinical models for selection of targeted therapies. *J Clin Invest*. 2011; 121: 2750–2767.
34. Orr GA, Verdier-Pinard P, McDaid H, Horwitz SB. Mechanisms of Taxol resistance related to microtubules. *Oncogene*. 2003; 22: 7280–7295.
35. Leandro-García LJ, Leskelä S, Landa I, Montero-Conde C, López-Jiménez E, Letón R, Cascón A, Robledo M, Rodríguez-Antona C. Tumoral and tissue-specific expression of the major human beta-tubulin isotypes. *Cytoskeleton (Hoboken)*. 2010; 67: 214–223.
36. Panda D, Miller HP, Banerjee A, Luduena RF, Wilson L. Microtubule Dynamics in-Vitro Are Regulated by the Tubulin Isotype Composition. *Proc Natl Acad Sci USA*. 1994; 91: 11358–11362.
37. Lu Q, Luduena RF. In vitro analysis of microtubule assembly of isotypically pure tubulin dimers. Intrinsic differences in the assembly properties of alpha beta II, alpha beta III, and alpha beta IV tubulin dimers in the absence of microtubule-associated proteins. *Journal of Biological Chemistry*. 1994; 269: 2041–2047.
38. Banerjee A, Roach MC, Trcka J, Luduena RF. Increased microtubule assembly in bovine brain tubulin lacking the type III isotype of beta-tubulin. *Journal of Biological Chemistry*. 1990; 265: 1794–1799.
39. Ameziane N, May P, Haitjema A, van de Vrugt HJ, van Rossum-Fikkert SE, Ristic D, Williams GJ, Balk J, Rockx D, Li H, et al. A novel Fanconi anaemia subtype associated with a dominant-negative mutation in RAD51. *Nature Communications*. 2015; 6: 8829.
40. Cox J, Hein MY, Luber CA, Paron I, Nagaraj N, Mann M. Accurate proteome-wide label-free quantification by delayed normalization and maximal peptide ratio extraction, termed MaxLFQ. *Mol Cell Proteomics*. 2014; 13: 2513–2526.
41. Tyanova S, Temu T, Sinitcyn P, Carlson A, Hein MY, Geiger T, Mann M, Cox J. The Perseus computational platform for comprehensive analysis of (prote)omics data. *Nat Meth*. 2016; 13: 731–740.
42. Korkmaz G, Lopes R, Ugalde AP, Nevedomskaya E, Han R, Myacheva K, Zwart W, Elkon R, Agami R. Functional genetic screens for enhancer elements in the human genome using CRISPR-Cas9. *Nature Biotechnology*. 2016; 34: 192–198.
43. Berns K, Sonnenblick A, Gennissen A, Brohée S, Hijmans EM, Evers B, Fumagalli D, Desmedt C, Loibl S, Denkert C, et al. Loss of ARID1A Activates ANXA1, which Serves as a Predictive Biomarker for Trastuzumab Resistance. *Clin Cancer Res*. 2016; 22: 5238–5248.

ABCB1 upregulation leads to Taxol resistance in cultured cells

2



3

Perturbations in 3D genome organization can promote acquired drug resistance

Anna G Manjón, Daniel Peric-Hupkes, Ning Qing Liu, Anoeek Friskes, Stacey Joosten, Hans Teunissen, Marleen Aarts, Stefan Prekovic, Wilbert Zwart, Elzo de Wit, Bas van Steensel, René H Medema

Manuscript under review

ABSTRACT

Acquired drug resistance is a major problem in the treatment of cancer. hTERT-immortalized, untransformed RPE-1 (RPE) cells can acquire resistance to Taxol by derepressing the *ABCB1* gene, encoding for the multidrug transporter P-gP. Here we have investigated how the *ABCB1* gene is derepressed. We show that activation of the *ABCB1* gene is associated with reduced DNA methylation, reduced H3K9 trimethylation and increased H3K27 acetylation at the *ABCB1* promoter. In addition, we find that the *ABCB1* locus has moved away from the nuclear lamina in the Taxol-resistant cells. This raises the question which of these alterations were causal to derepression. Directly modifying DNA methylation or H3K27 methylation had neither significant effect on *ABCB1* expression, nor did it promote drug resistance. In contrast, the disruption of Lamin B Receptor (LBR), a component of the nuclear lamina involved in genome organization, did promote the acquisition of a Taxol-resistant phenotype in a subset of cells. Using CRISPRa-mediated gene activation, we could further substantiate a model in which disruption of lamina association renders the *ABCB1* gene permissive to derepression. Based on these data we propose a model in which nuclear lamina dissociation of a repressed gene allows for its activation, implying that deregulation of the 3D genome topology could play an important role in tumor evolution and the acquisition of drug resistance.

INTRODUCTION

Chemotherapy, is one of the main pillars of cancer treatment. However, chemotherapeutic drugs loose efficacy over time due to acquired drug resistance^{1,2}. This acquired drug resistance can be the result of genetic mutations, as exemplified by mutations in receptor tyrosine kinases that causes resistance to tyrosine kinase inhibitors^{3,4}. Alternatively, drug resistance can arise through elevated gene expression of the drug target itself, or by altered expression of proteins involved in drug metabolism⁵. The cause of this altered gene expression can be a genetic mutation or amplification of one of its upstream regulators, but changes in gene expression can also be due to epigenetic changes^{6,7}. Well known examples of these, are changes in DNA methylation that result in altered gene expression in cancer⁸. How exactly these changes are induced during the evolution of drug resistance is currently unclear.

Here we have investigated the process of gene activation in the evolution of drug resistance in non-transformed immortalized human cells in culture. We have used derepression of the *ABCB1* gene as our model system to study gene regulation and acquired drug resistance.

Extensive research has shown that the *ABCB1* gene (also known as multidrug resistance gene or MDR) encoding the P-glycoprotein (P-gP) drug-efflux pump, is upregulated in many cancers cells exposed to increasing doses of Taxol and a variety of other chemotherapeutic drugs^{9,10}. The contribution of P-gP to Taxol resistance in patients is still debatable, with the possible exception of ovarian cancer, where it has been shown that Taxol resistance correlates with increased *ABCB1* expression¹¹. In this same tumor type, *ABCB1* has been found fused with active promoters in Taxol resistant samples^{12,13}.

Prior studies have investigated the mechanisms of the *ABCB1* upregulation in cellular systems, and found that DNA-copy number amplifications of *ABCB1* locus can be linked to acquired chemoresistance¹⁴. Additionally, recent studies have shown that epigenetic alterations can also drive the upregulation of *ABCB1*. Particularly, several studies in Taxol-resistant cancer cell lines demonstrated that loss of repressive marks of heterochromatin, such as DNA methylation, in the regulatory region was associated with active transcription of the *ABCB1* gene¹⁵⁻¹⁸.

Although prior reports suggest a role for the methylation status in *ABCB1* regulation, the influence of the higher-order chromatin structure on gene expression and drug resistance is not yet understood. In general, alterations in chromatin organization have been correlated to changes in gene expression¹⁹⁻²³, and consequently, dysregulation of these may influence the functionality of the genome, leading to pathogenesis. It is well understood that the three-dimensional genome is maintained by a multilayer of structural units like chromosome territories, nuclear compartments, Topological Associating Domains (TADs) and Lamina Associated Domains (LADs). While chromosome compartments are proposed to be mediated

by Condensin II and phase separation, TADs are often defined by CTCF and the cohesin complex²⁴⁻²⁶.

Several investigations have found alterations of the 3D genome involving TAD perturbations in cancer²⁶⁻²⁸ as well as in autoimmune diseases and limb malformations^{29,30}. Furthermore, a recent study reported genomic CTCF-binding site mutations in 200 patient samples of colorectal cancer³¹. In addition to genomic organization in TADs, in the cell nuclei extensive chromatin regions are associated with the Nuclear Lamina (NL), which are mostly transcriptionally repressed^{32,33}. This raises the question whether the NL could act as a repressive element for genes. Recent studies in *Drosophila* suggest that depletion of NL components alters gene expression of several chromatin regions, leading to defective cell differentiation³⁴⁻³⁶. However, in the context of drug resistance, it has not yet been examined whether 3D genome disorganization and detachment from the NL could be a potential mechanism of gene reactivation and consequently chemoresistance.

In order to explore novel mechanisms of gene re-activation and Taxol resistance, we generated Taxol-resistant cell lines derived from hTERT-immortalized, untransformed RPE-1 (RPE) cells. Consistent with our previous work³⁷, we find that these cells become resistant to Taxol through re-activation of the *ABCB1* gene. In Taxol-sensitive cells, *ABCB1* is located in a LAD together with other inactive genes. We show that modifying chromatin marks by drug inhibition of DNA and histone-methyltransferase enzymes does not have a significant effect on the *ABCB1* expression. In addition to the observed changes in chromatin modifications, we observe important changes of the 3D genome topology when comparing the Taxol-sensitive versus the Taxol-resistant lines, particularly in the NL interactions. Furthermore, the disruption of LBR, a NL component, is able to de-repress the locus leading to a Taxol-resistant phenotype. Therefore, this research provides a new understanding, from a high-order chromatin perspective, of how cells may gain resistance to chemotherapeutics such as Taxol.

RESULTS

Transcriptional activation of *ABCB1* drives Taxol resistance in RPE-TxR

In order to gain more insight in the processes that can lead to acquired drug resistance, we explored the molecular mechanism underlying *ABCB1* upregulation in the context of chemotherapy resistance. We made use of a previously described Taxol-resistant cell line derived from hTERT-immortalized, untransformed RPE-1 cells obtained after prolonged exposure to increasing doses of Taxol (RPE-Taxol Resistant, RPE-TxR)³⁷. The generated cell line can proliferate under a Taxol concentration 20-fold higher than the parental RPE-1 (RPE-Taxol Sensitive, RPE-TxS) (**Fig. 1A and B**). Inhibition of the drug efflux pump P-gP by Tariquidar showed a re-sensitization of the RPE-TxR, indicating that P-gP mediates resistance to Taxol in this cell line (**Fig. 1A**

and B)³⁷. We independently generated new Taxol-resistant RPE cell lines (TxR-3 and TxR-4) and confirmed that P-gP expression also conferred Taxol resistance in these lines (**Sup. Fig. 1A-B**). To interrogate whether enhanced P-gP protein expression was due to transcriptional activation of the *ABCB1* gene, we performed RT-qPCR analysis and observed that the mRNA level of *ABCB1* was increased in all of our clones (**Fig. 1C, Sup. Fig. 1C**). In addition, single-molecule RNA FISH (smRNA FISH) revealed an increased number of active *ABCB1* Transcription Sites (TS) in RPE-TxR compared to RPE-TxS (**Fig. 1D and E**). Taken together, we corroborate in three independently generated cell populations that the major mechanism underlying acquired Taxol resistance in RPE-1 cells is through transcriptional activation of the *ABCB1* gene.

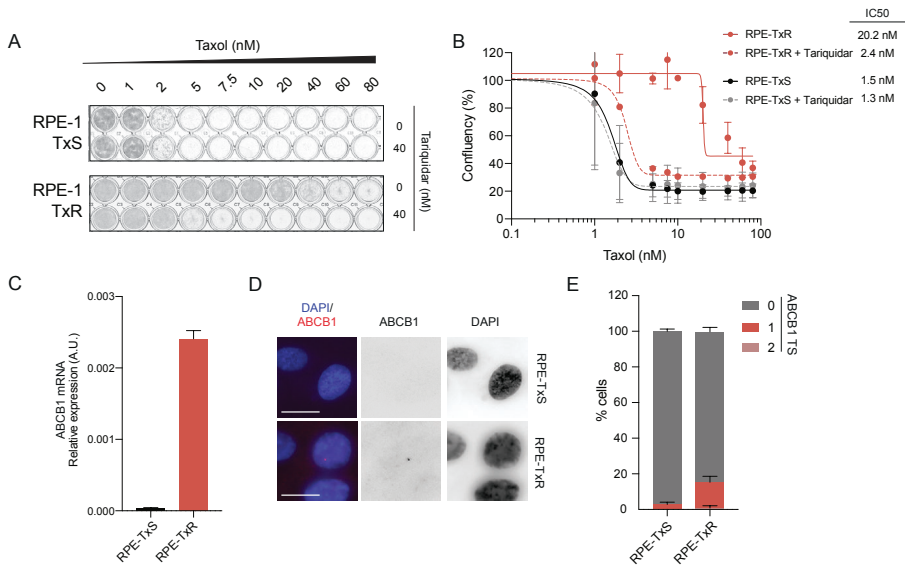


Figure 1 – Transcriptional activation of ABCB1 drives Taxol resistance in RPE-TxR

A) Crystal violet staining of viability assay on Taxol-naïve RPE-TxS and resistant RPE-TxR cell lines. **B)** Relative survival plots of the RPE-TxS and RPE-TxR cell lines. Error bars show the average \pm s.d. of two independent experiments and the calculated IC₅₀. The curve was drawn from the log(inhibitor) vs response equation $Y = \text{Bottom} + (\text{Top} - \text{Bottom}) / (1 + 10^{-(X - \text{LogIC}_{50})})$. **C)** ABCB1 mRNA levels determined by qRT-PCR and normalized to GAPDH expression levels, n=2. Error bars show the SD. **D)** Representative smRNA-FISH images of RPE-TxS and RPE-TxR for the ABCB1 gene and DAPI. The images are projections of 0.5 μm sections and a total 5 μm in thickness. Scale bar, 15 μm . **E)** Quantification of the number of ABCB1 transcription sites (TS) found per cell, n=2, 60 cells per condition.

ABCB1 gene activation in RPE-TxR is associated with changes in chromatin modifications and DNA contacts at the ABCB1 locus

In order to understand the mechanism of upregulation of *ABCB1* in RPE-TxR cells, we first aimed to investigate whether *ABCB1* expression is accompanied by changes in chromatin modifications at the *ABCB1* locus. To this end, we analyzed histone marks and DNA methylation patterns by Chromatin and Methylated Immunoprecipitation (Ch-IP and MeDIP). We found that RPE-TxR lost repressive modifications (H3K9me3 and DNA methylation) and gained active marks (H3K27ac and H2AZ) in the promoter region of the *ABCB1* gene (**Fig. 2A**), compared to RPE-TxS. Hi-C analysis demonstrated that *ABCB1* is found in a TAD together with two other genes, *ABCB4* and *RUNDC3B* (**Sup. Fig. 2A**). Interestingly, RNA-sequencing experiments showed, in addition to the 7-fold increase in the *ABCB1* mRNA levels, an upregulation of *ABCB4* and *RUNDC3B* in RPE-TxR (**Sup. Fig. 2B**). The same was seen in the additional independently generated RPE-1-derived Taxol-resistant cell lines (TxR-3 and TxR-4) (**Sup. Fig. 2C-D**). Because changes in gene regulation are often associated with local changes in chromosome folding³⁸, we performed Targeted Locus Amplification (TLA) in RPE-TxS and RPE-TxR. This strategy allows to selectively amplify and sequence DNA on the basis of the crosslinking of physically proximal sequences similarly to 4C-seq³⁹. We identified changes in chromatin contacts of the *ABCB1* locus in RPE-TxR compared to RPE-TxS (**Fig. 2B**). In RPE-TxS, *ABCB1* preferentially interacts with regions enriched for H3K9me3 and low for H3K36me3, associated with heterochromatin and transcriptionally active regions respectively^{40,41} (**Fig. 2B**). However, in RPE-TxR, contacts also occurred in less enriched H3K9me3 domains. Moreover, new interactions with the promoters of the transcribed genes *SLC25A40*, *CROT*, *DMTF1* and *TMEM243* were observed, marked by H3K36me3 and H3K4me3 (**Fig. 2B, Sup. Fig. 2E**). These new interactions were also enriched on H3K4me1, an enhancer-associated mark⁴², suggesting that the *ABCB1* gene could potentially be activated by proximal enhancers. Therefore, we conclude that chromatin marks undergo major changes at the *ABCB1* locus during the acquisition of Taxol-resistance. This is also the case for *ABCB1* DNA interactions, suggesting that genes are more likely to interact with regions with similar chromatin nature.

ABCB1 gene activation in RPE-TxR is associated with detachment from the NL

As gene silencing has been linked to association with the Nuclear Lamina (NL)⁴³, we also performed Lamin-DamID to study the *ABCB1*-NL interactions. We observed that in RPE-TxS, that the DamID signal intensity of the *ABCB1* locus is very high (**Fig. 2C**, blue line), indicating that it is in a lamina-associated domain (LAD). In contrast, in RPE-TxR cells the DamID signal intensity is greatly reduced (**Fig. 2C**, red line), indicating that a major NL detachment of the region containing *ABCB1* and its neighboring has taken place during the acquisition of drug resistance.

Perturbations in 3D genome organization can promote acquired drug resistance

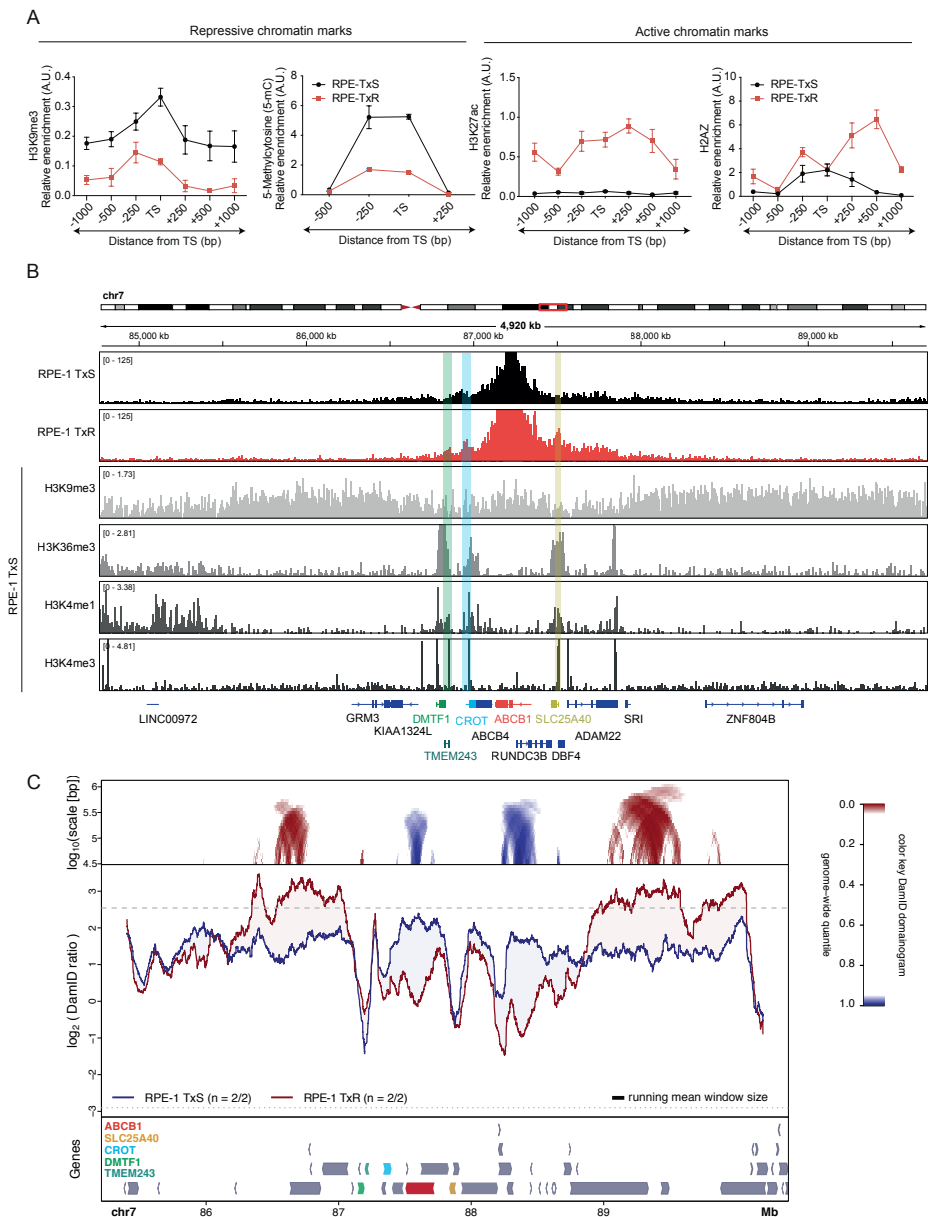


Figure 2 – ABCB1 gene activation in RPE-TxR is associated with changes in chromatin modifications and 3D genome

A) ChIP-qPCR of indicated chromatin and DNA methylation marks in the ABCB1 regulatory region for RPE-TxS and RPE-TxR. TS marks the transcription start site of the promoter. ChIP signal was normalized over input and a positive control specific for each mark, n=2. **B)** TLA analysis of the ABCB1 gene in RPE-TxS (first row) and RPE-TxR (second row), (gene annotation hg19). Sequencing expanding 5000kb shows that regions immediately neighboring the ABCB1 gene have higher

coverage. 3rd to 6th rows: ChIP-sequencing tracks of indicated histone modifications in RPE-TxS cells expanding 5000kb from the *ABCB1* gene (gene annotation hg19). Color lines show new contacts formed in RPE-TxR with the indicated colored genes. **C)** Change is NL interactions of *ABCB1* and flanking regions in RPE-TxR compared to RPE-TxS. Bottom panel: gene annotation track (hg38) with indicated colored genes. Middle panel: DamID tracks of NL interactions in RPE-TxS (blue line) and RPE-TxR cells (red line). Data are the average of 2 independent replicates. Noise was Suppressed by a running mean filter of indicated window size. Shading between the lines corresponds to the color of the sample with the highest value. Dotted lines mark the 5th and 95th percentiles of genome-wide DamID values. Top panel: domainograms; for every window of indicated size (vertical axis) and centered on a genomic position (horizontal axis), the pixel shade indicates the ranking of the change in DamID score (experimental minus control) in this window compared to the genome-wide changes in DamID scores across all possible windows of the same size. Blue: DamID score is highest in control samples; red: DamID score is highest in experimental samples.

Interestingly, *SLC25A40*, *CROT*, *DMTF1* and *TMEM243* are also found detached from the NL in RPE-TxS, suggesting that when *ABCB1* loses its interaction with the NL, it tends to interact with other inter-LAD (iLAD) genes, consistent with our TLA analysis (**Fig. 2B**). In addition to this, we could also observe a possibly 'compensatory' movement of the regions further from the *ABCB1* locus, which increased NL contacts in the Taxol-resistant cell lines (**Fig. 2C**, red line). Interestingly, this phenomena has been previously reported in other loci⁴⁴. Overall, these results indicate that a local rewiring of NL interactions occur in the *ABCB1* genomic region in the RPE-1 Taxol resistant cells.

Transition to Taxol-resistance is not primarily driven by repressive chromatin modifications of *ABCB1* genomic locus

In order to test whether altering the chromatin modifications of the *ABCB1* locus is sufficient to de-repress *ABCB1* in RPE-TxS, we made use of different drugs to perturb the epigenetic landscape. The addition of 5-aza deoxycytidine (5-AZA) for 24h was able to reduce the levels of DNMT1, the enzyme responsible for DNA methylation deposition (**Fig. 3A**). A similar trend for the levels of H3k27-trimethylation occurred when treating cells with GSK126 (EZH2 inhibitor), that interferes with H3K27me3 deposition (**Fig. 3A**). Under these treatments, we performed RT-qPCR in RPE-TxS to check *ABCB1* expression levels. We observed that both drugs were unable to induce transcription of the *ABCB1* gene (**Fig. 3B**). Thus, altering the levels of the H3K27-methyltransferase EZH2 or the DNA methyltransferase DNMT1 is not sufficient to derepress the *ABCB1* gene.

We next asked if altering H3K27-trimethylation or DNA methylation at the *ABCB1* promotor is sufficient to precondition the locus for derepression. To this end, we performed colony formation assays using a combination of the epigenetic drugs and Taxol. For the chromatin drugs we determined a dose that did not induce a proliferation defect (**Sup. Fig. 3A-B**). We pre-treated RPE-TxS cells with DNMT1i or

EZH2i for 24h followed by an over-night co-treatment with 20nM Taxol. Next morning the epigenetic drugs were washed out and only 20nM Taxol was present for 15 days. Neither the DNMT1 nor EZH2 inhibitor were able to increase the number of Taxol-resistant colonies (**Fig.3C-D**). In fact, DNMT1i in combination with Taxol led to a decrease in Taxol-resistant colonies compared to the DMSO control (**Fig.3C-D**). To boost the drug efficacy, we treated RPE-TxS cells for 72h with a higher dose of DNMT1i and maintained the same EZH2i dose. In addition, we included the H3k9me2 methyltransferase G9a inhibitor BIX01294. We observed a protein decrease on DNMT1, H3K27me3 and H3k9me2 when treating cells with DNMT1i, EZH2i and G9ai respectively or in combination (**Sup. Fig. 3C**). Moreover, an overall increase of the active mark H3k27ac and a decrease of the repressive mark H3k9me2 was detected by immunofluorescence in the cell nucleus (**Sup. Fig. 3D-E**). However, *ABCB1* mRNA levels quantified by qPCR remained similar to the DMSO-treated condition (**Sup. Fig. 3F**). Therefore, these data suggest that the disruption of chromatin-modifying enzymes by drug inhibition is unable to trigger activation of *ABCB1* gene transcription in RPE-1 cells, and thereby remain Taxol-sensitive.

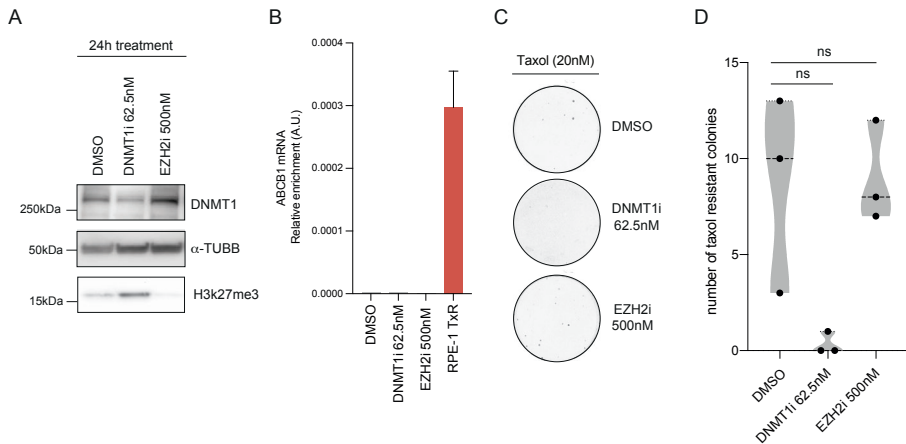


Figure 3 – Transition to Taxol-resistance is not primarily driven by repressive chromatin modifications of *ABCB1* genomic locus

A) Western Blot showing the levels of the chromatin proteins and controls (α -TUBB) upon treatment with the indicated epigenetic drugs with for 24h. **B)** *ABCB1* mRNA levels determined by qRT-PCR and normalized to GAPDH expression levels upon drug addition and RPE-TxR as a control for *ABCB1* expression, $n=2$. Error bars show the SD. **C)** Crystal violet staining of colony formation assay under 20nM of Taxol and the corresponding chromatin drug in RPE-1 iCut WT cells. **D)** Quantification of the number of Taxol resistant colonies from B. Black dots show an independent biological replicate. ns, $p>0,05$, Mann-Whitney test.

We next investigated whether potential upregulation of transcription factors (TFs) in RPE-TxR cells could be responsible for initiation of *ABCB1* gene expression, and

thereby change local chromatin modifications and 3D genome organization at the *ABCB1* locus. We first performed motif scan to identify the potential TFs binding to the promoters of the two *ABCB1* isoforms. Subsequently, we hypothesized that gain of Taxol resistance may be caused by aberrant expression of some of these TF interactors, and therefore we identified all the differentially expressed TF binders of the two promoters in RPE-TxR compared to RPE-TxS using mRNA sequencing (**Sup. Fig. 4A**). To further narrow down our searching, we speculated that the TFs responsible for the *ABCB1* derepression may potentially play an activation role for other upregulated genes in the resistant cells. Hence, we also performed a motif analysis for the promoters of all the upregulated genes in RPE-TxR in order to identify general promoter activators in the resistant cell line. We mainly found significantly enriched motifs belonging to the POU and LHX TF homeodomain family (**Sup. Fig. 4B-C**). This implies that these TFs may potentially be involved in the upregulation of many genes on the RPE-TxR cell lines, including *ABCB1*. To test this, we overexpressed *POU3F2*, *LHX6* and *ZIC5*, which showed a clear upregulation in the resistant cells (**Sup. Fig. 4A**), in the Taxol sensitive parental RPE cells. To that aim, we used the Cas9-VP64-transcription activation system (CRISPRa) to assess whether this would recapitulate *ABCB1* activation in the resistant cell line. Even though we observed by RT-qPCR a significant increase of mRNA expression of the three TFs, similar to the level of upregulation in RPE-TxR (**Sup. Fig. 4D**), this did not result in a Taxol-resistant phenotype (**Sup. Fig. 4E-F**). More importantly, downregulation of these TFs in RPE-TxR did not perturb the Taxol-resistant phenotype (**Sup. Fig. 4 G-I**), clearly indicating that *POU3F2*, *LHX6* and *ZIC5* are not required for expression of the *ABCB1* gene in RPE-TxR cells.

***ABCB1* upregulation in RPE-TxR is not caused by direct activation of the promoter by trans-acting factors**

We next wondered whether RPE-TxR cells upregulated additional TF that could lead to the activation of the *ABCB1* promoter. Therefore, to further exclude TF activation as the initial trigger for *ABCB1* gene activation, we carried out a luciferase reporter assay to assess the *ABCB1* promoter activity in RPE-1 Taxol-sensitive (TxS) and Taxol-resistant (TxR3-4) cells. To this end, the *ABCB1* promoter was cloned in a pGL3-basic vector followed by transfection into RPE-TxS or RPE-TxR. If similar luciferase activity was observed between cell lines, that would indicate that there are not differentially expressed trans-acting factors that lead to *ABCB1* promoter activation. However, if there is an increase of luciferase activity in RPE-TxR, a trans-acting factor may be upregulated therefore inducing *ABCB1* promoter activation. Activity of the *ABCB1* promoter was relatively low compared to the pGL3-promoter plasmid, but more importantly, we did not observe an increase of luciferase activity in Taxol-resistant cells compared to Taxol-sensitive (**Sup. Fig. 5A**). This suggests that RPE-1 TxR cells do not have a distinct transcriptional program or differentially expressed TFs which

could activate the *ABCB1* promoter. Instead, the 3D genome topology may be the determining factor for the *ABCB1* expression. Therefore, we hypothesized that NL detachment observed in RPE-TxR potentially could be a first step towards acquired drug resistance, subsequently allowing recruitment of available TFs leading to transcription activation of the *ABCB1* gene.

To further support the impact of NL in the regulation of *ABCB1*, we measured the *ABCB1* transcription levels in its native chromatin environment and outside of this context. We obtained these data from myelogenous leukemia K562 cells³². We used *GRO-cap* (global run-on sequencing with 5'cap selection) data as a measure of nascent RNA in native chromatin context. In order to detect transcription outside the chromatin context we used the plasmid-based assay *SuRE* (Survey of Regulatory Elements)⁴⁵. *ABCB1* exhibited a low *GRO-cap* activity and higher *SuRE* signal, suggesting that it is repressed by its native chromatin environment but can be activated when transcription activators have access to the regulatory region (**Sup. Fig. 5B**). All together, these results suggest that in RPE-1 WT cells, *ABCB1* is located in a repressive chromatin environment but has the ability to activate transcription if removed from this context.

LBR depletion facilitates acquisition of Taxol resistance

To further understand the importance of NL components in *ABCB1* gene expression we generated different knock-outs (KOs) of NL proteins using CRISPR-Cas9 technology in RPE-1 Cas9 cells (RPE-1 iCut)⁴⁶. We obtained a high cutting efficiency of the Lamin B Receptor (*LBR*) gene in a polyclonal cell population (**Fig. 4A**). Moreover, we could confirm by western blotting that *LBR* was depleted effectively (**Fig. 4B**). 7 days after the KO generation we performed colony formation assays using 20nM of Taxol. Upon *LBR* depletion, we observed an increase in the number of Taxol-resistant colonies in multiple independent experiments (**Fig. 4C-D**). Interestingly, the *ABCB1* mRNA levels were not increased in the polyclonal population (**Sup. Fig. 6A**). This implies that the loss of *LBR* can facilitate derepression of the *ABCB1* gene when cells are exposed to Taxol. Clearly, loss of *LBR* alone is not sufficient for full derepression of the *ABCB1* gene, because we find that only a fraction of cells in the population acquires Taxol-resistance. Moreover, the absolute number of Taxol-resistant colonies we obtained varied from experiment to experiment, suggesting the importance of other factors in activating the *ABCB1* gene. Nevertheless, the number of Taxol-resistant clones is significantly higher in *LBR* knock-out cells than what we observe in the parental lines. Complete depletion of Lamin B1 (*LMNB1*) or Lamin A/C (*LMNA*), structural and supporting components of the NL, had no obvious effect on Taxol resistance (**Sup. Fig. 6B-E**).

In order to investigate whether depletion of *LBR* induced *ABCB1* upregulation in other *in vitro* models, we performed RNA interference experiments in various cancer cell

lines. We selected a Triple Negative breast cancer (TNBC) cell line (MDA-MB-231), a head-and-neck squamous cell carcinoma (FaDu) and a lung adenocarcinoma cell line (A549). Using RT-qPCR analysis we found that MDA-MB-231 and FaDu had slightly higher *ABCB1* mRNA levels than RPE-1 cells. In contrast, the *ABCB1* mRNA levels detected in A549 were considerably increased (**Sup. Fig. 6F**). Depletion of *LBR* by siRNA led to a decrease of *LBR* protein levels 48h post-transfection in all cell lines (**Sup. Fig. 6G**). After 48h, colony formation assays under different concentrations of Taxol for each of the cell lines were performed. As control, we confirmed that depletion of *LBR* by siRNA led to an increase in number of Taxol-resistant colonies in RPE-1 cells (**Sup. Fig. 6H-I**). As expected, based on the high level of *ABCB1* expression, A549 cells were resistant to high levels of Taxol, and depletion of *LBR* had minimal effects (Sup. Fig. 6H-I). The effect of *LBR* depletion in MDA-MB-231 also resulted in increased numbers of Taxol-resistant colonies, similar to what we observe in RPE-1 cells (**Sup. Fig. 6H-I**). *LBR* depletion in FaDu cells resulted in a decrease of Taxol-resistant colonies (**Sup. Fig. 6H-I**). These data imply that loss of *LBR* can prime *ABCB1* for derepression in some cells, but additional factors are required to achieve derepression.

To explore the reorganization of the LAD landscape that takes place upon *LBR* depletion we performed Lamin-DamID in the polyclonal RPE-1 *LBR* KO cells. Overall, the LAD landscape of the parental RPE-1 cells was largely retained in the *LBR* KO cells, and only a subset of LADs was clearly altered. Detachment of the *ABCB1* locus from the NL was not detected in this polyclonal population, but a decrease on NL interactions was seen the neighboring regions (**Fig. 4E**, bottom panel). This change could destabilize the NL interactions of the locus and render the *ABCB1* locus more permissive for derepression. Alternatively, the effect of *LBR* depletion on NL interactions is not uniform across the entire population, causing the *ABCB1* locus to detach from the NL in a small subset of cells only. Finally, it is also possible that loss of *LBR* does not change the contacts of *ABCB1* with the NL, but instead causes a reduced repressive potential of the NL. In support of the latter model, *LBR* was previously found to interact with the repressive protein HP1.^{47,48} Based on these data we propose that in RPE-1 cells, and possibly across various other *in vitro* models, *LBR* may act as a regulator of the *ABCB1* gene expression and its depletion can contribute to acquired Taxol resistance. Additionally, these data suggest that NL-association may act as a critical threshold that needs to be overcome in order to derepress a gene, and as such loss of lamina-association might be a first step in the process of transcriptional derepression.

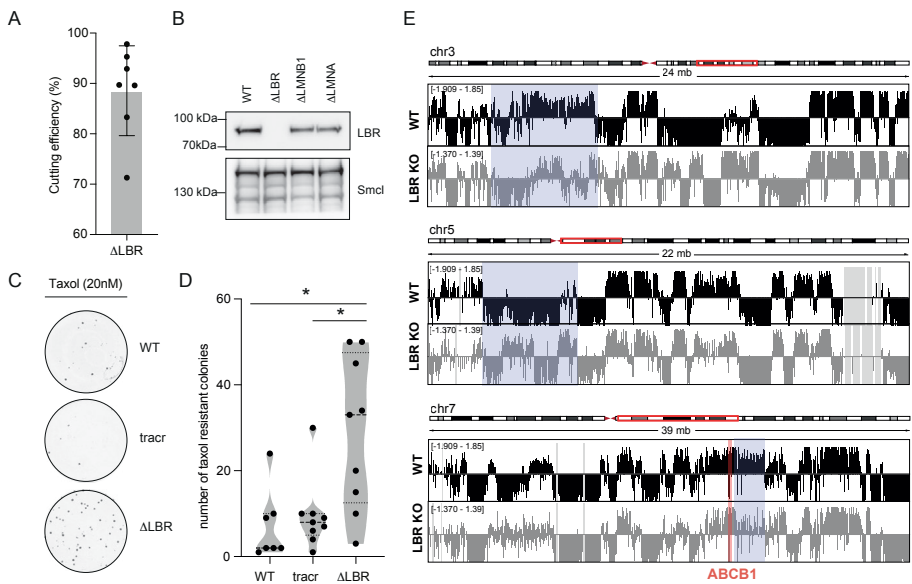


Figure 4 – LBR depletion facilitates acquisition of Taxol resistance

A) Percentage of disrupted sequence (cutting efficiency) in RPE-1 iCut cells transfected with crRNAs targeting the LBR gene and using TIDE analysis. Black dots show an independent biological replicate. Error bars show the SD. **B)** Western Blot showing the levels of LBR and control (SMC1) proteins 7 days after transfection of LBR, LMNA or LMNB1 crRNAs. **C)** Crystal violet staining of colony formation assay under 20nM of Taxol in RPE-1 iCut WT cells, transfected with only tracrRNA or tracrRNA and crRNA-LBR. **D)** Quantification of the number of Taxol resistant colonies under 20nM of Taxol in crRNA-LBR compared to WT and tracr only. Black dots show an independent biological replicate, *p<0,05, Mann-Whitney test. **E)** Change is NL interactions in LBR KO compared to RPE-TxS (WT) analyzed by DamID. Positive values indicate NL interactions, negative values indicate NL detachment. Three regions of the genome are shown. Blue: differences observed between WT and LBR KO. Red: ABCB1 genomic region.

Transcription-driven CRISPRa activation of neighboring genes can detach ABCB1 from the NL and lead to Taxol resistance

To further explore the role of NL in ABCB1 regulation, we examined whether NL detachment would lead to ABCB1 gene activation. It has been previously described that the CRISPRa induces detachment of genes from the NL, and in some instances this also causes detachment of flanking genes⁴⁴. We therefore attempted to detach ABCB1 from the NL by activation of its neighboring genes. We used CRISPRa to specifically activate the promoter of *ABCB1*, *ABCB4* or *RUNDC3B* or a combination of the latter two (**Fig. 5A**). Next, we performed Lamin-DamID to map NL interactions (**Fig. 5B-C**, **Sup. Fig. 7A-B**). We observed that in control cells, *ABCB1* is located at the NL, together with the *ABCB4* and *RUNDC3B* genes (**Fig. 5A-B**, **Sup. Fig. 7A-B**, blue lines). As expected and showed in previous research⁴⁴, upon CRISPRa single

gene activation local NL detachment was detected in the regulatory regions and most of the transcription units of these genes (**Sup. Fig. 7A-B**, red line). Strikingly, simultaneous activation of *ABCB4* and *RUNDC3B* caused not only detachment of these two genes, but also of *ABCB1* (**Fig. 5C**, red line). Next, we asked whether this was accompanied by upregulation of *ABCB1* expression. We observed that transcription activation of *ABCB1* by CRISPRa led to an expected increase of mRNA of *ABCB1* (**Fig. 5D**). Surprisingly, activating *ABCB4*, *RUNDC3B* or the combination via CRISPRa also triggered the activation of *ABCB1* (**Fig. 5D**, **Sup. Fig. 7C**), and was accompanied by an increase in occurrence of Taxol-resistant colonies (**Fig. 5E**, **Sup. Fig. 7D-G**). We next performed ChIP-qPCRs on the *ABCB1* regulatory region and observed a decrease in the H3K9me3 signal in both CRISPRa-*ABCB1* and CRISPRa *ABCB4-RUNDC3B* compared to the CRISPRa parental cell line (**Fig. 5F**, left). However, even though CRISPRa-*ABCB1* presented an enrichment of H3k27ac in the *ABCB1* promoter, the combination of *ABCB4* and *RUNDC3B* did not show this (**Fig. 5F**, right). To rule out the possibility that the *ABCB1* transcription initiation by *ABCB4* and *RUNDC3B* was a consequence of cross-activation of the *ABCB1* promoter, instead of a NL-detachment effect, we generated new sgRNAs targeting upstream and downstream of the *ABCB1* regulatory regions (**Sup. Fig. 7H**). We could confirm that these sgRNAs, even though in the same TAD as *ABCB1*, could not initiate transcriptional activation, as shown by RT-qPCR (**Sup. Fig. 7I**). Therefore, we could conclude that *ABCB1* transcription is linked to loss of H3K9me3 and NL detachment potentially caused by activation of *ABCB4* and *RUNDC3B* and not due to cross-activation of the sgRNAs.

DISCUSSION

In this study we describe a novel mechanism by which cells can upregulate *ABCB1*, a gene involved in Taxol resistance. Our data provide the first direct link between 3D genome reorganization and drug resistance. We have shown that Taxol resistance of RPE-TxR cells can be entirely attributed to the activity of the P-gP drug efflux pump³⁷. In RPE-TxR, *ABCB1*, the gene encoding for P-gP, is upregulated through transcriptional activation. This transcriptional activation coincides with an enrichment of active histone marks and a depletion of repressive marks in the chromatin environment of the *ABCB1* promoter. However, directly altering the chromatin landscape in RPE-TxS cells by drug inhibition of chromatin regulators did not lead to initiation of *ABCB1* expression. In addition to the altered chromatin modifications in the promoter region, we noted a clear detachment of the *ABCB1* locus from the NL in the Taxol-resistant cells. In conjunction with that, disruption of the *LBR*, a key NL protein, led to enhanced acquisition of drug-resistance, implying that NL detachment can prime the *ABCB1* locus for gene activation.

Perturbations in 3D genome organization can promote acquired drug resistance

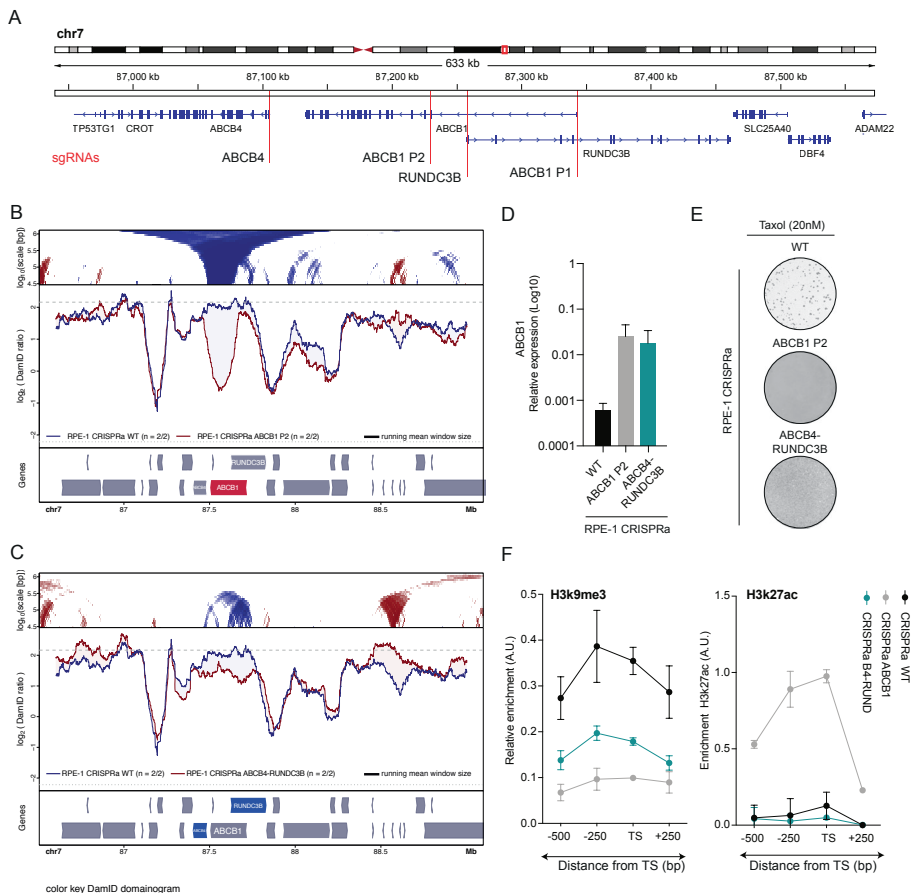


Figure 5 – Transcription-driven CRISPRa activation of neighboring genes can detach ABCB1 from the NL and lead to Taxol resistance

A) Schematic representation of the Chr7q21.12 region indicating the locations where the sgRNAs were targeting for CRISPRa ABCB1, ABCB4 or RUNDC3B activation. Two regions were independently targeted to upregulate ABCB1: P1 (proximal promoter, 6 sgRNA were used) and P2 (internal promoter, a single sgRNA was used). B) Local NL detachment caused by ABCB1 gene activation by CRISPRa in RPE-1 cells. C) Local NL detachment caused by simultaneously ABCB4 and RUNDC3B gene activation by CRISPRa in RPE-1 cells. D) ABCB1 mRNA levels determined by qRT-PCR and normalized to GAPDH upon CRISPRa activation of ABCB1 (P2) or combination of ABCB4 and RUNDC3B, n=2. Error bars show the SD. E) Crystal violet staining of viability assay on CRISPRa cell lines upon activation of ABCB1 (P2) and the combination of ABCB4 and RUNDC3B. F) ChIP-qPCR of H3K9me3 (left) and H3K27ac (right) in the ABCB1 regulatory region for CRISPRa WT, ABCB1 or the combination of ABCB4 and RUNDC3B (B4-RUND). TS marks the Transcription Start Site of the promoter. ChIP signal was normalized over input and a positive control specific for each mark, n=2.

Role of histone modifications and DNA methylation in the ABCB1 locus

ABCB1 gene regulation is thought to be driven by DNA methylation⁴⁹. Some studies have shown that low DNA methylation status of the *ABCB1* promoter is linked to gene activation^{15,16}. However, other studies were unable to confirm these findings^{17,18}. Here we show that there is a switch from inactive to active chromatin in the *ABCB1* promoter in RPE-TxR cells, as well as a change in DNA methylation pattern. Depletion of the DNA methyltransferase DNMT1 in RPE-TxS cells did not directly alter *ABCB1* gene expression or Taxol sensitivity. The same was observed when inhibiting the H3K27 methyltransferase EZH2, suggesting that the active chromatin environment observed in the *ABCB1* promoter region in RPE-TxR cells may be secondary to gene activation during the process of transcriptional derepression.

How depletion of LBR may de-repress ABCB1

Studies in *Drosophila* have found that depletion of lamins can lead to de-repression of NL-associated genes^{35,50}. Here, we found that *ABCB1* is partially activated upon depletion of LBR but not lamins. We speculate that depletion of *LBR* may lead to leaky *ABCB1* gene expression in at least two different ways. In one model, loss of *LBR* may cause stochastic detachment of *ABCB1* from the NL. In mouse and human cells LBR has been implicated in anchoring heterochromatin to the NL⁵¹⁻⁵³. In our study, the frequency of heterochromatin detachment after LBR depletion may be too low to be detectable by DamID. However, if stable contact with the NL is essential for robust repression of *ABCB1*, then occasional detachment could account for the stochastic occurrence of Taxol-resistant clones in *LBR*-depleted cells. Indeed, NL interactions can be intrinsically stochastic, and the NL contact frequency is inversely linked to gene expression^{54,55}. This may explain why only a small proportion of cells acquires Taxol resistance. In a second model, depletion of *LBR* may not affect the *ABCB1* – NL contact frequency, but rather may compromise the repressive potential of the NL. *LBR* may play a direct role in this repression, e.g. through its interaction with HP1⁴⁷, or indirectly by controlling the protein composition of the NL. This partially defective repression in *LBR*-depleted cells could then allow for emergence of Taxol-resistant clones. In both models, interactions of *ABCB1* with the NL contribute to its repression.

Forced detachment of ABCB1 from the NL coincides with gene activation

The generation of CRISPRa cell lines targeting *ABCB4* and *RUNDC3B* allowed for detachment of *ABCB1* from the NL, and we find that this is associated with *ABCB1* gene activation. This further suggests a causal effect between NL detachment and *ABCB1* gene activation. However, we cannot fully rule out that the activated *ABCB4* and *RUNDC3B* promoters act as enhancers of the nearby *ABCB1* promoter, because enhancer activity has been observed for many promoters⁵⁶. Interestingly, a decrease

Perturbations in 3D genome organization can promote acquired drug resistance

of gene expression has previously been observed by tethering chromosomes to the nuclear periphery⁵⁷⁻⁵⁹. Interestingly, recent research has shown that intrinsic features of promoters influence their sensitivity to the repressive LAD environment³². According to this study, *ABCB1* promoter is classified as repressed in K562 cells and thereby to have the potential to be activated if taken out from their native repressive LAD environment.

Celltype-specific roles of LBR and lamins

We find that depletion of *LBR*, but not Lamin A/C, or B, can render the *ABCB1* locus permissive to gene activation. In another study, Lamin A/C together with *LBR* were shown to be involved in tethering heterochromatin to the nuclear periphery during development⁵³. Interestingly, a recent study shows that loss of Lamin B1 leads to detachment of LADs together with global chromatin re-distribution and de-compaction, supporting the idea that NL have a role in chromatin dynamics and potentially in gene regulation⁶¹. Our results show that only *LBR* depletion has a positive effect on the induction of Taxol resistance in RPE-1 cells. This could be because in differentiated cells, NL components may have different relevance on gene repression. Certainly, *LBR* may have celltype-specific effects, as we observed with the depletion of *LBR* in the various cancer cell lines.

Taken together, we propose that acquisition of Taxol resistance in RPE-1 cells requires detachment of the *ABCB1* locus from the nuclear lamina as a priming event. When this priming event is followed by gene activation, this could induce changes to the local chromatin state that might help to keep the locus detached from the NL. Whether lamina detachment is the most critical step in the derepression of an inactive gene likely depends on the contribution of lamina-association in the regulation of gene expression of a given gene. One could envision that 3D genome rearrangements are an important priming step in the activation of a gene that is tightly associated to the NL, while activation of a TF is more likely to be the crucial event for activation of genes that display are more relaxed lamina-association.

MATERIALS AND METHODS

Cell lines and cell culture conditions

hTert-immortalized retinal pigment epithelium (RPE-1) and derived cell lines were maintained in DMEM/F-12 + Glutamax (Gibco, Life Technology) Supplemented with 1% penicillin/streptomycin and 6% fetal bovine serum (FBS, S-FBS-EU-015, Serana). A549 cancer cell lines were grown in Advanced RPMI 1640 (Gibco, Life Technology) Supplemented with 1% penicillin/streptomycin, 1% sodium pyruvate, 2% HEPES buffer and 10% fetal bovine serum. MDA-MB-231 and FADU cell lines were maintained in DMEM (Gibco, Life Technology) Supplemented with 1% penicillin/

streptomycin, 1% sodium pyruvate, 2% HEPES buffer and 10% fetal bovine serum. All cell lines were routinely checked for mycoplasma.

Drug treatments

Drugs were dissolved in DMSO and prepared at stock concentrations before usage at varying final concentrations as indicated in each Figure. For the 24h assay, cells were treated for 24h with the specific epigenetic drug dose, adding 20nM of Taxol overnight followed by a wash out of the drugs and subsequently addition of 20nM Taxol again for 15 days. For the epigenetic drug treatment combination (Combo), 250nM of 5-Aza-2'-deoxycytidine, 150nM of GSK126 and 2mM of BIX-01294 were used.

Luciferase Assay

The *ABCB1* promoter was cloned in a pGL3-basic (Promega) vector (pGL3-Basic Vector GenBank® Accession Number U47295). The *ABCB1* internal promoter region (1kb) was PCR amplified from RPE-1 genomic DNA and inserted downstream of the luciferase reporter gene. The primers used were: gatcAAGCTTCATTAGCCAAATGCATGAGC (FWD) and GATCGGTACCTGGAAACATCCTCAGACTATGC (REV). pGL3-promoter (Promega) vector (pGL3-Promoter Vector GenBank® Accession Number U47298) was used as a control to assess transfection efficiency. For transfection of the pGL3 vectors, 2 million RPE-1 cells (TxS, TxR.3 or TxR.4) were resuspended in nucleofection buffer (Solution I and II 4:1). Solution I (125 mM Na₂HPO₄, 12.5 mM KCl, pH 7.75) Solution II (55 mM MgCl₂). After co-transfection of 100ng of Renilla plasmid (pRL-SV40 Vector GenBank® Accession Number AF025845) and 1 µg pGL3-basic-empty, 1 µg pGL3-basic-*ABCB1* or 1ug pGL3-promoter plasmid, cells were electroporated in an Amaxa 2D Nucleofector using program U-023. Cells were plated in 6-well plates and next day medium was changed. Luciferase reporter assay was performed 48h after nucleofection using a Dual-Luciferase Reporter assay kit (Promega). Cells were lysed directly on the plate with passive lysis buffer for 15 min at room temperature. Luciferase and Renilla activity were measured with the substrates from the kit using TECAN Infinite M200 PRO machine.

Generation of CRISPRa cell lines

For RPE-1 CRISPRa, sgRNAs targeting human *ABCB1* P1, *ABCB1* P2, *ABCB4*, *RUNDC3B*, intronic regions and *POU3F2*, *LHX6* and *ZIC5* were individually cloned into the lentiCRISPR v2 plasmid. Specific sequences are found on **Sup. Table 1**. CRISPR vectors were co-expressed with 3rd generation viral vectors in HEK293T cells using Fugene6 Transfection Reagent. After lentivirus production, the medium was

Perturbations in 3D genome organization can promote acquired drug resistance

harvested and transferred to the designated cell lines. Two days post infection cells were put on puromycin selection for two weeks.

tracrRNA:crRNA design and transfections in RPE-1 iCut

Alt-R crRNA (Integrated DNA technologies) for LBR, LMNB1 and LMNA were obtained from the Human CRISPR Knockout Pooled Library (GeCKO v2)⁶². Specific sequences are found on **Sup. Table 2**. tracrRNA:crRNA duplex was transfected according to the manufacturer's protocol⁶³.

siRNA transfections

ON-TARGETplus SMARTpool set of 4 siRNAs targeting LBR, POU3F2, LHX6 or ZIC5 were from Dharmacon and were transfected using RNAiMAX (Life Technologies) according to manufacturer's protocol⁶³ at a final concentration of 20nM. All transfections were performed 48h before experiment, if not specified on the Figure legend.

Density and Colony Formation Assays

1 million cells were treated indicated dose of Taxol and allowed to grow out for 15 days. Plates were fixed in 80% Methanol and stained with 0.2% Crystal Violet solution. Cell density was measured in ImageJ and normalized to control (WT) plate. For colony formation assays, the number of Taxol resistant cells were counted.

Viability assays

For viability assays, 1000 cells were plated in a 96-well plate and treated for 7 days with indicated drug concentrations. Subsequently, plates were fixed in 80% Methanol and stained with 0.2% Crystal Violet solution.

RNA isolation and qRT-PCR analysis

RNA isolation was performed by using Qiagen RNeasy kit and quantified using NanoDrop (Thermo Fisher Scientific). cDNA was synthesized using Bioscript reverse transcriptase (Bioline), Random Primers (Thermo Fisher), and 1000 ng of total RNA according to the manufacturer's protocol. Primers were designed with a melting temperature close to 60 degrees to generate 90–120-bp amplicons, mostly spanning introns. cDNA was amplified for 40 cycles on a cycler (model CFX96; Bio-Rad Laboratories) using SYBR Green PCR Master Mix (Applied Biosystems). Target cDNA levels were analyzed by the comparative cycle (Ct) method and values

were normalized against GAPDH expression levels. qRT-PCR oligo sequences are summarized in **Sup. Table 3**.

Immunofluorescence

Cells were fixed with 3.7% formaldehyde and permeabilized with 0.2% Triton-X100 for 10 minutes. After, cells were blocked in 4% bovine serum albumin (BSA) in PBS Supplemented with 0.1% Tween (PBS-T) for 1h. Cells were incubated for 2h at 4°C with primary antibody in PBS-T with 3% BSA, washed three times with PBS-T, and incubated with secondary antibody and DAPI in PBS-T with 3% BSA for 1h at room temperature (RT). Images were acquired with the use of a DeltaVision Elite (Applied Precision) equipped with a 60x 1.45 numerical aperture (NA) lens (Olympus) and cooled CoolSnap CCD camera. Nuclear intensity of the different chromatin marks was evaluated in ImageJ using an in-house developed macro that enables automatic and objective analysis. The following antibodies were used for immunofluorescence experiments: H3K27ac (Actif Motif #39133, 1:500), and H3K9me2 (ab1220, 1:500). Secondary antibodies were anti-rabbit Alexa 488 (A11008 Molecular probes, 1:600), anti-mouse Alexa 568 (A11004 Molecular probes, 1:600). DAPI was used at a final concentration of 1µg/mL.

Western Blots

For western blot experiments, equal amounts of cells were lysed with Laemmli buffer and separated by SDS–polyacrylamide gel electrophoresis followed by transfer to a nitrocellulose membrane. Membranes were blocked in 5% milk in PBST for 1h at RT before overnight incubation with primary antibody in PBST with 3% BSA at 4°C. Membranes were washed three times with PBST followed by incubation with secondary antibody in PBST with 5% milk for 2h at RT. Antibodies were visualized using enhanced chemiluminescence (ECL) (GE Healthcare). The following antibodies were used for western blot experiments: SMC1 (Bethyl, A300-055a), α -Tubulin (Sigma t5168), DNMT1 (Sigma, D4692), H3K27me3 (Actif Motif #39156), H3k27ac (Actif Motif #39133), H3k9me2 (ab1220), LaminB1 (ab16048), Lamin A (sc6215) and Lamin B Receptor (ab232731). For secondary antibodies, peroxidase-conjugated goat anti-rabbit (P448 DAKO, 1:2000), goat anti-mouse (P447 DAKO, 1:2000) and rabbit anti-goat (P449) were used.

RNA FISH

RPE-1 cells were plated on glass coverslips and washed twice with BS before fixation in 4% PFA in PBS for 10 minutes at room temperature. After two additional washes in 1x PBS coverslips were incubated in 70% ethanol at 4°C overnight. Coverslips were incubated for pre-hybridization in wash buffer (2x saline-sodium citrate (SSC)

with deionized formamide (Sigma) 10%) for 2-5 minutes at room temperature. RNA FISH probe mix wash dissolved in hybridization buffer (wash buffer Supplemented with 10% dextran sulfate). 38 probes labelled with Cy5 were targeted to the intronic regions of ABCB1 (Biosearch technologies). Coverslips were incubated in hybridization solution for at least 4h at 37°C. Then coverslips were washed twice for 30 minutes with wash buffer followed by a quick rinse with 2x SSC. Finally, coverslips were washed once for 5 minutes in 1x PBS before mounting on slides using Prolong gold DAPI mounting medium (Life Technologies). Images were acquired with the use of a DeltaVision Elite (Applied Precision) equipped with a 60x 1.45 numerical aperture (NA) lens (Olympus) and cooled CoolSnap CCD camera. ABCB1 transcription start site quantification was performed manually double blind.

ChIP-sequencing of RPE-1 hTERT cells

Chromatin immunoprecipitations (ChIP) were performed as described previously⁶⁴ with minor adjustments. For ChIP of histone marks, approximately $7.0 \cdot 10^6$ million cells, 50 μ L of Protein A magnetic beads (Invitrogen) and 5 μ g of antibody were used. Antibodies were H3K27ac (Activ Motif #39133), H3K9me3 (ab8898), H2AZ (ab4174), 5-methylcytosine (ab10805). For ChIP-seq, samples were processed for library preparation (Part# 0801-0303, KAPA Biosystems kit), sequenced using an Illumina Hiseq2500 genome analyzer (65bp reads, single end) and aligned to the Human Reference Genome (hg19) using Burrows-Wheeler Aligner (bwa) version 0.5.9. Mapped reads were filtered based on mapping quality of 20 using samtools version 0.1.19. For ChIP-qPCR analysis, DNA was amplified for 40 cycles on a cycler (model CFX96; Bio-Rad Laboratories) using SYBR Green PCR Master Mix (Applied Biosystems). Target DNA levels were analyzed by the comparative cycle (Ct) method and values were normalized against input DNA and positive control region (specific for each chromatin mark). ChIP-qPCR oligo sequences are summarized in **Sup. Table 3**.

RNA-sequencing

Total RNA from cultured cells was extracted using RLT (Quiagen). Strand-specific libraries were generated using the TruSeq PolyA Stranded mRNA sample preparation kit (Illumina). In brief, polyadenylated RNA was purified using oligo-dT beads. Following purification, the RNA was fragmented, random-primed and reverse transcribed using SuperScript II Reverse Transcriptase (Invitrogen). The generated cDNA was 3' end-adenylated and ligated to Illumina Paired-end sequencing adapters and amplified by PCR using HiSeq SR Cluster Kit v4 cBot (Illumina). Libraries were analyzed on a 2100 Bioanalyzer (Agilent) and subsequently sequenced on a HiSeq2000 (Illumina). We performed RNAseq alignment using TopHat 2.1.1. Differentially expressed genes were called with DESeq2, with an adjusted p-value threshold of 0.05.

TLA analysis

TLA was performed as previously described with minor modifications³⁹. TLA libraries were sequenced on a MiSeq and were analyzed with a custom TLA mapping pipeline. TLA ligation data were mapped to hg19. Normalization and downstream analysis were done using peakC16.

DamID-seq

DamID-seq was performed as described⁶⁵ with minor modifications. Dam fused to human LMNB1 protein (Dam-LMNB1) or unfused Dam were expressed in cells by lentiviral transduction⁶⁶. Three days after infection, cells were collected for genomic DNA (gDNA) isolation. gDNA was pre-treated with SAP (10 U, New England Biolabs #M0371S) in CutSmart buffer in a total volume of 10 μ l at 37°C for 1h, followed by heat-inactivation at 65°C for 20 min to suppress signal from apoptotic fragments. This gDNA was then digested with DpnI (10 U, New England Biolabs #R0176L) in CutSmart buffer in a total volume of 10 μ l at 37°C for 8h followed by heat inactivation at 80 °C for 20 min. Fragments were ligated to 12.5 pmol DamID adapters using T4 ligase (2.5 U, New England Biolabs ##) in T4 ligase buffer in a total volume of 20 μ l incubated at 16°C for 16h. The reaction was heat-inactivated for 10 minutes at 65°C. Products were then digested with DpnII to destroy partially methylated fragments. DpnII buffer and DpnII (10 U, New England Biolabs #R0543L) were added in a total volume of 50 μ l and incubated at 37 °C for 1 h. Next, 8 μ l of DpnII-digested products was amplified by PCR with MyTaq Red Mix (Bioline #BIO-25044) and 1.25 μ M primers Adr-PCR-Rand1 in a total volume of 40 μ l. PCR settings were 8 min at 72 °C (1 \times) followed by 20 s at 94 °C, 30 s at 58 °C, 20 s at 72 °C (24 \times for Dam, 28 \times for Dam-LMNB1 samples) and 2 minutes at 72°C (1 \times). Remaining steps were performed as previously described. Samples were sequenced on an Illumina HiSeq2500.

Motif analysis

Genomic coordinates of all the genes were obtained from GRCh37 (Ensembl version 75) using biomaRt package⁶⁷ and transcription starting sites of the genes were extended 1 kb to both up- and down-stream to identify the promoter regions. The motifs presenting in the promoters were identified using GimmeMotifs⁶⁸ against the non-redundant Cis-bp database (version 3.0). To identify the overrepresented motifs, we used a similar method as described in our previous publication (<https://www.nature.com/articles/s41588-020-00744-4>, will be online next Monday). Briefly, we calculated for every motif the frequency in the promoters of the upregulated genes and all the expressed genes. We computed relative motif frequency by dividing the individual motif frequency by the total number of identified motifs. We calculated the log₂-enrichment score by calculating the ratio of relative motif frequency between the promoters of up-regulated genes and all the expressed

Perturbations in 3D genome organization can promote acquired drug resistance

genes. The p-value was calculated using the Fisher exact test on the following 2x2 table: for every motif M, we determine the number of the promoters belonging to the upregulated genes with or without M and for the promoters of the expressed genes with or without M.

Processing of RPE-1 DamID data

DamID-seq was performed as described in⁴⁴

GEO accession information

All sequencing raw and processed data files generated in this study are available in GEO with the GEO accession code GSE163315.

3

Supplementary Table 1 – sgRNAs for RPE-1 CRISPRa

ABCB1 Promoter 1	Target Sequence
abcb1-P1-1	gtagctcctcctctgtact
abcb1-P1-2	gctacatgaactaaggcaggc
abcb1-P1-3	gataagtttgggtggaggaaggg
abcb1-P1-4	gtgatcttttctaaaggtgt
abcb1-P1-5	gagttacatggcttagggat
abcb1-P1-6	gttgagaagtttagccagaat
ABCB1 Promoter 2	
abcb1-P2-1	TCAATGCCCGTGTTTTCCA
ABCB4 Promoter	
abcb4-1	TGCAACGGTAGGCGTTTCCC
RUNDC3B Promoter	
rundc3b-1	GCTGCTTTAAAGGTCCGCG
INTRONIC sgRNAs	
abcb1-P1-rundc3b-1	actctctattgtccggca
abcb1-P1-rundc3b-2	ctctctattgtccggca
abcb1-P2-rundc3b-1	agagtgttctaatccgg
abcb1-P2-rundc3b-2	taggtaaagcagctcgaggt
TF sgRNAs	
POU3F2-P1	Ggaggactaccaagaggggg
LHX6-P1	GCCCCGGGTGAGGAAGAAGC
ZIC5-P1	GTGCAACTTGGGCATCCCCG
Supplementary Table 2 – crRNA for RPE-1 icut KO	
Gene name	Target Sequence
LBR_1	GCCGATGGTGAAGTGGTAAG
LMNB1_3	TCGTTGTCAGAGCCTTACTG
LMNA_2	GCCGAGCCTGAGCAGCTATC

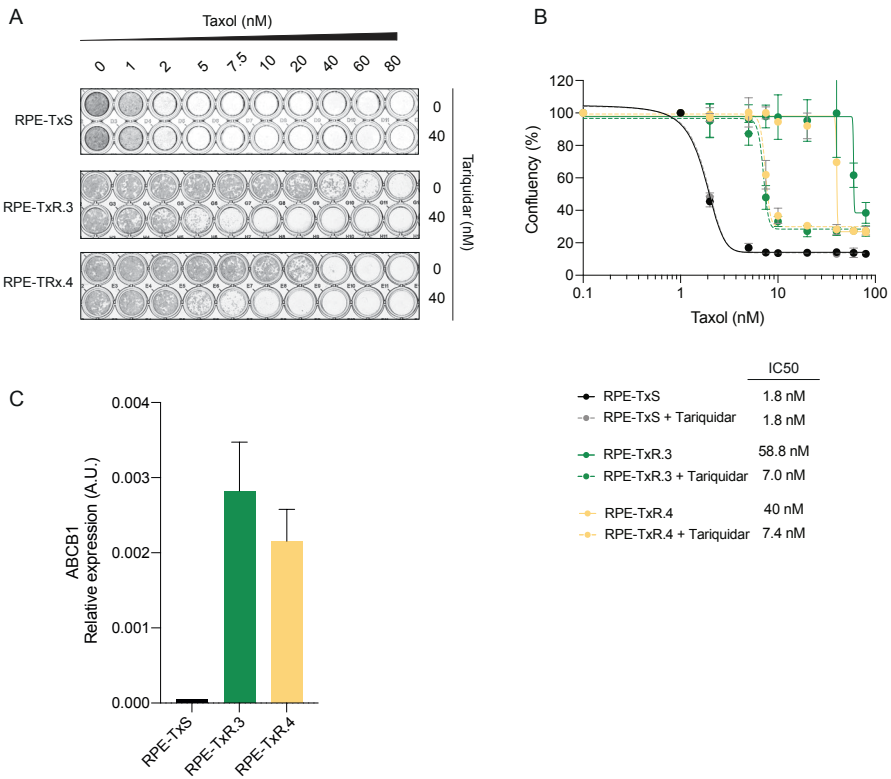
Supplementary Table 3 – RT-qPCR and ChiP-qPCR primers

RT-qPCR Primers	FWD	REV
ABCB1 P1	GGAGGCCAACATACATGCCT	GCTGTCTAACAAAGGGCACGA
ABCB1 P2	ACAGCACGGAAGGCCTAATG	GTCTGGCCCTTCTTCACCTC
ABCB4	ATAGCTCACGGATCAGGTCTC	GGATTTAGCGACAAGGAAA
RUNDC3B	GATGGCAGTTTTCTGTCTGT	AGGAAAGGAGGTCCGACATT
GAPDH	TGCACCACCAACTGCTTA	GGATGCAGGGATGATGTTT
POU3F2_qPCR_F1	GCGGATCAAACCTGGGATTTA	AAAGGCTTCAGCTTGACAT
LHX6_qPCR_F2	CTCGAGATCTGGACCGATA	CGAATCGGCTGAAGTAGTCC
ZIC5_qPCR_F1	CAGTCCTCCAGAAGCAGAC	AGCCCTGCTCCAAAACTTTC
ChiP-qPCR Primers	FWD	REV
H3K9me3 positive control	TGAAGACACATCTGCGAACC	TCGCGCACTCATACTGTTTC
H3k27ac positive control	TGCCACACACCAGTGACTTT	ACAGCCAGAAGCTCCAAAAA
5-mC positive control	CAGAGTAGGGTGGGAAAGCA	TTCCAAAAGCCTGTGATGC
H2AZ positive control	CGTGGGAACCTCTGTCTTT	AGGGCAGCTCAGATAACAGG
ABCB1_P2_-1000	GGCGACCAACACCAC TT	GTCTTGGTGTGCCTCTTTCT
ABCB1_P2_1000	TTCCTGTCCACTATTTACTTCAA	GCTCTGATGTGAGTTAGCATT
ABCB1_P2_-500	TTCTGCTCTAAGCAGGGATATTG	CTAGCCTCCAGCTCTGAAATAAA
ABCB1_P2_500	CTACAGGACGTAGTTAAGGGAAAT	AGGAGGCAGAAAGGTGATACAG
ABCB1_P2_-250	CCATTCCGACCTGAAGAGAAA	CTCTTACTGCTCTCTGGCTTC
ABCB1_P2_250	GAAGAGCCGCTACTCGAATG	ATCTGTGGTGAGGCTGATTG
ABCB1_P2_TS	GGGTCTCCAGCATCTCCAC	GTGGGTGGGAGGAAGCATC

Supplementary Table 4 – RT-qPCR primers position

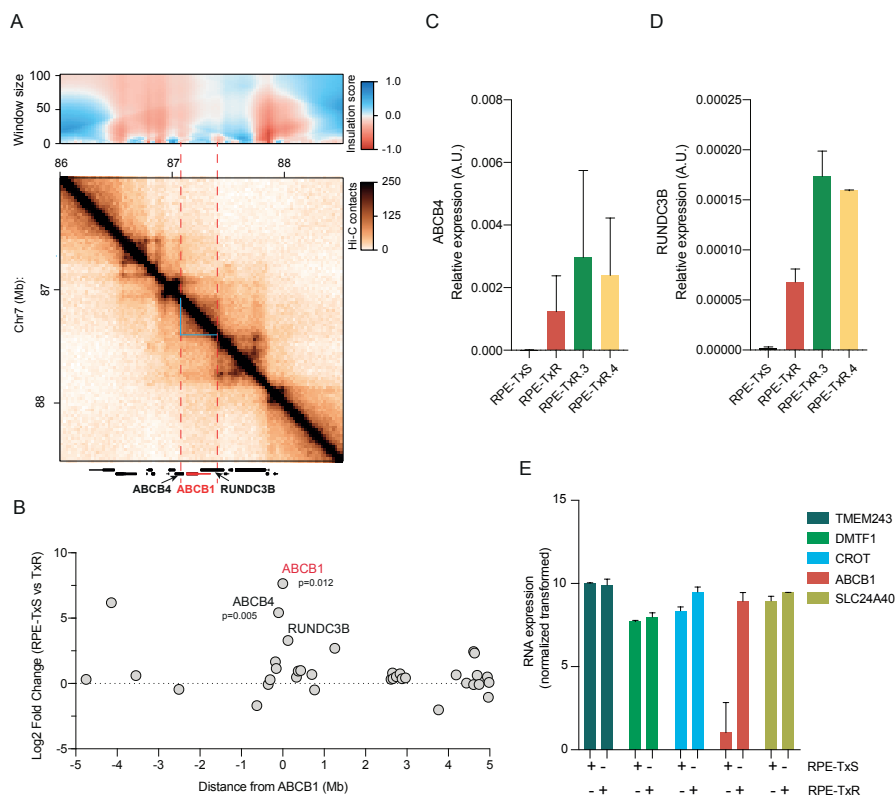
		Hg19 position	Exon
ABCB1 P1	FWD	87138611	27
	REV	87135269	28
ABCB1 P2	FWD	87145828	25
	REV	87144635	26
ABCB4	FWD	87092147	4
	REV	87083890	Junction 5-4
RUNDC3B	FWD	87370893	7
	REV	87400026	8

Perturbations in 3D genome organization can promote acquired drug resistance



Supplementary Figure 1 – Transcriptional activation of ABCB1 drives Taxol resistance in independently generated RPE-TxR

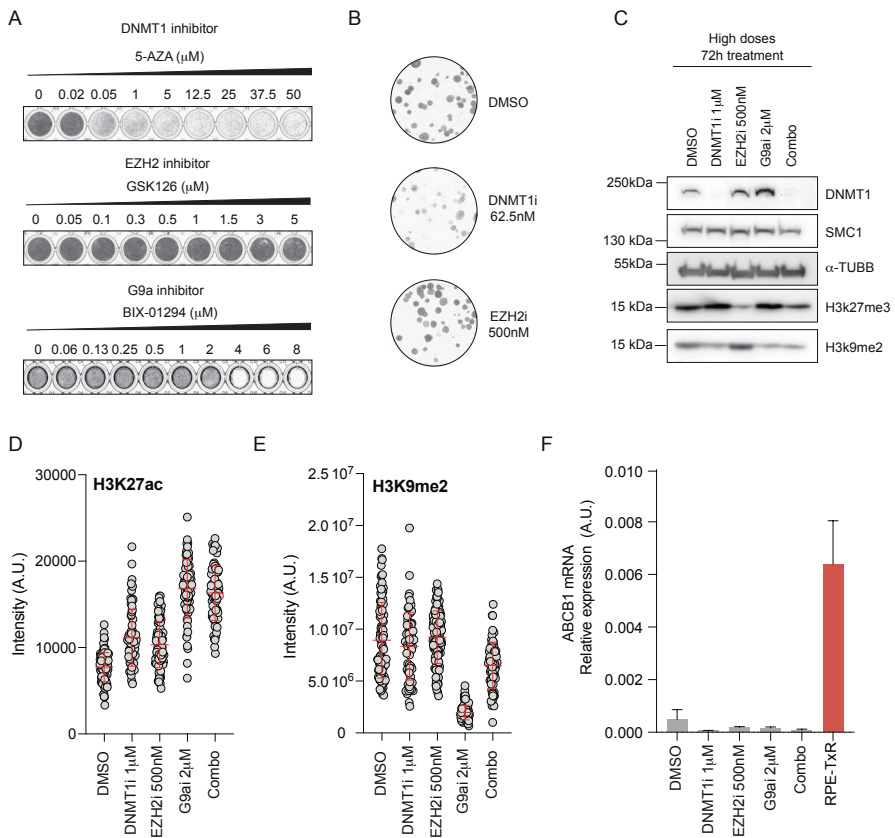
A) Crystal violet staining of viability assay on Taxol-naïve RPE-TxS and two independently generated Taxol resistant cell lines (RPE-TxR3 and RPE-TxR4). **B)** Relative survival plots of the RPE-TxS and RPE-TxR3 and TxR4 cell lines. Error bars show the average \pm s.d. of two independent experiments and the calculated IC50. The curve was drawn from the $\log(\text{inhibitor})$ vs response equation $Y = \text{Bottom} + (\text{Top} - \text{Bottom}) / (1 + 10^{-(X - \text{LogIC50})})$. **C)** ABCB1 mRNA levels determined by qRT-PCR and normalized to GAPDH expression in RPE-TxS, RPE-TxR3 and RPE-TxR4, n=2. Error bars show the SD.



Supplementary Figure 2 – RPE-TxR undergo changes in gene expression

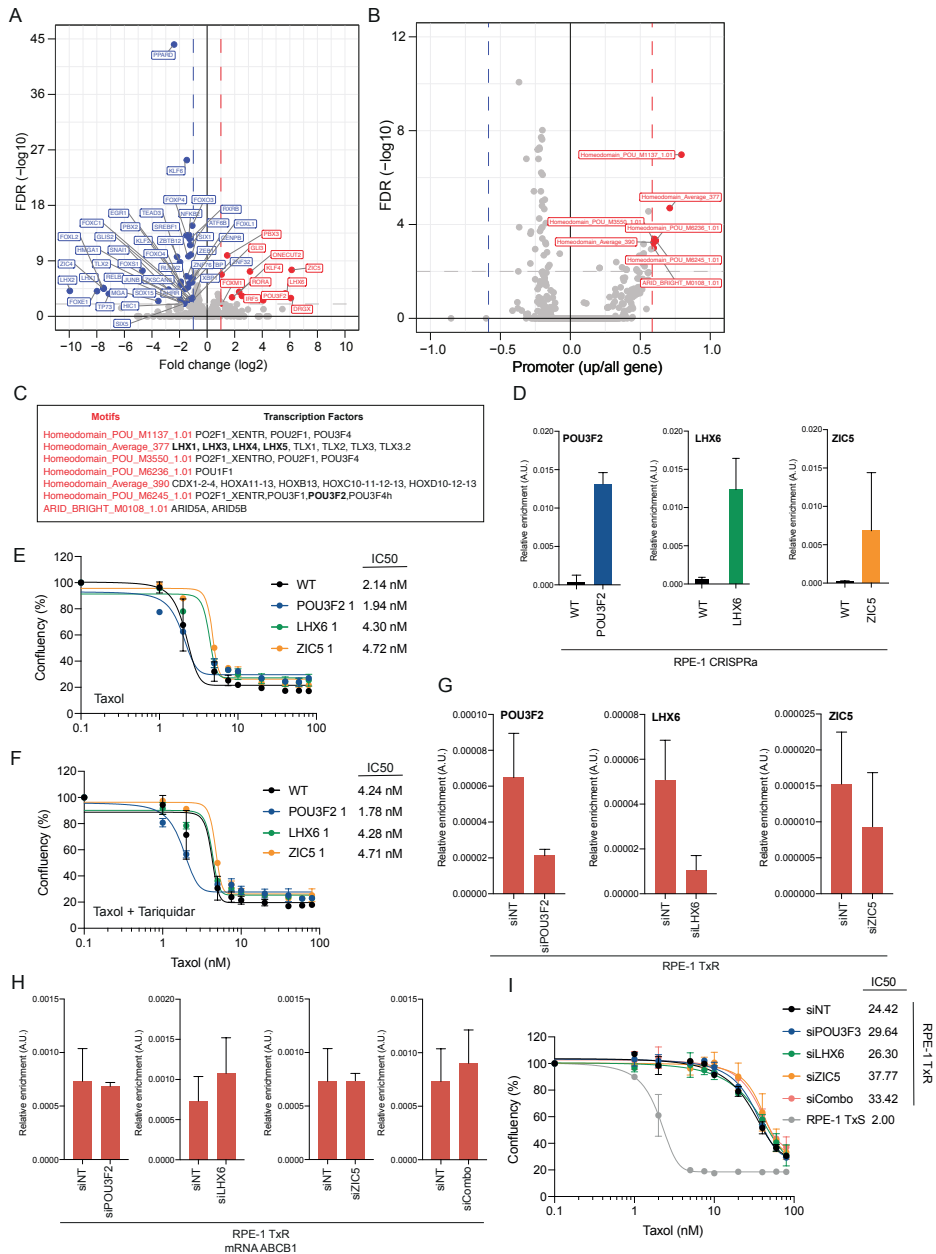
A) Hi-C contact matrix of RPE-1 WT generated by Aiden Lab. For TAD calling, we calculated the insulation score for each bin at 25kb resolution using the software GENOVA⁶⁹. Blue lines show the TAD called where *ABCB1* is located together with *ABCB4* and *RUNDC3B*. **B)** Log₂ Fold change of RNA expression levels of genes across 5Mb +/- *ABCB1* comparing RPE-TxS to RPE-TxR, n=2. Every dot indicates a gene. **C)** *ABCB4* and **D)** *RUNDC3B* mRNA levels determined by qRT-PCR and normalized to *GAPDH* expression in RPE-TxS, RPE-TxR, RPE-TxR3 and RPE-TxR4, n=2. Error bars show the SD. **E)** Normalized RNA expression of *ABCB1* and its neighbor transcribed genes in RPE-TxS and RPE-TxR cells.

Perturbations in 3D genome organization can promote acquired drug resistance



Supplementary Figure 3 – 5-AZA and GSK126 inhibitors validations

A) Crystal violet staining of viability assay on RPE-TxS with increasing concentration of the epigenetic drugs 5-Aza-2'-deoxycytidine (5-AZA, DNMT1 inhibitor), GSK126 (EZH2 inhibitor) and BIX-01294 (G9a inhibitor). **B)** Crystal violet staining of colony formation assay under the indicated drug doses without Taxol. 100 cells were plated per condition and let grown for 15 days in parallel to Fig. 3C. **C)** Western Blot showing the levels of the chromatin proteins and controls (SMC1 an α -TUBB) upon treatment with single drugs or the combination (Combo) for 72h. **D)** Immunofluorescence quantification of nuclear H3K27ac and **E)** H3K9me2 levels after 72h drug addition by ImageJ in-house foci macro, n=1, 60 cells per condition. Error bars show the SD. **F)** *ABCB1* mRNA levels determined by qRT-PCR and normalized to *GAPDH* expression levels upon high drug addition and RPE-TxR as a control for *ABCB1* expression, n=3 technical replicates. Error bars show the SD.

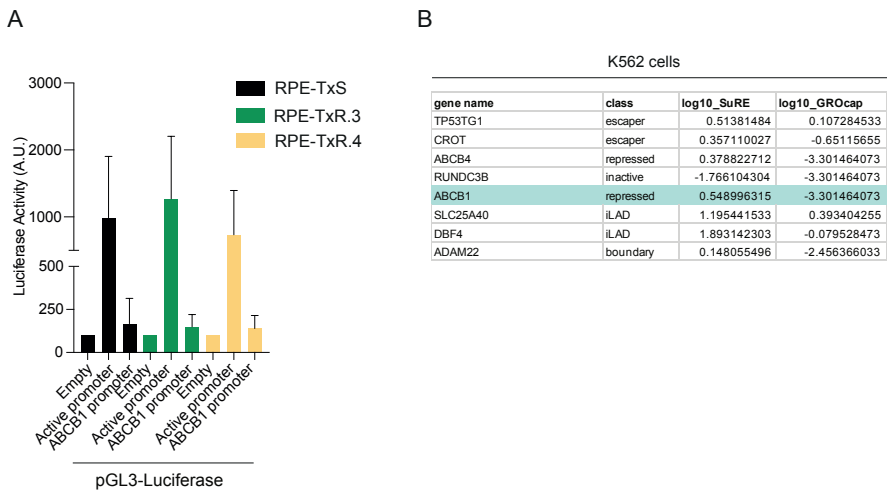


Supplementary Figure 4 – POU3F2, LHX6 or ZIC5 are not responsible for initiation of ABCB1 gene expression in RPE-TxR cells

A) RNA-seq analysis identified the differentially regulated transcription factors genes in the Taxol resistant RPE-TxR cells (n=2) compared to RPE-TxS cells (n=3). **B)** Motif analysis revealed the potential promoter activators in the RPE-TxR cell line. **C)** Table showing the corresponding TF binding the significant motifs found on B. **D)** mRNA levels determined by qRT-PCR and normalized to *GAPDH*

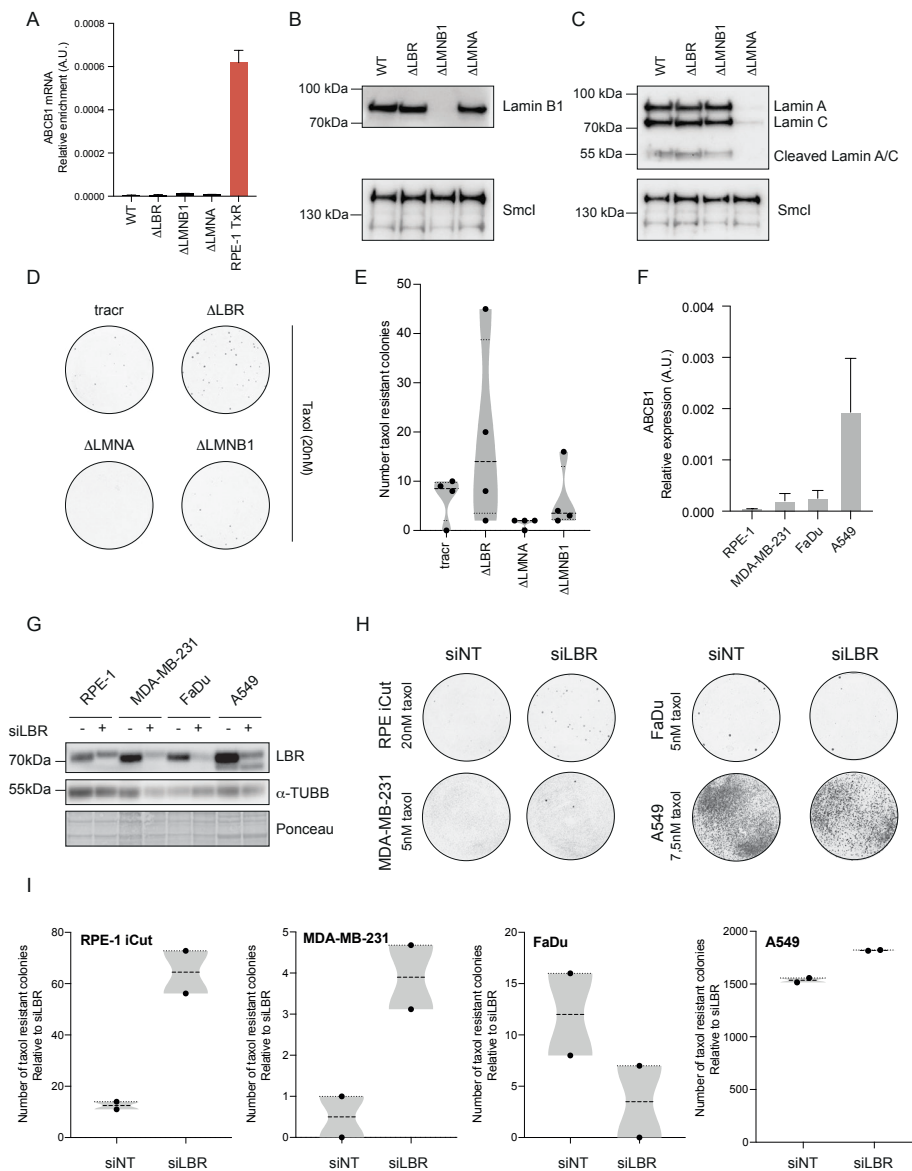
Perturbations in 3D genome organization can promote acquired drug resistance

expression in RPE-1 CRISPRa targeted with sgRNA for *POU3F2*, *LHX6* or *ZIC5*, n=2. Error bars show the SD. **E and F**) Relative survival plots of the same TFs CRISPRa cell lines. Error bars show the average +/- s.d. of two independent experiments and the calculated IC50. The curve was drawn from the log(inhibitor) vs response equation $Y=Bottom + (Top-Bottom)/(1+10^{-(X-LogIC50)})$. **G**) mRNA levels of the TF candidates or **H**) *ABCB1* determined by qRT-PCR and normalized to *GAPDH* expression in RPE-TxR transfected with siRNA NT, siPOU3F2 or siZIC5. Error bars show the SD, n=2. **I**) Relative survival plots of the respective siRNA transfections. Error bars show the average +/- s.d. of two independent experiments and the calculated IC50.



Supplementary Figure 5 – ABCB1 upregulation in RPE-TxR is not caused by direct activation of the promoter by trans-acting factors

A) Relative luciferase activity calculated by dividing the luciferase activity to that of Renilla luciferase. Data shown represent average +/- s.d, n = 3. **B)** Promoter classification of the genes neighboring ABCB1 based on GROcap and SuRE in K562 cells.

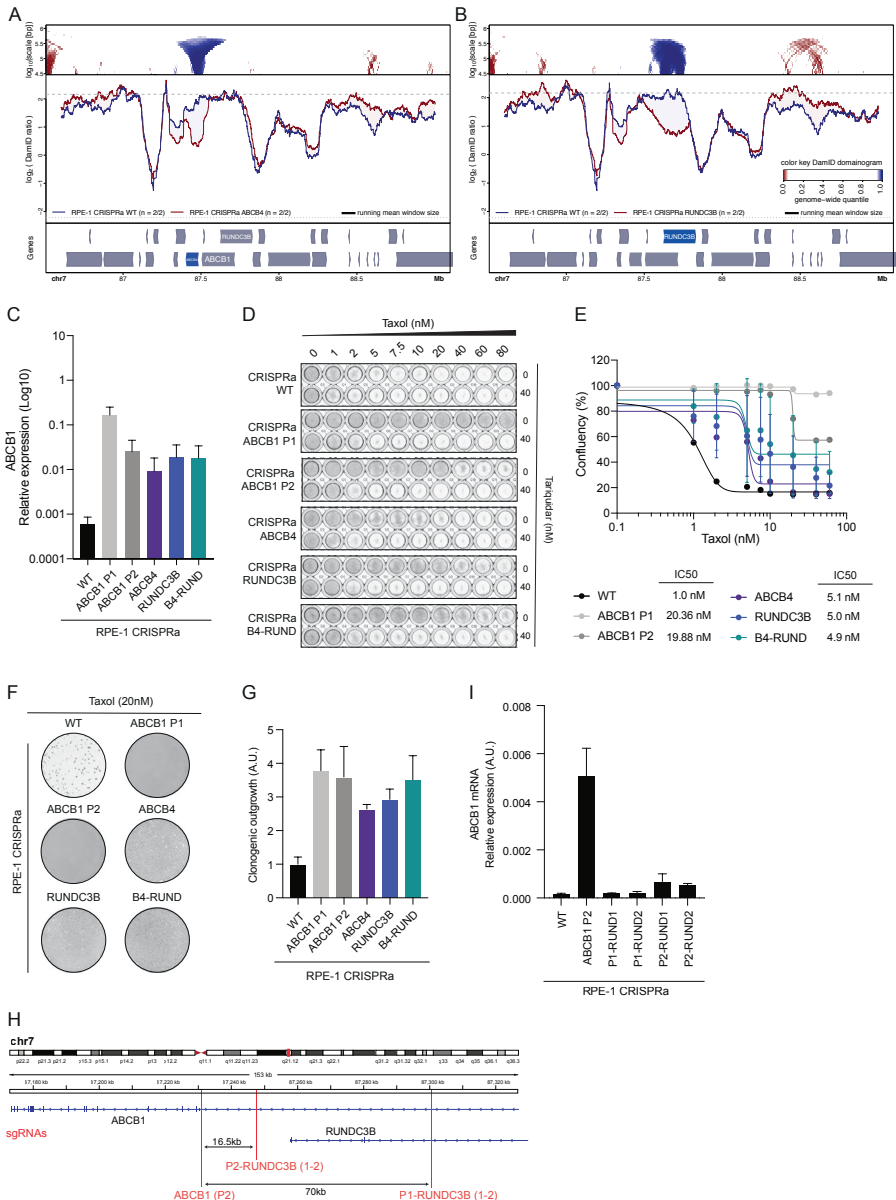


Supplementary Figure 6 – LBR, LMNB1 and LMNA knockout and knockdown validations

A) ABCB1 mRNA levels determined by qRT-PCR and normalized to GAPDH expression in RPE-1 iCut in WT cells or 7 days after transfection of *LBR*, *LMNA* or *LMNB1* crRNAs. n=2. Error bars show the SD. **B)** Western Blot showing Lamin B1 and control (SMC1) protein levels upon the different KO in RPE-1 iCut cells. **C)** Western Blot showing LaminA/C and control (SMC1) protein levels upon the different KO in RPE-1 iCut cells. **D)** Crystal violet staining of colony formation assay under 20nM of Taxol in RPE-1 iCut WT, transfected only with tracrRNA or together with the specific crRNA to generate a KO. **E)** Quantification of the number of Taxol resistant colonies under 20nM of Taxol in the different KO, n=2. Error bars show the SD. Black dots show an independent biological replicate.

Perturbations in 3D genome organization can promote acquired drug resistance

F) ABCB1 mRNA levels determined by qRT-PCR and normalized to GAPDH in RPE-1 and the different cancer cell lines, $n=3$. Error bars show the SD of technical replicates. **G)** Western Blot showing *LBR* and control (a-TUBB) protein levels in the different cancer cell lines upon *LBR* siRNA depletion. **H)** Crystal violet staining of colony formation assay in RPE-1 iCut and cancer cell lines under indicated concentration of Taxol. Cells were treated for 72hrs prior to colony formation plating with siNT or *siLBR*. **I)** Quantification of the number of Taxol resistant colonies in G. Black dots show an independent biological replicate.



Supplementary Figure 7 – Validation of CRISPRa cell lines

A) Local NL detachment caused by ABCB4 gene activation or **B)** RUNDC3B by CRISPRa in RPE-1 cells. **C)** ABCB1 mRNA levels determined by qRT-PCR and normalized to GAPDH upon CRISPRa activation of individual genes or combination of ABCB4 and RUNDC3B (B4-RUND), n=2. Error bars show the SD. **D)** Crystal violet staining of viability assay on CRISPRa cell lines upon activation of ABCB1 (P1 and P2), ABCB4, RUNDC3B or the combination. **E)** Relative survival plots of CRISPRa cell lines targeting ABCB1 (P1 and P2), ABCB4, RUNDC3B or the combination of the last two. Error bars show the average +/- s.d. of two independent experiments and the calculated IC50. The curve was drawn from the log(inhibitor) vs response equation $Y=Bottom + (Top-Bottom)/(1+10^{-(X-LogIC50)})$. **F)** Crystal violet staining of density assays of CRISPRa cells targeting the different genes upon 20nM of Taxol. WT, ABCB1 P2 and B4-RUND are duplicated from Figure 5E. **G)** ImageJ quantification of density assays of CRISPRa cells targeting the different genes upon 20nM of Taxol, n=2. Error bars show the SD. **H)** Schematic representation of the Chr7q21.12 region indicating the locations where the sgRNAs were targeting intronic regions for the ABCB1 gene. **I)** ABCB1 mRNA levels determined by qRT-PCR and normalized to GAPDH in CRISPRa cells upon sgRNA targeting of the different intronic regions, n=2. Error bars show the SD.

REFERENCES

1. Holohan, C., Van Schaeybroeck, S., Longley, D. B. & Johnston, P. G. Cancer drug resistance: An evolving paradigm. *Nature Reviews Cancer* vol. 13 714–726 (2013).
2. Rebutti, M. & Michiels, C. Molecular aspects of cancer cell resistance to chemotherapy. *Biochemical Pharmacology* vol. 85 1219–1226 (2013).
3. Du, Z. & Lovly, C. M. Mechanisms of receptor tyrosine kinase activation in cancer. *Molecular Cancer* vol. 17 (2018).
4. Rosenzweig, S. A. Acquired Resistance to Drugs Targeting Tyrosine Kinases. in *Advances in Cancer Research* vol. 138 71–98 (Academic Press Inc., 2018).
5. General Mechanisms of Drug Resistance - Holland-Frei Cancer Medicine - NCBI Bookshelf. <https://www.ncbi.nlm.nih.gov/books/NBK12424/>.
6. Jaenisch, R. & Bird, A. Epigenetic regulation of gene expression: How the genome integrates intrinsic and environmental signals. *Nature Genetics* vol. 33 245–254 (2003).
7. Albertson, D. G. Gene amplification in cancer. *Trends in Genetics* vol. 22 447–455 (2006).
8. Dedes, K. J. *et al.* Synthetic lethality of PARP inhibition in cancers lacking *BRCA1* and *BRCA2* mutations. *Cell Cycle* **10**, 1192–1199 (2011).
9. Housman, G. *et al.* Drug resistance in cancer: An overview. *Cancers* vol. 6 1769–1792 (2014).
10. Goldstein, L. J. MDR1 gene expression in solid tumours. *Eur. J. Cancer* **32**, 1039–1050 (1996).
11. Vaidyanathan, A. *et al.* ABCB1 (MDR1) induction defines a common resistance mechanism in paclitaxel- and olaparib-resistant ovarian cancer cells. *Br. J. Cancer* **115**, 431–441 (2016).
12. Christie, E. L. *et al.* Multiple ABCB1 transcriptional fusions in drug resistant high-grade serous ovarian and breast cancer. *Nat. Commun.* **10**, 1–10 (2019).
13. Patch, A. M. *et al.* Whole-genome characterization of chemoresistant ovarian cancer. *Nature* **521**, 489–494 (2015).
14. Yasui, K. *et al.* Alteration in Copy Numbers of Genes as a Mechanism for Acquired Drug Resistance. *Cancer Res.* **64**, 1403–1410 (2004).
15. Desiderato, L., Davey, M. W. & Piper, A. A. Demethylation of the human MDR1 5' region accompanies activation of P-glycoprotein expression in a HL60 multidrug resistant subline. *Somat. Cell Mol. Genet.* **23**, 391–400 (1997).
16. Chen, K. G. *et al.* Genetic and epigenetic modeling of the origins of multidrug-resistant cells in a human sarcoma cell line. *Cancer Res.* **65**, 9388–9397 (2005).
17. Li, A. *et al.* Hypermethylation of ATP-binding cassette B1 (ABCB1) multidrug resistance 1 (MDR1) is associated with cisplatin resistance in the A549 lung adenocarcinoma cell line. *Int. J. Exp. Pathol.* **97**, 412–421 (2016).
18. Reed, K. *et al.* Hypermethylation of the ABCB1 downstream gene promoter accompanies ABCB1 gene amplification and increased expression in docetaxel-resistant MCF-7 breast tumor cells. *Epigenetics* **3**, 270–280 (2008).
19. Kalmykova, A. I., Nurminsky, D. I., Ryzhov, D. V. & Shevelyov, Y. Y. Regulated chromatin domain comprising cluster of co-expressed genes in *Drosophila melanogaster*. *Nucleic Acids Res.* **33**, 1435–44 (2005).
20. Razin, S. V., Farrell, C. M. & Recillas-Targa, F. Genomic domains and regulatory elements operating at the domain level. *Int. Rev. Cytol.* **226**, 63–125 (2003).
21. Dillon, N. Gene regulation and large-scale chromatin organization in the nucleus. *Chromosom. Res.* **14**, 117–126 (2006).
22. Hansen, J. C. Linking genome structure and function through specific histone acetylation. *ACS chemical biology* vol. 1 69–72 (2006).
23. Sproul, D., Gilbert, N. & Bickmore, W. A. The role of chromatin structure in regulating the expression of clustered genes. *Nature Reviews Genetics* vol. 6 775–781 (2005).
24. Hildebrand, E. M. & Dekker, J. Mechanisms and Functions of Chromosome Compartmentalization. *Trends Biochem. Sci.* **45**, 385–396 (2020).
25. Razin, S. V. & Gavrilov, A. A. The Role of Liquid-Liquid Phase Separation in the Compartmentalization of Cell Nucleus and Spatial Genome Organization. *Biochemistry (Moscow)* vol. 85 643–650 (2020).
26. Flavahan, W. A. *et al.* Insulator dysfunction and oncogene activation in IDH mutant gliomas. *Nature* **529**, 110–114 (2016).
27. Seaman, L. *et al.* Nucleome analysis reveals structure-function relationships for colon cancer. *Mol. Cancer Res.* **15**, 821–830 (2017).
28. Hnisz, D. *et al.* Activation of proto-oncogenes by disruption of chromosome neighborhoods. *Science (80-.)*. **351**, 1454–1458 (2016).
29. Martin, P. *et al.* Capture Hi-C reveals novel candidate genes and complex long-range interactions with related autoimmune risk loci. *Nat. Commun.* **6**, 1–7 (2015).
30. Lupiáñez, D. G. *et al.* Disruptions of topological chromatin domains cause pathogenic rewiring of gene-enhancer interactions. *Cell* **161**, 1012–1025 (2015).
31. Katainen, R. *et al.* CTCF/cohesin-binding sites are frequently mutated in cancer. *Nat. Genet.* **47**, 818–821 (2015).
32. Leemans, C. *et al.* Promoter-Intrinsic and Local Chromatin Features Determine Gene Repression in LADs. *Cell* **177**, 852–864.e14 (2019).
33. Peric-Hupkes, D. *et al.* Molecular Maps of the Reorganization of Genome-Nuclear Lamina Interactions during Differentiation. *Mol. Cell* **38**, 603–613 (2010).
34. Chen, H., Zheng, X. & Zheng, Y. Age-associated loss of lamin-b leads to systemic inflammation and gut hyperplasia. *Cell* **159**, 829–843 (2014).
35. Shevelyov, Y. Y. *et al.* The B-type lamin is required for somatic repression of testis-specific gene clusters. *Proc. Natl. Acad. Sci. U. S. A.* **106**, 3282–3287 (2009).

36. Ito, K., Awano, W., Suzuki, K., Hiromi, Y. & Yamamoto, D. The *Drosophila* mushroom body is a quadruple structure of clonal units each of which contains a virtually identical set of neurones and glial cells. *Development* **124**, 761–771 (2010).
37. Tame, M. A., Manjón, A. G., Belokhovostova, D., Raaijmakers, J. A. & Medema, R. H. TUBB3 overexpression has a negligible effect on the sensitivity to Taxol in cultured cell lines. *Oncotarget* **8**, 71536 (2017).
38. Wang, X. Q. D. & Dostie, J. Chromosome folding and its regulation in health and disease. *Current Opinion in Genetics and Development* vol. 43 23–30 (2017).
39. de Vree, P. J. P. *et al.* Targeted sequencing by proximity ligation for comprehensive variant detection and local haplotyping. *Nat. Biotechnol.* **32**, 1019–25 (2014).
40. Huang, C. & Zhu, B. Roles of H3K36-specific histone methyltransferases in transcription: antagonizing silencing and safeguarding transcription fidelity. *Biophys. reports* **4**, 170–177 (2018).
41. Nicetto, D. & Zaret, K. S. Role of H3K9me3 heterochromatin in cell identity establishment and maintenance. *Curr. Opin. Genet. Dev.* **55**, 1–10 (2019).
42. Heintzman, N. D. *et al.* Distinct and predictive chromatin signatures of transcriptional promoters and enhancers in the human genome. *Nat. Genet.* **39**, 311–8 (2007).
43. van Steensel, B. & Belmont, A. S. Lamina-Associated Domains: Links with Chromosome Architecture, Heterochromatin, and Gene Repression. *Cell* vol. 169 780–791 (2017).
44. Brueckner, L. *et al.* Local rewiring of genome–nuclear lamina interactions by transcription. *EMBO J.* 685255 (2020) doi:10.1101/685255.
45. Van Arensbergen, J. *et al.* Genome-wide mapping of autonomous promoter activity in human cells. *Nat. Biotechnol.* **35**, 145–153 (2017).
46. Van Den Berg, J. *et al.* A limited number of double-strand DNA breaks is sufficient to delay cell cycle progression. *Nucleic Acids Res.* **46**, 10132–10144 (2018).
47. Polioudaki, H. *et al.* Histones H3/H4 form a tight complex with the inner nuclear membrane protein LBR and heterochromatin protein 1. *EMBO Rep.* **2**, 920–925 (2001).
48. Olins, A. L., Rhodes, G., Welch, D. B. M., Zwerger, M. & Olins, D. E. Lamin B receptor multi-tasking at the nuclear envelope. *Nucleus* **1**, 53–70 (2010).
49. Zappe, K. & Cichna-Markl, M. Aberrant DNA Methylation of ABC Transporters in Cancer. *Cells* vol. 9 (2020).
50. Ulianov, S. V. *et al.* Nuclear lamina integrity is required for proper spatial organization of chromatin in *Drosophila*. *Nat. Commun.* **10**, 1–11 (2019).
51. Poleshko, A. *et al.* The Human Protein PRR14 Tethers Heterochromatin to the Nuclear Lamina during Interphase and Mitotic Exit. *Cell Rep.* **5**, 292–301 (2013).
52. Clowney, E. J. *et al.* Nuclear aggregation of olfactory receptor genes governs their monogenic expression. *Cell* **151**, 724–737 (2012).
53. Solovei, I. *et al.* LBR and lamin A/C sequentially tether peripheral heterochromatin and inversely regulate differentiation. *Cell* **152**, 584–598 (2013).
54. Kind, J. *et al.* Genome-wide maps of nuclear lamina interactions in single human cells. *Cell* **163**, 134–47 (2015).
55. Rooijers, K. *et al.* Simultaneous quantification of protein–DNA contacts and transcriptomes in single cells. *Nat. Biotechnol.* **37**, 766–772 (2019).
56. Medina-Rivera, A., Santiago-Algarra, D., Puthier, D. & Spicuglia, S. Widespread Enhancer Activity from Core Promoters. *Trends Biochem. Sci.* **43**, 452–468 (2018).
57. Finlan, L. E. *et al.* Recruitment to the nuclear periphery can alter expression of genes in human cells. *PLoS Genet.* **4**, e1000039 (2008).
58. Reddy, K. L., Zullo, J. M., Bertolino, E. & Singh, H. Transcriptional repression mediated by repositioning of genes to the nuclear lamina. *Nature* **452**, 243–247 (2008).
59. Dialynas, G., Speese, S., Budnik, V., Geyer, P. K. & Wallrath, L. L. The role of *Drosophila* Lamin C in muscle function and gene expression. *Development* **137**, 3067–3077 (2010).
60. Kumaran, R. I. & Spector, D. L. A genetic locus targeted to the nuclear periphery in living cells maintains its transcriptional competence. *J. Cell Biol.* **180**, 51–65 (2008).
61. Chang, L. *et al.* Nuclear peripheral chromatin–lamin B1 interaction is required for global integrity of chromatin architecture and dynamics in human cells. *Protein Cell* 1–23 (2020) doi:10.1007/s13238-020-00794-8.
62. Sanjana, N. E., Shalem, O. & Zhang, F. Improved vectors and genome-wide libraries for CRISPR screening. *Nature Methods* vol. 11 783–784 (2014).
63. Jacobi, A. M. *et al.* Simplified CRISPR tools for efficient genome editing and streamlined protocols for their delivery into mammalian cells and mouse zygotes. *Methods* **121–122**, 16–28 (2017).
64. Stelloo, S. *et al.* Endogenous androgen receptor proteomic profiling reveals genomic subcomplex involved in prostate tumorigenesis. *Oncogene* **37**, 313–322 (2018).
65. Brueckner, L., van Arensbergen, J., Akhtar, W., Pagie, L. & van Steensel, B. High-throughput assessment of context-dependent effects of chromatin proteins. *Epigenetics Chromatin* **9**, 43 (2016).
66. Vogel, M. J., Peric-Hupkes, D. & van Steensel, B. Detection of in vivo protein–DNA interactions using DamID in mammalian cells. *Nat. Protoc.* **2**, 1467–78 (2007).
67. Durinck, S. *et al.* BioMart and Bioconductor: A powerful link between biological databases and microarray data analysis. *Bioinformatics* **21**, 3439–3440 (2005).
68. van Heeringen, S. J. & Veenstra, G. J. C. GimmeMotifs: A de novo motif prediction pipeline for ChIP-sequencing experiments. *Bioinformatics* **27**, 270–271 (2011).

Perturbations in 3D genome organization can promote acquired drug resistance

69. Van Der Weide, R. H. *et al.* Hi-C Analyses with GENOVA: a case study with cohesin variants. *bioRxiv* 2021.01.22.427620 (2021) doi:10.1101/2021.01.22.427620.



4

DNA damage-dependent chromatin dynamics as a potential cause of acquired Taxol-resistance

Anna G. Manjón, Stefano Manzo, Tom van Schaik, Anoeek Friskes, Hans Teunissen,
Dorine Hintzen, André Koch, Elzo de Wit, Bas van Steensel, René H. Medema

ABSTRACT

The maintenance of chromatin and three-dimensional genome organization is crucial to preserve cellular functions and organism viability. Yet, (epi)genome maintenance is challenged when the DNA is damaged. During the DNA damage response, the chromatin surrounding the lesion is altered in several ways in order to allow the repair machinery to faithfully repair the damage. Whether chromatin and 3D genome organization are perfectly restored to the state they were in before the break is currently not entirely clear. Here, we investigated if DNA damage can induce lasting alterations to the epigenetic state of a locus. We show that upon break formation in the *ABCB1* gene, the locus moves to the nuclear interior. Strikingly, a subset of cells derepress the *ABCB1* gene upon DSB induction, which leads to acquired Taxol-resistance. In these cells, *ABCB1* is retained in the nuclear interior and acquires active histone modifications. Inhibition of non-homologous end-joining (NHEJ) yields an increased number of Taxol-resistant cells, implying that resection-dependent repair can induce the required reprogramming at the locus. We hypothesize that in a small subset of cells that engage in resection-dependent repair, the epigenome is not faithfully restored after damage induction, leading to *ABCB1* gene re-activation and acquisition of Taxol-resistance. Based on these data, we propose a model in which epigenetic scars that result from DNA damage can lead to genome plasticity, allowing for the acquisition of drug resistance.

INTRODUCTION

DNA is subjected to constant chemical modifications and damage, which can perturb cellular integrity leading to cancer or cell death¹. Double-strand breaks (DSBs), i.e. breakage of both DNA strands at proximal sites in a double-stranded helix, are the most deleterious form of DNA damage. To counter this, cells have evolved several mechanisms to repair DSBs^{2,3}, including homologous recombination (HR), non-homologous end joining (NHEJ) or micro-homology-mediated end-joining (MMEJ). While NHEJ ligates the broken ends together, often causing small nucleotide insertions and deletions, HR employs resection and a DNA template to repair the damage⁴⁻⁶.

The DNA repair process occurs in the context of chromatin. DNA is highly organized and packed forming nucleosome structures containing histone proteins. Modifications of histone tails by acetylation, methylation and phosphorylation are known to be necessary for gene regulation. In addition, there is a range of histone modifications that are induced during DNA repair processes, most notably the phosphorylation of H2AX and the ubiquitination of H2A^{7,8}. Moreover, a large number of studies have shown that chromatin de-condensation, nucleosome loss and DNA mobility are additionally needed in response to DNA damage. This spatiotemporal regulation of chromatin is required in order to make the DSB accessible to the repair machinery allowing for DNA repair pathway engagement⁹⁻¹¹.

More specifically, it has been shown that nuclear compartmentalization influences DSB repair pathway choice. The eukaryotic nucleus is structured in chromosome territories and active and inactive compartments. While DSBs in the nuclear interior can be repaired by several pathways, some studies have shown that heterochromatin-associated regions are preferentially repaired by NHEJ¹²⁻¹⁴. On the other hand, it has been shown that pericentromeric heterochromatin breaks relocate to the nuclear periphery to complete repair by HR^{15,16}. Other studies show that replication stress foci and telomeric lesions display similar DNA mobility^{17,18}. Indeed, this could suggest that high compaction levels in heterochromatin may lead to difficulties in DNA repair. Importantly, CRISPR-Cas9 technology allows us to target specific chromatin domains and nuclear compartments to study differences in DSB repair dynamics.

Even though the importance of epigenetic changes and 3D genome dynamics during the DNA damage response has become clear, less is known about the reversal of these changes following completion of DNA repair. Reestablishing the original chromatin and 3D genome state is required to preserve (epi)genome integrity, but long-term retention of the DSB-induced chromatin changes could modulate gene expression and cell identity. In this study we show that a Cas9-induced DSB in the *ABCB1* gene, encoding for the P-glycoprotein (PgP) drug efflux pump, is able to transcriptionally activate this locus. PgP is a membrane transporter known to pump out different drugs, including Taxol. In RPE-1 cells, *ABCB1* is transcriptionally

inactive and found in a heterochromatin repressive environment, leading to a Taxol-sensitive phenotype. We found that upon break induction in the regulatory region of *ABCB1*, a subset of RPE-1 cells acquire Taxol resistance by upregulation of this gene. Furthermore, the *ABCB1* locus undergoes major 3D genome changes upon DSB induction, including relocalization to the nuclear interior. Interestingly, DSB-induced Taxol-resistant clones, which stably maintain *ABCB1* transcriptionally active, also reveal detachment from the Nuclear Lamina (NL). Further experiments confirm that even though some clones upregulate *ABCB1* through DSB-dependent genetic rearrangements, others may do it by DSB-induced 3D genome and chromatin changes. We hypothesize that DNA damage-dependent chromatin modifications are not always faithfully restored, and if so, they can lead to gene expression changes and cellular plasticity, ultimately leading to acquisition of a Taxol-resistant phenotype.

RESULTS

Induction of DSB in the *ABCB1* promoter leads to acquired Taxol-resistance

In order to understand whether a DSB could lead to epigenetic alterations at the damage site, consequently resulting in gene activation, we decided to introduce a DSB in a transcriptionally silent gene that we could easily select for when activated. In RPE-1 cells, *ABCB1* is found in a heterochromatic environment and transcriptionally repressed. As previously shown, in RPE-1 cells the Taxol-resistant phenotype is attributed to activation of the *ABCB1* gene^{19,20}. To investigate if a DNA lesion could result in de-repression of the *ABCB1* gene, we induced a DSB in the *ABCB1* regulatory region and subsequently added a lethal dose of Taxol to the culture medium to select for Taxol-resistant clones. *ABCB1* is transcribed from two promoters²¹. The majority of transcripts originates from the downstream or inner promoter²² while the upstream promoter, located 112kb upstream in the *RUNDC3B* gene, is active only in some cells^{23,24} (**Fig. 1A**). Therefore, we generated several synthetic CRISPR RNAs (crRNAs) targeting the inner promoter region (**Fig. 1A**). Cutting efficiency of the different *ABCB1*-crRNAs was calculated by TIDE analysis²⁵, demonstrating that all of the designed crRNAs were able to efficiently cut their respective target site, with indel frequencies ranging from 40-80% (**Fig. 1B**). Seven days after break induction, one million cells were plated for clonogenic assays in the presence of 20 nM of Taxol, after which colonies were allowed to grow out for 15 days. Strikingly, a DSB in the *ABCB1* promoter, regardless of the crRNA used, led to the formation of Taxol-resistant clones (**Fig. 1C and D**). In order to exclude that recruitment of Cas9, rather than break induction, is sufficient to open the *ABCB1* locus and trigger transcriptional activation, we generated a short crRNA derived from the *ABCB1* targeting crRNA #6. It has been previously shown that a crRNA of 15 nucleotides (nt) can localize Cas9 to the target site without inducing cleavage²⁶. Indeed, the 15-nt modified crRNA #6 did not yield Taxol-resistant colonies (**Sup. Fig. 1A and B**), confirming that a DSB is

needed to acquire Taxol resistance in RPE-1 cells. These data imply that de-silencing of the *ABCB1* can be induced by DNA lesions in the regulatory region of the gene. It should be noted, however, that less than one in 10,000 cells become Taxol-resistant, while cutting efficiencies range from 40-80%. This implies that repair of the lesion is associated with maintenance or restoration of the original repressed state, while in rare cases the repressed state cannot be maintained or restored. Therefore, we concluded that a CRISPR-Cas9-induced DSB in the regulatory region of *ABCB1* can lead to gene activation in a subset of cells, thus inducing Taxol resistance.

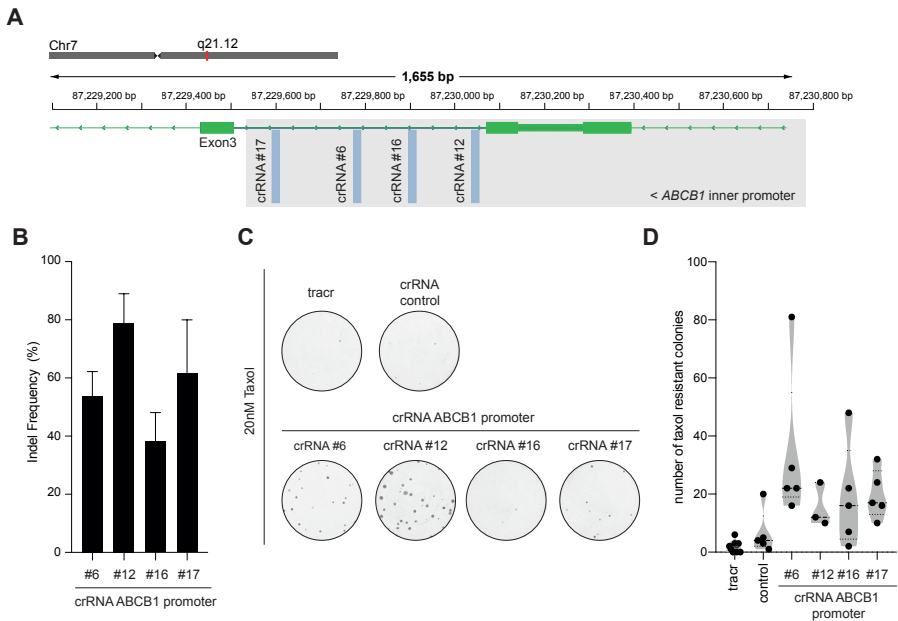


Figure 1. A DSB in the regulatory region of *ABCB1* induces Taxol-resistant colonies.

A) Graphical panel of the *ABCB1* regulatory region showing the locations of the crRNAs. **B)** Indel frequency determined by TIDE of crRNAs targeting *ABCB1*. **C)** Crystal violet staining of colony formation assay on RPE iCut cells with the different crRNAs targeting *ABCB1* under 20 nM Taxol. **D)** Quantification of number of Taxol-resistant colonies from C.

DSB-induced clones acquire Taxol resistance through *ABCB1* upregulation

In order to further characterize the Taxol-resistant clones produced through DSB-formation in the *ABCB1* promoter, we isolated and expanded several single colonies from the clonogenic assays belonging to crRNA #6 and #12. We kept these clones under constant Taxol selection (8 nM) for several weeks to ensure that we recovered Taxol-resistant lines. In order to examine the Taxol response of these clones, we performed viability assays with increasing doses of Taxol (**Fig. 2A** and **B**). Interestingly, we observed a variable level of resistance, with IC₅₀s varying from 10 nM to 60 nM depending on the clone (**Fig. 2B**). RT-qPCRs analysis confirmed that

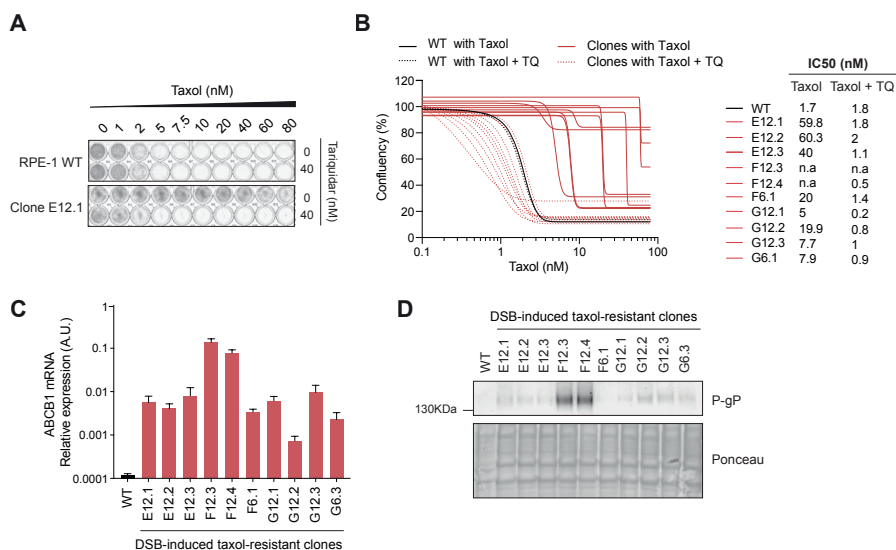


Figure 2. DSB-induced Taxol-resistant colonies upregulate ABCB1.

A) Crystal violet staining of proliferation assay of a Taxol-resistant clone derived from crRNA #12 and the parental cell line. **B)** Relative survival plots of **A** including other Taxol-resistant clones and the calculated IC50. **C)** ABCB1 mRNA levels determined by qRT-PCR and normalized to GAPDH expression levels. **D)** Western Blot of PgP in the different Taxol-resistant clones.

ABCB1 mRNA was upregulated in all the clones compared to the RPE-1 parental cell line (WT) (**Fig. 2C**). Also, levels of the drug efflux pump P-glycoprotein (PgP) encoded by the *ABCB1* gene, were upregulated in the resistant clones, as shown by western blot (**Fig. 2D**). The absolute expression levels of *ABCB1* mRNA and PgP protein differed within each clone, in line with the observed differences in IC50s across the various clones. Importantly, addition of Tariquidar (TQ), an inhibitor of PgP, restored Taxol sensitivity of all DSB-induced clones to levels observed in the parental RPE-1 cells (**Fig. 2A** and **B**). These data indicate that the Taxol resistance is entirely due to upregulation of the *ABCB1* gene, which is activated by DSB-formation in its promoter region.

To further characterize the transcriptional response of the *ABCB1* gene in the Taxol-resistant clones, we performed single-molecule smRNA FISH using fluorescently labelled DNA probes recognizing the intronic sequence of the *ABCB1* mRNA. Using these probes, we can visualize pre-mRNA molecules that are transcribed and spliced at the *ABCB1* locus. Since these probes only detect pre-mRNA, this method allows for quantification of the number of actively transcribed *ABCB1* alleles in the DSB-induced Taxol-resistant clones. All analyzed clones displayed an increased percentage of cells with active *ABCB1* transcription sites as compared to the parental RPE-1 cells (**Sup. Fig. 2A** and **B**). Even though the number of cells with active transcription sites of *ABCB1* varied between clones, the majority appear to only activate a single

ABCB1 allele. Interestingly, almost all analyzed cells from Clone F12.4, derived from crRNA #12 break induction, showed two active transcription sites (**Sup. Fig. 2A and B**). Altogether, this data demonstrate that RPE-1 cells can upregulate the *ABCB1* gene by DSB induction in its regulatory region leading to stable *ABCB1* transcription activation and a Taxol-resistance phenotype.

Genetic mutations and chromosome re-arrangements do not fully explain the DSB-induced Taxol-resistant phenotype

It is well described that genetic re-arrangements and DNA mutations can lead to *ABCB1* transcriptional activation²⁷⁻²⁹. In order to understand whether this was the mechanism of DSB-dependent gene re-activation, we set out to establish the genetic landscape of the DSB-induced Taxol-resistant clones. To further characterize the genetic background of the Taxol-resistant clones in more detail, we performed Targeted Locus Amplification (TLA) analysis. TLA allows robust detection of structural genetic re-arrangements such as gene fusions, translocations and deletions via selective amplification of a locus and its physically proximal sequences, similar to 4C-seq³⁰. With this method we found that in the majority of DSB-induced Taxol-resistant clones, *ABCB1* interacts with nearby regions close to its genomic location in chromosome 7, in a similar arrangement that is found in parental RPE-1 cells (**Fig. 3A**). However, Clone F12.4 showed a *de novo* interaction with a chromosome region megabases (Mb) downstream from the *ABCB1* locus (**Fig. 3A**, F12.4 red circle). A zoom-in in this region indicated that, in Clone F12.4 but not in parental RPE-1, *ABCB1* was interacting with the LINC-PINT locus, a highly expressed long intergenic non-coding RNA (**Sup. Fig. 3A and B**). smRNA FISH showed that this clone actively transcribes both *ABCB1* alleles (**Sup. Fig. 2A**). Of the other analyzed clones, none displayed signs of structural genetic rearrangements (**Fig. 3A**), indicating that other mechanisms must be driving the upregulation of PgP expression.

In order to assess whether *ABCB1* gene amplification in RPE-1 cells is sufficient to promote *ABCB1* upregulation and Taxol resistance, we performed Taxol-tolerance assays in a cell line with three copies of chromosome 7, where *ABCB1* is located. Strikingly, *ABCB1* amplification did not lead to increased mRNA levels or acquired Taxol-resistance (**Sup. Fig. 3C-E**). This suggests that in order for RPE-1 cells to activate transcription of *ABCB1* (hence acquire Taxol-resistance), a modification of its chromatin landscape is needed rather than accumulating increased copies of *ABCB1*. We also evaluated whether the DSB-induced Taxol-resistant clones had the *ABCB1* gene amplified by genomic DNA quantitative PCR. We observed that all clones had comparable genomic transcript levels to the parental cell line when assessing the *ABCB1* locus (**Sup. Fig. 3F**), confirming that only two copies of *ABCB1* were present in these cells.

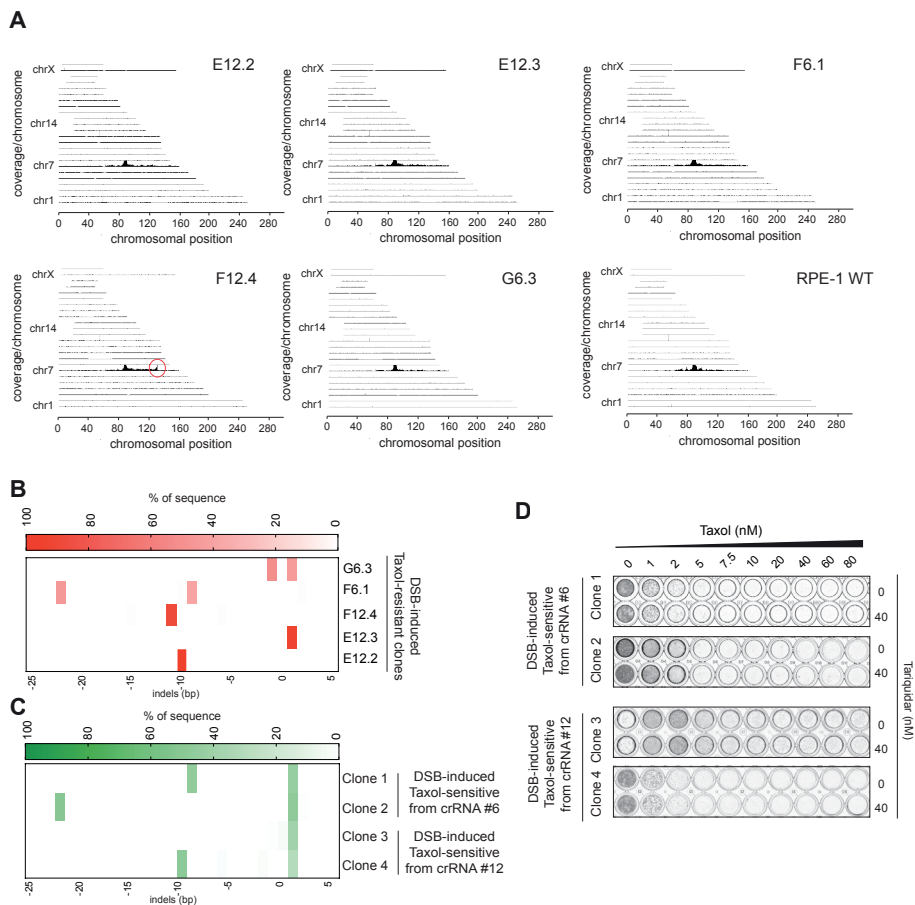


Figure 3. Genetic alterations and chromosome re-arrangements do not fully explain the DSB-induced Taxol-resistant phenotype.

A) Genome-wide TLA coverage plot showing all chromosomes in Taxol-resistant clones and parental cell line. Red circle shows a genetic re-arrangement. **B)** Heat map of TIDE analysis showing the indel frequency in each Taxol-resistant clone. 100% refers to all alleles having the same indel while 50% means that the alleles have different indels. **C)** Heat map of TIDE analysis showing the indel frequency in the Taxol-sensitive clones generated from crRNA #6 and crRNA #12. **D)** Crystal violet staining of proliferation assay on a Taxol-sensitive clone derived from crRNA #6 and crRNA #12.

We next used TIDE analysis to assess the mutation pattern of these clones at the DSB site³¹ and observed a variety of insertions and deletions, when assessing five different DSB-induced Taxol-resistant clones. For example, Clone G6.3 had a 1nt deletion in one allele and 1nt insertion in the other allele (**Fig. 3B**). Interestingly, F12.4 and E12.2 clones showed homozygous deletions of 11nt and 10nt respectively. In order to determine whether these indels could lead to transcriptional activation

of the *ABCB1* gene, we generated RPE-1 cells with similar indels in the same DSB location (**Fig. 3C**). Even though Clone 1 and Clone 2 had the same 9nt and 22nt deletions as F6.1 and G6.3, they did not acquire a Taxol-resistant phenotype (**Fig. 3C and D**). Similarly, Clone 4 had a 10nt deletion similar to the resistant clone E12.2, yet it was sensitive to Taxol (**Fig. 3B-D**). These data suggest that the small indels generated during CRISPR-Cas9-mediated DSB formation and repair in the *ABCB1* locus do not *per se* lead to *ABCB1* gene activation. However, we cannot rule out that the generated indels could destabilize the repression of the gene leading to gene activation in a subset of cells. Yet, we speculate that there could be genetic and non-genetic drivers of Taxol resistance in these clones.

DSB-induced Taxol-resistant clones exhibit changes in chromatin and 3D organization

We have previously revealed that RPE-1 cells that spontaneously acquire Taxol-resistance display alterations in the chromatin landscape surrounding the *ABCB1* locus²⁰. We showed that heterochromatic marks are lost at the *ABCB1* promoter region, in exchange for an enrichment of euchromatic histone modifications²⁰. Interestingly, others have reported that the chromatin landscape surrounding a DNA lesion is altered during DSB repair, in order to ensure accessibility to the damaged region⁹. This suggests that DSB-induced transcriptional activation of the *ABCB1* gene could be a consequence of a failure to restore chromatin compaction and repressive chromatin marks following completion of repair. Therefore, we set to study whether the DSB-induced Taxol-resistant clones also altered the chromatin landscape at the *ABCB1* locus. For this analysis we focused on the clones for which a non-genetic mechanism was likely driving enhanced gene expression (E12.2, G12.3, F6.1 and G6.3). ChIP-qPCRs for 5-methylcytosine (5-mC) showed an overall decrease in DNA methylation levels in the DSB-induced Taxol-resistant clones compared to RPE-1 WT (**Fig. 4A and B**). Given that only one allele of *ABCB1* is activated in the clones, we do not expect a total loss of DNA methylation. DNA methylation levels in region 1 were only reduced in Clone F12.4, but we observed a clear reduction in DNA methylation levels in region 2 of the *ABCB1* promoter in all of the clones (**Fig. 4B**). ChIP-qPCRs for the active chromatin mark H3K4me3 showed that all DSB-induced Taxol-resistant clones contain increased levels of H3K4me3 in both regions of the *ABCB1* promoter (**Fig. 4C**).

We next determined if there were any changes in the 3D genome organization of the *ABCB1* locus in the resistant clones that could contribute to gene activation. It is known that the Nuclear Lamina (NL) is associated with transcriptional gene repression³²⁻³⁴. Interestingly, we have previously shown that in Taxol-resistant cells, *ABCB1* shows a decrease in NL contacts and this is directly associated with *ABCB1* gene activation^{20,33}. Indeed, pA-DamID showed that Clone F6.1 and G6.3, both

obtained after DSB-induction with crRNA #6, display a clear decrease in *ABCB1* NL contacts compared to RPE-1 WT (**Fig. 4D**). This decreased NL interaction was not

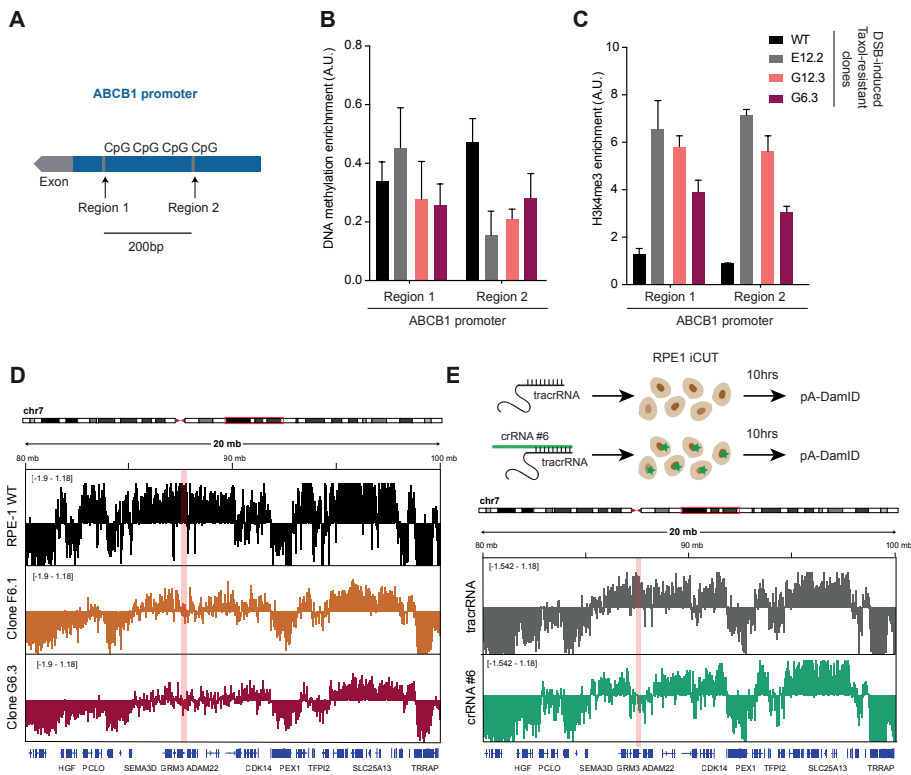


Figure 4. DSB-induced Taxol-resistant clones exhibit changes in chromatin and 3D organization.

A) Graphical representation of the *ABCB1* promoter and the first transcribed exon. CpG refers to CpG islands that can be methylated. Arrows show the locations where qPCR primers from B and C bind to and the distance between them. **B)** DNA methylation IP (MeDIP) qPCR in Taxol-resistant clones compared to WT in two regions of the *ABCB1* promoter. **C)** ChIP-qPCR of H3k4me3 in Taxol-resistant clones and WT cell line. **D)** Change in NL interactions in two Taxol resistant clones compared to WT analyzed by DamID. Positive values indicate NL interactions, negative values indicate NL detachment. Red: *ABCB1* genomic region. **E)** Graphical representation of the time line of crRNA #6 transfection in RPE-1 iCut cells and DSB induction. 10h post-crRNA transfection cells were harvested for pA-DamID. **F)** Change in NL interactions in RPE-1 iCut cells 10h post-transfection with crRNA #6 compared to tracrRNA analyzed by DamID.

limited to the *ABCB1* locus (**Fig. 4D, red line**) but spread ~10 Mb from the break point. This detachment could either be an (in)direct consequence of gene activation, or inversely, NL detachment during DSB repair could allow for gene activation. We therefore wanted to investigate if this observed detachment from the NL already

occurs during *ABCB1* DSB induction and repair. To this end we transfected RPE-1 cells with the *tracrRNA* or the hybrid *tracrRNA:crRNA#6* targeting *ABCB1*. We next performed pA-DamID at 10h after crRNA transfection, when we expected DSB repair to be in progress (**Fig. 4E**). We observed a remarkable detachment of the *ABCB1* locus from the NL (**Fig. 4E, red line**) in cells exposed to crRNA#6, while transfection of the control *tracrRNA* maintained *ABCB1* in close contact with the NL. Importantly, the size of the detachment differed between the 10hrs crRNA transfection and the Taxol-resistant clones. This demonstrates that DSB formation in this NL-associated locus results in displacement away from the NL. We speculate that this occurs during repair and could lead to a failure to re-store the initial pre-DSB genome organization that could subsequently lead to gene activation and the formation of DSB-induced Taxol-resistant clones.

Inhibition of NHEJ during *ABCB1* DSB repair can boost the amount of developing Taxol-resistant clones

It has been previously reported that DSBs in heterochromatic regions can only engage in HR after they have moved out of the heterochromatin domain^{15,35}. This re-localization is thought to prevent recombination of repetitive sequences that are enriched in heterochromatic regions, thus preventing unwanted genetic rearrangements. In order to force RPE-1 cells to repair the DSB by HR we inhibited DNAPK, a protein involved in NHEJ, at the time of DSB induction. After seven days of DSB induction and repair, we performed clonogenic assays under Taxol selection. We observed a trend in increase Taxol-resistant colonies when DNAPK was inhibited during DSB repair (**Fig. 5A and B**). However, depletion of Mre11, a protein involved in DSB end-resection, and DNAPK by small interference RNA (siRNA) did not show a clear decrease and increase in the number of Taxol-resistant colonies respectively (**Sup. Fig. 4A-C**).

While the NHEJ repair pathway generates small insertions and deletions in the break site, other resection-dependent pathways either yield deletions (MMEJ), and perfect repair (HR). In order to understand the effect of DNAPK inhibition on the different pathways, we performed TIDE analysis in a polyclonal population three days after break induction. Indeed, we found that DNAPK inhibition led to a decrease in the frequency of 1nt insertions (associated with NHEJ) and an increase in longer deletions (associated with MMEJ), or no alteration (0, representing either uncut sequences or a product of HR) (**Fig. 5C**). This confirms that DNAPK inhibition results in preferential repair of DSBs by HR or MMEJ, both resection-dependent pathways of repair. In order to further characterize the resulting Taxol-resistant cells, we isolated and expanded colonies from both the DMSO- and DNAPKi-treated clonogenic assays. Viability assays indicated that these clones were resistant to Taxol and re-sensitized to Taxol upon inhibition of PgP with Tariquidar (**Fig. 5D**). Interestingly, the DSB break

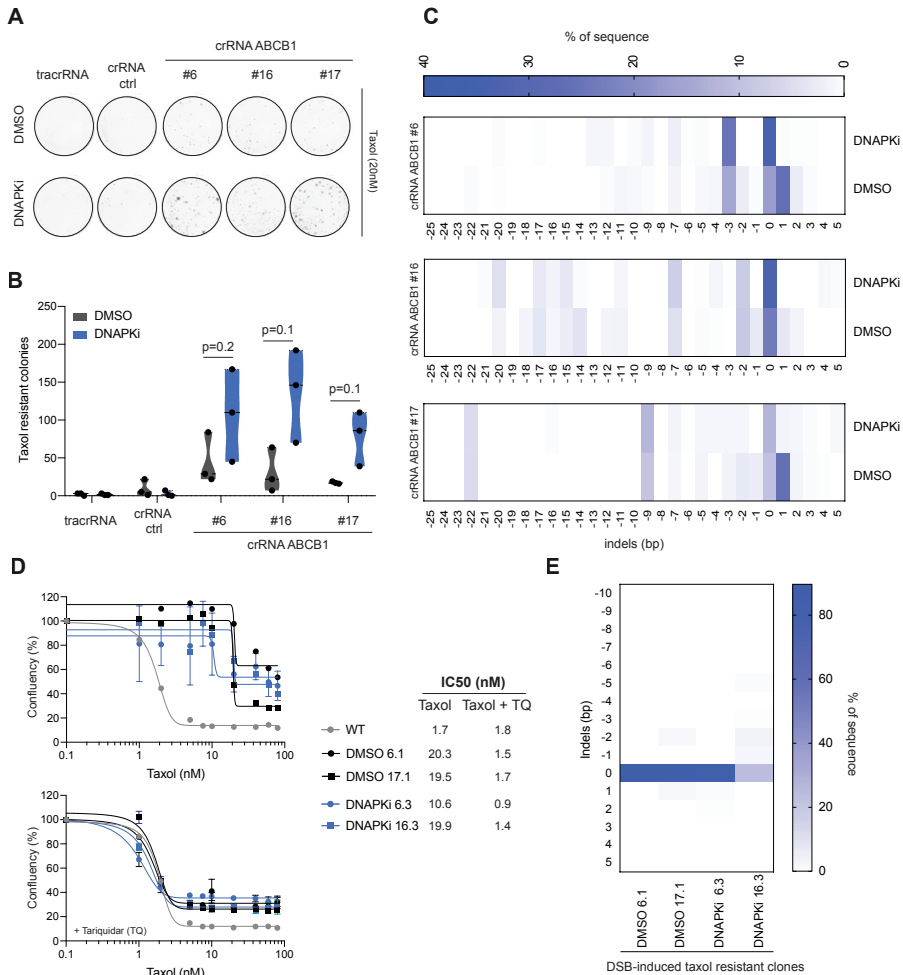


Figure 5. Inhibition of NHEJ during ABCB1 DSB repair can boost the formation of Taxol-resistant clones.

A) Crystal violet staining of colony formation assay on RPE iCut cells with the different crRNAs targeting ABCB1 under 20 nM Taxol treated with DMSO or DNAPKi during DSB induction. **B)** Quantification of number of Taxol-resistant colonies from A. p-values analyzed from Mann-Whitney test comparing DMSO vs DNAPKi. **C)** Heat map of TIDE analysis showing the indel frequency in DMSO- or DNAPKi-treated cells from a 72h post-break induction. Polyclonal population of cells transfected with crRNA #6, #16 and #17 are shown. **D)** Relative survival plots of Taxol-resistant clones obtained from A and the calculated IC50. **E)** Heat map of TIDE analysis showing the indel frequency in the Taxol-resistant clones obtained from A.

sites in these clones appeared to be perfectly repaired, presumably by HR, as TIDE analysis revealed that the DNA sequence showed no signs of indels (**Fig. 5E**).

Relocalization of heterochromatin DSBs occurs by directed motion along nuclear actin filaments (F-actin)^{36–38}. In order to understand whether F-actin was driving *ABCB1* transcriptional activation and acquisition of drug resistance, presumably by driving *ABCB1* detachment from the NL, we made use of the F-actin polymerization inhibitor CK-666. We induced a DSB in *ABCB1* in the presence or absence of CK-666, followed by clonogenic assays in the presence of 20 nM Taxol. While TIDE analysis showed no major changes in the indel pattern of these DSBs (**Sup. Fig. 4D**), a reduction, even though not significant, in the number of Taxol-resistant colonies was observed (**Sup. Fig. 4E and F**).

Based on these data, we propose a model where *ABCB1* re-localization from the NL during DSB repair allows for epigenetic reprogramming of the locus, eventually leading to de-repression of the locus in a subset of cells. Possibly, F-actin could drive this re-localization as its depletion decreases the ability of these cells to acquire Taxol-resistance.

DISCUSSION

In this study we show that the induction of a DSB in the *ABCB1* promoter region can lead to gene activation and the acquisition of Taxol-resistance in RPE-1 cells. We confirmed that *ABCB1* is upregulated in the DSB-induced resistant clones and drives the resistance phenotype. We could show that in a subset of the clones, genetic rearrangements gave rise to *ABCB1* upregulation and consequently Taxol-resistance. However, in the majority of clones, we did not find any evidence of genetic mutations or rearrangements that could explain the re-activation of the *ABCB1* gene. Here we hypothesize that changes in histone modifications and the 3D genome alterations that take place during the course of damage induction and repair could play a role in *ABCB1* gene re-activation. In support of such a model, we show that the *ABCB1* gene detaches from the NL during the DDR response. This displacement could go hand in hand with a decrease in DNA methylation and repressive histone marks that could arise as a consequence of DNA resection. Resection can directly remove methylated cytosines, and could result in the displacement of nucleosomes. We speculate that NL detachment is needed in order to repair the *ABCB1* locus by HR outside of the heterochromatin domain, while resection could trigger epigenetic reprogramming. Interestingly, F-actin could play a role in facilitating the re-localization of the *ABCB1* locus (**Fig. 6**).

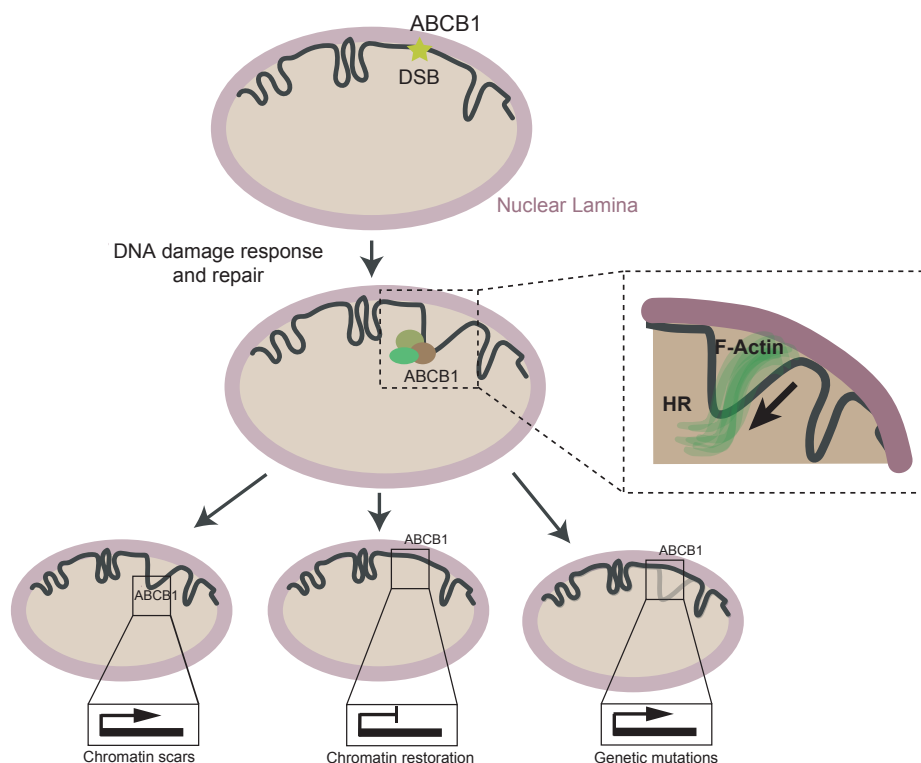


Figure 6. DNA damage-dependent chromatin dynamics as a potential cause of acquired Taxol-resistance.

When a DSB occurs in the regulatory region of ABCB1, this gene detaches from the Nuclear Lamina (NL) in order to complete DNA repair. We hypothesize that this re-localization is needed to perform HR and may be driven by F-actin. Once repair is completed, the majority of cells restore the original 3D genome organization with ABCB1 in the NL, keeping transcription repressed. Other cells undergo genetic re-arrangements in ABCB1 leading to transcriptional activation. We hypothesize that a third group of cells are not able to restore the DNA-damage induced chromatin modifications and NL displacement creating a chromatin 'scar', which allows ABCB1 to activate.

DNA breaks in the ABCB1 promoter region leading to genetic mutations and re-arrangements

Repair of a DNA lesion does not always occur error-free, resulting in point-mutations, deletions or translocations. We observe a variety of these events in our DSB-induced ABCB1 system. We show that a DSB in the ABCB1 promoter can lead to fusions with distant genomic regions. If this fusion takes place with a highly active regulatory region, this can lead to ABCB1 transcriptional activation. Interestingly, it has been reported that ovarian cancer patients could acquire Taxol-resistance by fusing the ABCB1 promoter with the highly active SLC25A40 promoter, a gene 100Kb away

from *ABCB1*²⁹. Other DSB-induced Taxol-resistant clones without evident gene fusions displayed homozygous indel patterns at the break site (**Fig. 3B**, E12.3 E12.2). It is unlikely that with all possible indel outcomes both alleles acquire the same mutation. We believe that other genetic re-arrangements undetectable by TIDE could be arising. Using TLA, we were able to identify clones in which a translocation occurred, versus clones in which only small indels were induced. In this former clone the *ABCB1* gene was brought in close proximity to a highly expressed long intergenic non-coding RNA. However, in other clones we were unable to identify genetic events other than small indels in the *ABCB1* promoter region, measured by TIDE. By generating independent clones with similar indels, we show that these indels themselves are unable to induce transcriptional activation in the overall cell population. However, we can reason that these genetic mutations could still increase the chance of gene de-repression, by for example, decrease the binding affinity of a repressive transcription factor. In order to test this possibility, we should perform Taxol colony formation assays in the indel-generated clones.

NL detachment during DSB repair

Chromatin undergoes major alterations during DNA damage induction and repair. Some of these changes are required for binding of components of the repair machinery, others are required to make the damage accessible for repair^{7,39-41}. In addition, resection-dependent repair can cause the displacement of nucleosomes and the removal of methylated cytosines, which altogether shape the chromatin landscape of a locus^{42,43}.

It has been shown by many researchers that DNA lesions are highly dynamic and can undergo directional movements within the cell nucleus^{44,45}. Particularly, DSBs occurring in heterochromatin need to move away from this compartment in order to undergo HR-mediated repair^{15,46}. This is because the repair protein Rad51 can only be recruited to the lesion outside of heterochromatic regions^{15,35}. In line with this, binding of HR proteins is reduced upon artificial tethering of a locus to the NL¹³. If the locus remains associated with the NL, HR repair proteins might not have access to the lesion, and it will have to be repaired by NHEJ.

Strikingly, our pA-DamID experiments show that *ABCB1* detaches from the NL during DNA repair. Nuclear actin polymerization has been shown to be required for DNA mobility during DNA damage^{36,38,47}. Our preliminary experiments argue that inhibition of actin polymerization by CK-666 inhibits DSB-induced upregulation of the *ABCB1* gene. It would be very interesting to test whether perturbations of F-actin polymerization could interfere with *ABCB1* NL detachment.

NL detachment of the *ABCB1* locus suggests that a significant fraction of the DSBs which are made in the promoter region of *ABCB1* are repaired via HR. Additionally, we observe an increase in DSB-induced Taxol-resistant colonies when DNA-PK is inhibited, causing more breaks to be repaired via HR. Based on these observations

we propose that NL detachment and subsequent HR prime the *ABCB1* locus for transcriptional activation.

Interestingly, several investigations have shown a role for the heterochromatin protein 1 (HP1) in promoting HR⁴⁸⁻⁵¹. However, movements of HP1-rich regions of the chromatin during damage and repair have not been studied, so it is unclear if these also detach from the NL during DNA repair. Possibly, HP1 is needed to promote NL detachment, and in this way stimulates HR repair.

Chromatin dynamics leading to *ABCB1* upregulation

Apart from the clones showing gene re-arrangements, the other DSB-induced Taxol-resistant clones did not show any evidence of genetic alterations that could explain the upregulation of the *ABCB1* gene. However, our data clearly show that the DSB induction is necessary for *ABCB1* re-activation and the acquisition of Taxol-resistance. Thus, in these latter clones, the upregulation of *ABCB1* has likely occurred via a non-genetic alteration. We hypothesize that the changes that happen to the chromatin during repair of the double-stranded lesion are causal to *ABCB1* transcription activation. Two other studies have suggested that chromatin modifications that are acquired during DNA replication stress or DNA repair can be stably inherited and can lead to changes in gene expression^{52,53}. However, both of these earlier studies were performed using an exogenous reporter locus. Here we show that permanent epigenetic alterations can also occur on endogenous loci. Furthermore, we show that not only histone modifications, but also 3D genome organization can be dysregulated in response to DNA damage.

It is known that *ABCB1* gene expression is associated with NL detachment^{20,33}. We show that the *ABCB1* gene detaches from the NL during repair, and is detached from the NL in some of the DSB-induced Taxol-resistant clones. While this does not formally prove that both observations are causally linked, it is tempting to speculate that the histone modifications and 3D genome changes observed in the Taxol-resistant clones were established during the DSB induction and were not restored after repair was completed. This could have caused the de-repression of the *ABCB1* gene, leading to its transcriptional activation and acquisition of the Taxol-resistant phenotype.

Epigenetic scars: epigenome integrity vs. plasticity

Our data imply that repair of a double-stranded DNA lesion can lead to an epigenetic 'scar' that results in the reprogramming of a gene from repressed to active. Our clonogenic assays allow us to calculate the frequency at which the *ABCB1* gene switches states after a DNA lesion is inflicted in its promoter region. We find that chromatin-dependent re-activation of *ABCB1* is still a rare event (~1:10.000). This implies that in the majority of cases the chromatin landscape and 3D genome

organization is faithfully restored during repair, ensuring that the *ABCB1* gene is maintained in a repressed state. This indicates that epigenome integrity is most often maintained during DNA repair. Yet, how restoration of the initial chromatin state is regulated is still a matter of debate. Interestingly, it has been suggested that upon DNA damage, a damaged scar with altered epigenetic marks could persist on chromatin, therefore regulating gene expression¹⁰. Here we show that this can indeed happen, but at a very low frequency. This raises two intriguing questions; how is the original chromatin state restored in the majority of cases, and how does a ‘scar’ arise in a minority of cases.

These observations could prove important in light of tumor evolution. Possibly, epigenetic ‘scars’ that arise from ongoing DNA damage on chromatin could result in epigenetic heterogeneity that could have relevant consequences in the pathogenic context. Indeed, we show that epigenetic activation of the *ABCB1* locus occurs following a DNA lesion in its promoter region, and can trigger drug resistance. Given the high number of cancer patients exposed to genotoxic treatments, as well as the ongoing replicative stress in a tumor, epigenetic ‘scars’ could be responsible for a high level of tumor heterogeneity in the clinical context. Thus, further work is warranted to fully understand the role of DNA damage-dependent chromatin changes and its contribution during tumor evolution.

MATERIALS AND METHODS

Cell lines and cell culture conditions

hTert-immortalized retinal pigment epithelium (RPE-1) and derived cell lines were maintained in DMEM/F-12 + Glutamax (Gibco, Life Technology) Supplemented with 1% penicillin/streptomycin and 6% fetal bovine serum (FBS, S-FBS-EU-015, Serana). DSB-induced Taxol-resistant clones were grown under 8 nM Taxol.

Drug treatments

Drugs were dissolved in DMSO and prepared at stock concentrations before usage at varying final concentrations as indicated in each Figure. For the DNAPK inhibitor (M3814), a final concentration of 1 mM was used. For Arp2/3 inhibitor (CK-666) a final concentration of 400 nM was used. For Tariquidar, a final concentration of 40 nM was used.

tracrRNA:crRNA design and transfections in RPE-1 iCut

ABCB1 crRNAs were generated by Integrated DNA technologies. Specific sequences are found in **Supplementary Table 1**. tracrRNA:crRNA duplex was transfected according to the manufacturer’s protocol⁵⁴.

siRNA transfections

ON-TARGETplus SMARTpool set of four siRNAs targeting Mre11 and DNAPK were from Dharmacon and were transfected using RNAiMAX (Life Technologies) according to manufacturer's protocol⁵⁴ at a final concentration of 20 nM. All transfections were performed 48h before experiment, if not specified on the Figure legend.

Colony Formation Assays (CFAs) with Taxol

Seven days prior to CFAs, RPE-1 iCut cells were transfected with a specific crRNA. 24h later, the transfection was washed and cells were expanded. 1×10^6 cells were treated with indicated doses of Taxol and allowed to grow out for 15 days under drug selection in 15-cm dishes. Plates were fixed in 80% Methanol and stained with 0.2% Crystal Violet solution.

Viability assays

For viability assays, 1×10^3 cells were plated in a 96-well plate and treated for seven days with indicated drug concentrations. Subsequently, plates were fixed in 80% Methanol and stained with 0.2% Crystal Violet solution. IC₅₀ was calculated from the log(inhibitor) vs response equation $Y = Bottom + (Top - Bottom) / (1 + 10^{-(X - LogIC_{50})})$.

RNA isolation and qRT-PCR analysis

RNA isolation was performed by using Qiagen RNeasy kit and quantified using NanoDrop (Thermo Fisher Scientific). cDNA was synthesized using Bioscript reverse transcriptase (Bioline), Random Primers (Thermo Fisher), and 1000 ng of total RNA according to the manufacturer's protocol. Primers were designed with a melting temperature close to 60 degrees to generate 90–120-bp amplicons, mostly spanning introns. cDNA was amplified for 40 cycles on a cycler (model CFX96; Bio-Rad Laboratories) using SYBR Green PCR Master Mix (Applied Biosystems). Target cDNA levels were analyzed by the comparative cycle (Ct) method and values were normalized against GAPDH expression levels. qRT-PCR oligo sequences are summarized in **Supplementary Table 2**.

Western Blot

For western blot experiments, equal amounts of cells were lysed with Laemmli buffer and separated by SDS–polyacrylamide gel electrophoresis followed by transfer to a nitrocellulose membrane. Membranes were blocked in 5% milk in PBS/0.1% Tween-20 (PBST) for 1h at RT before overnight incubation with primary antibody in PBST with 3% milk at 4°C. Membranes were washed three times with PBST followed by incubation with secondary antibody in PBST with 5% milk for

2h at RT. Antibodies were visualized using enhanced chemiluminescence (ECL) (GE Healthcare). The following antibodies were used for western blot experiments: MDR1/PgP (Santa Cruz, sc-8312), MRE11 (Genetex, GTX70212), DNAPK (Santa Cruz, sc9051). For secondary antibodies, peroxidase-conjugated goat anti-rabbit (P448 DAKO, 1:2000), goat anti-mouse (P447 DAKO, 1:2000) and rabbit anti-goat (P449 DAKO, 1:2000) were used.

Single-molecule RNA FISH

RPE-1 cells were plated on glass coverslips and washed twice with 1x PBS before fixation in 4% PFA in PBS for 10 minutes at RT. After two additional washes in 1x PBS coverslips were incubated in 70% ethanol at 4°C overnight. Coverslips were incubated for pre-hybridization in wash buffer (2x saline-sodium citrate (SSC) with deionized formamide (Sigma) 10%) for 2-5 minutes at RT. RNA FISH probe mix wash dissolved in hybridization buffer (wash buffer Supplemented with 10% dextran sulfate). 38 probes labelled with Cy5 were targeted to the intronic regions of ABCB1 (Biosearch technologies). Coverslips were incubated in hybridization solution for at least 4h at 37°C. Then coverslips were washed twice for 30 minutes with wash buffer followed by a quick rinse with 2x SSC. Finally, coverslips were washed once for 5 minutes in 1x PBS before mounting on slides using Prolong gold DAPI mounting medium (Life Technologies). Images were acquired with the use of a DeltaVision Elite (Applied Precision) equipped with a 60x 1.45 numerical aperture (NA) lens (Olympus) and cooled CoolSnap CCD camera. ABCB1 transcription start site quantification was performed manually double blind.

ChIP-sequencing of RPE-1 hTERT cells

Chromatin immunoprecipitations (ChIP) were performed as described previously⁵⁵ with minor adjustments. For ChIP of histone marks, approximately 7×10^6 cells, 50 μ L of Protein A magnetic beads (Invitrogen) and 5 μ g of antibody (H3K4me3 (Abclonal, A2357 and 5-methylcytosine (ab10805)). For ChIP-seq, samples were processed for library preparation (Part# 0801-0303, KAPA Biosystems kit), sequenced using an Illumina Hiseq2500 genome analyzer (65bp reads, single end) and aligned to the Human Reference Genome (hg19) using Burrows-Wheeler Aligner (bwa) version 0.5.9. Mapped reads were filtered based on mapping quality of 20 using samtools version 0.1.19. For ChIP-qPCR analysis, DNA was amplified for 40 cycles on a cycler (model CFX96; Bio-Rad Laboratories) using SYBR Green PCR Master Mix (Applied Biosystems). Target DNA levels were analyzed by the comparative cycle (Ct) method and values were normalized against input DNA and positive control region (specific for each chromatin mark). ChIP-qPCR oligo sequences are summarized in **Supplementary Table 2**.

RNA-sequencing

Total RNA from cultured cells was extracted using RLT (Qiagen). Strand-specific libraries were generated using the TruSeq PolyA Stranded mRNA sample preparation kit (Illumina). In brief, polyadenylated RNA was purified using oligo-dT beads. Following purification, the RNA was fragmented, random-primed and reverse transcribed using Sup.erScript II Reverse Transcriptase (Invitrogen). The generated cDNA was 3' end-adenylated and ligated to Illumina Paired-end sequencing adapters and amplified by PCR using HiSeq SR Cluster Kit v4 cBot (Illumina). Libraries were analyzed on a 2100 Bioanalyzer (Agilent) and subsequently sequenced on a HiSeq2000 (Illumina). We performed RNAseq alignment using TopHat 2.1.1. Differentially expressed genes were called with DEseq2, with an adjusted p-value threshold of 0.05.

Copy number variation analysis

Detailed description of the methods used for CNV can be found on⁵⁶.

Determination of nucleotide insertions and deletions by TIDE

TIDE analysis was performed as previously described³¹.

TLA analysis

TLA was performed as previously described with minor modifications³⁰. TLA libraries were sequenced on a MiSeq and were analyzed with a custom TLA mapping pipeline. TLA ligation data were mapped to hg19. Normalization and downstream analysis were done using peakC16.

DamID-seq

DamID-seq was performed as described⁵⁷ with minor modifications. Dam fused to human LMNB1 protein (Dam-LMNB1) or unfused Dam were expressed in cells by lentiviral transduction⁵⁸. Three days after infection, cells were collected for genomic DNA (gDNA) isolation. gDNA was pre-treated with SAP (10 U, New England Biolabs #M0371S) in CutSmart buffer in a total volume of 10 μ L at 37°C for 1h, followed by heat-inactivation at 65°C for 20 min to suppress signal from apoptotic fragments. This gDNA was then digested with DpnI (10 U, New England Biolabs #R0176L) in CutSmart buffer in a total volume of 10 μ L at 37°C for 8h followed by heat inactivation at 80°C for 20 min. Fragments were ligated to 12.5 pmol DamID adapters using T4 ligase (2.5 U, New England Biolabs ##) in T4 ligase buffer in a total volume of 20 μ L incubated at 16°C for 16h. The reaction was heat-inactivated for 10 minutes at 65°C. Products were then digested with DpnII to destroy partially

methylated fragments. DpnII buffer and DpnII (10 U, New England Biolabs #R0543L) were added in a total volume of 50 μ L and incubated at 37 °C for 1 h. Next, 8 μ L of DpnII-digested products was amplified by PCR with MyTaq Red Mix (Bioline #BIO-25044) and 1.25 μ M primers Adr-PCR-Rand1 in a total volume of 40 μ L. PCR settings were 8 min at 72°C (1 \times) followed by 20 s at 94°C, 30 s at 58°C, 20 s at 72°C (24 \times for Dam, 28 \times for Dam-LMNB1 samples) and 2 minutes at 72°C (1 \times). Remaining steps were performed as previously described. Samples were sequenced on an Illumina HiSeq2500.

Processing of RPE-1 DamID data

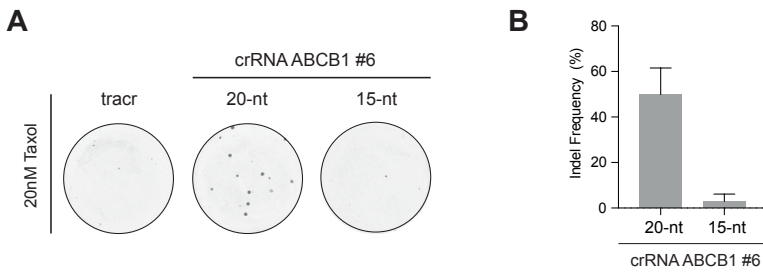
DamID-seq was performed as described in ³³.

Supplementary Table 1 – crRNA for *ABCB1* DSB induction

	Target Sequence
crRNA #6	CCTCCCGGTTCCAGTCGCCG
crRNA #6 short	CGGTTCAGTCGCCG
crRNA #16	GAGCAGCGCCCAAACCGTAG
crRNA #17	CTGCTCTCTGGCTTCGACGG
crRNA Control (chr3.2)	CGTTTCATGGGCACTATTGC

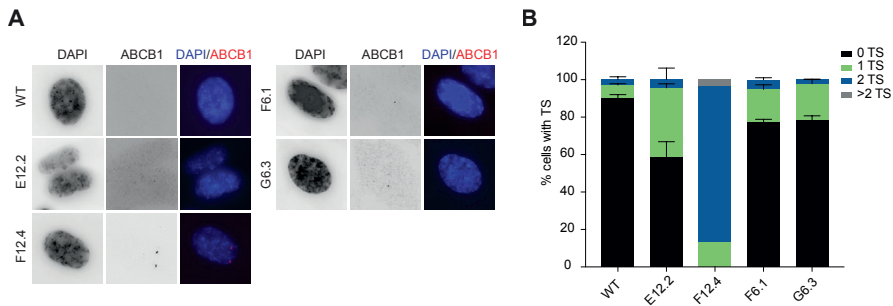
Supplementary Table 2 – RT-qPCR and ChIP-qPCR primers

RT-qPCR Primers	FWD	REV
ABCB1 P1	GGAGGCCAACATACATGCCT	GCTGTCTAACAAGGGCACGA
ABCB1 P2	ACAGCACGGAAGGCCTAATG	GTCTGGCCCTTCTCACCTC
GAPDH	TGCACCACCAACTGCTTA	GGATGCAGGGATGATGTTT
ChIP-qPCR Primers	FWD	REV
H3K4me3 positive control (XBP1)	TCTCTGGGCTGGCACCAT	GCGGTGCGTAGTCTGGAG
5-mC positive control (OCT4)	cagagtagggtgggaaagca	ttccaaaagcctgtgatgc
ABCB1_Region1_P3	GGTCCCTTCAAGATCCATTC	CCTTTACTGCTCTCTGGCTTC
ABCB1_Region2_MSPI	GGGTCTCCAGCATCTCCAC	GTGGGTGGGAGGAAGCATC



Supplementary Figure 1. A DSB in the regulatory region of *ABCB1* induces Taxol-resistant colonies.

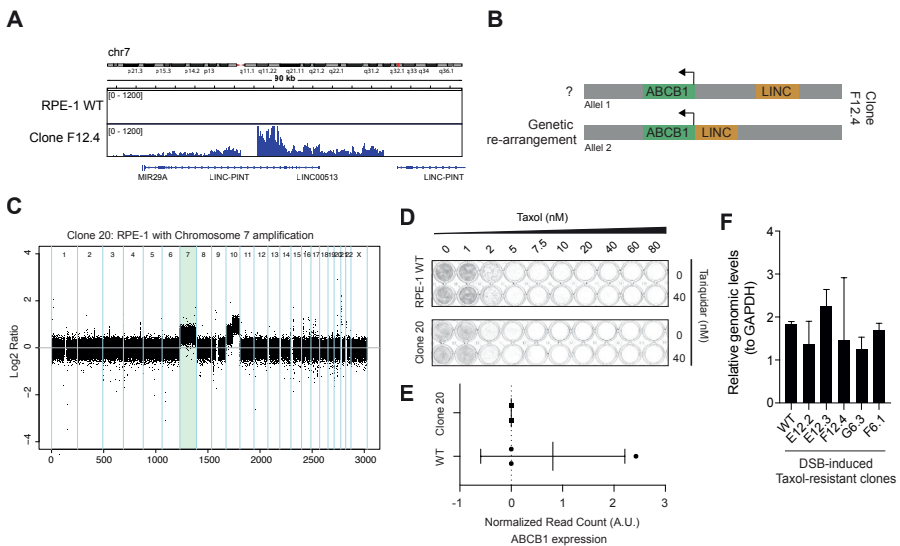
A) Crystal violet staining of colony formation assay on RPE iCut cells with the short and long version of crRNA #6 targeting *ABCB1* under 20 nM Taxol. **B)** Cutting efficiency determined by TIDE of crRNA #6 short and long targeting *ABCB1*.



Supplementary Figure 2. DSB-induced Taxol-resistant colonies upregulate *ABCB1*.

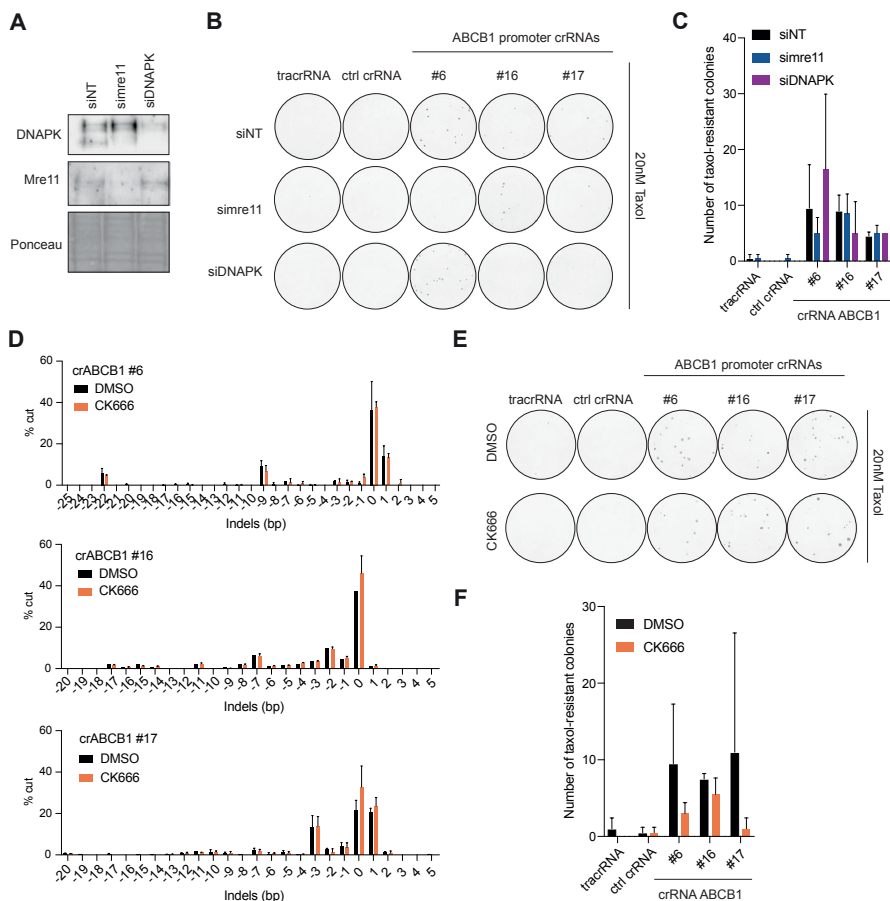
A) Representative smRNA-FISH images of Taxol-resistant clones and parental cell line for the *ABCB1* gene and DAPI. **B)** Quantification of the number of *ABCB1* transcription sites (TS) found per cell in the different Taxol-resistant clones.

DNA damage-dependent chromatin dynamics leading to Taxol resistance



Supplementary Figure 3. Genetic alterations and chromosome re-arrangements do not fully explain the DSB-induced Taxol-resistant phenotype.

A) TLA analysis of the *ABCB1* gene in RPE-1 parental cells and the Taxol-resistant clone F12.4. TLA coverage shows *de novo* interactions in F12.4 with the LINC-PINT locus. **B)** Graphical representation of the two alleles from Clone F12.4. Both alleles are transcriptionally active as shown by smRNA FISH. One of them having *de novo* re-arrangement and the other unknown. **C)** Copy number analysis showing all chromosomes in RPE-1 cells (Clone 20). Chromosome 7, with one extra copy, is highlighted in green, where *ABCB1* is found. **D)** Crystal violet staining of viability assay on Clone 20 from C and RPE-1 parental cells. **E)** RNA sequencing data showing the normalized read counts of the *ABCB1* gene in WT vs Clone 20 from C. **F)** gDNA levels relative to GAPDH calculated by qPCR in RPE-1 WT cells and the DSB-induced Taxol-resistant clones to show no amplifications.



Supplementary Figure 4. DSB-induced Taxol-resistant clones exhibit changes in chromatin and 3D organization.

A) Western Blot of DNAPK and Mre11 proteins upon 72h post siRNA transfection with non-targeting (siNT), siRNA for Mre11 or siRNA for DNAPK. **B)** Crystal violet staining of colony formation assay on RPE iCut cells with the different crRNAs targeting *ABCB1* under 20 nM Taxol treated with the different siRNAs. **C)** Quantification of number of Taxol-resistant colonies from B. **D)** TIDE analysis showing the percentage of indels formation in the different crRNAs targeting *ABCB1*. DMSO-treated cells shown in black and CK666-treated cells in orange. **E)** Crystal violet staining of colony formation assay on RPE iCut cells with the different crRNAs targeting *ABCB1* under 20 nM Taxol treated with DMSO or CK666. 400 μ M of CK666 were added 8h post-crRNA transfection during 1h. **F)** Quantification of number of Taxol-resistant colonies from E.

REFERENCES

1. Roos, W. P., Thomas, A. D. & Kaina, B. DNA damage and the balance between survival and death in cancer biology. (2016) doi:10.1038/nrc.2015.2.
2. Valerie, K. & Povirk, L. F. Regulation and mechanisms of mammalian double-strand break repair. *Oncogene* vol. 22 5792–5812 (2003).
3. Her, J. & Bunting, S. F. How cells ensure correct repair of DNA double-strand breaks. *Journal of Biological Chemistry* vol. 293 10502–10511 (2018).
4. Scully, R., Panday, A., Elango, R. & Willis, N. A. DNA double-strand break repair-pathway choice in somatic mammalian cells. *Nature Reviews Molecular Cell Biology* vol. 20 698–714 (2019).
5. Jackson, S. P. Sensing and repairing DNA double-strand breaks. *Carcinogenesis* vol. 23 687–696 (2002).
6. Vitor, A. C., Huertas, P., Legube, G. & de Almeida, S. F. Studying DNA Double-Strand Break Repair: An Ever-Growing Toolbox. *Frontiers in Molecular Biosciences* vol. 7 24 (2020).
7. Jackson, S. P. & Bartek, J. The DNA-damage response in human biology and disease. *Nature* vol. 461 1071–1078 (2009).
8. van Attikum, H. & Gasser, S. M. Crosstalk between histone modifications during the DNA damage response. *Trends in Cell Biology* vol. 19 207–217 (2009).
9. Polo, S. E. & Almouzni, G. Chromatin dynamics after DNA damage: The legacy of the access-repair-restore model. *DNA Repair* vol. 36 114–121 (2015).
10. Dabin, J., Fortuny, A. & Polo, S. E. Epigenome Maintenance in Response to DNA Damage. *Mol. Cell* **62**, 712–727 (2016).
11. Soria, G., Polo, S. E. & Almouzni, G. Prime, Repair, Restore: The Active Role of Chromatin in the DNA Damage Response. *Molecular Cell* vol. 46 722–734 (2012).
12. Davis, A. J. & Chen, D. J. DNA double strand break repair via non-homologous end-joining. *Translational Cancer Research* vol. 2 130–143 (2013).
13. Lemaître, C. *et al.* Nuclear position dictates DNA repair pathway choice. *Genes Dev.* **28**, 2450–2463 (2014).
14. Schep, R. *et al.* Impact of chromatin context on Cas9-induced DNA double-strand break repair pathway balance. (2021) doi:10.1016/j.molcel.2021.03.032.
15. Chiolo, I. *et al.* Double-strand breaks in heterochromatin move outside of a dynamic HP1a domain to complete recombinational repair. *Cell* **144**, 732–744 (2011).
16. Ryu, T. *et al.* Heterochromatic breaks move to the nuclear periphery to continue recombinational repair. **17**, (2015).
17. Lamm, N. *et al.* Nuclear F-actin counteracts nuclear deformation and promotes fork repair during replication stress. *Nat. Cell Biol.* **22**, 1460–1470 (2020).
18. Pinzaru, A. M. *et al.* Replication stress conferred by POT1 dysfunction promotes telomere relocalization to the nuclear pore. *Genes Dev.* **34**, 1619–1636 (2020).
19. Tame, M. A., Manjón, A. G., Belokhovostova, D., Raaijmakers, J. A. & Medema, R. H. TUBB3 overexpression has a negligible effect on the sensitivity to Taxol in cultured cell lines. *Oncotarget* **8**, 71536 (2017).
20. Manjón, A. G. *et al.* Perturbations in 3D genome organization can promote acquired drug resistance. *bioRxiv* 2021.02.02.429315 (2021) doi:10.1101/2021.02.02.429315.
21. Ueda, K. *et al.* The human multidrug resistance (*mdr1*) gene. cDNA cloning and transcription initiation. *J. Biol. Chem.* **262**, 505–508 (1987).
22. JE, C., R, S., KE, N., K, C. & IB, R. Structure and expression of the human MDR (P-glycoprotein) gene family. *Mol. Cell. Biol.* **9**, 3808–3820 (1989).
23. S, R. *et al.* Production of P-glycoprotein from the MDR1 upstream promoter is insufficient to affect the response to first-line chemotherapy in advanced breast cancer. *Int. J. cancer* **122**, 1058–1067 (2008).
24. S, R. *et al.* Activation of the MDR1 upstream promoter in breast carcinoma as a surrogate for metastatic invasion. *Clin. Cancer Res.* **10**, 2776–2783 (2004).
25. Brinkman, E. K., Chen, T., Amendola, M. & van Steensel, B. Easy quantitative assessment of genome editing by sequence trace decomposition. *Nucleic Acids Res.* **42**, e168–e168 (2014).
26. Dahlman, J. E. *et al.* Orthogonal gene knockout and activation with a catalytically active Cas9 nuclease. *Nat. Biotechnol.* **33**, 1159–1161 (2015).
27. Huff, L. M., Lee, J. S., Robey, R. W. & Fojo, T. Characterization of gene rearrangements leading to activation of MDR-1. *J. Biol. Chem.* **281**, 36501–36509 (2006).
28. Fojo, T. Multiple paths to a drug resistance phenotype: Mutations, translocations, deletions and amplification of coding genes or promoter regions, epigenetic changes and microRNAs. *Drug Resist. Updat.* **10**, 59–67 (2007).
29. Patch, A. M. *et al.* Whole-genome characterization of chemoresistant ovarian cancer. *Nature* **521**, 489–494 (2015).
30. de Vree, P. J. P. *et al.* Targeted sequencing by proximity ligation for comprehensive variant detection and local haplotyping. *Nat. Biotechnol.* **32**, 1019–25 (2014).
31. Brinkman, E. K., Chen, T., Amendola, M. & Van Steensel, B. Easy quantitative assessment of genome editing by sequence trace decomposition. *Nucleic Acids Res.* **42**, (2014).
32. Shevelyov, Y. Y. *et al.* The B-type lamin is required for somatic repression of testis-specific gene clusters. *Proc. Natl. Acad. Sci. U. S. A.* **106**, 3282–3287 (2009).
33. Brueckner, L. *et al.* Local rewiring of genome–nuclear lamina interactions by transcription. *EMBO J.* 685255 (2020) doi:10.1101/685255.
34. van Steensel, B. & Belmont, A. S. Lamina-Associated Domains: Links with Chromosome Architecture, Heterochromatin, and Gene Repression. *Cell* vol. 169 780–791 (2017).

35. Ryu, T. *et al.* Heterochromatic breaks move to the nuclear periphery to continue recombinational repair. *Nat. Cell Biol.* **17**, 1401–1411 (2015).
36. Caridi, C. P. *et al.* Nuclear F-actin and myosins drive relocalization of heterochromatic breaks. *Nature* **559**, 54–60 (2018).
37. Amaral, N., Ryu, T., Li, X. & Chiolo, I. Nuclear Dynamics of Heterochromatin Repair. *Trends Genet.* **33**, 86–100 (2017).
38. Rawal, C. C., Caridi, C. P. & Chiolo, I. Actin' between phase separated domains for heterochromatin repair. *DNA Repair (Amst)*. **81**, 102646 (2019).
39. Dantuma, N. P. & Attikum, H. Spatiotemporal regulation of posttranslational modifications in the DNA damage response. *EMBO J.* **35**, 6–23 (2016).
40. Nair, N., Shoib, M. & Sørensen, C. S. Chromatin dynamics in genome stability: Roles in suppressing endogenous DNA damage and facilitating DNA repair. *International Journal of Molecular Sciences* vol. 18 (2017).
41. Mari, P. O. *et al.* Dynamic assembly of end-joining complexes requires interaction between Ku70/80 and XRCC4. *Proc. Natl. Acad. Sci. U. S. A.* **103**, 18597–18602 (2006).
42. Adkins, N. L., Niu, H., Sung, P. & Peterson, C. L. NUCLEOSOME DYNAMICS REGULATE DNA PROCESSING. *Nat. Struct. Mol. Biol.* **20**, 836 (2013).
43. Goldstein, M., Derheimer, F. A., Tait-Mulder, J. & Kastan, M. B. Nucleolin mediates nucleosome disruption critical for DNA double-strand break repair. *Proc. Natl. Acad. Sci.* **110**, 16874–16879 (2013).
44. Caridi, C. P. *et al.* Quantitative Methods to Investigate the 4D Dynamics of Heterochromatic Repair Sites in *Drosophila* Cells. in *Methods in Enzymology* vol. 601 359–389 (Academic Press Inc., 2018).
45. Miné-Hattab, J. & Chiolo, I. Complex Chromatin Motions for DNA Repair. *Frontiers in Genetics* vol. 11 800 (2020).
46. Chiolo, I. *et al.* Double-Strand Breaks in Heterochromatin Move Outside of a Dynamic HP1a Domain to Complete Recombinational Repair. *Cell* **144**, 732–744 (2011).
47. Caridi, C. P., Plessner, M., Grosse, R. & Chiolo, I. Nuclear actin filaments in DNA repair dynamics. *Nature Cell Biology* vol. 21 1068–1077 (2019).
48. Alagoz, M. *et al.* SETDB1, HP1 and SUV39 promote repositioning of 53BP1 to extend resection during homologous recombination in G2 cells. *Nucleic Acids Res.* **43**, 7931–7944 (2015).
49. Baldeyron, C., Soria, G., Roche, D., Cook, A. J. L. & Almouzni, G. HP1a recruitment to DNA damage by p150CAF-1 promotes homologous recombination repair. *J. Cell Biol.* **193**, 81–95 (2011).
50. Lee, Y. H., Kuo, C. Y., Stark, J. M., Shih, H. M. & Ann, D. K. HP1 promotes tumor suppressor BRCA1 functions during the DNA damage response. *Nucleic Acids Res.* **41**, 5784–5798 (2013).
51. Soria, G. & Almouzni, G. Differential contribution of HP1 proteins to DNA end resection and homology-directed repair. *Cell Cycle* **12**, 422–429 (2013).
52. Papadopoulou, C., Guilbaud, G., Schiavone, D. & Sale, J. E. Nucleotide Pool Depletion Induces G-Quadruplex-Dependent Perturbation of Gene Expression. *Cell Rep.* **13**, 2491–2503 (2015).
53. O'Hagan, H. M., Mohammad, H. P. & Baylin, S. B. Double strand breaks can initiate gene silencing and SIRT1-dependent onset of DNA methylation in an exogenous promoter CpG island. *PLoS Genet.* **4**, (2008).
54. Jacobi, A. M. *et al.* Simplified CRISPR tools for efficient genome editing and streamlined protocols for their delivery into mammalian cells and mouse zygotes. *Methods* **121–122**, 16–28 (2017).
55. Stelloo, S. *et al.* Endogenous androgen receptor proteomic profiling reveals genomic subcomplex involved in prostate tumorigenesis. *Oncogene* **37**, 313–322 (2018).
56. Soto, M. *et al.* p53 Prohibits Propagation of Chromosome Segregation Errors that Produce Structural Aneuploidies. *Cell Rep.* **19**, 2423–2431 (2017).
57. Brueckner, L., van Arensbergen, J., Akhtar, W., Pagie, L. & van Steensel, B. High-throughput assessment of context-dependent effects of chromatin proteins. *Epigenetics Chromatin* **9**, 43 (2016).
58. Vogel, M. J., Peric-Hupkes, D. & van Steensel, B. Detection of in vivo protein-DNA interactions using DamID in mammalian cells. *Nat. Protoc.* **2**, 1467–78 (2007).



5

Unexpected gene activation following CRISPR-Cas9-mediated genome editing

Anna G. Manjón, Simon Linder, Hans Teunissen, Wilbert Zwart, Elzo de Wit, René
H. Medema

Manuscript under review

ABSTRACT

The discovery of the Clustered Regularly-Interspaced Short Palindromic Repeats (CRISPR) and its development as a genome editing tool has revolutionized the field of molecular biology. In the DNA damage field, CRISPR has brought an alternative to induce endogenous double-strand breaks (DSB) at desired genomic locations and study the DNA damage response and its consequences. Many systems for sgRNA delivery have been reported in order to efficiently generate this DSB, including lentiviral vectors. However, some of the consequences of these systems are yet not well understood. Here we report that lentiviral-based sgRNA vectors can integrate into the endogenous genomic target location, leading to undesired activation of the target gene. By generating a DSB in the regulatory region of the *ABCB1* gene using a lentiviral sgRNA vector, we can induce the formation of Taxol-resistant colonies. We show that these colonies upregulated *ABCB1* via integration of the *EEF1A1* and the U6 promoters from the sgRNA vector. We believe that this is an unreported CRISPR/Cas9 artefact that researchers need to be aware of when using lentiviral vectors for genome editing.

INTRODUCTION

The discovery of the Clustered Regularly-Interspaced Short Palindromic Repeats (CRISPR), their role in the prokaryotic immune system and subsequent development as a genome editing tool has revolutionized the field of molecular biology¹⁻⁶. In recent years, many laboratories have developed CRISPR/Cas9 as a tool that can be applied to study many different biological questions⁷. In the DNA damage field, CRISPR has brought an alternative to induce endogenous double-strand breaks (DSB) at desired genomic locations. This system allowed for the study of the DNA damage response and its consequences in different genome compartments or structures⁸. Combining imaging and high throughput technologies with DSB-induced Cas9 systems allows one to examine processes such as transcription, chromatin dynamics, and DNA replication⁹⁻¹².

The CRISPR/Cas9 system needs to be delivered in an accurate manner for efficient gene editing.

On the one hand, the Cas9 protein needs to be expressed in the host system or delivered in a form of a Ribonucleoprotein (RNP) complex¹³. On the other hand, a target-specific single guide RNA (sgRNA) – formed by CRISPR RNA (crRNA) and transactivating CRISPR RNA – needs to direct Cas9 to the target site¹⁴. It is important to choose the right delivery strategy for the sgRNA to survive the degradation processes in the cell and translocate into the nucleus to allow for gene editing. To date, we can classify sgRNA delivery methods into viral and non-viral, based on whether viral constructs are used for transfection⁷.

Viral vectors include gamma-retroviruses, adenovirus, adeno-associated viruses (AAVs) and lentiviruses (LVs)¹⁵. Specially in LVs, Cas9 and sgRNA are relatively easy to clone, produce and efficiently transduced into the host cell. However, the bigger challenge of these systems is the random integration of the construct into the genome¹⁶. We can divide the non-viral methods into physical and chemical. Physical methods include microinjections – where the sgRNAs are directly injected by a needle – and electroporation – where electric currents open the cell membrane for the delivery of molecules into the cell^{17,18}. Chemical delivery methods comprise a DNA or RNA form of the sgRNA that can be transfected into the host by liposome-based and non-leptosomic reagents^{19,20}. With RNA delivery methods, the transfection efficiency can be lower, but they are a safer alternative, as random viral integrations do not occur.

Even though targeting genomic regions with the CRISPR/Cas9 system is tightly controlled and specific, it is known that off-target cutting activity could still occur^{5,21,22}. Other limitations of CRISPR include the requirement for a protospacer adjacent motif (PAM) to the target DNA sequence and the DNA-damage toxicity triggered after the CRISPR-induced DSB²³. Nonetheless, valuable efforts have been made to understand and minimize these drawbacks. However, much less is known

about how viral CRISPR/Cas9 delivery methods may affect genome integrity and gene expression when randomly integrated into the host genome.

Here we show that a LV-based sgRNA vector can integrate into the endogenous genomic target location thereby affecting gene expression of the target gene. By generating a DSB in the regulatory region of the *ABCB1* gene with this system, we can produce Taxol resistant clones that upregulated *ABCB1* through transcriptional activation via the *EEF1A1* and the U6 promoters from the sgRNA vector. We believe that this unreported gene activation mechanism following CRISPR-Cas9-mediated genome editing needs to be taken into consideration when inducing DSBs with a sgRNA lentiviral method.

RESULTS

A LentiGuide-induced DSB in the *ABCB1* promoter leads to upregulation of *ABCB1*

We have previously shown that in human retinal pigment epithelial-1 (RPE-1), the major mechanism of Taxol resistance is transcriptional activation of the *ABCB1* gene, that encodes for the multi-drug resistance protein MDR1 or P-Glycoprotein (PgP)^{24,25}. Using the lentiviral system lentiGuide-Puro from the Zhang Lab²⁶, we cloned different sgRNAs targeting different non-coding regions across the *ABCB1* locus to induce a DSB (**Fig. 1A**). We chose non-coding regions to avoid the possibility that a break-induced change in coding sequence could result in acquired Taxol resistance. Seven days after lentiviral infection and puromycin selection we treated the RPE-1 cells with 8nM of Taxol in order to select cells that over-expressed PgP. Surprisingly, we observed that only cells treated with sgRNAs targeting the promoter of *ABCB1* became resistant to Taxol (**Fig. 1A** and **Sup. Fig. 1A**), as we observed a considerable number of RPE-1 colonies growing under Taxol pressure. In order to better understand the mechanisms responsible for the acquisition of the Taxol-resistant phenotype, we decided to individually characterize the Taxol-resistant clones from the sgRNA targeting the *ABCB1* promoter. Therefore, we expanded under Taxol pressure the resistant colonies observed in the colony outgrowth assays. When performing a viability assay with increasing doses of Taxol, we observed that all clones were resistant to high concentrations of Taxol, and could be re-sensitized with Tariquidar, a PgP inhibitor (**Fig. 1B**). As expected, with Western Blot and qRT-PCR assays we could confirm that the Taxol-resistant clones expressed high levels of PgP as well as mRNA respectively (**Fig. 1C-D**). Thus, confirming that the mechanism of Taxol resistance was through *ABCB1* upregulation. By performing intronic smRNA-FISH, which allows for visualization of active transcription sites, we demonstrated that only one allele was actively transcribing *ABCB1* (**Fig. 1E**), confirming that *ABCB1* copy number amplifications were not observed in these clones. Importantly, we also performed lentiviral infection with the same sgRNAs targeting *ABCB1* in human

Unexpected gene activation following CRISPR-Cas9-mediated genome editing

mammary epithelial cells (HMEC) expressing Cas9. Here we observed as well that the sgRNAs targeting the promoter of *ABCB1* lead to Taxol-resistant colonies (**Sup. Fig. 1B**). Thus, confirming that this phenomenon can be reproduced in other cell lines.

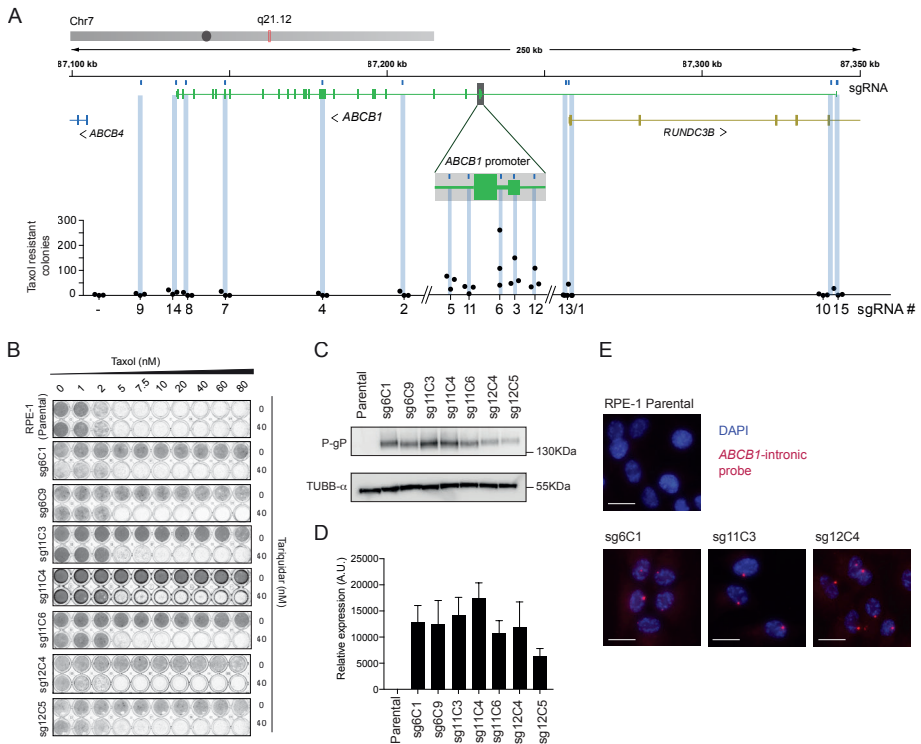


Figure 1 – A DSB in the promoter of *ABCB1* causes gene upregulation and Taxol-resistance
A) Graphical representation of the *ABCB1* genomic region and the location of the gRNA targeting the gene. RPE-1 cells were infected with a Lentivirus carrying one of the gRNAs and after 7 days of puromycin selection one million cells were plate with 8nM of Taxol for Colony Outgrowth Assay. Taxol resistant cells were counted and plotted in the graph. N=3. **B**) Crystal violet staining of viability assay on RPE-1 Parental cells and Taxol resistant clones obtained from A. For the clones' nomenclature, sg# represents the sgRNA from where they are derived and C# the clone number. **C**) Western Blot showing the levels of the PgP and control (α -TUBB) in RPE-1 Parental and Taxol resistant clones. **D**) *ABCB1* mRNA levels determined by qRT-PCR and normalized to GAPDH expression levels, n=2. Error bars show the SD. **E**) Representative smRNA-FISH images of RPE-1 Parental and clones for the *ABCB1* gene and DAPI. The images are projections of 0,5 μ m sections and a total 5 μ m in thickness. Scale bar, 15 μ m.

The LentiGuide vector integrates and drives gene expression upon a DSB in the *ABCB1* promoter

To exclude that DNA translocations or insertions might be induced by the DSB and could modify the activity of the *ABCB1* promoter, we performed Targeted Locus Amplification (TLA), a chromosome conformation capture-based technique, enabling the identification of single nucleotide variation and genomic rearrangements in a specific locus using a single PCR reaction²⁷. We selectively amplified and sequenced the DNA flanking the *ABCB1* promoter. We compared RPE-1 Parental cells with a Taxol-resistant clone derived from the sgRNA #6 targeting the promoter of *ABCB1* (sg6C9). Surprisingly, we found that our TLA experiments for the *ABCB1* promoter amplified a 1.3kb region from chromosome 6 in the Taxol-resistant clone (**Fig. 2A**, green arrow). When zooming in on that region, we discovered that the promoter of the *EEF1A1* gene was amplified in the sg6C9 Taxol-resistant clone (**Fig. 2B**). The read distribution over the *EEF1A1* promoter is reminiscent of genomic insertions previously mapped with TLA²⁷. To confirm the fusion of the *ABCB1* and *EEF1A1*, we performed PCRs on genomic DNA using either *Forward* and *Reverse* primers amplifying the *ABCB1* break site or a *Forward* primer binding the promoter region of *EEF1A1* together with a *Reverse* from the *ABCB1* promoter. Only when *EEF1A1* and *ABCB1* are juxtaposed in the genome this will result in a PCR product (**Fig. 2C**). Remarkably, we found out that not only the Taxol-resistant clone sg6C9 but also all the other clones derived from the sgRNA #6 and some others from #3, #5, #11 and #12, all generating a DSB in the promoter of *ABCB1*, gave a PCR product when using the *ABCB1* and *EEF1A1* primers (**Fig. 2D**). We could also observe a higher band appearing when amplifying the sequence over the break site with *Forward* and *Reverse* *ABCB1* primers (**Fig. 2E**). These data confirm that the *EEF1A1* promoter was integrated in the break site in the regulatory region of *ABCB1*. When we sequenced the PCR products from the different clones, we observed that there were other sequences belonging to the U6 promoter and the puromycin-resistant cassette integrated (data not shown). We next decided to align the sequence reads of the TLA experiment analyzing the sg6C9 Taxol-resistant clone to the LentiGuide vector sequence that was used to clone the *ABCB1*-targeting sgRNAs to induce the DSB. We found that in the sg6C9 Taxol-resistant clone, there was a large region aligning with the LentiGuide vector, suggesting that the *EEF1A1* integration found in the *ABCB1* promoter belonged to the LentiGuide vector and not to the endogenous gene found on chromosome 6 (**Fig. 2F**). We therefore conclude that the lentiGuide-Puro vector had been integrated into the *ABCB1* promoter, most likely due to the presence of the CRISPR-induced DSB in that region. As the U6 promoter is an RNA Pol III promoter most likely this will not result in mRNA and protein translation. Therefore, most probably the *EEF1A1* promoter from this vector induced the transcriptional activation of *ABCB1*.

Unexpected gene activation following CRISPR-Cas9-mediated genome editing

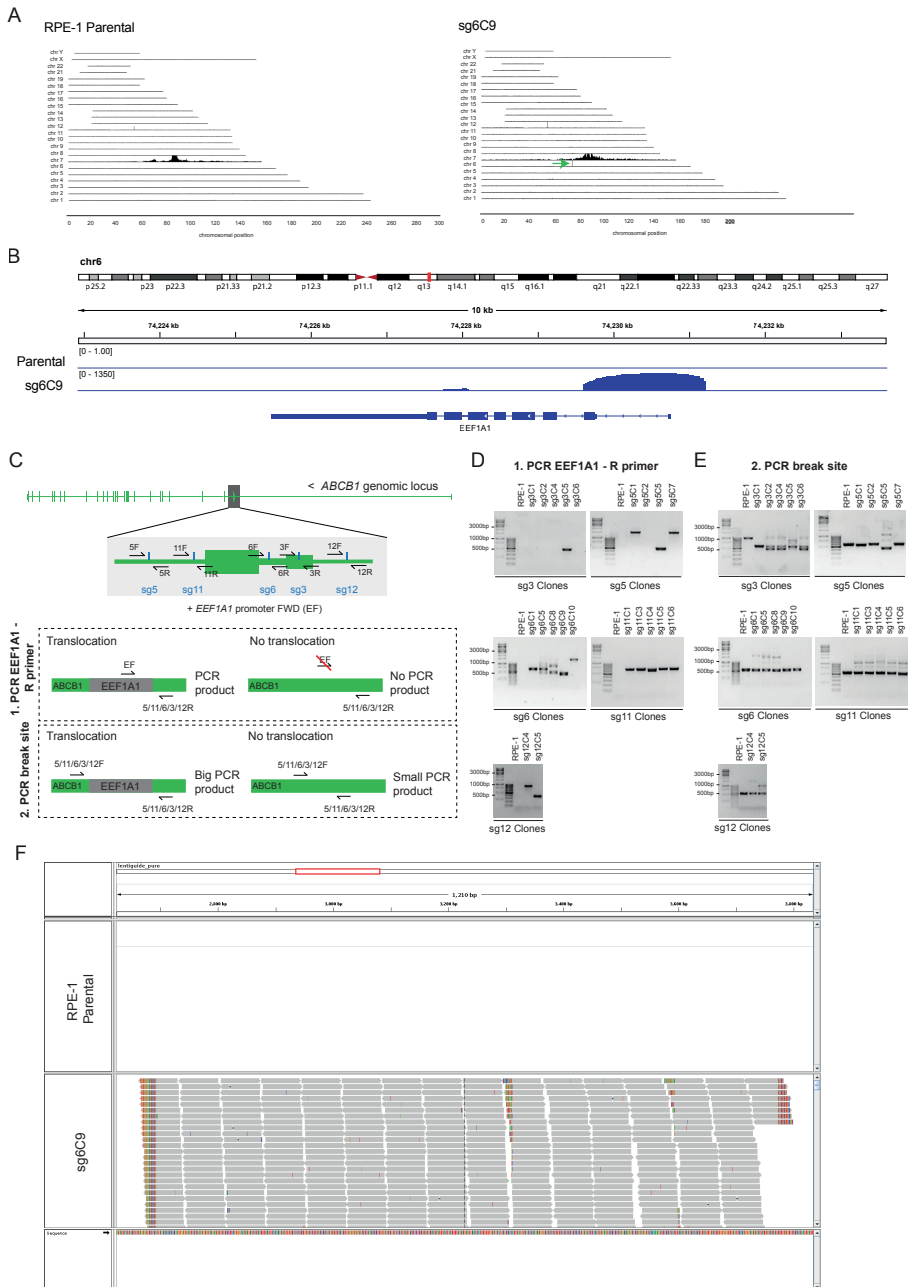


Figure 2 – sgRNA integration and transcription activation of ABCB1

A) TLA analysis for ABCB1 contacts in RPE-1 Parental and Taxol resistant clone sg6C9 covering the whole genome. Green arrow in sg6C9 shows a de novo interaction found between ABCB1 and a region in chromosome 6. **B)** TLA analysis for RPE-1 Parental and sg6C9. Zoom in the region of chr6 with de novo interaction for sg6C9. **C)** Graphical representation of the PCR products to assess vector integration. Two different primer pairs were used to PCR the vector integration: 1) a common EEF1A1

5

Forward (F) primer with a specific Reverse for each break site (5/11/6/3/12R). Only when *EEF1A1* is integrated in cis we will obtain a PCR product. 2) A forward and Reverse primer to amplify each specific break site (5/11/6/3/12F and R). If *EEF1A1* is integrated in the break site, the PCR product will be bigger. **D)** PCR products using the primers in C(1) over the *ABCB1* and *EEF1A1* regions in RPE-1 Parental and the different Taxol resistant clones. **E)** PCR products using the primers in C(2) over the specific break site in the *ABCB1* promoter in RPE-1 Parental and the different Taxol resistant clones. **F)** IGV screen shot where the reads of the TLA experiments are aligned to the lenti-guide puro sequence. In sg6C9, reads align to the lenti-guide vector.

Chromatin changes in the *ABCB1* promoter region upon LentiGuide vector integration

We next decided to compare the chromatin landscape in the *ABCB1* promoter in RPE-1 parental cells and the Taxol-resistant clones with the lentiGuide-Puro integration. It is known that in RPE-1 parental cells, *ABCB1* is found in a repressive chromatin environment consequently leading to transcriptional repression²⁵. We therefore performed ChIP-sequencing for the repressive histone modification H3K9me3. ChIP-sequencing tracks of this chromatin mark showed that in RPE-1 parental cells *ABCB1* is located in a region that contains intermediate level of H3K9me3, and flanked by regions with high levels of H3K9me3 (**Fig. 3A**, black track). Importantly, the seven Taxol-resistant clones derived from different sgRNAs also displayed a similar H3K9me3 patterns (**Fig. 3A**). In order to better quantify the levels of H3K9me3, we performed ChIP-qPCRs in the *ABCB1* promoter spanning up to 10kb surrounding the transcriptional start site (**Fig. 3B**). Interestingly, we observed that while some Taxol-resistant clones had lower levels of H3K9me3 (sg6C1, sg6C9 and sg12C5), others had similar levels compared to the parental cell line (sg11C3-4-6 and sg12C4) (**Fig. 3B** and **Sup. Fig. 3A-B**). It has been suggested that the DNA methylation profile of the *ABCB1* promoter can regulate its transcriptional status^{28,29}. Therefore, we set out to study whether the DNA methylation pattern was altered in the Taxol-resistant clones. By performing a DNA methylation array, we could assess the relative methylation status of 11 CpG islands located in the *ABCB1* promoter close by the sgRNAs targeting regions (**Fig. 3C-D**). In RPE-1 parental, only two CpG islands were nearly fully methylated (CpG 1 and 2), and maintained the same status in four out of seven Taxol-resistant clones (**Fig. 3D**). The rest of CpG islands were hemimethylated in the parental cell line and vary between clones (**Fig. 3D**). Therefore, even though some Taxol-resistant clones have lower levels of repressive chromatin marks, others maintain them still leading to *ABCB1* gene activation. Possibly the DNA damage-repair process induced by the sgRNA-Cas9 system could cause the erasure of repressive chromatin marks, but this does not fully explain *ABCB1* gene activation. Therefore, we suggest that the endogenous *ABCB1* promoter remains repressed in the Taxol-resistant clones that contain the lentiGuide-Puro integration, and that transcription activation occurs via the *EEF1A1* promoter in that vector.

Unexpected gene activation following CRISPR-Cas9-mediated genome editing

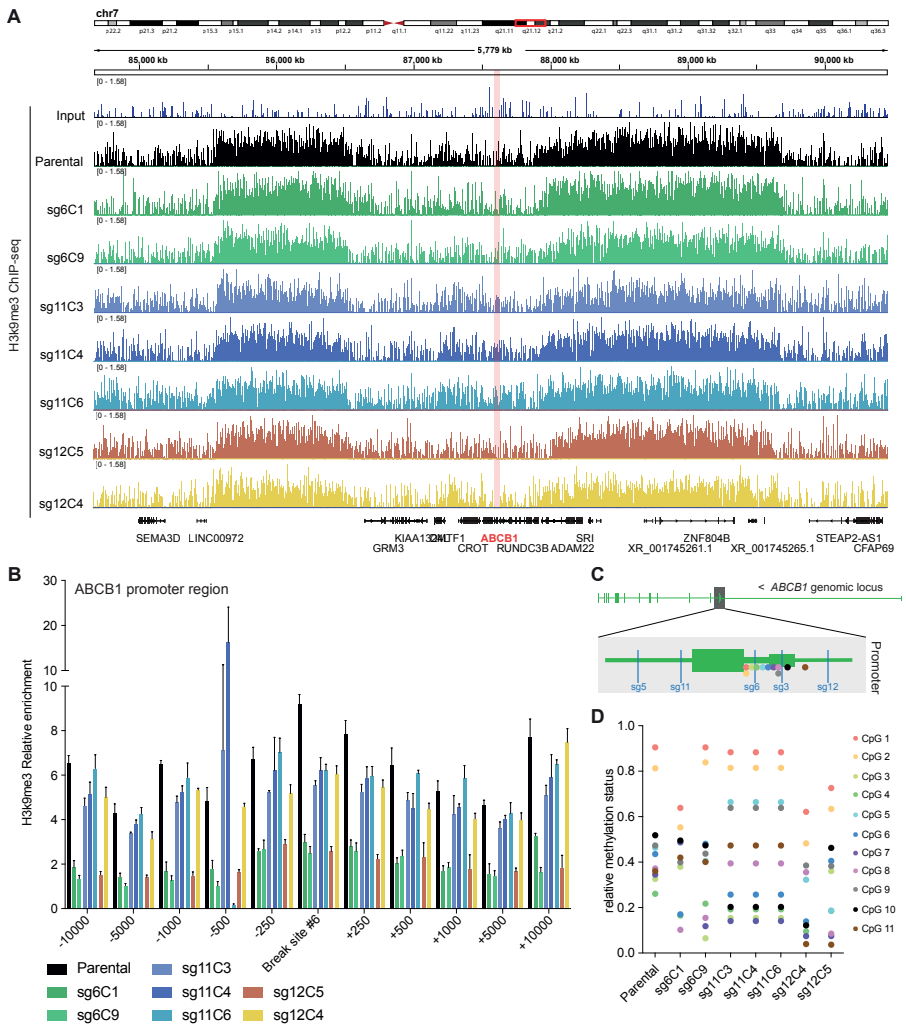


Figure 3 – Chromatin landscape in the ABCB1 promoter region upon LentiGuide vector integration

A) H3K9me3 ChIP-sequencing tracks from the q21.12 arm of chromosome 7 in RPE-1 cells (Parental and Taxol-resistant clones). The ABCB1 gene region is shown in pink. **B)** H3K9me3 ChIP-qPCR in the ABCB1 promoter region. Bar graph show primer pairs amplifying the sgRNA#6 break and spanning this region (+/- base pairs) for each Taxol-resistant clone compared to the Parental. **C)** Graphical representation of the ABCB1 promoter region. The location of the sgRNAs targeting the promoter are shown in blue. The location of the eleven CpG islands analyzed in the methyl array are shown in colored dots. **D)** Relative methylation status (1: methylated, 0: non-methylated) of the eleven CpG islands shown in C for RPE-1 Parental and the Taxol-resistant clones.

DISCUSSION

We show here that a lentiviral sgRNA delivery system to induce a DSB close the transcriptional start site of a gene can result in integration of the vector in the break site, and activation of the gene. When generating a DSB in the regulatory region of *ABCB1* with this system, we were able to find cells with genetic alterations that contained the U6 and *EE1A1* promoters of the lentiviral vector. We believe that the DSB increased the probability of the vector to integrate into this location. In RPE-1 cells *ABCB1* is repressed and the cells are sensitive to Taxol. The integration of these promoters allowed for gene activation and produced a Taxol resistant phenotype (**Figure 4**). This mechanism does not appear to be of high frequency, but selection of cells with high transcriptional levels of *ABCB1* by Taxol increased its occurrence. Nonetheless, as seen by colony formation outgrowth, we found that this event may happen in up to three cells out of a thousand, suggesting that this type of genetic alterations have to be taken into consideration.

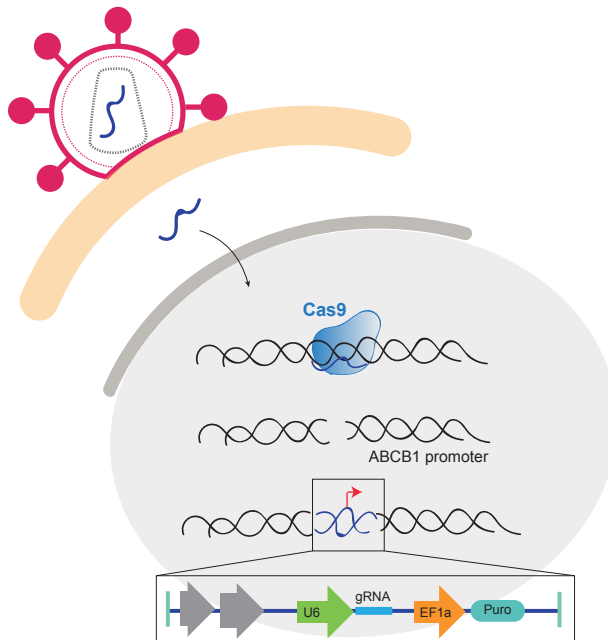


Figure 4 – Model of sgRNA integration in endogenous *ABCB1* locus

When a lenti-guide Puro vector is used to deliver a gRNA to induce a DSB, the gRNA can be integrated into the break site. The DSB was induced in the promoter of *ABCB1* and therefore the highly active promoters of the vector were driving the expression of the *ABCB1* gene. In this case, we were selecting for cells that upregulated *ABCB1* and therefore the frequency of this event was higher.

HIV-1-based lentiviral vectors convert single-strand RNA into double-strand DNA by reverse transcription and subsequently insertion into the genome of post-mitotic

cells⁷. Lentiviral vectors have become important tools to deliver components of the CRISPR/Cas9 system for genome editing. However, in gene therapy, stable viral integrations come with concerns regarding safety³⁰. Among them, the deregulation of genes caused by the insertions and mutagenesis found in gene therapy for immunodeficiencies in patients³¹.

Many researchers are currently using lentiviral vectors for delivery of CRISPR/Cas9 components, as sgRNAs are relatively easy to clone into them⁷. Lentiviral sgRNA-delivery systems are used in functional genetic screens to find lethal interactions of specific biological processes³². Even though many limitations are known regarding off targets or difference in efficiency between sgRNAs³³⁻³⁵, little is known about how lentiviral-based CRISPR can affect gene transcription changes. We speculate that targeted viral integration could result in deregulation of genes that may affect biological functions and therefore lead to false positive candidates when performing functional screens. Thus, when performing screens, it is important to have a good sgRNA complexity and reproducible results.

Furthermore, as CRISPR enables the induction of DNA breaks at specific endogenous loci, more and more researchers are using several Cas9 systems to study of DSB repair and its biological consequences^{8,36,37}. As we show here, inducing a DSB in a gene regulatory region could have consequence in gene expression thus leading to incorrect interpretation of the results. Therefore, to study long term consequence of the DNA damage response we suggest to employ non-integrative systems such as synthetic gRNAs delivered in an RNA form³⁸.

MATERIALS AND METHODS

Cell lines and cell culture conditions

RPE-1 cells are hTert-immortalized human retinal pigment epithelium non-tumoral cells. HMEC cells are hTert-immortalized human mammary epithelial non-tumoral cells. RPE-1 and HMEC cell lines were maintained in DMEM/F-12 + Glutamax (Gibco, Life Technology) supplemented with 1% penicillin/streptomycin and 6% fetal bovine serum (FBS, S-FBS-EU-015, Serana).

Taxol and Tariquidar treatment

Taxol and Tariquidar were dissolved in DMSO and prepared at stock concentrations before usage at varying final concentrations as indicated in each Figure.

sgRNA designed and cloning

The sgRNAs targeting *ABCB1* were cloned into a lenti-guidePuro (Addgene plasmid # 52963) using the BsmBI restriction site. sgRNA sequences are summarized in **Table 1**.

Table 1 – gRNA sequences targeting ABCB1

Name	Target gene	gRNA sequence
lentiGuide-Puro-ABCB1 #1	ABCB1	GCTGCTTTAAAAGGTCCGCG
lentiGuide-Puro-ABCB1 #2	ABCB1	AGAAAGCTCCATCAACCGCA
lentiGuide-Puro-ABCB1 #3	ABCB1	GCTGGGCAGGAACAGCGCCG
lentiGuide-Puro-ABCB1 #4	ABCB1	TGTGACTGCTGATCACCGCA
lentiGuide-Puro-ABCB1 #5	ABCB1	GCTTTCCTGCCCCAGACAGG
lentiGuide-Puro-ABCB1 #6	ABCB1	CCTCCCGGTTCCAGTCGCCG
lentiGuide-Puro-ABCB1 #7	ABCB1	CTGCTCCTCCAAATGAAAGG
lentiGuide-Puro-ABCB1 #8	ABCB1	GGTTTCCCCTGTAAATAGA
lentiGuide-Puro-ABCB1 #9	ABCB1	CCTATTGCTCTGCTATGGCG
lentiGuide-Puro-ABCB1 #10	ABCB1	ATACAATCCAAGAAAAACAA
lentiGuide-Puro-ABCB1 #11	ABCB1	ACAAACTTCTGCTCTAAGCA
lentiGuide-Puro-ABCB1 #12	ABCB1	TCAATGCCCGTGTTTTCCA
lentiGuide-Puro-ABCB1 #13	ABCB1	ATATTATCCCTGTTAATGCA
lentiGuide-Puro-ABCB1 #14	ABCB1	CCAAGAAGAATGAAGCCAGA
lentiGuide-Puro-ABCB1 #15	ABCB1	CTAAGCCATGTAACTCTTCG

sgRNA lentiviral infection and Colony Formation Assays

400.000 RPE-1 or HMEC cells were infected with a specific lenti-sgRNA in 1:4 ratio. Next day, cells were trypsinized and 1:750 of 10mg/ml of Puromycin was added. Cells were allowed to grow under Puromycin selection for seven days. Following selection, one million cells were seeded and treated with 8nM of Taxol and allowed to grow out for 15 days. Plates were fixed in 80% Methanol and stained with 0.2% Crystal Violet solution. After fixation, the number of Taxol resistant cells were counted.

Viability assays

For viability assays, 1000 cells were plated in a 96-well plate and treated for seven days with indicated drug concentrations. Subsequently, plates were fixed in 80% Methanol and stained with 0.2% Crystal Violet solution

RNA isolation and qRT-PCR analysis

RNA isolation was performed by using Qiagen RNeasy kit and quantified using NanoDrop (Thermo Fisher Scientific). cDNA was synthesized using Bioscript reverse transcriptase (Bioline), Random Primers (Thermo Fisher), and 1000 ng of total RNA according to the manufacturer's protocol. Primers were designed with a melting temperature close to 60 degrees to generate 90–120-bp amplicons, mostly spanning introns. cDNA was amplified for 40 cycles on a cycler (model CFX96;

Unexpected gene activation following CRISPR-Cas9-mediated genome editing

Bio-Rad Laboratories) using SYBR Green PCR Master Mix (Applied Biosystems). Target cDNA levels were analyzed by the comparative cycle (Ct) method and values were normalized against GAPDH expression levels. qRT-PCR oligo sequences are summarized in **Table 2**.

Table 2 – RT-qPCR primers

RT-qPCR Primers	FWD	REV
ABCB1	ACAGCACGGAAGGCCTAATG	GTCTGGCCCTTCTTCACCTC
GAPDH	TGCACCACCAACTGCTTA	GGATGCAGGGATGATGTTT

Western Blots

For western blot experiments, equal amounts of cells were lysed with Laemmli buffer and separated by SDS–polyacrylamide gel electrophoresis followed by transfer to a nitrocellulose membrane. Membranes were blocked in 5% milk in PBST for 1h at RT before overnight incubation with primary antibody in PBST with 5% milk at 4°C. Membranes were washed three times with PBST followed by incubation with secondary antibody in PBST with 5% milk for 2h at RT. Antibodies were visualized using enhanced chemiluminescence (ECL) (GE Healthcare). The following antibodies were used for western blot experiments: α -Tubulin (Sigma t5168), MDR(PgP) (sc-8313). For secondary antibodies, peroxidase-conjugated goat anti-rabbit (P448 DAKO, 1:2000), goat anti-mouse (P447 DAKO, 1:2000) and rabbit anti-goat (P449) were used.

smRNA FISH

RPE-1 cells were plated on glass coverslips and washed twice with BS before fixation in 4% PFA in PBS for 10 minutes at room temperature. After two additional washes in 1x PBS coverslips were incubated in 70% ethanol at 4°C overnight. Coverslips were incubated for pre-hybridization in wash buffer (2x saline-sodium citrate (SSC) with deionized formamide (Sigma) 10%) for 2-5 minutes at room temperature. RNA FISH probe mix wash dissolved in hybridization buffer (wash buffer supplemented with 10% dextran sulfate). 38 probes labelled with Cy5 were targeted to the intronic regions of ABCB1 (Biosearch technologies). Coverslips were incubated in hybridization solution for at least 4h at 37°C. Then coverslips were washed twice for 30 minutes with wash buffer followed by a quick rinse with 2x SSC. Finally, coverslips were washed once for 5 minutes in 1x PBS before mounting on slides using Prolong gold DAPI mounting medium (Life Technologies). Images were acquired with the use of a DeltaVision Elite (Applied Precision) equipped with a 60x 1.45 numerical aperture (NA) lens (Olympus) and cooled CoolSnap CCD camera. ABCB1 transcription start site quantification was performed manually double blind.

TLA analysis

TLA was performed as previously described with minor modifications. TLA libraries were sequenced on a MiSeq and were mapped to genome using *bwa bwawsw*³⁹ to enable partial mapping of sequence reads. Reads were mapped to hg19 reference of the human genome.

ChIP-sequencing/qPCR of RPE-1 hTERT cells

Chromatin immunoprecipitations (ChIP) were performed as described previously⁴⁰ with minor adjustments. Approximately 7×10^6 cells per condition were fixed, 50 μ L of Protein A magnetic beads (Invitrogen) and 5 μ g of antibody H3K9me3 (abcam ab8898). For ChIP-seq, samples were processed for library preparation (Part# 0801-0303, KAPA Biosystems kit), sequenced using an Illumina HiSeq2500 genome analyzer (65bp reads, single end) and aligned to the Human Reference Genome (hg19) using Burrows-Wheeler Aligner (*bwa*) version 0.5.9. Mapped reads were filtered based on mapping quality of 20 using *samtools* version 0.1.19. For ChIP-qPCR analysis, DNA was amplified for 40 cycles on a cycler (model CFX96; Bio-Rad Laboratories) using SYBR Green PCR Master Mix (Applied Biosystems). Target DNA levels were analyzed by the comparative cycle (Ct) method and values were normalized against input DNA and positive control region (specific for each chromatin mark). ChIP-qPCR oligo locations are summarized in **Table 3**.

Table 3 – ChIP-qPCR primers

RT-qPCR Controls	FWD	REV
7 (negative control)	TGCCACACACCAGTGACTTT	ACAGCCAGAAGCTCCAAAAA
S2 (negative control)	CTAGGAGGGTGGAGGTAGGG	GCCCCAAACAGGAGTAATGA
KS6 (positive control)	TGAAGACACATCTGCGAACC	TCGCGCACTCATAAGTTTC
KS7 (positive control)	CAATTGGCCATATCTTTACG	CATGTTCTCGAAAGCAAGCA

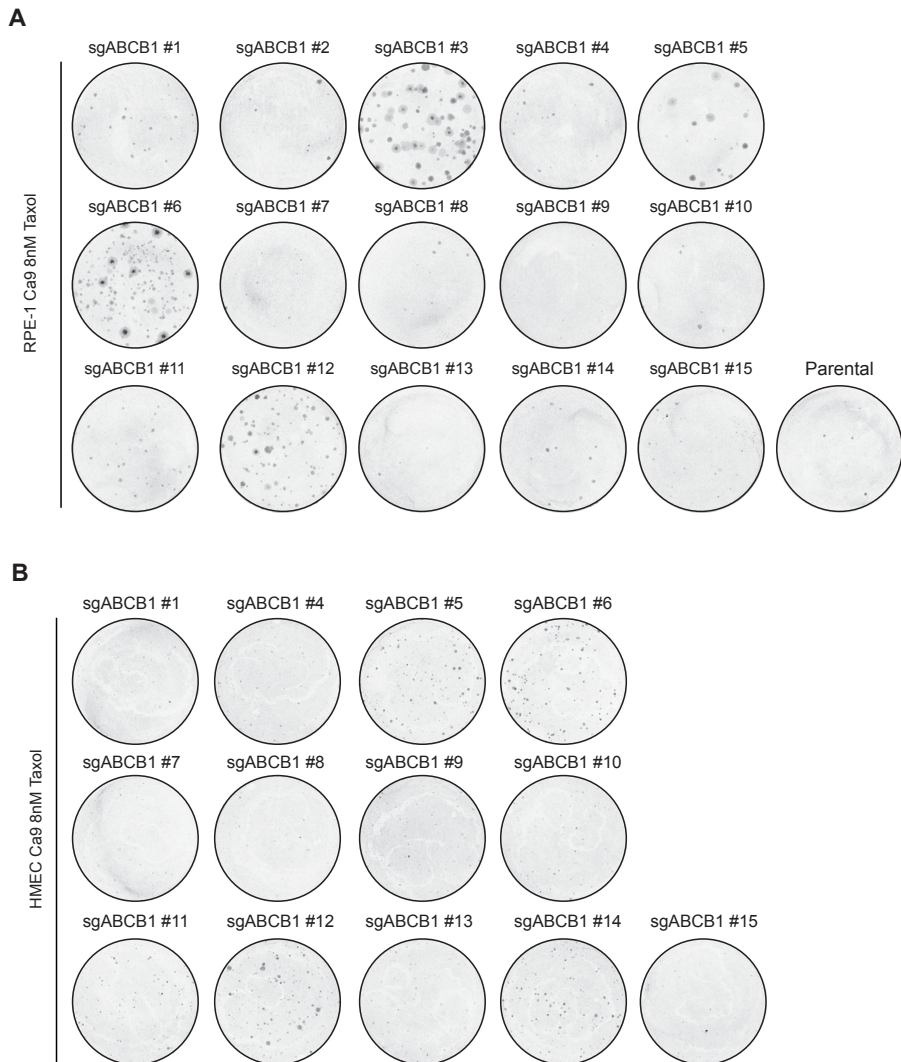
RT-qPCR ABCB1	Location (hg19)	RT-qPCR ABCB1	Location (hg19)
250-	chr7:87229476,87229676	250+	chr7:87230176,87230376
500-	chr7:87229226,87229426	500+	chr7:87230426,87230626
1000-	chr7:87228726,87228926	1000+	chr7:87230926,87231126
5000-	chr7:87224726,87224926	5000+	chr7:87234926,87235126
10000-	chr7:87219726,87219926	10000+	chr7:87239926,87240126

DNA Methylation array

DNA methylation was measured with the Infinium MethylationEPIC BeadChip (Illumina Inc., San Diego, CA) according to the manufacturers protocol. In short, 500 ng of genomic DNA was bisulfite converted using the EZ-96 DNA Methylation Deep-Well Kit (Zymo Research, Irvine, CA, USA). The samples were plated in a randomized

Unexpected gene activation following CRISPR-Cas9-mediated genome editing

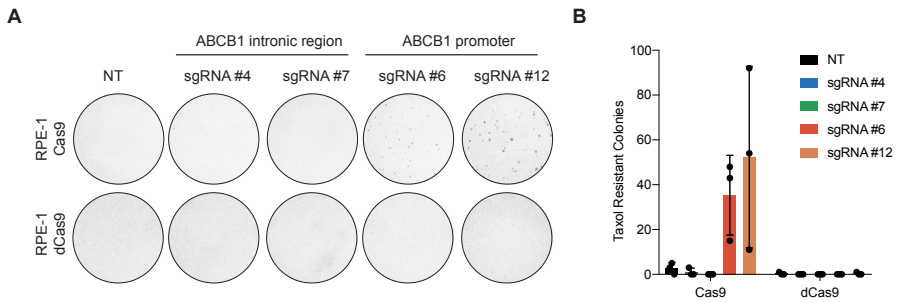
order. The bisulfite conversion was performed according to the manufacturers protocol with the following modifications. For binding of the DNA 15 μ l MagBinding Beads was used. The conversion reagent incubation was done according to the following cycle protocol: 16 cycles of 95°C for 30 seconds followed by 50 °C for 1 hour. After the cycle protocol the DNA is incubated for 10 minutes at 4 °C. Next, DNA samples were hybridized on the Infinium MethylationEPIC BeadChip (Illumina Inc., San Diego, CA) according to the manufacturers protocol.



Supplementary Figure 1 – A DSB in the promoter of ABCB1 causes gene upregulation and Taxol-resistance

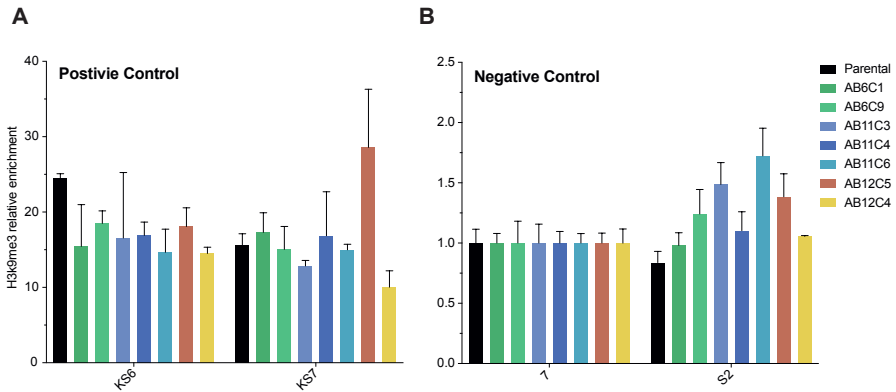
A) Example replicate of crystal violet staining of Colony Formation Assays with 8nM of Taxol for RPE-1 WT cells quantified in Figure 1A and **B)** HMEC-1 (Parental) and cells infected with Lenti-guides targeting the ABCB1 gene (sgRNAs #1 to #15).

Unexpected gene activation following CRISPR-Cas9-mediated genome editing



Supplementary Figure 2 – A DSB is needed to induce Taxol-resistant colonies

A) Example replicate of crystal violet staining of Colony Formation Assays with 8nM of Taxol for RPE-1 Cas9 and RPE-1 dCas9 cells infected with the indicated sgRNAs targeting ABCB1. **B)** Quantification of A, Error bars show the SD of three biological replicates (n=3).



Supplementary Figure 3 – Chromatin landscape of the ABCB1 promoter in the Taxol-resistant clones

A) H3K9me3 ChIP-qPCR showing two primer pairs amplifying positive regions for H3K9me3 (KS6 and KS7) in RPE-1 Parental and Taxol-resistant clones. **B)** H3K9me3 ChIP-qPCR showing two primer pairs amplifying negative regions for H3K9me3 (7 and S2) in RPE-1 Parental and Taxol-resistant clones.

REFERENCES

- Mojica, F. J. M., Juez, G. & Rodríguez-Valera, F. Transcription at different salinities of Haloferax mediterranei sequences adjacent to partially modified PstI sites. *Mol. Microbiol.* **9**, 613–621 (1993).
- Mojica, F. J. M., Díez-Villaseñor, C., García-Martínez, J. & Soria, E. Intervening sequences of regularly spaced prokaryotic repeats derive from foreign genetic elements. *J. Mol. Evol.* **60**, 174–182 (2005).
- van der Oost, J., Jore, M. M., Westra, E. R., Lundgren, M. & Brouns, S. J. J. CRISPR-based adaptive and heritable immunity in prokaryotes. *Trends in Biochemical Sciences* vol. 34 401–407 (2009).
- Jinek, M. *et al.* A programmable dual-RNA-guided DNA endonuclease in adaptive bacterial immunity. *Science (80-.)*. **337**, 816–821 (2012).
- Cong, L. *et al.* Multiplex genome engineering using CRISPR/Cas systems. *Science (80-.)*. **339**, 819–823 (2013).
- Mali, P. *et al.* RNA-guided human genome engineering via Cas9. *Science (80-.)*. **339**, 823–826 (2013).
- Lino, C. A., Harper, J. C., Carney, J. P. & Timlin, J. A. Delivering crispr: A review of the challenges and approaches. *Drug Delivery* vol. 25 1234–1257 (2018).
- Vitor, A. C., Huertas, P., Legube, G. & de Almeida, S. F. Studying DNA Double-Strand Break Repair: An Ever-Growing Toolbox. *Frontiers in Molecular Biosciences* vol. 7 24 (2020).
- Clouaire, T. & Legube, G. A Snapshot on the Cis Chromatin Response to DNA Double-Strand Breaks. *Trends in Genetics* vol. 35 330–345 (2019).
- Aymard, F. *et al.* Genome-wide mapping of long-range contacts unveils clustering of DNA double-strand breaks at damaged active genes. *Nat. Struct. Mol. Biol.* **24**, 353–361 (2017).
- Miné-Hattab, J. & Chiolo, I. Complex Chromatin Motions for DNA Repair. *Frontiers in Genetics* vol. 11 800 (2020).
- D'Alessandro, G. & d'Adda di Fagagna, F. Transcription and DNA Damage: Holding Hands or Crossing Swords? *Journal of Molecular Biology* vol. 429 3215–3229 (2017).
- Jinek, M. *et al.* Structures of Cas9 endonucleases reveal RNA-mediated conformational activation. *Science (80-.)*. **343**, (2014).
- Doudna, J. A. & Charpentier, E. The new frontier of genome engineering with CRISPR-Cas9. *Science* vol. 346 (2014).
- Warnock, J. N., Daigre, C. & Al-Rubeai, M. Introduction to Viral Vectors. *Methods Mol. Biol.* **737**, 1–25 (2011).
- Kotterman, M. A., Chalberg, T. W. & Schaffer, D. V. Viral Vectors for Gene Therapy: Translational and Clinical Outlook. *Annual Review of Biomedical Engineering* vol. 17 63–89 (2015).
- de Melo, J. & Blackshaw, S. In vivo electroporation of developing mouse retina. In *Methods in Molecular Biology* vol. 1715 101–111 (Humana Press Inc., 2018).
- Horii, T. *et al.* Validation of microinjection methods for generating knockout mice by CRISPR/Cas-mediated genome engineering. *Sci. Rep.* **4**, (2014).
- Liang, X. *et al.* Rapid and highly efficient mammalian cell engineering via Cas9 protein transfection. *J. Biotechnol.* **208**, 44–53 (2015).
- PL, F. *et al.* Lipofection: a highly efficient, lipid-mediated DNA-transfection procedure. *Proc. Natl. Acad. Sci. U. S. A.* **84**, 7413–7417 (1987).
- Hsu, P. D. *et al.* DNA targeting specificity of RNA-guided Cas9 nucleases. *Nat. Biotechnol.* **31**, 827–832 (2013).
- Pattanayak, V. *et al.* High-throughput profiling of off-target DNA cleavage reveals RNA-programmed Cas9 nuclease specificity. *Nat. Biotechnol.* **31**, 839–843 (2013).
- Uddin, F., Rudin, C. M. & Sen, T. CRISPR Gene Therapy: Applications, Limitations, and Implications for the Future. *Frontiers in Oncology* vol. 10 1387 (2020).
- Tame, M. A., Manjón, A. G., Belokhovostova, D., Raaijmakers, J. A. & Medema, R. H. TUBB3 overexpression has a negligible effect on the sensitivity to Taxol in cultured cell lines. *Oncotarget* **8**, 71536 (2017).
- Manjón, A. G. *et al.* Perturbations in 3D genome organization can promote acquired drug resistance. *bioRxiv* 2021.02.02.429315 (2021) doi:10.1101/2021.02.02.429315.
- Sanjana, N. E., Shalem, O. & Zhang, F. Improved vectors and genome-wide libraries for CRISPR screening. *Nat. Methods* **11**, 783 (2014).
- de Vree, P. J. P. *et al.* Targeted sequencing by proximity ligation for comprehensive variant detection and local haplotyping. *Nat. Biotechnol.* **32**, 1019–25 (2014).
- Reed, K., Hembruff, S. L., Sprowl, J. A. & Parisenti, A. M. The temporal relationship between ABCB1 promoter hypomethylation, ABCB1 expression and acquisition of drug resistance. *Pharmacogenomics J.* **10**, 489–504 (2010).
- Chen, K. G. *et al.* Genetic and epigenetic modeling of the origins of multidrug-resistant cells in a human sarcoma cell line. *Cancer Res.* **65**, 9388–9397 (2005).
- Rothe, M., Modlich, U. & Schambach, A. Biosafety Challenges for Use of Lentiviral Vectors in Gene Therapy. *Curr. Gene Ther.* **13**, 453–468 (2014).
- Hacein-Bey-Abina, S. *et al.* A Serious Adverse Event after Successful Gene Therapy for X-Linked Severe Combined Immunodeficiency. *N. Engl. J. Med.* **348**, 255–256 (2003).
- Mulero-Sánchez, A., Pogacar, Z. & Vecchione, L. Importance of genetic screens in precision oncology. *ESMO Open* **4**, (2019).
- Cao, J. X., Wang, Y. L. & Wang, Z. X. Advances in precise regulation of CRISPR/Cas9 gene editing technology. *Yi chuan = Hered.* **42**, 1168–1177 (2020).
- Kosicki, M., Tomberg, K. & Bradley, A. Repair of double-strand breaks induced by CRISPR–Cas9 leads to large deletions and complex rearrangements. *Nat. Biotechnol.* **36**, 765–771 (2018).
- Zhang, X. H., Tee, L. Y., Wang, X. G., Huang, Q. S. & Yang, S. H. Off-target effects in CRISPR/Cas9-mediated genome engineering. *Molecular Therapy - Nucleic Acids* vol. 4 e264 (2015).

Unexpected gene activation following CRISPR-Cas9-mediated genome editing

36. Van Den Berg, J. *et al.* A limited number of double-strand DNA breaks is sufficient to delay cell cycle progression. *Nucleic Acids Res.* **46**, 10132–10144 (2018).
37. Schep, R. *et al.* Impact of chromatin context on Cas9-induced DNA double-strand break repair pathway balance. *bioRxiv* 2020.05.05.078436 (2020) doi:10.1101/2020.05.05.078436.
38. Yan, S., Schubert, M., Young, M. & Wang, B. *Applications of Cas9 nickases for genome engineering.* www.idtdna.com.
39. Li, H. & Durbin, R. Fast and accurate long-read alignment with Burrows-Wheeler transform. *Bioinformatics* **26**, 589–595 (2010).
40. Stelloo, S. *et al.* Endogenous androgen receptor proteomic profiling reveals genomic subcomplex involved in prostate tumorigenesis. *Oncogene* **37**, 313–322 (2018).
41. Brinkman, E. K., Chen, T., Amendola, M. & van Steensel, B. Easy quantitative assessment of genome editing by sequence trace decomposition. *Nucleic Acids Res.* **42**, e168–e168 (2014).



6

Uncovering the contribution of different DDR factors in repair pathway choice in the context of chromatin

Anna G. Manjón*, Xabier Vergara*, Ben Morris, Roderick Beijersbergen, Bas van Steensel, René H. Medema

* Contributed equally

Manuscript in preparation

ABSTRACT

In order to deal with DNA damage, cells have developed several DNA repair pathways to fix these lesions. It is now clear that the local chromatin context can influence repair pathway choice. However, the effect of chromatin on individual DNA damage factors is poorly understood. Using the multiplex reporter assay of Schep et al. we set out to understand how different DNA damage repair (DDR) factors affect repair pathway choice in the context of distinct chromatin states. Employing a clonal cell line containing 19 copies of a pathway reporter, integrated at sites of varying chromatin states, we successfully implemented a CRISPR-Cas9-based screen for 527 DDR factors. Depletion of DDR factors was followed by Cas9-induced break formation in the 19 reporter integrations. Preliminary data revealed that depletion of single factors is able to switch repair pathway balance between NHEJ and MMEJ. Remarkably, the majority of observed perturbations are independent of the chromatin context. Yet, the screen could help to better understand the contribution of DDR factors to the NHEJ and MMEJ repair pathways.

INTRODUCTION

The integrity of the genome is continuously challenged by DNA lesions arising from endogenous and exogenous sources. DNA double-strand breaks (DSBs) are considered the most lethal form of DNA damage in eukaryotic organisms. In addition to triggering cell death, DSBs can also produce genetic mutations and chromosomal rearrangements leading to cancer onset and progression. CRISPR-Cas9 is widely applied for genome editing, but it also provides a means to induce endogenous DSBs at desired genomic locations¹⁻⁶. This property has increased the use of CRISPR-Cas9-induced breaks to study possible differences in the DNA damage response across different genome compartments or structures⁷.

Multiple cellular pathways can repair DSBs, including non-homologous end-joining (NHEJ), homologous recombination (HR) and microhomology-mediated end-joining (MMEJ) (reviewed in⁸). While NHEJ directly ligates together the blunt-ended DSBs, often producing small insertions and deletions, HR utilizes the intact sister chromatid of the damaged locus as a template allowing for error-free repair. In contrast, MMEJ uses short homologous sequences close to the break site to align the broken ends prior to ligation, resulting in small deletions. DSB repair pathway choice can be influenced by the local DNA sequence where the damage occurred⁹⁻¹¹ as well as by the cell cycle phase¹² and DNA end complexity¹³. In addition, DSB repair occurs in the context of the local chromatin¹⁴⁻¹⁷.

Most research has focused on understanding the interplay between NHEJ and HR. In these studies, DSBs are generated at different genomic locations, which makes the contribution of DNA sequence and chromatin inseparable. Schep et al. have recently reported a strategy that measures the contributions of NHEJ and MMEJ in the chromatin context where the sequence context remains unaltered¹⁷. Exploiting CRISPR-Cas9 technology, they used a TRIP-based reporter¹⁸ inserted in >1,000 genomic locations (Integrated Pathway Reporter, IPR) that, when cut with Cas9, measures repair by NHEJ and MMEJ across the entire chromatin landscape using breaks of identical sequence.

Despite recent advances on understanding the importance of chromatin state in regulating repair pathway choice, the contribution of individual DNA damage repair (DDR) factors across varying chromatin states remains elusive. DDR components have been extensively described and assigned to a specific repair pathway. But clearly, these factors must be recruited within the context of chromatin. Here, we report a novel application of the TRIP-based multiplexed reporter assay from Schep et al. We demonstrate that CRISPR-Cas9 screens can be successfully implemented in this system to uncover the contribution of individual DDR factors in repair pathway choice in the context of chromatin. We generated a 96-well format synthetic gRNA library with 527 genes involved in the DNA damage response. KO generation by transfection of the gRNAs into a K562 clone with 19 integrated pathway reporters was followed by Cas9-induced DSB in the reporters. Preliminary data indicated that

the depletion of DDR proteins is able to shift the pathway balance towards NHEJ or MMEJ depending on the depleted factor. Strikingly, the majority of observed NHEJ or MMEJ perturbations are independent of the chromatin context. Altogether, we demonstrate that the use of CRISPR screens can help us understand the implications of each individual protein in DNA repair pathway choice across the entire chromatin environment.

RESULTS

CRISPR-Cas9 screen of DDR proteins in the multiplex reporter assay: Screen set up

In order to understand if the contribution of known DDR factors varies across different chromatin states, we modified the TRIP-based multiplex reporter assay from Schep et al. to perform a CRISPR-Cas9-based screen. To carry out this approach, we selected the K562 Clone #5, a very well characterized cell line with 19 Integrated Pathway Reporters (IPRs) located across most major chromatin types¹⁷. Each of the IPRs contains a short DNA sequence (derived from the LBR gene) that is edited when targeted with a CRISPR RNA (from now on LBR-crRNA) and the Cas9 endonuclease. It has been previously described that the two most common indels that result from this editing procedure, a +1 insertion or a -7 deletion, are the result of NHEJ and MMEJ repair, respectively^{17,19}. The CRISPR-Cas9-based screen was performed in a 96-well format, where each well contains four crRNAs targeting the same gene (**Fig. 1A**). The crRNAs were distributed in six 96-well plates, leaving the column #6 for control samples on each plate. Clone 5 was co-transfected with the corresponding crRNA together with the tracrRNA (see Material and Methods for details) and treated with Shield-1 for Cas9 activation to create a knock-out for each respective gene in the library. Five days later, the LBR-crRNA was co-transfected with the tracrRNA to induce the DSB in the 19 IPRs in the context of each KO (**Fig. 1B**). Column #6 was transfected with LBR-crRNA to normalize and analyze the results obtained in the screen. After 3 days of DSB induction in the IPRs, cells were lysed in 96-well PCR plates and libraries were prepared for sequencing to determine the indel patterns that were produced in each individual well (**Fig. 1C**).

Evaluation of noise levels in WT and KOs for MMEJ scores and cutting efficiency

Three independent replicates were performed in order to obtain a reliable measure of pathway balance perturbations. Cutting efficiency was calculated and correlated among three replicates in WT wells (**Fig. 2A**, upper row) and KO wells (**Fig. 2B**, upper row). 60 to 70% cutting efficiency was observed in WT wells, while KO wells had a bigger cutting efficiency spread. In this last category, some outlier wells did not correlate well between replicates. The relative frequency of MMEJ (MMEJscore) was

CRISPR-Cas9 screen to characterize chromatin influence upon DSB

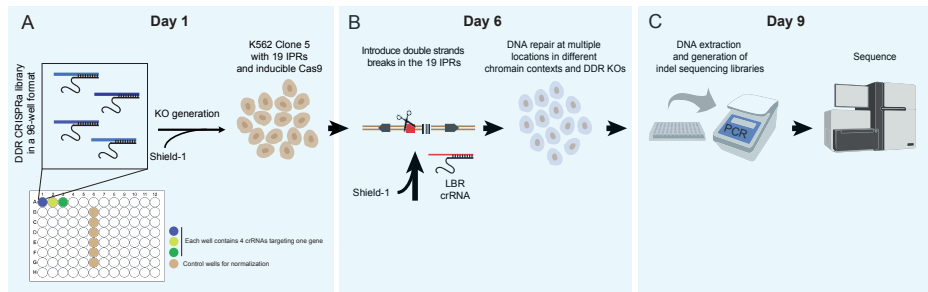


Figure 1 – CRISPR-Cas9 screen of DDR proteins in the multiplex reporter assay: Screen set up.

A) A combination of four crRNAs targeting a single DDR protein for KO generation are found in a single well of a 96-well plate. Column 6 does not contain any crRNA. For KO generation in Clone 5, the four crRNAs were co-transfected with a tracrRNA and Shield-1 and kept in individual wells. **B)** After 5 days, the LBR-crRNA and tracrRNA were co-transfected to induce DSBs in the 19 IPRs. This will happen in the context of a specific DDR protein KO. **C)** 72h after IPR-DSB induction cells were lysed and kept in 96-well PCR tubes for further processing and library preparation followed by Illumina sequencing.

calculated dividing the frequency of -7 by the sum of -7 and +1 indel frequencies ($\text{freq}_{-7}/(\text{freq}_{-7}+\text{freq}_{+1})$). We obtained a MMEJ score per IPR in each WT well and DDR protein KO. Next, we averaged the 19 MMEJ scores per well and compared them between replicates (**Fig. 2A and B**, lower row). Importantly, we detected a very consistent MMEJ score across WT wells (**Fig. 2A**, lower row) that allowed us to set baseline to compare to the KO wells. The MMEJ scores of the KOs clearly correlated between replicates even though some outliers were as well observed (**Fig. 2B**, lower row). Next, we used MMEJ score from WT wells ($n = 38$) as a null population to compute the z-score per IPRs of each KO. Z-scores for IPRs in similar types of chromatin were combined together to get MMEJ score per each chromatin category (**Fig. 2C, Sup. Fig. 1**). Negative values of Z-scores refer to a switch from MMEJ towards NHEJ repair (less -7 and more +1) while positive z-scores imply lower NHEJ and higher MMEJ repair (less +1 and more +7). While the majority of KOs were found distributed around the 0 value, we could observe several KOs with a significant change in their z-score in every chromatin type (**Fig. 2C**).

Gene knock-outs that perturb the NHEJ and MMEJ pathway balance

We next decided to further examine genes whose depletion caused a perturbation in pathway balance in different chromatin states. In the screen set up we included *POLQ*, a gene known to be involved in MMEJ, as a positive control. Indeed, *POLQ* depletion led to the highest reduction in MMEJ (z-score around -20) in all chromatin types (**Fig. 3A**, green dots). Interestingly, we observed a higher number of KOs leading to negative z-scores (**Fig. 3A**, red dots), suggesting that more proteins in

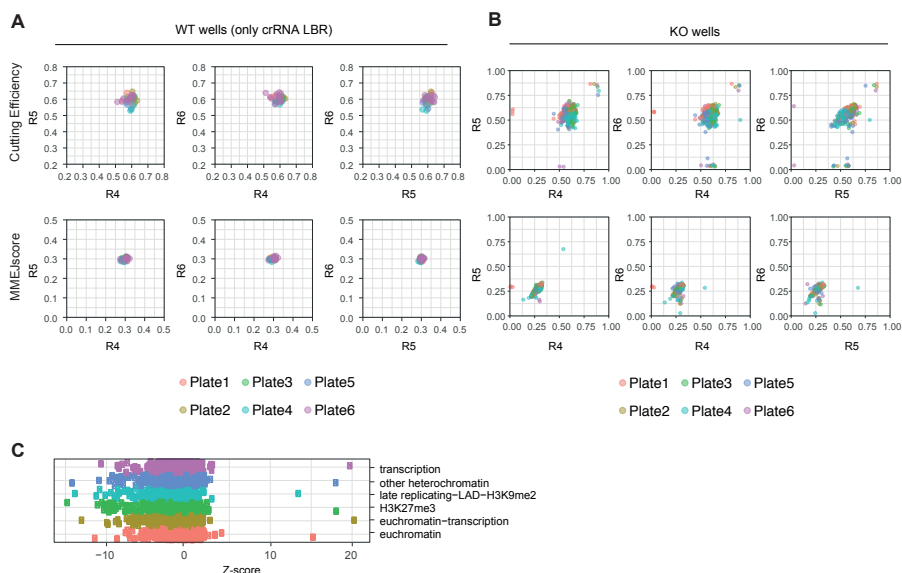


Figure 2 – Evaluation of noise levels in WT and KO for MMEJ scores and cutting efficiency.

A) Correlation plots between the three replicates in the WT wells only targeted with the crRNA-LBR. Upper row shows cutting efficiency correlation and lower row shows MMEJ score correlations. Every dot represents a well color-coded by plate. **B)** Correlation plots between the three replicates in the KO wells (same as **A**). **C)** Z-scores calculated over the three replicates in every chromatin type. Every dot represents a gene. Negative z-score values determine perturbations in MMEJ while positive represent perturbations in NHEJ.

our library are involved in regulating MMEJ than NHEJ. We then set a threshold of z-score ± 1.65 in order to consider a protein a hit, where in all three replicates at least one chromatin type was $+1.65$ or -1.65 (**Fig. 3B**). In order to visualize whether some DDR factors had distinct roles among chromatin states, we plotted all the hits of the screen in a heatmap representing the different chromatin states (**Fig. 3B**). Red indicates a KO switching pathway balance towards NHEJ (MMEJ perturbation) and blue means a perturbation in favor of the MMEJ pathway. Here again we can verify that in our DDR factor library more genes are involved in regulating MMEJ than NHEJ. Remarkably, *POLL*, the gene encoding for the polymerase λ ($\text{Pol } \lambda$) shows the highest z-score in all chromatin types, indicating that its perturbation decreases NHEJ (**Fig. 3B**). We observed that the majority of depleted DDR proteins perturb NHEJ or MMEJ independently of the chromatin type (**Fig. 3B**), *POLL* and *RAD50* being respectively in the extremes. Interestingly, members of the MRN complex and the Fanconia Anemia pathway appear to have a greater effect on perturbing MMEJ.

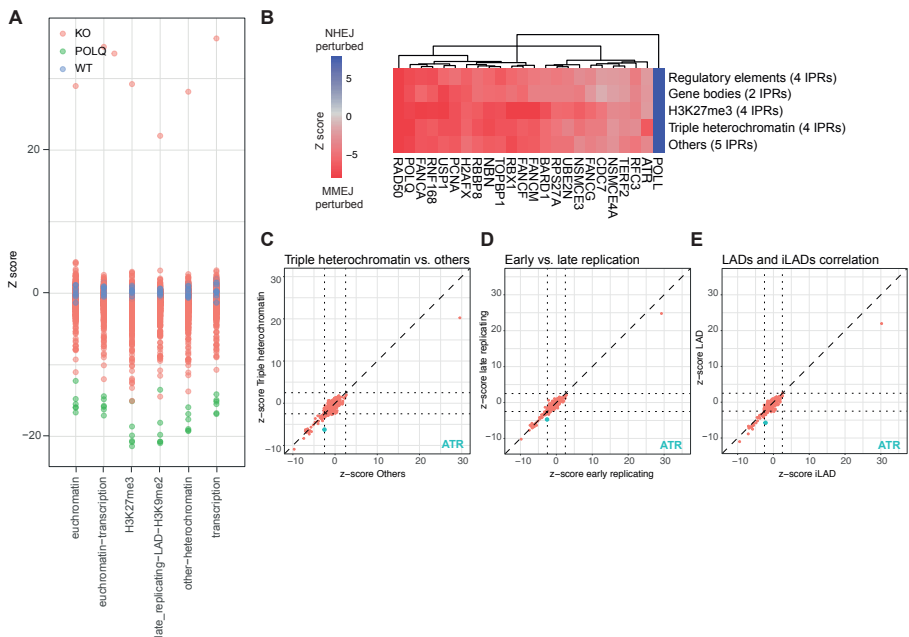


Figure 3 – Preliminary genes detected to perturb the NHEJ and MMEJ pathway balance. **A)** Z-score plot color-coding WT and KO wells. POLQ control gene shows the higher perturbations on MMEJ (lower z-scores) as expected as being a key regulator of this pathway. WT wells used to calculate z-scores have z-score values of 0. KO genes are distributed around WT z-scores depending on the effect they have on MMEJ and NHEJ pathway balance. **B)** Heat map of genes with absolute z-score ≥ 1.65 at least in one chromatin type and in all three replicates classified by hierarchical clustering in all chromatin states. Red scale shows pathway balance switching towards NHEJ (MMEJ perturbed). Blue colors show pathway switching towards MMEJ (NHEJ perturbed). **C)** Correlation plot of MMEJ z-scores in barcodes located in triple heterochromatin vs other types of chromatin of all DDR factors. Every dot shows the average z-score from three replicates. Blue dot shows the ATR gene. **D)** Correlation plot of MMEJ z-scores in barcodes located in early vs late replicating regions of all DDR factors. **E)** Correlation plot of MMEJ z-scores in barcodes located in LADs vs iLADs of all DDR factors.

Only *ATR* appeared to have a chromatin context specific role. Specifically, in triple heterochromatin, *ATR* had a consistent lower z-score, suggesting a role in MMEJ in heterochromatin regions (**Fig. 3B**). To better visualize the effect of *ATR* depletion in this chromatin state, we correlated the MMEJ z-scores of all KOs stratified by barcodes located in triple heterochromatin vs barcodes located somewhere else (**Fig. 3C**). Indeed, *ATR* was the gene that deviated the most from the diagonal, suggesting a role in MMEJ specifically in triple heterochromatin. Triple heterochromatin can be defined by three features: H3k9me2, lamina-associated domains (LADs) and late replication regions¹⁷. Again, when generating correlation plots for early vs late replicating regions (**Fig. 3D**) or LAD vs iLADs (**Fig. 3E**), we could observe *ATR* having

a differentially effect on MMEJ. Overall, these results suggest that the majority of DDR proteins regulate NHEJ or MMEJ pathway balance mainly independently of the chromatin context. Exceptionally, *ATR* could have a specific role depending on the chromatin context where the DSB is induced.

DISCUSSION

In this study we describe a high-throughput approach based on CRISPR-Cas9-mediated genome editing to systematically interrogate the DNA repair pathway choice of DDR proteins in the context of chromatin. We demonstrate that the multiplexed DSB repair reporter from Schep et al. can be scaled to perform CRISPR screens targeting DNA damage proteins in a 96-well format. As this reporter has very well characterized indels; +1 for NHEJ and -7 for MMEJ, we can study the contribution of DDR proteins to each of this mutation patterns in different chromatin context. We clearly detect perturbations in the expected repair pathways upon depletion of previously described DDR factors. Surprisingly, preliminary analysis does not show major differences in the repair pathway choice of specific DDR factors depending on the chromatin environment where the DSB takes place. This may be explained by the CRISPR library generation, where primarily core repair factors were included. These proteins have very specific roles in the DNA damage response and repair, which could leave the chromatin environment with a negligent role.

Advances in CRISPR Cas9-based screening have generated a broad gene repository involved in many different biological processes and pathways²⁰⁻²³. Many of these have been done against DNA-damaging agents in order to identify novel regulators of the DNA damage response²⁴. Other screens have been performed targeting known DDR proteins to reveal novel gene-drug interactions^{25,26}. Here we describe for the first time a screen approach that aims to uncover the interrelationship between chromatin and DNA damage factors. On the one hand, high-resolution investigations have determined that upon DSB induction chromatin is modified on several different levels^{27,28}. On the other hand, it is known that different DNA repair pathways have different chromatin signatures¹⁴. Here we aimed to understand which role the original chromatin landscape plays in regulating specific DDR proteins and repair pathway choice. Schep et al. have recently unraveled how the repair of Cas9 breaks is influenced by the local chromatin context independent of the sequence¹⁷. Specifically, while NHEJ shows higher incidence in all chromatin contexts, heterochromatin environments had a bias towards MMEJ. Here we show that depletion of the DDR factors in our library mostly perturbs MMEJ, as shown by more negative z-scores compared to positive, implying that MMEJ is more tightly controlled than NHEJ.

We also show that DDR genes with a related function are typically clustering together independently of the local chromatin state. For instance, proteins belonging to the

MRN complex (*RAD50*, *NBN*, *RBBP8*) known to be involved in short-range resection, show a decrease in MMEJ when depleted. It is known that the MMEJ repair pathway depends on resecting the broken ends by the MRN complex²⁹. We also observe similar MMEJ reduction levels with *POLQ* KO, the downstream polymerase q (Pol q) required to extend the resected ends to complete MMEJ. Therefore, we can hypothesize that both loss of upstream resection factors or downstream effectors of the MMEJ pathway can switch the repair towards NHEJ. Interestingly, proteins from the Fanconi anemia (FA) pathway (*FANCA*, *FANCF*, *FANCM*) are also found to alter the pathway balance towards NHEJ, suggesting a role in MMEJ. FA proteins are known to repair interstrand crosslink (ICL) lesions, which consist in a covalent bond between the two strands of DNA. Interesting links exist between MMEJ and the Fanconi anemia genes^{30,31}. Specially, *FANCA* is able to catalyze single-strand annealing (SSA) in DSBs, a repair pathway that shares many features with MMEJ³². Interestingly, the strongest hit (with a z-score ~ 20) is polymerase I (Pol I), a protein encoded in *POLL* gene. Pol I is involved in the gap-filling step of NHEJ pathway, which will further bind XRCC4-ligase IV complex to complete the final ligation³³. We can speculate that depletion of Pol I would interfere with the formation of the +1 insertion in the reporter system and therefore MMEJ repair pathway and Pol q ligation would take place. Taken together, our screen allows us to more carefully categorize the function of known DDR regulators and their engagement in the MMEJ/NHEJ repair pathway choice.

Yet, the strongest hallmark of the screen was the potential to detect the influence of chromatin on repair pathway choice in the different DDR factors. However, we can only detect limited DDR factors that potentially employ different repair pathways depending on the chromatin context. Interestingly, *ATR* depletion showed a stronger decrease in MMEJ in triple heterochromatin regions compared to other types of chromatin. In *Drosophila*, it has been shown that ATRIP foci (ATR interacting protein) are recruited to resected DSBs and appear brighter and faster in heterochromatin³⁴. In fact, *ATR* inhibition in *Drosophila* also has been reported to show defects on heterochromatin expansion and DSB movement³⁵. We could speculate that *ATR* is required in LADs and other triple heterochromatin regions to promote chromatin expansion and DSB-resection engagement.

Overall, this preliminary analysis confirms the functionality of genetic screens in this multiplexed DSB repair reporter of Schep et al. Even though chromatin appears to have relatively minor role in regulating different DDR factors, we can further study how an extensive network of DDR proteins affects the NHEJ and MMEJ repair pathway choice.

MATERIALS AND METHODS

Cell lines and cell culture conditions

We used clonal cell like K562 #5 derived from female human K562 cell line (ATCC) stably expressing DD-Cas9³⁶. K562 cells were cultured in RPMI 1640 (GIBCO) Supplemented with 10% fetal bovine serum (FBS, Sigma), 1% penicillin/streptomycin.

Synthetic DDR gRNA library generation

Gene Ontology terms descriptive of biological processes (GOTERM_BP) were used to select the DDR genes included in the library. DDR (GO:0006281~DNA repair) and DSBR (GO:0006302~doublestrand break repair) gene lists were combined with an in-house shRNA DDR library. Afterwards, manual filtering was performed with the help of the DNA damage expert researchers Jacqueline Jacobs, Heinz Jacobs and Jeroen van den Berg to end up with a list of 527 genes. The crRNA library was generated by Integrated DNA Technologies (IDT) and contained 4 gRNA per gene that were pooled together in the same well. The crRNAs were distributed in 6 96-well plates. The crRNAs were delivered in a lyophilized RNA form.

gRNA transfections and KO generation

96-well transfections were performed with the help of the robotics facility at the NKI making use of Hamilton Research and Development platform (R&D). Two transfections were done in order to carry out the DDR CRISPR screen. The first transfection involved individually combining the 527 DDR proteins crRNAs with the tracrRNA forming a duplex to guide Cas9 to the break site. Next, 15.000 K562 were reverse transfected per well with the crRNA:tracrRNA duplex and the lipofectamine DharmaFECT 4 transfection reagent (Horizon discovery). Cells were grown in 96-wells and splitted 1:10 the 5th day. For the second transfection at day 6, a crRNA targeting the IPRs (GCCGATGGTGA-AGTGGTAAG) and tracrRNA were reverse transfected in K562 KO cells in the same ways as transfection 1. Four wells per plate (and nine extra wells in plate 6) were only transfected with crRNA targeting the IPRs, and were used for normalization when analyzing the results. At Day 9 cells were lysed with DirectPCR Lysis Reagent (Cell) (Catalog No: 301-C) to proceed with the generation of indel sequencing libraries. crRNA and tracrRNA were transfected at a final concentration of 20nM each. 2x DharmaFECT 4 was used. Shield-1 (Aeobius, Cat#: AOB1848) was added in K562 cells prior to transfections in a final concentration of 500nM.

Two biological independent CRISPR-Cas9 screens were performed in separate months. Each biological experiment was organized in three technical replicates (every 96-well plate was represented 3 times).

Generation of indel sequencing libraries

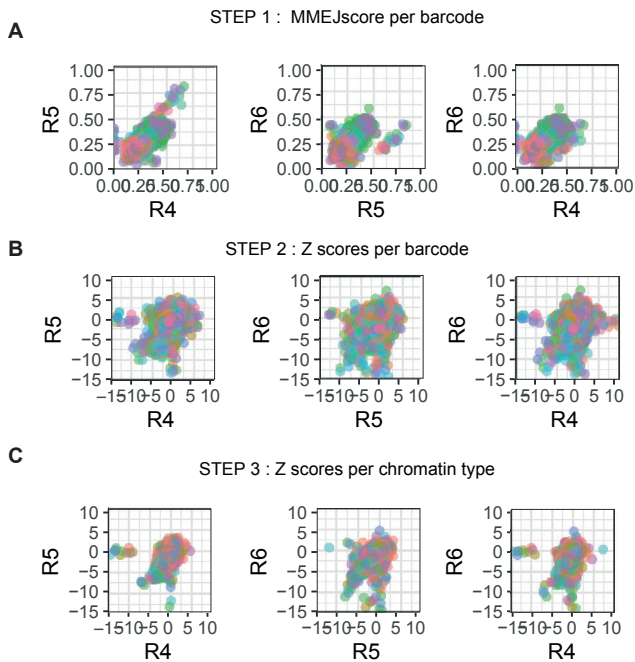
After 72 hours of the IPR crRNA transfection, cells were collected by the robot, and genomic DNA was extracted using Direct Lysis with proteinase K. PCRs for library generation were conducted as described in¹⁷.

Indel scoring

Indel reads were analyzed and counted in the same way as in ¹⁷. To assess the MMEJ repair, we calculated the MMEJ score (frequency of -7/(frequency of -7 + frequency of +1).

MMEJ score data processing

MMEJ scores were converted into z-scores to account for small differences in dynamic range. Z-scores were calculated by using the mean and standard deviation of the MMEJ score in WT wells and KO wells. MMEJ score processing contains three different steps: 1. Selection of WT background breaks (null population) and calculation of z-scores based on mean & SD of the null distribution (per barcode and replicate) 2. Combination of IPRs by chromatin type as dependent variables. 3. Combination of replicates as independent variables.



Supplementary Figure 1 - Z-scores calculation with MMEJ scores from WT wells and KO wells.

MMEJ scores were converted into z-scores to account for small differences in dynamic range. Z-scores were calculated by using the mean and standard deviation of the MMEJ score in WT wells and KO wells. **A)** Correlation between replicates of the MMEJ scores per barcodes of the KO genes. **B)** Correlation between replicates of the z-score per barcode of KO genes. **C)** Correlation between replicates of the z-scores per chromatin type of the KO genes.

REFERENCES

- Mojica, F. J. M., Juez, G. & Rodriguez-Valera, F. Transcription at different salinities of *Haloferax mediterranei* sequences adjacent to partially modified PstI sites. *Mol. Microbiol.* **9**, 613–621 (1993).
- Mojica, F. J. M., Díez-Villaseñor, C., García-Martínez, J. & Soria, E. Intervening sequences of regularly spaced prokaryotic repeats derive from foreign genetic elements. *J. Mol. Evol.* **60**, 174–182 (2005).
- van der Oost, J., Jore, M. M., Westra, E. R., Lundgren, M. & Brouns, S. J. J. CRISPR-based adaptive and heritable immunity in prokaryotes. *Trends in Biochemical Sciences* vol. 34 401–407 (2009).
- Jinek, M. *et al.* A programmable dual-RNA-guided DNA endonuclease in adaptive bacterial immunity. *Science* (80-.). **337**, 816–821 (2012).
- Cong, L. *et al.* Multiplex genome engineering using CRISPR/Cas systems. *Science* (80-.). **339**, 819–823 (2013).
- Mali, P. *et al.* RNA-guided human genome engineering via Cas9. *Science* (80-.). **339**, 823–826 (2013).
- Vitor, A. C., Huertas, P., Legube, G. & de Almeida, S. F. Studying DNA Double-Strand Break Repair: An Ever-Growing Toolbox. *Frontiers in Molecular Biosciences* vol. 7 24 (2020).
- Mladenov, E., Magin, S., Soni, A. & Iliakis, G. DNA double-strand-break repair in higher eukaryotes and its role in genomic instability and cancer: Cell cycle and proliferation-dependent regulation. *Seminars in Cancer Biology* vols 37–38 51–64 (2016).
- Allen, F. *et al.* Predicting the mutations generated by repair of Cas9-induced double-strand breaks. *Nat. Biotechnol.* **37**, 64–82 (2019).
- Chakrabarti, A. M. *et al.* Target-Specific Precision of CRISPR-Mediated Genome Editing. *Mol. Cell* **73**, 699–713.e6 (2019).
- Shen, M. W. *et al.* Predictable and precise template-free CRISPR editing of pathogenic variants. *Nature* **563**, 646–651 (2018).
- Hustedt, N. & Durocher, D. The control of DNA repair by the cell cycle. *Nature Cell Biology* vol. 19 1–9 (2017).
- Schipler, A. & Iliakis, G. DNA double-strand-break complexity levels and their possible contributions to the probability for error-prone processing and repair pathway choice. *Nucleic Acids Res.* **41**, 7589–7605 (2013).
- Thomas Clouaire, A. *et al.* Comprehensive Mapping of Histone Modifications at DNA Double-Strand Breaks Deciphers Repair Pathway Chromatin Signatures. *Mol. Cell* **72**, 250–262.e6 (2018).
- Clouaire, T. & Legube, G. DNA double strand break repair pathway choice: A chromatin based decision? *Nucleus* **6**, 107–113 (2015).
- Kalousi, A. & Soutoglou, E. Nuclear compartmentalization of DNA repair. *Current Opinion in Genetics and Development* vol. 37 148–157 (2016).
- Schep, R. *et al.* Impact of chromatin context on Cas9-induced DNA double-strand break repair pathway balance. (2021) doi:10.1016/j.molcel.2021.03.032.
- Akhtar, W. *et al.* XChromatin position effects assayed by thousands of reporters integrated in parallel. *Cell* **154**, 914–927 (2013).
- Brinkman, E. K. *et al.* Kinetics and Fidelity of the Repair of Cas9-Induced Double-Strand DNA Breaks Molecular Cell Article Kinetics and Fidelity of the Repair of Cas9-Induced Double-Strand DNA Breaks. *Mol. Cell* **70**, 801–813 (2018).
- Joung, J. *et al.* Genome-scale CRISPR-Cas9 knockout and transcriptional activation screening. *Nat. Protoc.* **12**, 828–863 (2017).
- Zhang, F., Wen, Y. & Guo, X. CRISPR/Cas9 for genome editing: Progress, implications and challenges. *Hum. Mol. Genet.* **23**, R40–R46 (2014).
- Wu, X., Kriz, A. J. & Sharp, P. A. Target specificity of the CRISPR-Cas9 system. *Quantitative Biology* vol. 2 59–70 (2014).
- Cong, L. *et al.* Multiplex genome engineering using CRISPR/Cas systems. *Science* (80-.). **339**, 819–823 (2013).
- Olivieri, M. *et al.* A Genetic Map of the Response to DNA Damage in Human Cells. *Cell* **182**, 481–496.e21 (2020).
- Breuer, G. A. *et al.* Targeted DNA Damage Repair CRISPR/Cas9 Knockout Screen Identifies Novel Classification of Poly-ADP Ribose Polymerase Inhibitors Based on Key Base Excision Repair Proteins. *bioRxiv* 2020.10.18.333070 (2020) doi:10.1101/2020.10.18.333070.
- Su, D. *et al.* CRISPR/CAS9-based DNA damage response screens reveal gene-drug interactions. *DNA Repair (Amst.)* **87**, (2020).
- Polo, S. E. & Almouzni, G. Chromatin dynamics after DNA damage: The legacy of the access-repair-restore model. *DNA Repair* vol. 36 114–121 (2015).
- Clouaire, T. & Legube, G. A Snapshot on the Cis Chromatin Response to DNA Double-Strand Breaks. *Trends in Genetics* vol. 35 330–345 (2019).
- Sfeir, A. & Symington, L. S. Microhomology-Mediated End Joining: A Back-up Survival Mechanism or Dedicated Pathway? *Trends in Biochemical Sciences* vol. 40 701–714 (2015).
- McVey, M. & Lee, S. E. MMEJ repair of double-strand breaks (director's cut): deleted sequences and alternative endings. *Trends in Genetics* vol. 24 529–538 (2008).
- Howard, S. M., Yanez, D. A. & Stark, J. M. DNA Damage Response Factors from Diverse Pathways, Including DNA Crosslink Repair, Mediate Alternative End Joining. *PLoS Genet.* **11**, 1004943 (2015).
- Benitez, A. *et al.* FANCA Promotes DNA Double-Strand Break Repair by Catalyzing Single-Strand Annealing and Strand Exchange The single-strand annealing activity of FANCA plays a direct role in DSB repair Molecular Cell FANCA Promotes DNA Double-Strand Break Repair by Catalyzing Single-Strand Annealing and Strand Exchange. *Mol. Cell* **71**, 621–628 (2018).
- Van Loon, B., Hübscher, U. & Maga, G. Living on the Edge: DNA Polymerase Lambda between Genome Stability and Mutagenesis. *Chemical Research in Toxicology* vol. 30 1936–1941 (2017).
- Amaral, N., Ryu, T., Li, X. & Chiolo, I. Nuclear Dynamics of Heterochromatin Repair. *Trends Genet.* **33**, 86–100 (2017).
- Janssen, A., Colmenares, S. U. & Karpen, G. H. Heterochromatin : Guardian of the Genome. (2018).
- Brinkman, E. K. *et al.* Kinetics and Fidelity of the Repair of Cas9-Induced Double-Strand DNA Breaks. *Mol. Cell* **70**, 801–813.e6 (2018).



7

General Discussion

Anna G. Manjón, René H. Medema

Functional importance of (epi)genome integrity

All cells in an organism contain essentially the same DNA, yet, it is estimated that the human body is comprised of 210 histologically distinct cell types¹. This is achieved through differential gene expression programs that establish specialized cellular functions. Importantly, the regulation of gene expression relies on epigenetic modifications and organization of the genome within the nucleus. Epigenetics has been extensively described as the study of heritable gene expression changes that are not caused by changes in the DNA sequence². Changes in the epigenome include changes in DNA methylation, post-translation modifications of histones (PTMs), histone positioning or non-histone chromatin components³⁻⁶. In addition to this, the higher-order chromatin structure and distribution of the genome across distinct nuclear compartments also plays an important role in regulating the transcriptional program and cellular plasticity. Thus, chromatin can be seen as a complex biochemical network that can integrate environmental signals to regulate gene expression through changes in epigenetic marks. Yet, cellular processes such as transcription, replication or DNA damage and repair can induce alterations to the chromatin and the three-dimensional organization of the genome and thereby challenge the integrity of the epigenome.

In this thesis we have described various mechanisms that can compromise (epi) genome integrity, resulting in changes in gene expression and cellular phenotype, specifically the acquisition of drug resistance. In **Chapter 2** we describe the cellular model we have used to study acquisition of a Taxol-resistant phenotype, and show that this occurs via transcriptional activation of the *ABCB1* gene. Furthermore, we show that *ABCB1* activation can happen spontaneously, in cells exposed to increasing doses of Taxol over an extended period of time. In **Chapter 3** we further demonstrate the important role that 3D genome organization plays in gene regulation and cellular plasticity. Specifically, we show that perturbations in Nuclear Lamina (NL) interactions within *ABCB1* can lead to changes in gene expression and acquisition of a Taxol-resistant phenotype. Since chromatin is heavily modified during the DNA damage response, we wanted to study how epigenome integrity is affected and restored upon double-strand break (DSB) induction (**Chapter 4**). During the course of that work we uncovered that genetic DNA re-arrangements induced by CRISPR-Cas9-mediated genome editing also impact the three-dimensional genome organization and contribute to changes in gene expression that can affect cellular physiology (**Chapter 5**). Finally, in **Chapter 6** we have shifted the research focus to describe how local chromatin environment can affect the DNA damage response. The work presented in this thesis aims to emphasize the importance of chromatin and 3D genome organization in modulating cellular functions. We have aimed to resolve how epigenetic alterations that can promote gene activation can be induced in manners that could be highly relevant during tumor evolution.

Nuclear organizational changes leading to gene dis-regulation

The nucleus is organized in many layers ranging from high-order chromatin structures, such as the chromosomes, to smaller scale frameworks, for instance, DNA loops between regulatory regions. This nuclear organization influences transcriptional output in different ways. It is clear that enhancer-promoter interactions are necessary to modulate gene transcription, as changes in DNA contacts and chromatin looping have been shown to affect gene expression^{7,8}. Yet, it is unclear how higher-order genome organization is controlled during adaptive changes of a transcriptional program. Even though positioning of chromosome territories (CT) correlates with transcription, repositioning of CTs does not always cause changes in gene expression^{9,10}. Importantly, chromatin regions that are associated with the NL are mostly transcriptionally repressed^{11,12}. Several studies have shown that tethering chromosomes to the nuclear periphery decreases gene expression¹³⁻¹⁵. Also, triggering transcriptional activation in genes located at the NL using a dCas9-VP64 system can induce NL detachment¹⁶. Yet, the causal effect of the NL on repressing transcription is still a matter of debate. Researchers have tried to answer this question by perturbing NL components and observing the consequences on transcriptional outcome. Studies in *Drosophila* have found that depletion of lamins can lead to de-repression of NL-associated genes^{17,18}. In **Chapter 3** we set out to better understand whether the repressive environment of the NL could regulate *ABCB1* gene expression. *ABCB1* transcriptional activation is the main mechanism through which RPE-1 cells acquire Taxol resistance (**Chapter 2**). We found that *ABCB1* becomes more permissive to transcriptional activation upon depletion of *LBR*, but not after depletion of lamins. Interestingly, forced *ABCB1* detachment from the NL, without recruiting dCas9-VP64 to this locus, was associated with gene activation. Another investigation has shown that hundreds of human promoters become active when displaced from the NL, confirming the potential of the NL to form a repressive environment¹¹. However, that analysis also demonstrated that there is another set of promoters present inside LADs that are able to maintain active transcription¹⁹. This suggests that the NL influences but does not fully determine transcriptional outputs in all genomic regions similarly. Given the potential importance of the NL in regulating various cellular functions through its effect on gene expression, we can speculate that the 3D genome organization could have a role in the pathogenesis and progression of diseases. Indeed, several investigations have tried to address the changes in 3D genome alterations that occur during tumorigenesis²⁰⁻²². Three-dimensional genome organization has been analyzed in models of various cancer types, including breast, prostate, glioma and several hematological cancers²³⁻²⁶. Strikingly, no major differences within A/B compartments, Topological Associated Domains (TADs) and chromatin loops were found between healthy and cancer cells. However, in some cancers of the hematopoietic system, 20% of genomic regions were reported to undergo a compartmental switch (from A to B and vice versa)^{23,27,28}. It would

be interesting to assess whether loss of B compartments, specifically LADs is a consequence of mutations or downregulation of NL components such as Lamin A or *LBR* in those cancer types. Interestingly, a small molecule inhibitor that can compromise long-range promoter-enhancer interactions has been recently developed²⁹. Of course, it is highly debatable whether the three-dimensional genome can be fine-tuned with such inhibitors that detrimental interactions are disrupted, while other essential interactions are maintained. Nonetheless, this opens up new avenues of research that allow us to study the consequences of alterations in 3D genome organization in more detail.

As described in **Chapter 2** and **3**, small regions of the 3D genome can be re-organized leading to large phenotypic changes, such as acquisition of drug resistance. It is important to consider that anticancer drugs targeting the 3D genome could also have a negative outcome by dis-regulating oncogene gene expression. As new 3D genome analysis techniques have helped us to study chromatin organization changes in disease, we can then learn more about crucial changes and develop predictive biomarkers and potential new targets for anti-cancer therapy.

DNA rearrangements leading to transcriptional activation in response to DNA damage

DNA damage is one of the major threats to genome integrity. DNA double-strand breaks (DSBs) are one of the most deleterious forms of DNA damage that can lead to significant genomic mutations and rearrangements. These genomic alterations can create considerable challenges for the maintenance of a stable transcriptional program.

In **Chapter 4** of this thesis we describe a mechanism by which cells can rewire their transcriptional program, specifically re-activating the *ABCB1* gene, via genomic rearrangements that occur following DSB induction. This genetic perturbation leads to altered gene expression, through which cells acquire resistance to the chemotherapeutic drug Taxol. In our system, a DSB lesion in the regulatory region of the *ABCB1* gene, combined with selective pressure applied through the addition of Taxol to the culture medium, leads to fusions of the *ABCB1* locus with an active genomic region. It is known that HR and NHEJ repair pathways, even though important for genome stability, also generate a certain level of genome instability, due to the fact that repair is not always completely error-free³⁰. For instance, in some cases, long range resection which cannot be followed up by HR can lead to the use of microhomologies by engagement of microhomology-mediated end-joining (MMEJ). This can give rise to complex breakpoints and genomic rearrangements³¹. We can speculate that an event like this could have happened in some cells upon Cas9-induced break formation, followed by Taxol selection. The drug selection process enriches for a cell population that activates *ABCB1*, including rare genetic perturbations. Interestingly, recurrent translocations have been identified in many

tumors. Specifically, in ovarian cancer, among 114 samples of patients treated with Taxol, 36 rearrangements were captured, which included two recurrent promoter fusions between *ABCB1* and *SLC25A40*³². Even though in our system we did not observe fusions with *SLC25A40*, this is also a highly transcribed gene that leads to the transcriptional activation of *ABCB1*. This confirms that genetic rearrangements can occur in patients undergoing selective pressure, but *ABCB1* might not always be the driver of drug resistance in the clinical setting.

Additionally, other complex genetic rearrangements have been observed in the *ABCB1* locus, which also lead to acquired Taxol resistance. Among them we can include gene amplifications and extra chromosomal DNA sequences containing the *ABCB1* gene³³⁻³⁶. Our lab has generated Taxol-resistant cells from HeLa and p53-deficient RPE-1 cells in a similar manner as described in **Chapter 2**. Strikingly, while the HeLa cervical cancer cell line was able to acquire Taxol-resistance by generating extra chromosomal DNA sequences of *ABCB1* (data not shown), RPE-1 cells acquired resistance by upregulating *ABCB1* through non-genetic mechanisms. This suggests that transformed cell lines, potentially with higher levels of genomic instability, might be more prone to rewire the transcriptional program by accumulating genomic rearrangements, leading to cellular physiological changes.

In **Chapter 5** we introduced a DSB in the regulatory region of the *ABCB1* gene, but instead of a synthetic CRISPR RNA (crRNA), a lentiviral sgRNA delivery system was used. Interestingly, an artificial genetic alteration was also observed here, where the sgRNA-U6/EE1A1 promoters from the lentiviral delivery system were integrated in the DSB site thereby driving the transcriptional activation of *ABCB1*. It is important to take this research into consideration, as increasing advances in the CRISPR field are occurring. We speculate that random viral integration that can occur during CRISPR/Cas9-mediated genome editing could result in deregulation of genes that may affect biological functions. Interestingly, a serious adverse event was reported in immunodeficient patients undergoing gene therapy. Months after retrovirally mediated transfer of the *gc* gene into immune cells, one patient showed aberrant expression of the LMO-2 transcript in T-cells, a gene reported to cause acute lymphoblastic leukemia. Indeed, a proviral integration was found to drive LMO-2 expression³⁷.

In conclusion, DSB repair can play a triple role; on one hand, faithful repair can lead to the maintenance of genomic stability. On the other hand, DNA repair can generate genetic instability and significant genomic rearrangements via the errors that occur in the process. Importantly, our data reveal that DSBs can also act at a third level, namely to affect the epigenetic landscape of a gene, representing a novel way to regulate the transcription of the genes and create cell plasticity.

Influence of nuclear organization and local chromatin environment on the response to DNA damage

Local chromatin context and DNA repair pathway choice

As any other molecular process in the cell nucleus, DSB induction and repair occurs within a highly organized chromatin structure. Our understanding of the interplay between chromatin features and the repair process has increased in recent years due to the development of novel tools that allow for DSB formation at well-defined sites in the human genome. This was initially done by introduction of an ectopic I-SceI restriction site in the human genome that can be cleaved upon expression of I-SceI. As an alternative, recruitment of Fok1 to specific target sites was achieved using TALEN technology³⁸⁻⁴¹. In addition to this, several rare-cutting restriction enzymes have been expressed in mammalian cells that target a number of sites in the genome simultaneously, such as PpoI and AsiSI⁴². For instance, the DivA (DSB inducible via AsiSI) system enables the induction of DSB at known positions across the genome, where the different AsiSI sites vary in chromatin context⁴³⁻⁴⁵. These, and other tools, have shown that chromatin can regulate DNA repair at multiple levels and influence repair pathway choice. For example, it has been shown that actively transcribed regions enriched by H3k36me3 are preferentially repaired by HR⁴⁶. It has also been described that H3k9me3 heterochromatic regions recruit the acetyltransferase Tip60 via the MRN complex, suggesting that Tip60-dependent nucleosome removal could target HR to heterochromatin breaks⁴⁷⁻⁴⁹. Paradoxically, studies in *Drosophila* and mouse models revealed that gIR and Cas9-induced DSBs in heterochromatin are repaired by both NHEJ and HR with similar kinetics^{50,51}.

Recently, the group of Bas van Steensel developed a barcoded reporter system which randomly integrates in thousand locations in the genome and used this to unravel how DNA repair pathway choice is influenced by the local chromatin context⁵². Specifically, the reporter contains a sequence that when cleaved by Cas9 gives rise to specific indel signatures: a single nucleotide insertion (+1) associated with NHEJ and a 7 nucleotides deletion (-7) linked with MMEJ repair. While NHEJ was predominant in all chromatin environments, MMEJ repair was enhanced in heterochromatin environments. Specifically, H3k9me2 regions associated with the NL had a pronounced bias towards MMEJ.

In **Chapter 4** we induce DSBs with CRISPR/Cas9 in the *ABCB1* locus, a region defined by heterochromatin marks and its association with the NL. TIDE analysis after break induction in this location reveal different indel patterns depending on the crRNA used. If we consider indel formation as a readout for repair pathway usage, these data indicate that DNA sequence plays a prominent role in repair pathway choice. While crRNA#6 and #17 induce a pronounced +1, associated with NHEJ, crRNA #16 does not produce +1 insertions, indicating it triggers alternate repair pathways. Indeed, it has been shown that repair pathway choice also depends on the local DNA sequence⁵³⁻⁵⁵. We can also observe other resection-associated mutation patterns, suggesting that DSBs in heterochromatic regions can be repaired by multiple

pathways. In **Chapter 6** we describe the role of DNA damage proteins in regulating NHEJ and MMEJ depending on the chromatin context. Employing the TRIP-based repair reporter system with 19 well-annotated integrations in major chromatin contexts⁵², we perform a CRISPR-based screen using a library of crRNAs targeting all DNA damage-associated proteins. Interestingly, the predominant changes in repair pathway choice that are induced upon knock-down appear to be independent of the chromatin context. For instance, perturbing DNA damage response (DDR) regulators of resection affects MMEJ in all chromatin types. Indeed, it has been shown that NHEJ and MMEJ regulators bind to this reporter independently of the chromatin context⁵², suggesting that proteins of all major pathways regulate repair in both heterochromatin and euchromatin DSBs. Importantly, repair pathway choice does determine the repair accuracy and mutation rate of a DSB occurring in the genome.

Heterochromatin as a barrier for DNA damage repair

It has been hypothesized that heterochromatin represents a challenge for DNA damage repair due to its highly condensed nature. It is therefore thought that heterochromatin needs to be de-compacted for repair factors to gain access to the site of damage^{47,56}. Several investigations have suggested a role for KAP1 phosphorylation in mediating chromatin decondensation and subsequent release of HP1-b from heterochromatin⁵⁷. Moreover, it has been reported that pericentromeric heterochromatin regions in *Drosophila* relocalize outside of the heterochromatic domain to allow for repair by HR upon DSB induction by gIR⁵⁸⁻⁶¹. These breaks migrate to the nuclear periphery where they anchor to the nuclear pores, to allow for the recruitment of Rad51. It has been hypothesized that relocalization helps to avoid recombination with other repetitive heterochromatin regions thus preventing genomic instability. Similar relocalization of DSBs has been observed in mouse cells upon gIR of chromocenters, another heterochromatin structure⁶². Interestingly, recent investigations have determined that nuclear actin (N-actin) and myosin-dependent forces drive the relocalization of DNA breaks in heterochromatic regions in mouse cells⁶³. The mechanisms of DSB relocalization might also occur in other heterochromatin-like structures such as telomeres^{64,65}, where actin polymerization is also involved in the DNA movement. Whether this relocalization could have consequences on gene expression has never been exploited. In **Chapter 4** we hypothesize that DNA dynamics that are induced upon DSB formation could have a role in acquisition of Taxol resistance through transcriptional activation of *ABCB1*. Indeed, switching repair towards HR, via inhibition of DNAPK, caused an increase in the number of Taxol resistant cells. We speculate that *ABCB1* could re-localize outside of the heterochromatin domain to complete HR repair, where transcriptional activation could take place. Failure to restore the original chromatin state could subsequently lead to stable *ABCB1* transcriptional activation in a subset of cells. This model is substantiated by the evidence we present for NL detachment of the *ABCB1* locus by pA-DamID after DSB induction.

Higher-order genome organization and its influence on DNA repair

DNA damage and repair also takes place in the context of higher-order chromatin structures^{66,67}. Indeed, nuclear organization plays a critical role in regulating not only gene expression, but also maintaining genomic stability⁶⁸. Nuclear compartments include the nuclear periphery (NL and nuclear pores), nucleoli and nuclear bodies such as PML bodies and Cajal bodies⁶⁹. As described above, some DSBs display extensive mobility towards the nuclear periphery to finalize repair. Apart from NL-associated domains, it has also been reported that DSBs induced at nucleolar rDNA repeats lead to reorganization of the nucleolar structure. Somewhat similar to the breaks at the NL, it has been shown that rDNA breaks relocalize towards the nucleolar periphery in order to be accessible to DDR factors and engage HR⁷⁰⁻⁷².

A limited number of studies have been performed inducing DSBs in the nuclear periphery, specifically at LADs. One of these studies aimed to determine repair pathway engagement on an I-SceI site introduced in a locus tethered to the nuclear lamina using the lacO/LacI system⁷³. Interestingly, HR factors such as BRCA1 and Rad51 could not be recruited to the LAD and the DSBs were mainly repaired by NHEJ. On the other hand, when DSBs were induced at nuclear pores (a more open chromatin domain) using the same system, they could be repaired by both NHEJ and HR. This suggests that the chromatin environment of different genomic domains plays a role in repair pathway choice. Remarkably, the authors confirmed by super resolution imaging that DSBs associated with the NL do not migrate to more permissive environments to perform HR. These findings are contrary to our observations in **Chapter 4**, where we observe NL detachment of *ABC1* upon DSB induction. We speculate that these differences may have at least three different explanations. Firstly, I-SceI DSBs may behave differently than CRISPR-Cas9 induced ones. Even though endonucleases such as I-SceI are powerful tools to induce site-specific DSBs, they are limited to the site targeted by the endonuclease⁷⁴. Moreover, while I-SceI induces staggered breaks and leaves 3' overhangs, Cas9 mainly generates blunt ends^{75,76}. Second, the tethering of the LacO/I-SceI system to the NL could limit the potential mobility for DSB repair. Third, DDR-dependent transcriptional activation could be the trigger of NL detachment. Recent studies have suggested that transcription can be initiated upon DSB induction, generating non-coding RNAs which will regulate DNA repair^{77,78}. As the LacO/I-SceI is an exogenous non-coding locus, transcriptional activation and consequent DSB re-localization might not take place.

In conclusion, inducing DNA damage at specific nuclear domains has a major impact on genome stability, DNA mobility and repair pathway choice. Further studies will be needed to better address the role of NL in regulating DNA repair and relocalization of DSBs.

Chromatin alterations as part of the DNA repair process

Chromatin is modified at multiple levels during the repair process, which has been shown to also have an influence in the repair pathway choice and genome stability^{67,79,80}. It has become clear that chromatin around DSBs contains several *de novo* histone post-translation modifications, which are part of a complex crosstalk that ensures recruitment of the proper DDR proteins and completion of repair⁸¹. In **Chapter 4** we showed that DSB-induced Taxol-resistant clones exhibit changes in histone modifications, yet, we still do not understand exactly when these alterations are acquired. We speculate that during DSB induction and repair in the *ABCB1* gene, local chromatin remodeling and *de novo* histone PTMs are triggered. It would be crucial to investigate whether we can detect histone PTM depositions within the whole DSB repair process by time course experiments. In response to DSB formation the phosphorylated form of histone H2AX (γH2AX) spreads around the break site. It has been described that this spreading is confined to the damaged TAD^{82,83}. This suggests that in response to DSB induction histone dynamics are spatially regulated by the initial chromatin architecture surrounding the DSB. In **Chapter 3** we characterize the 3D organization of the *ABCB1* gene within the nucleus by Hi-C. We observed that *ABCB1* is located in close proximity with *ABCB4* and *RUNDC3B*, and further away from other genes within this TAD. Interestingly, when in **Chapter 4** we evaluate the *ABCB1* displacement from NL upon DSB induction, we observe that the detachment is also restricted to the TAD where *ABCB1* is located, with very clear boundaries that localize to CTCF sites. Therefore, our research corroborates previous observations on γH2AX spreading. We can speculate that both histone modifications and higher-order chromatin structures such as LADs are influenced by the initial chromatin architecture surrounding the DSB.

It is also clear that chromatin de-compaction needs to occur in order to allow repair factors to have physical access to the broken sequence. Indeed, the nucleosome structure acts as a barrier to repair DNA, independently of the lesion. For instance, in UVC irradiation or laser micro-irradiation-induced DNA damage a loss of density of histones has been observed^{84–87}. It could therefore also be interesting to perform chromatin accessibility assays, such as ATAC-seq, following DSB induction in the *ABCB1* locus. The DamID technique can allow to identify accessible genomic regions when using the freely diffusing Dam protein⁸⁸. Interestingly, in **Chapter 4**, when we performed pA-DamID to assess *ABCB1* NL-interactions upon DSB induction, we did not observe chromatin accessibility changes with the Dam-only control. This suggests that NL detachment is the major chromatin re-modeling event occurring and that chromatin de-compaction could be secondary to *ABCB1* NL detachment. Taken together, it is important to consider that chromatin both influences and is modified by the DNA damage and repair process. While our knowledge of the nature and function is increasingly growing, more research is necessary to understand the crosstalk between these mechanisms and their role in genome integrity.

Transcriptional regulation during DSB induction

As noted in the introduction, increasing evidences show that transcription is necessary for a full activation of the DNA damage response^{77,89}. So far, the majority of studies have focused on understanding the role of transcriptional activation in the repair of exogenous loci and ectopically introduced I-SceI sites^{90,91}. As shown in **Chapter 2**, *ABCB1* upregulation is closely linked to Taxol resistance in human RPE1 cells. Therefore, it would be of major interest to understand if the *ABCB1* gene is transcriptionally activated during the repair process. Specially, chromatin de-compaction and loss of heterochromatic repressive marks are associated with transcription activation^{92,93}. Following the results obtained in **Chapter 4**, we hypothesize that upon DSB induction in the *ABCB1* gene, transcriptional activation and chromatin remodeling could take place in two different ways. First, DNA damage has been shown to recruit RNA Polymerase II (Pol II) to DSB sites which subsequently will form damage-induced non-coding RNAs⁹⁴. As we are targeting the promoter of *ABCB1*, recruitment of Pol II could also well trigger transcriptional activation of the *ABCB1* gene itself. NL rewiring has been observed when targeting the VP64 transcriptional activation to specific loci (**Chapter 3** and ¹⁶). This is known to enhance gene expression by recruiting Pol II to the target promoter⁹⁵. Thus, it is possible that the damage-induced transcription directly triggers NL detachment. In the second model, DNA damage-dependent chromatin remodelers could trigger chromatin de-compaction and NL detachment consequently leading to *ABCB1* transcriptional activation. We can test these models by inhibiting transcription during the formation and repair of a DSB in the *ABCB1* gene and exploring if *ABCB1* contacts with the NL change by pA-DamID.

Epigenome integrity vs plasticity after DNA damage

As described in the previous sections, we have increasing knowledge of the chromatin and higher-order nuclear organization changes taking place during DSB induction and repair. However, little is known about the restoration of the initial chromatin organization once repair is completed. Indeed, whether the epigenome is reliably restored is still a matter of debate⁶⁷. We can speculate that faithful re-establishment of the epigenetic landscape is required to maintain the integrity of the transcriptional program and cellular functions. Yet, stable inheritance of DSB-dependent chromatin changes could modulate the epigenome and thereby deregulate gene expression. Few studies have suggested that DNA damage can cause heritable changes to the chromatin and lead to transcriptional changes. In 2008, O'Hagan et al. suggested that a DSB occurring in an exogenous E-cadherin promoter could recruit silencing factors, resulting in an increase in repressive chromatin marks. Upon DSB repair, in a small fraction of cells the promoter became stably silenced and gene expression was lost⁹⁶. Other studies have approached this question by inducing damage in a replication-dependent manner^{97,98}. This allowed

the authors to show that Hydroxyurea treatment induces loss of active histone marks in the Bu-1 reporter locus in chicken DT40 cells, leading to a subset of cells with low Bu-1 expression levels 7 days post-treatment. Indeed, similar mechanisms are described to happen during DNA replication and repair leading to transient chromatin rearrangements possibly contributing to epigenetic plasticity^{67,99}.

These investigations are especially important for our system developed in **Chapter 4**, where a DSB induced in the *ABCB1* gene generates a subset of cells acquiring Taxol resistance by *ABCB1* gene re-activation. Even though we find that in some of these cells genetic re-arrangements cause *ABCB1* upregulation, we show that genetic events are unlikely to cause Taxol-resistance in other clones, and that these could acquire stable DSB-induced chromatin changes (referred as “chromatin scars”⁶⁷) that reshape the epigenome. Importantly, our investigation and the others, as described above, refer to chromatin scars as rare events, as only a small population of cells acquire permanent epigenetic changes. This suggests that the majority of cells faithfully restore the pre-existing chromatin landscape upon genotoxic stress. It is tempting to speculate that each of these studies, including our own, have used easily selectable systems to study a possible epigenetic switch of the locus under investigation. This allows one to select for rare events, but requires for the gene under investigation to be in a clear on/off state in the parental cells. In case of the *ABCB1* gene, it is tightly repressed in parental RPE1, coincident with the presence of a variety of repressive marks, such as DNA methylation, H3K9 methylation and NL-association. It is possible that all marks are affected during repair, but only rarely completely lost, explaining why de-repression is such an infrequent event.

The functional relevance of epigenome plasticity after DNA damage has been emphasized in recent reviews^{67,99}. It was speculated that chromatin scars could act as a “damage memory” mark helping cells to respond to secondary stresses. On the other hand, chromatin scars could also be the result of erroneous reestablishment of the initial histone code and genome topology. We could speculate that the formation of chromatin scars could be relevant for tumor evolution. For example, in response to genotoxic agents where DNA damage is induced, chromatin scars could contribute to the transcriptional reprogramming of tumor cells. Interestingly, overexpression of protein kinases such as EGFR are very well known in cancer models driving tumor evolution¹⁰². We could hypothesize that overexpression of specific oncogenes is caused by chromatin scars. Therefore, understanding the mechanisms of chromatin scars and epigenome plasticity could open new therapeutic strategies to modulate gene expression and benefit cancer treatments.

Taxol resistance and the clinic

The overall purpose of this thesis was to understand the molecular mechanisms underlying spontaneous gene re-activation, employing the *ABCB1* gene as a tool which easily enables the selection of cells that upregulate *ABCB1*. Taxol interferes

with cell division leading to cell death and has been used to treat solid tumors since 1992 as a microtubule stabilizer^{103,104}. Despite the efficacy for many different cancer types, acquired Taxol resistance remains a major obstacle to improve the survival of cancer patients. Taxol resistance has been described to be caused by multifactorial mechanisms, which include PgP over-expression, expression of tubulin variants and alterations in microtubule dynamics^{105,106}. Resistance via PgP leads to an increased drug efflux that lowers the intracellular drug concentration in an ATP-dependent manner¹⁰⁷. On the other hand, over-expression of bIII-tubulin, an isotype of β -tubulin, has also been associated with Taxol resistance^{108,109}. It has been suggested that bIII-tubulin may enhance the rate of tubulin depolymerization thereby rendering microtubules less sensitive to the microtubule-stabilizing activity of Taxol¹¹⁰⁻¹¹². In **Chapter 2** we found that TUBB3 depletion in several cancer cell lines results in a marginal increase in Taxol sensitivity. Instead, the major mechanism of Taxol resistance was attributed to *ABCB1* transcriptional activation and PgP over-expression.

Despite the overwhelming amount of studies correlating PgP expression with Taxol resistance in cell lines and mouse models, the development of PgP inhibitors for the clinic has been unsuccessful^{105,113,114}. Importantly, the first clinical trials with PgP inhibitors were designed in 1995 for acute myeloid leukemia (AML)¹¹³. Thanks to the whole-genome analysis of tumors it is now known that only 13% of AML cancers express PgP. In fact, many of these clinical trials were randomized and did not select patients based on PgP expression¹¹⁵. With the introduction in the clinical practice of tumor sequencing and increasing use of cancer targeted therapies, it was recently suggested to revisit the role of PgP and other ABC transporters in drug resistance¹¹⁴. To achieve this, it is essential to first develop reliable methods to detect PgP protein expression and use it as a biomarker to target these specific tumor sub-types.

Concluding remarks and future challenges

In recent years, the importance of genome integrity for proper cellular functions and viability has become clear. Both nuclear architecture and histone modifications need to be properly established for faithful regulation of the transcriptional program. However, genome integrity is certainly perturbed in response to DNA damage. In this thesis we suggest a role for the NL in regulating *ABCB1* gene expression. We also demonstrate that NL-association is perturbed upon DSB induction in the *ABCB1* locus. We hypothesize that the altered epigenetic landscape is not always faithfully restored leading to chromatin scars, transcriptional dysregulation and cellular plasticity. Clearly, a deeper understanding on how DNA damage repair affects chromatin and genome topology is necessary as well as its impact on transcription regulation (**Fig. 1**). Future studies will determine whether DSB-dependent chromatin changes are capable of shaping the epigenome to promote cellular plasticity, both in development and cancer progression.

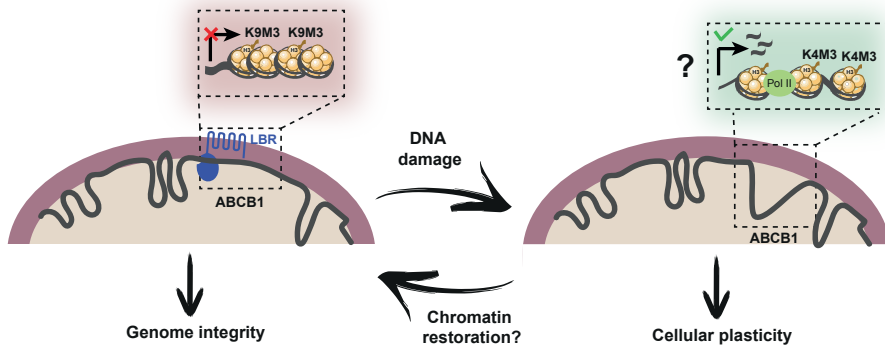


Figure 1 - The role of DNA damage in genome integrity vs cellular plasticity (Left) In RPE-1 naïve cells, *ABCB1* is located in the NL and it is associated with repressive histone marks. In this context, *ABCB1* transcription is shut down. We suggest that *LBR* could have a role in regulating this process. (Right) Upon DNA damage, chromatin is remodeled, specifically by rewiring of NL interactions within the *ABCB1* locus. We hypothesize that during this process there is also a gain in active histone modifications and potentially recruitment of RNA Polymerase II (Pol II). Altogether, this complex crosstalk could allow for *ABCB1* transcription activation. We speculate that faithful chromatin restoration could occur in the majority of cells, thus maintaining genome integrity. However, some cells could stably gain the DSB-dependent chromatin alterations thus contributing to cellular plasticity.

REFERENCES

1. Stueve, T. R., Marconett, C. N., Zhou, B., Borok, Z. & Laird-Offringa, I. A. The importance of detailed epigenomic profiling of different cell types within organs. *Epigenomics* vol. 8 817–829 (2016).
2. Waterland, R. A. Epigenetic mechanisms and gastrointestinal development. *J. Pediatr.* **149**, (2006).
3. Maze, I., Noh, K. M., Soshnev, A. A. & Allis, C. D. Every amino acid matters: Essential contributions of histone variants to mammalian development and disease. *Nature Reviews Genetics* vol. 15 259–271 (2014).
4. Schübeler, D. Function and information content of DNA methylation. *Nature* vol. 517 321–326 (2015).
5. Bannister, A. J. & Kouzarides, T. Regulation of chromatin by histone modifications. *Cell Research* vol. 21 381–395 (2011).
6. Margueron, R. & Reinberg, D. The Polycomb complex PRC2 and its mark in life. *Nature* **469**, 343–9 (2011).
7. Greenwald, W. W. *et al.* Subtle changes in chromatin loop contact propensity are associated with differential gene regulation and expression. *Nat. Commun.* **10**, 1–17 (2019).
8. Schoenfelder, S. & Fraser, P. Long-range enhancer–promoter contacts in gene expression control. *Nature Reviews Genetics* vol. 20 437–455 (2019).
9. Morey, C., Da Silva, N. R., Perry, P. & Bickmore, W. A. Nuclear reorganisation and chromatin decondensation are conserved, but distinct, mechanisms linked to Hox gene activation. *Development* **134**, 909–919 (2007).
10. Cavalli, G. & Misteli, T. Functional implications of genome topology. *Nature Structural and Molecular Biology* vol. 20 290–299 (2013).
11. Leemans, C. *et al.* Promoter-Intrinsic and Local Chromatin Features Determine Gene Repression in LADs. *Cell* **177**, 852–864.e14 (2019).
12. Peric-Hupkes, D. *et al.* Molecular Maps of the Reorganization of Genome-Nuclear Lamina Interactions during Differentiation. *Mol. Cell* **38**, 603–613 (2010).
13. Finlan, L. E. *et al.* Recruitment to the nuclear periphery can alter expression of genes in human cells. *PLoS Genet.* **4**, e1000039 (2008).
14. Reddy, K. L., Zullo, J. M., Bertolino, E. & Singh, H. Transcriptional repression mediated by repositioning of genes to the nuclear lamina. *Nature* **452**, 243–247 (2008).
15. Dyalynas, G., Speese, S., Budnik, V., Geyer, P. K. & Wallrath, L. L. The role of Drosophila Lamin C in muscle function and gene expression. *Development* **137**, 3067–3077 (2010).
16. Brueckner, L. *et al.* Local rewiring of genome–nuclear lamina interactions by transcription. *EMBO J.* 685255 (2020) doi:10.1101/685255.
17. Ulianov, S. V. *et al.* Nuclear lamina integrity is required for proper spatial organization of chromatin in Drosophila. *Nat. Commun.* **10**, 1–11 (2019).
18. Shevelyov, Y. Y. *et al.* The B-type lamin is required for somatic repression of testis-specific gene clusters. *Proc. Natl. Acad. Sci. U. S. A.* **106**, 3282–3287 (2009).
19. Leemans, C. *et al.* Promoter-Intrinsic and Local Chromatin Features Determine Gene Repression in LADs Article Promoter-Intrinsic and Local Chromatin Features Determine Gene Repression in LADs. *Cell* **177**, 852–864.e14 (2019).
20. Kantidze, O. L., Gurova, K. V., Studitsky, V. M. & Razin, S. V. The 3D Genome as a Target for Anticancer Therapy. *Trends in Molecular Medicine* vol. 26 141–149 (2020).
21. Wang, D. C. & Wang, X. Genome dimensions control biological and toxicological functions; myth or reality? *Cell Biology and Toxicology* vol. 34 333–336 (2018).
22. Li, R. *et al.* 3D genome and its disorganization in diseases. *Cell Biology and Toxicology* vol. 34 351–365 (2018).
23. Wu, P. *et al.* 3D genome of multiple myeloma reveals spatial genome disorganization associated with copy number variations. *Nat. Commun.* **8**, 1–11 (2017).
24. Hnisz, D. *et al.* Activation of proto-oncogenes by disruption of chromosome neighborhoods. *Science (80-.)*. **351**, 1454–1458 (2016).
25. Braun, R. *et al.* Single Chromosome Aneuploidy Induces Genome-Wide Perturbation of Nuclear Organization and Gene Expression. *Neoplasia (United States)* **21**, 401–412 (2019).
26. Taberlay, P. C. *et al.* Three-dimensional disorganization of the cancer genome occurs coincident with long-range genetic and epigenetic alterations. *Genome Res.* **26**, 719–731 (2016).
27. Barutcu, A. R. *et al.* Chromatin interaction analysis reveals changes in small chromosome and telomere clustering between epithelial and breast cancer cells. *Genome Biol.* **16**, (2015).
28. Nagai, L. A. E., Park, S. J. & Nakai, K. Analyzing the 3D chromatin organization coordinating with gene expression regulation in B-cell lymphoma. *BMC Med. Genomics* **11**, 19–29 (2019).
29. Kantidze, O. L. *et al.* The anti-cancer drugs curaxins target spatial genome organization. *Nat. Commun.* **10**, 1–11 (2019).
30. So, A., Le Guen, T., Lopez, B. S., Ee Guirouilh-Barbat, J. & Guirouilh-Barbat, J. Genomic rearrangements induced by unscheduled DNA double strand breaks in somatic mammalian cells. *FEBS J.* **284**, 2324–2344 (2017).
31. Hartlerode, A. J., Willis, N. A., Rajendran, A., Manis, J. P. & Scully, R. Complex Breakpoints and Template Switching Associated with Non-canonical Termination of Homologous Recombination in Mammalian Cells. *PLoS Genet.* **12**, e1006410 (2016).
32. Patch, A. M. *et al.* Whole-genome characterization of chemoresistant ovarian cancer. *Nature* **521**, 489–494 (2015).
33. Genovese, I., Ilari, A., Assaraf, Y. G., Fazi, F. & Colotti, G. Not only P-glycoprotein: Amplification of the ABCB1-containing chromosome region 7q21 confers multidrug resistance upon cancer cells by coordinated overexpression of an assortment of resistance-related proteins. *Drug Resist. Updat.* **32**, 23–46 (2017).

34. Vaidyanathan, A. *et al.* ABCB1 (MDR1) induction defines a common resistance mechanism in paclitaxel- and olaparib-resistant ovarian cancer cells. *Br. J. Cancer* **115**, 431–441 (2016).
35. Reed, K., Hembruff, S. L., Sprowl, J. A. & Parissenti, A. M. The temporal relationship between ABCB1 promoter hypomethylation, ABCB1 expression and acquisition of drug resistance. *Pharmacogenomics J.* **10**, 489–504 (2010).
36. Ruiz, J. C., Choi, K. H., von Hoff, D. D., Roninson, I. B. & Wahl, G. M. Autonomously replicating episomes contain *mdr1* genes in a multidrug-resistant human cell line. *Mol. Cell. Biol.* **9**, 109–115 (1989).
37. Hacein-Bey-Abina, S. *et al.* A Serious Adverse Event after Successful Gene Therapy for X-Linked Severe Combined Immunodeficiency. *N. Engl. J. Med.* **348**, 255–256 (2003).
38. Overcash, J. M., Aryan, A., Myles, K. M. & Adelman, Z. N. Understanding the DNA damage response in order to achieve desired gene editing outcomes in mosquitoes. *Chromosome Res.* **23**, 31 (2015).
39. Joung, J. K. & Sander, J. D. TALENs: a widely applicable technology for targeted genome editing. *Nat. Rev. Mol. Cell Biol.* **14**, 49 (2013).
40. T, S., L, P., E, W. & A, L. I-SceI endonuclease: a new tool for DNA repair studies and genetic manipulations in streptomyces. *Appl. Microbiol. Biotechnol.* **87**, 1525–1532 (2010).
41. M, H. *et al.* Non-homologous end-joining for repairing I-SceI-induced DNA double strand breaks in human cells. *DNA Repair (Amst)*. **6**, 781–788 (2007).
42. RJ, M., AF, H. & MA, C. Generation of highly site-specific DNA double-strand breaks in human cells by the homing endonucleases I-PpoI and I-CreI. *Biochem. Biophys. Res. Commun.* **255**, 88–93 (1999).
43. Iacovoni, J. S. *et al.* High-resolution profiling of yh2AX around DNA double strand breaks in the mammalian genome. *EMBO J.* **29**, 1446–1457 (2010).
44. Massip, L., Caron, P., Iacovoni, J. S., Trouche, D. & Legube, G. Deciphering the chromatin landscape induced around DNA double strand breaks. *Cell Cycle* vol. 9 3035–3044 (2010).
45. Clouaire, T. *et al.* Comprehensive Mapping of Histone Modifications at DNA Double-Strand Breaks Deciphers Repair Pathway Chromatin Signatures. *Mol. Cell* **72**, 250–262.e6 (2018).
46. Aymard, F. *et al.* Transcriptionally active chromatin recruits homologous recombination at DNA double-strand breaks. *Nat. Struct. Mol. Biol.* **21**, 366–374 (2014).
47. Goodarzi, A. A. *et al.* ATM Signaling Facilitates Repair of DNA Double-Strand Breaks Associated with Heterochromatin. *Mol. Cell* **31**, 167–177 (2008).
48. Sun, Y. *et al.* Histone H3 methylation links DNA damage detection to activation of the tumour suppressor Tip60. *Nat. Cell Biol.* **11**, 1376–1382 (2009).
49. Clouaire, T. & Legube, G. DNA double strand break repair pathway choice: A chromatin based decision? *Nucleus* **6**, 107–113 (2015).
50. Kallimasioti-Pazi, E. M. *et al.* Heterochromatin delays CRISPR-Cas9 mutagenesis but does not influence the outcome of mutagenic DNA repair. *PLoS Biol.* **16**, (2018).
51. Janssen, A. *et al.* A single double-strand break system reveals repair dynamics and mechanisms in heterochromatin and Euchromatin. *Genes Dev.* **30**, 1645–1657 (2016).
52. Schep, R. *et al.* Impact of chromatin context on Cas9-induced DNA double-strand break repair pathway balance. (2021) doi:10.1016/j.molcel.2021.03.032.
53. Allen, F. *et al.* Predicting the mutations generated by repair of Cas9-induced double-strand breaks. *Nat. Biotechnol.* **37**, 64–82 (2019).
54. Chakrabarti, A. M. *et al.* Target-Specific Precision of CRISPR-Mediated Genome Editing. *Mol. Cell* **73**, 699–713.e6 (2019).
55. Chen, W. *et al.* Massively parallel profiling and predictive modeling of the outcomes of CRISPR/Cas9-mediated double-strand break repair. *Nucleic Acids Res.* **47**, 7989–8003 (2019).
56. Noon, A. T. *et al.* 53BP1-dependent robust localized KAP-1 phosphorylation is essential for heterochromatic DNA double-strand break repair. *Nat. Cell Biol.* **12**, 177–184 (2010).
57. Ayoub, N., Jeyasekharan, A. D., Bernal, J. A. & Venkitaraman, A. R. HP1- β mobilization promotes chromatin changes that initiate the DNA damage response. *Nature* **453**, 682–686 (2008).
58. Chiolo, I. *et al.* Double-Strand Breaks in Heterochromatin Move Outside of a Dynamic HP1a Domain to Complete Recombinational Repair. *Cell* **144**, 732–744 (2011).
59. Ryu, T. *et al.* Heterochromatic breaks move to the nuclear periphery to continue recombinational repair. *Nat. Cell Biol.* **17**, 1401–1411 (2015).
60. Chiolo, I., Tang, J., Georgescu, W. & Costes, S. V. Nuclear dynamics of radiation-induced foci in euchromatin and heterochromatin. *Mutation Research - Fundamental and Molecular Mechanisms of Mutagenesis* vol. 750 56–66 (2013).
61. Jakob, B. *et al.* DNA double-strand breaks in heterochromatin elicit fast repair protein recruitment, histone H2AX phosphorylation and relocation to euchromatin. *Nucleic Acids Res.* **39**, 6489–6499 (2011).
62. Jakob, B. *et al.* DNA double-strand breaks in heterochromatin elicit fast repair protein recruitment, histone H2AX phosphorylation and relocation to euchromatin. *Nucleic Acids Res.* **39**, 6489–6499 (2011).
63. Caridi, C. P. *et al.* Nuclear F-actin and myosins drive relocalization of heterochromatic breaks. *Nature* **559**, 54–60 (2018).
64. Lamm, N. *et al.* Nuclear F-actin counteracts nuclear deformation and promotes fork repair during replication stress. *Nat. Cell Biol.* **22**, 1460–1470 (2020).
65. Pinzaru, A. M. *et al.* Replication stress conferred by POT1 dysfunction promotes telomere relocalization to the nuclear pore. *Genes Dev.* **34**, 1619–1636 (2020).
66. Kalousi, A. & Soutoglou, E. Nuclear compartmentalization of DNA repair. *Current Opinion in Genetics and Development* vol. 37 148–157 (2016).
67. Dabin, J., Fortuny, A. & Polo, S. E. Epigenome Maintenance in Response to DNA Damage. *Mol. Cell* **62**, 712–727 (2016).

68. Misteli, T. & Soutoglou, E. The emerging role of nuclear architecture in DNA repair and genome maintenance. *Nature Reviews Molecular Cell Biology* vol. 10 243–254 (2009).
69. Handwerger, K. E. & Gall, J. G. Subnuclear organelles: New insights into form and function. *Trends in Cell Biology* vol. 16 19–26 (2006).
70. Kruhlak, M. *et al.* The ATM repair pathway inhibits RNA polymerase I transcription in response to chromosome breaks. *Nature* **447**, 730–734 (2007).
71. van Sluis, M. & McStay, B. A localized nucleolar DNA damage response facilitates recruitment of the homology-directed repair machinery independent of cell cycle stage. *Genes Dev.* **29**, 1151–1163 (2015).
72. Harding, S. M., Boiarsky, J. A. & Greenberg, R. A. ATM Dependent Silencing Links Nucleolar Chromatin Reorganization to DNA Damage Recognition. *Cell Rep.* **13**, 251–259 (2015).
73. Lemaître, C. *et al.* Nuclear position dictates DNA repair pathway choice. *Genes Dev.* **28**, 2450–2463 (2014).
74. Miné-Hattab, J. & Chiolo, I. Complex Chromatin Motions for DNA Repair. *Frontiers in Genetics* vol. 11 (2020).
75. Cong, L. *et al.* Multiplex genome engineering using CRISPR/Cas systems. *Science (80-. J.)* **339**, 819–823 (2013).
76. Jinek, M. *et al.* RNA-programmed genome editing in human cells. *Elife* **2013**, (2013).
77. Capozzo, I., Iannelli, F., Francia, S. & d’Adda di Fagagna, F. Express or repress? The transcriptional dilemma of damaged chromatin. *FEBS Journal* vol. 284 2133–2147 (2017).
78. Caron, P., van der Linden, J. & van Attikum, H. Bon voyage: A transcriptional journey around DNA breaks. *DNA Repair (Amst.)* **82**, 102686 (2019).
79. Clouaire, T. & Legube, G. A Snapshot on the Cis Chromatin Response to DNA Double-Strand Breaks. *Trends in Genetics* vol. 35 330–345 (2019).
80. Polo, S. E. & Almouzni, G. Chromatin dynamics after DNA damage: The legacy of the access-repair-restore model. *DNA Repair* vol. 36 114–121 (2015).
81. Dantuma, N. P. & Attikum, H. Spatiotemporal regulation of posttranslational modifications in the DNA damage response. *EMBO J.* **35**, 6–23 (2016).
82. Arnould, C. & Legube, G. The Secret Life of Chromosome Loops upon DNA Double-Strand Break. *Journal of Molecular Biology* vol. 432 724–736 (2020).
83. Lee, C.-S., Lee, K., Legube, G. & Haber, J. E. Dynamics of yeast histone H2A and H2B phosphorylation in response to a double-strand break. *Nat. Publ. Gr.* **21**, (2013).
84. Luijsterburg, M. S. *et al.* DDB2 promotes chromatin decondensation at UV-induced DNA damage. *J. Cell Biol.* **197**, 267–281 (2012).
85. Kruhlak, M. J. *et al.* Changes in chromatin structure and mobility in living cells at sites of DNA double-strand breaks. *J. Cell Biol.* **172**, 823–834 (2006).
86. Smeenk, G. *et al.* Poly(ADP-ribosyl)ation links the chromatin remodeler SMARCA5/SNF2H to RNF168-dependent DNA damage signaling. *J. Cell Sci.* **126**, 889–903 (2013).
87. Strickfaden, H. *et al.* Poly(ADP-ribosyl)ation-dependent transient chromatin decondensation and histone displacement following laser microirradiation. *J. Biol. Chem.* **291**, 1789–1802 (2016).
88. van Schaik, T., Vos, M., Peric-Hupkes, D., HN Celie, P. & van Steensel, B. Cell cycle dynamics of lamina-associated DNA. *EMBO Rep.* **21**, e50636 (2020).
89. D’Alessandro, G. & d’Adda di Fagagna, F. Transcription and DNA Damage: Holding Hands or Crossing Swords? *Journal of Molecular Biology* vol. 429 3215–3229 (2017).
90. Francia, S. *et al.* Site-specific DICER and DROSHA RNA products control the DNA-damage response. *Nature* **488**, 231–235 (2012).
91. Michelini, F. *et al.* Damage-induced lncRNAs control the DNA damage response through interaction with DDRNAs at individual double-strand breaks. *Nat. Cell Biol.* **19**, 1400–1411 (2017).
92. Jaenisch, R. & Bird, A. Epigenetic regulation of gene expression: How the genome integrates intrinsic and environmental signals. *Nature Genetics* vol. 33 245–254 (2003).
93. Gorkin, D. U., Leung, D. & Ren, B. The 3D genome in transcriptional regulation and pluripotency. *Cell Stem Cell* vol. 14 762–775 (2014).
94. Rzeszutek, I. & Betlej, G. The role of small noncoding rna in dna double-strand break repair. *International Journal of Molecular Sciences* vol. 21 1–13 (2020).
95. Mittler, G. *et al.* A novel docking site on Mediator is critical for activation by VP16 in mammalian cells. *EMBO J.* **22**, 6494–6504 (2003).
96. O’Hagan, H. M., Mohammad, H. P. & Baylin, S. B. Double strand breaks can initiate gene silencing and SIRT1-dependent onset of DNA methylation in an exogenous promoter CpG island. *PLoS Genet.* **4**, (2008).
97. Papadopoulou, C., Guilbaud, G., Schiavone, D. & Sale, J. E. Nucleotide Pool Depletion Induces G-Quadruplex-Dependent Perturbation of Gene Expression. *Cell Rep.* **13**, 2491–2503 (2015).
98. Sale, J. E. The Effects of Replication Stress on S Phase Histone Management and Epigenetic Memory. (2016) doi:10.1016/j.jmb.2016.11.011.
99. Stewart-Morgan, K. R., Petryk, N. & Groth, A. Chromatin replication and epigenetic cell memory. *Nat. Cell Biol.* **22**, 1–11 (2020).
100. Ma, Y., Kanakousaki, K. & Buttitta, L. How the cell cycle impacts chromatin architecture and influences cell fate. *Frontiers in Genetics* vol. 5 (2015).
101. de Castro, I. J., Gokhan, E. & Vagnarelli, P. Resetting a functional G1 nucleus after mitosis. *Chromosoma* vol. 125 607–619 (2016).
102. Cincenas, J., Zalyte, E., Bairoch, A. & Gaudet, P. Kinases and cancer. *Cancers* vol. 10 (2018).
103. Torres, K. & Horwitz, S. B. Mechanisms of Taxol-induced Cell Death Are Concentration Dependent. *Cancer Res.* **58**, (1998).
104. Weaver, B. A. How Taxol/paclitaxel kills cancer cells. *Molecular Biology of the Cell* vol. 25 2677–2681 (2014).
105. Gottesman, M. M., Fojo, T. & Bates, S. E. Multidrug resistance in cancer: Role of ATP-dependent transporters. *Nature Reviews Cancer* vol. 2 48–58 (2002).

106. Kavallaris, M. Microtubules and resistance to tubulin-binding agents. *Nature Reviews Cancer* vol. 10 194–204 (2010).
107. Ambudkar, S. V. *et al.* Biochemical, cellular, and pharmacological aspects of the multidrug transporter. *Annual Review of Pharmacology and Toxicology* vol. 39 361–398 (1999).
108. Kavallaris, M. *et al.* Taxol-resistant epithelial ovarian tumors are associated with altered expression of specific β -tubulin isotypes. *J. Clin. Invest.* **100**, 1282–1293 (1997).
109. Mariani, M. *et al.* Clas- III β -tubulin in normal and cancer tissues. *Gene* vol. 563 109–114 (2015).
110. Derry, W. B., Wilson, L., Khan, I. A., Ludueña, R. F. & Jordan, M. A. Taxol differentially modulates the dynamics of microtubules assembled from unfractionated and purified β -tubulin isotypes. *Biochemistry* **36**, 3554–3562 (1997).
111. Lu, Q. & Luduena, R. F. In vitro analysis of microtubule assembly of isotypically pure tubulin dimers. Intrinsic differences in the assembly properties of $\alpha\beta$ II, $\alpha\beta$ III, and $\alpha\beta$ IV tubulin dimers in the absence of microtubule-associated proteins. *J. Biol. Chem.* **269**, 2041–2047 (1994).
112. Hari, M., Yang, H., Zeng, C., Canizales, M. & Cabral, F. Expression of class III β -tubulin reduces microtubule assembly and confers resistance to paclitaxel. *Cell Motil. Cytoskeleton* **56**, 45–56 (2003).
113. Leonard, G. D., Fojo, T. & Bates, S. E. The Role of ABC Transporters in Clinical Practice. *Oncologist* **8**, 411–424 (2003).
114. Robey, R. W. *et al.* Revisiting the role of ABC transporters in multidrug-resistant cancer. *Nature Reviews Cancer* vol. 18 452–464 (2018).
115. W. Robey, R., R. Massey, P., Amiri-Kordestani, L. & E. Bates, S. ABC Transporters: Unvalidated Therapeutic Targets in Cancer and the CNS. *Anticancer. Agents Med. Chem.* **10**, 625–633 (2011).



APPENDIX

NEDERLANDSE SAMENVATTING

Alle cellen in een organisme bevatten in wezen hetzelfde DNA, maar toch bestaat het menselijk lichaam uit ongeveer 210 histologisch verschillende celtypen. Dit wordt bereikt door middel van differentiële genexpressieprogramma's die cellen gebruiken om gespecialiseerde cellulaire functies tot stand te brengen. Belangrijk is dat de regulatie van genexpressie afhankelijk is van zowel epigenetische modificaties en de organisatie van het genoom in de kern. Epigenetica is uitgebreid beschreven als de studie van erfelijke genexpressieveranderingen die niet worden veroorzaakt door veranderingen in de DNA-sequentie. Veranderingen in het epigenoom omvatten veranderingen in DNA-methylatie, post-translatiemodificaties van histonen (PTMs), histonpositionering of niet-histonchromatinecomponenten. Daarnaast speelt de hogere-orde van de chromatinestructuur en de distributie van het genoom over verschillende nucleaire compartimenten ook een belangrijke rol bij het reguleren van het transcriptionele programma en de cellulaire plasticiteit. Hierdoor kan chromatine worden gezien als een complex biochemisch netwerk dat omgevingssignalen kan integreren, om zo genexpressie te reguleren door veranderingen in epigenetische kenmerken. Cellulaire processen zoals transcriptie, replicatie of DNA-schade en de reparatie hiervan kunnen veranderingen in het chromatine en de driedimensionale organisatie van het genoom veroorzaken, en daardoor de integriteit van het epigenoom op de proef stellen.

In dit proefschrift hebben we verschillende mechanismen beschreven die de integriteit van het (epi)genoom in gevaar kunnen brengen, resulterend in veranderingen in genexpressie en cellulaire fenotypes, met name het verwerven van resistentie tegen geneesmiddelen. In **Hoofdstuk 2** beschrijven we het cellulaire model dat we hebben gebruikt om de acquisitie van een Taxol-resistent fenotype te bestuderen, en laten we zien dat dit gebeurt via transcriptionele activatie van het ABCB1 gen. We laten zien dat ABCB1-activering spontaan kan plaatsvinden in cellen die gedurende langere tijd aan toenemende doses Taxol zijn blootgesteld. In **Hoofdstuk 3** demonstreren we verder de belangrijke rol die 3D-genoomorganisatie speelt in genregulatie en cellulaire plasticiteit. In het bijzonder laten we zien dat verstoringen in Nuclear Lamina (NL) interacties binnen ABCB1 kunnen leiden tot veranderingen in genexpressie en verwerving van een Taxol-resistent fenotype. Omdat chromatine sterk verandert tijdens de DNA-schadereactie, wilden we bestuderen hoe de integriteit van het epigenoom wordt aangetast en hersteld na DSB-inductie (**Hoofdstuk 4**). In de loop van dat werk ontdekten we dat genetische DNA-herschikkingen geïnduceerd door CRISPR-Cas9-gemedieerde genoombewerking ook een impact hebben op de driedimensionale genoomorganisatie en bijdragen aan veranderingen in genexpressie die de cellulaire fysiologie kunnen beïnvloeden (**Hoofdstuk 5**). Ten slotte hebben we in **Hoofdstuk 6** de dingen vanuit de tegenovergestelde hoek bekeken en beschreven hoe de lokale chromatine-omgeving de DNA-schadereactie kan beïnvloeden. Het werk dat in dit

proefschrift wordt gepresenteerd, heeft tot doel het belang van chromatine en 3D-genoomorganisatie bij het moduleren van cellulaire functies te benadrukken. We hebben geprobeerd op te lossen hoe epigenetische veranderingen die genactivering kunnen bevorderen, kunnen worden geïnduceerd op manieren die zeer relevant kunnen zijn tijdens tumorevolutie.

RESUMEN EN ESPAÑOL

Todas las células del organismo contienen esencialmente el mismo ADN. Sin embargo, se estima que en el cuerpo humano hay 210 tipos de células histológicamente distintas. Esto se logra a través de programas de expresión génica que emplean las células para establecer funciones celulares especializadas. La regulación de la expresión génica está influenciada por modificaciones epigenéticas y la organización del genoma dentro del núcleo. La epigenética se ha descrito ampliamente como el estudio de los cambios hereditarios en la expresión génica que no son causados por cambios en la secuencia del ADN. Los cambios en el epigenoma incluyen cambios en la metilación del ADN, modificaciones post-traduccionales de histonas (PTM), el posicionamiento nuclear de histonas o componentes de cromatina que no son histonas. Además de esto, la estructura de la cromatina y la distribución del genoma a través de distintos compartimentos nucleares también juega un papel importante en la regulación del programa transcripcional y la plasticidad celular. Por lo tanto, la cromatina puede verse como una red bioquímica compleja que puede integrar señales ambientales para regular la expresión génica a través de cambios en las marcas epigenéticas. Sin embargo, los procesos celulares como la transcripción, la replicación o el daño y la reparación del ADN pueden inducir alteraciones en la cromatina y la organización tridimensional del genoma y, por lo tanto, desafiar la integridad del epigenoma.

En esta tesis hemos descrito varios mecanismos que pueden comprometer la integridad del (epi)genoma, dando como resultado cambios en la expresión génica y fenotipos celulares, específicamente centrándonos en la adquisición de resistencia a medicamentos. En el **Capítulo 2** describimos el modelo celular que hemos utilizado para estudiar la adquisición de resistencia a Taxol y mostramos que esto ocurre mediante la activación transcripcional del gen *ABCB1*. Mostramos que la activación de *ABCB1* puede ocurrir de manera espontánea, en células expuestas a dosis crecientes de Taxol durante un período de tiempo prolongado. En el **Capítulo 3** demostramos el importante papel que desempeña la organización del genoma 3D en la regulación génica y la plasticidad celular. Específicamente, mostramos que las perturbaciones en las interacciones de la lámina nuclear (NL) y *ABCB1* pueden conducir a cambios en la expresión génica y la adquisición de resistencia a Taxol. Dado que la cromatina se modifica en gran medida durante la respuesta al daño del ADN, hemos querido estudiar cómo se ve afectada y restaurada la integridad



del epigenoma tras la inducción de doble rotura en el ADN (DSB) (**Capítulo 4**). Durante el curso de ese trabajo, descubrimos que los reordenamientos genéticos del ADN inducidos por el sistema de CRISPR-Cas9 también afectan la organización del genoma tridimensional y contribuyen a cambios en la expresión génica que pueden afectar la fisiología celular (**Capítulo 5**). Finalmente, en el **Capítulo 6** hemos analizado las cosas desde el ángulo opuesto y describimos cómo el ambiente local de la cromatina puede afectar la respuesta al daño del ADN. El trabajo presentado en esta tesis tiene como objetivo enfatizar la importancia de la cromatina y la organización del genoma 3D en la modulación de las funciones celulares. Hemos tratado de resolver cómo se pueden inducir alteraciones epigenéticas que pueden promover la activación de genes de formas que podrían ser de gran relevancia durante la evolución del tumor.

CURRICULUM VITAE

Anna González Manjón was born on July 10th 1993 in Barcelona, Spain. She graduated pre-university secondary education (Bachillerato) in 2011 from FEDAC Horta with Honors. In 2011 she started her studies of Human Biology at Universitat Pompeu Fabra (Barcelona) obtaining her BSc. degree in 2015. During this time, she worked as a researcher assistant in Fundación Jimenez Diaz (Madrid) with Dr. Germán Peces-Barba studying the role of Liver Growth Factor in the regeneration of lung emphysema. She also worked on cell cycle regulation by p38 in cancer cell models as a researcher assistant with Dr. Francesc Posas in Barcelona Biomedical Research Park (PRBB). Following her BSc, she enrolled in the Master in Pharmaceutical and Biotechnology Industry in Universitat Pompeu Fabra (Barcelona) in 2016. Following her interest in cell biology, she joined the lab of Prof. Rene Medema at the Netherlands Cancer Institute (Amsterdam) as part of her MSc. There she studied how chromatin could be modified upon DNA damage and regulate gene expression. This prompted her interest in chromatin plasticity and epigenome maintenance and continued in the lab of Prof. Rene Medema where she started her Ph.D in 2016. The results of her work are presented in this thesis. From 2022 onwards, she will continue examining genomic instability in cancer models as a postdoctoral researcher in the lab of Anthony Cesare at the Children Medical Research Institute (CMRI) in Sydney, Australia.

PUBLICATIONS AND PREPRINTS

TUBB3 overexpression has a negligible effect on the sensitivity to Taxol in cultured cell lines

Mihoko A. Tame*, [Anna G. Manjón*](#), Daria Belokhvostova, Jonne A. Raaijmakers, René H. Medema. *Oncotarget*, vol. 8, no. 42, p. 71536, Sep. 2017, doi: 10.18632/oncotarget.17740.

A limited number of double-strand DNA breaks is sufficient to delay cell cycle progression

Jeroen van den Berg, [Anna G. Manjón](#), Karoline Kielbassa, Femke M. Feringa, Raimundo Freire, René H. Medema. *Nucleic Acids Res.*, vol. 46, no. 19, pp. 10132–10144, Nov. 2018, doi: 10.1093/nar/gky786.

Perturbations in 3D genome organization can promote acquired drug resistance

[Anna G. Manjón](#), Daan Peric Hupkes, Ning Qing Liu, Anoek Friskes, Stacey Joosten, Hans Teunissen, Marleen Aarts, Stefan Prekovic, Wilbert Zwart, Elzo de Wit, Bas van Steensel#, René H. Medema#. *bioRxiv*, p. 2021.02.02.429315, Feb. 2021, doi: 10.1101/2021.02.02.429315.

In revision (Cell Reports)

Predicting clinical drug response from model systems by non-linear subspace-based transfer learning

Soufiane Mourragui, Marco Loog, Daniel J. Vis, Kat Moore, [Anna G. Manjón](#), Mark A. van de Wiel, Marcel JT Reinders, Lodewyk FA Wessels. *bioRxiv*, p. 2020.06.29.177139, Jun. 2020, doi: 10.1101/2020.06.29.177139.

Accepted (PNAS)

Unexpected gene activation following CRISPR-Cas9-mediated genome editing

[Anna G. Manjón](#), Simon Linder, Hans Teunissen, Wilbert Zwart, Elzo De Wit, Rene H. Medema. *bioRxiv*, p. 2021.06.14.448328, Jun. 2021, doi: 10.1101/2021.06.14.448328.

In revision (EMBO Reports)



Glucocorticoid receptor triggers a reversible drug-tolerant dormancy state with acquired therapeutic vulnerabilities in lung cancer

Stefan Prekovic*, Karianne Schuurman*, Isabel Mayayo-Peralta, [Anna G. Manjón](#), Mark Buijs, Selçuk Yavuz, Max D. Wellenstein, Alejandro Barrera, Kim Monkhorst, Anne Huber, Ben Morris, Cor Liefink, Theofilos Chalkiadakis, Ferhat Alkan, Joana Silva, Balázs Györffy, Liesbeth Hoekman, Bram van den Broek, Hans Teunissen, Donna O. Debets, Tesa Severson, Jos Jonkers, Timothy Reddy, Karin E. de Visser, William Faller, Roderick Beijersbergen, Maarten Altelaar, Elzo de Wit, Rene Medema, Wilbert Zwart. Nat. Commun. 2021 121, vol. 12, no. 1, pp. 1–18, Jul. 2021, doi: 10.1038/s41467-021-24537-3.

*Equal contribution

Corresponding authors

ACKNOWLEDGEMENTS

I would like to thank everyone that have contributed in some way to the completion of this thesis. If you are reading this, you are one of them.

Rene, I still remember the first weeks in the lab as a student and your challenging “make me famous” quote. Thanks for believing in me and offering me a PhD position (in the most challenging project). You gave me all opportunities and freedom that I could wish for to develop my research, from which I learned a lot. I have always admired your leadership and dedication for science and for your group. I truly had a great time working in the Medema group.

Special thank you to my co-promoter, **Bas**. I have always appreciated our project discussions, which taught me the importance of a critical point of view in science. You also welcomed me as part of your group for performing experiments and lab meetings. Thanks for all the support received over the years.

Thanks to the reading committee that spent time going to the foundations of this thesis. **Tineke**, **Fred** and **Kees** thanks for being part of my PhD committee. With you, year evaluations have been smooth and fun more than stressful.

To my paranympths, **Louise**, it was great to start with you the PhD journey. Since the first day cutting decoration for Femke’s defense until now, five years later. Your constant support has made smoother this journey. Thanks for all the moments inside and outside the lab that made our friendship evermore. Even though my time in the Netherlands have ended, you will be one of the reasons for me to come back every year. **Xabi**, I will always remember how we pushed you to come climbing the

day of your PhD interview. Since then we have spent great time together, specially doing Lipofectamine optimizations. I am very grateful to have spent with you these last years in Amsterdam. I admire your enthusiasm for science as well as your nasty Basque jokes. Collaborating with you during my PhD has been a great pleasure.

And to my other paranymphs, two very important persons that I could not leave behind. **Živa**, what to say, you have always been there. Science, (random) trips, hikes, climbing, brunches... You have been a pillar during all these years in Amsterdam and I am so happy to have developed this beautiful friendship with you. Thank you for your wisdom and endless support. You always have the right word to say and made easier the hard moments. Yet, the endless happy moments will be the ones to remember. **Antonio**, el alma de la fiesta, the most social person in the world with some FOMO-related abilities similar to mines. Having to know you and sharing so many moments with you (which I cannot even write down here) has been one of my highlights of Amsterdam. Thank you for ALWAYS being there. Aquí, o en la otra punta del mundo seguiremos sumando momentos. ¡Empezando por Yeste!

To the **Medema** group, having to spent my PhD with you was amazing. Many people have come and gone in these years, but I am grateful I shared with you a part of my stay. Thank you all for all the good moments and great science. **Apostolos**, thank you for bring in such a positive energy in the lab. Your optimism as well as your Greek cookies are so necessary in a daily day. It has been a pleasure to have you around during all my PhD. **Jonne**, the experience and knowledge you bring to the lab is so much needed. Thanks for all the discussions and input you gave me during all these years. I am sure the Raaijmakers group will keep growing. **Lenno**, as my grand-supervisor, it was great to have you back in the lab for my last half of the PhD! Thanks for all the helpful discussions. I hope *ATR* will bring you great publications next year (even more than 10!). **Michael**, finally we got a computational scientist in the lab! Even though R proved to be harder than expected... It was actually much fun having you joining bouldering. **Lisa**, it has been lovely to have you around these years. You are such a good scientist, don't let yourself think the opposite. **Anoek**, you bring fun and energy to the lab, and you are always up for helping everyone. Keep strong and fearless to finish the PhD! You are capable of everything. **Dorine**, your happiness and optimism in the lab are so much needed. You make things look simple and easy. I am sure you will have great coming years! **Mila**, what a nice surprise meeting you in my last year. And another *ABCB1* lover! It was very nice to have you around (even though too shortly). All the best of luck with your DM. I will miss to have you as my bench neighbor. Come and visit me soon! **Rob**, you are an essential pillar in the lab. Thanks for your help, over all these years. **Mariet** and **Marianne**, your organization and administrative work keeps the lab running. Thanks for all the hard work.



To **Marleen** and **Leon**, that made me discover what is like to be a supervisor. Thanks for all your hard work and time invested on *ABCB1*. I wish you all the luck for new exciting times to come as scientist!

And to all the rest of people that left the lab, you will always be part of my PhD times. **Jeroen**, it was great to have you as my supervisor. Your help during the first years made me able to become an independent scientist after you left. Thank you for everything you did for me. **Mar, Iraia, Rita, Chantal, Mihoko, Andre, Femke, Ahmed**, thanks for the good old times.

To the **Rowlands** and **Jacobs** groups, thanks for all Monday work discussions over the years. Your input has always been very helpful to develop my projects. **Judith, Claire, Roel, Angela, Demi, Marjon, Roan, Alberto, Sus** I am happy you joined B5 again! The lab is so much fun with cohesion around. To the **Jalink** and **Sonenberg** groups, it has been a pleasure to share departments with you.

To all B4, thanks for hosting me as one more in your department, your input and help has been very valuable during all my PhD. Without your help this thesis will not look like it is. **Ruben, Christ, Eva**, thanks for many monthly discussions over these years. It was great to be involved in your projects. **Elzo**, your help made us realize that we were working with an artefact. It was hard to assimilate but this led to good collaborations. Thank you for willing to help and discuss in all my projects. **Stefano** and **Tom**, thanks for sharing with me the art of the pA-Dam ID, it has been great (long) days spent at your benches. **Ningqing**, library preps are not exactly fun, but I will be happy to join you for hotpot again. Thanks for all the input, analysis and fun moments over all these years! **Dan, Miguel, Koen, Luca, Michela, Hans, Marcel, Chistine, Lisse, Heta, Aleksandra** and all the rest, thanks for all fun moments spent at the department, borrels and parties.

To the **Zwart** group, thanks for all the help I got over the years. Coming to H5 felt always like being in my own department. Also, ChIPing with you is much fun!

Special thanks to **Piet Borst**, for all your knowledge and input on ABC transporters and multidrug resistance.

The NKI (Mafia) family, when I came in 2016 for my internship I never imagined I would meet this amazing group of people. You are the reason why I decided to do my PhD at the NKI. **Joao**, you welcome me in the group, and since then you have been there. We have also spent great moments together at Diepenbeekplantsoen partying, watching Gran Hotel, cooking for me... I wish you the best for the new beginnings that are soon to arrive. **Ale**, you made me feel at home when I first arrive to the lab as a student. It was fun when you were there but even more all the good

moments that came after. **Isa**, your energy and happiness is contagious. Thanks for being always there, for the fun and for the needed moments. **Mariana**, I admire your strength and straightforward lifestyle. You know what you want and you will get it. Thanks for so many fun moments (including spilling wine) over the years. **Simon**, being students together at B5 was so much fun! I am glad you decided to come back to Amsterdam. I can't wait for many climbing trips to come. **Ronak**, thanks for your kindness and good moments we spent together. **Mathias**, always up for a party, bike trip or a random plan! Thanks for the happiness and energy that you bring to the group. **Eric**, it needs a lot of courage to leave the comfort zone and start a new degree. It has been always nice to have you around and remember our Catalan *peseteros* background. **Migurk**, todo un personaje, your inspirational monologues and way of life amaze me. I will miss so much your bad jokes in Australia.

And to the rest of the people that joined over the years and made my stay even better. **Stefan**, you have always been there, for the good and less good moments. Our weekly coffees and conversations are so much needed. Thank you for all your help, your endless support in science and in life made everything easier. **Dario**, the flammenkuchen after climbing sessions have been a way out of many hard work days. Thanks for always being up for everything. **Julia**, so nice to have someone from la Pompeu! It's being nice to continue doing science (and not so much science) together! **Soufiane**, thanks for all the good moments together! I enjoyed our Paclitaxel discussions bringing computers and biology together. **Marjolo**, I love your passion for science and cohesin! But it has also been so much fun to hang out outside the lab for trips, triathlons, weekends in Utrecht... It has been a pleasure to share our PhD journeys. **Angela**, having you as a flatmate has been fun, and even better as friend. Thanks for all dinners, runs and time we spent together. You are a tough girl that can deal with everything. **Alberto**, you leave such good vibes in the lab (and also in the parties). Thanks for being always there for a lab break.

Alba, Veronika, Nils, Santi, Inés, Aniek, Karianne, Liqin, Rodrigo, Ben, Roderick, Leila, Daan, Shanna, Christel, Max, Luuk, Lorenzo, Olga, Ana, Rebeca, Maria, Celia, Clara, Miriam, Theresa, Bruno, Roxanne, Elisa, Irune, and all the rest of people that made my stay unbeatable, thanks for all good moments spent together.

Dani and Francisca, you have been my best surprise in Amsterdam. I would have never imagined sharing my Amsterdam time with you both. I am so happy to see you growing together.

Elena, Robert, mi triángulo. Todos estos años, cada uno por su lado y seguimos como hace diez años. Muchas gracias por seguir allí todo este tiempo, por las aventuras que seguimos compartiendo y vuestro apoyo incondicional. Os quiero muchísimo. **Maria, Roser, Carla**, mis chicas de Horta, esperadme unos años más



y me tendréis haciendo el vermut cada fin de semana en Plaza Ibiza :D **Champi, Cata, Pedro, Oscar, Nuria**, gracias por todos los fines de semanas de vuelta a casa y estar siempre allí. Volver a veros siempre es una alegría. **Mar, Clara, Mirna, Agnès, Julia i Isshak**, gràcies per tots aquests anys que tot hi veient-nos poc hem continuat sumant moments junts.

Jérémy, my main support in the hard moments, the last push in the scary rappels and best partner in life. For many more adventures together.

Y por último, gracias a toda mi familia por todo el apoyo recibido durante estos años aun y estando lejos. Mama, Papa y Laura, gracias a vosotros he llegado hasta aquí. Y a ti Yayo, que no puedo escribir esto sin lagrimas en los ojos, me hubiera gustado tanto darte este libro en persona. Siempre has sido mi motor para seguir adelante, gracias por creer en mi.

Gracias a todos <3

Anna



